ABSTRACT

Title of Dissertation: MOLECULAR STRUCTURE AND SURFACE ORGANIZATION: A STUDY OF LIQUID/VAPOR INTERFACES USING NEWLY DEVELOPED SUM FREQUENCY METHODS

Okan Esenturk, Doctor of Philosophy, 2004

Dissertation Directed By: Professor Robert A. Walker
Department of Chemistry and Biochemistry

Vibrational sum frequency spectroscopy (VSFS) is a surface specific nonlinear technique that provides vibrational spectra of molecules at interfaces. Studies presented in this thesis use VSFS to examine surface structure of common liquids at liquid/vapor interfaces. The goal of this work is to correlate molecular structure and molecules functionality with the structure adopted by molecules at liquid surfaces.

The first part of this work describes the instrumental design and components of the newly developed VSFS. New methods are developed to overcome experimental difficulties associated with data collection for an entire spectral region of interest. The methods for data analysis and spectral post processing are also presented.

Surface vibrational studies of linear alkanes ranging in length from 9 to 17 carbon atoms investigated dependence of surface order on chain length. The linear alkane liquid surfaces evince a surprising degree of conformational order and this surface structure becomes more disordered as chain length increases. Halogenated alkane studies showed that replacing one terminal methyl group of linear alkanes with CH_2X (X=Cl or Br) for chain lengths 10, 14 and 16 leads to a mixed surface layer primarily occupied by CH_2X. These results are attributed to dipole-dipole interactions between the CH_2X and are indicative of a higher surface activity of the halogenated ends compared to the unsubstituted ends.

Additional experiments have investigated the effect of stronger interactions on the surface structure of 1-, 3-, and 5-nonanols and their ketone analogs namely 1-, 3-, and 5-nonanones. Results showed an increasing order as the OH or =O group advances toward the center of the molecule. A surprising result is a slightly lower surface order for nonanones compared to nonanols hints at the relative importance of simple dipolar interactions and highly directional hydrogen bonding in determining the surface structure. In addition, vibrational studies are carried out for 1- and 3-octanol at liquid/vapor interfaces. The results confirm observations from the nonanols by having a higher order for the 3-octanol. However, monolayer of 1-octanol on aqueous surface have a much higher surface order compared to 3-octanol. The increased order is attributed to the strong hydrogen bonding with water molecules.

MOLECULAR STRUCTURE AND SURFACE ORGANIZATION:

A STUDY OF LIQUID/VAPOR INTERFACES

USING NEWLY DEVELOPED SUM FREQUENCY METHODS

By

OKAN ESENTÜRK

Dissertation submitted to the Faculty of the Graduate School of the
University of Maryland, College Park, in partial fulfillment
of the requirements for the degree of
Doctor of Philosophy
2004

Advisory Committee:

Professor Robert A. Walker, Chair
Professor John D. Weeks
Professor John Tossell
Professor Douglas English
Professor Michael A. Coplan

DEDICATION

To my wife and my parents

TABLE OF CONTENTS

LIST OF TABLES

LIST OF FIGURES

Chapter 1

Introduction

The aim of this thesis is to explore how the surface structure of common liquids depends on a liquids' molecular structure using a surface vibrational spectrometer developed in our laboratory. Molecular structures of different liquids are systematically varied in terms of both size and intermolecular interactions. Changes in surface structure are observed in the vibrational spectra acquired with the sum frequency spectrometer. The present chapter motivates the need for studying the surface structure of liquids and describes the sum frequency generation technique. In addition, the chapter introduces the Walker group sum frequency spectrometer and systems studied.

1.1. Importance of Surface Vibrational Studies and Solvent Surface Structure

Frequently, discoveries made about the microscopic behavior of solutes in solution lead to advances in different industrial processes and products. For example, understanding forces responsible micellization lead to better detergents and phase transfer catalysis.[1] Many techniques have been developed to probe and identify these interactions in bulk solution. Tools available to study solvation at liquid surfaces are more limited. Particle based techniques such as neutron[2] or X-ray diffraction[3] lack the ability to reach buried interfaces between two condensed phases. Thermodynamic methods such as ellipsometry[3,4] fail to provide detailed information about the molecular structure at interfaces and total internal reflection infrared spectroscopy lacks surface specificity.[5] In contrast, vibrational sum frequency spectroscopy (VSFS)

is a technique ideally suited for studies of intermolecular interactions at liquid surfaces. Our research will use VSFS - a surface specific vibrational spectroscopy - to investigate the surface structure at liquid/vapor interfaces in order to help establish a predictive understanding of how interfacial structure is controlled by molecular shapes and intermolecular interactions. Knowing how solvent molecules arrange themselves at surfaces will enable us to begin to better understand interfacial processes and properties such as solvation and solution phase surface chemistry.

Accomplishing these goals requires direct knowledge of how solvents interact within the interfacial region. Previous studies in our laboratory have examined how the interfacial dielectric environment depends not only on the substrate composition but also on solvent identity.[6,7] Results demonstrated that interfacial solvent polarity changes with solvent structure even when two solvents have similar bulk dielectric properties. These conclusions are based on observed shifts in electronic transitions due to solute solvatochromic behavior. Such information, however, only provides details about the interfacial environment and overall orientation of a solute's electronic transition moment. Missing is direct information about interfacial structure and intermolecular forces. These forces will control conformation, orientation, and long-range order of molecules near the interface. With VSFS, we can investigate these effects by measuring vibrational band shifts, relative band intensities, and orientation of vibrational transition dipoles. The following study concentrates on the characteristics of the variety of the alkane surfaces, mainly solvent liquid/vapor interfaces. A common structural element possessed by all solvents is an alky chain.

Our work focuses specifically on conformations and geometries adopted by alkyl chains at liquid/vapor interface.

Alkanes might be considered the simplest type of organic molecules because of their chemical homogeneity and weakly interacting nature. Nonetheless, alkanes play complex roles in biological systems such as lipids, surfactants, and liquid crystals, and alkanes constitute the dominant component of fuels and lubricants. Although, the bulk properties of alkanes are well described,[8-16] the characterization of alkane surface structure and surface properties remain incomplete. The surface properties of alkane systems have been studied by various surface methods ranging from newly developed optical techniques (i.e sum-frequency (SF) spectroscopy) to conventional surface techniques such as surface IR, X-ray, neutron and light scattering, and ellipsometry.[3,4,17-23] Most of these studies seek to characterize the surface properties by varying either the experimental conditions such as temperature and pressure or by varying the chain length of the alkanes.

The surface structure of liquid alkanes is controlled by weak, van der Waals interactions between adjacent solvent molecules. Here, the term surface structure refers to any net ordering of liquid molecules at the liquid/vapor interface due to intrinsic interfacial anisotropy. Surface structure – those functional groups of a solvent molecule presented to the vapor phase – is different than long-range surface order, a term that refers to the relative positions and conformations of interfacial solvent molecules at the liquid/vapor boundary. This distinction becomes quite apparent when comparing the results of room temperature X-ray scattering from the n-hexadecane/vapor interface to vibrational spectra acquired from the same system.

X-ray scattering data from the n-hexadecane liquid/vapor interface show no diffraction features leading Ocko and coworkers to conclude that at room temperature, this surface possesses no long-range order.[3] In contrast, vibrational spectra of the n-hexadecane/vapor interface show a very pronounced feature assigned to a methyl symmetric stretch.[19] With fourteen methylene groups and only two methyl groups, one would not anticipate such a strong methyl response unless there existed surface structure having a non-statistical number of methyl groups aligned perpendicular to the interfacial plane. This apparent discrepancy between X-ray and vibrational data simply reflects differences in the properties probed by the two techniques. Long chain alkanes can possess surface structure (e.g. methyl groups oriented towards the vapor phase) without having any long-range order (e.g. beneath the terminal methyl groups, the solvent structure is randomized).

Predicting how surface structure changes with subtle alterations in a solvent's molecular structure is far from straightforward. For example, if one end of a long chain n-alkane were replaced with a weak dipole, one might guess that the polar ends of the solvent should be preferentially solvated due to solvation and surface free energy considerations. Preferential solvation would lead to a distinct absence of polar endgroups at the liquid/vapor interface. However, an alternative perspective presents a surface excess of polar endgroups so that dipoles can interact more freely without the steric constraints imposed by the accompanying long chains in bulk solution. These two pictures – polar ends solvated vs. surface active polar ends – predict liquid surfaces having very different properties. In the case where the polar ends are solvated, the liquid/vapor interface will be very inert and chemically similar to the

surface of other liquid alkanes. The surface having an excess of polar endgroups is much more polarizable and more likely to promote efficient adsorption of gas phase species and, perhaps, enhanced reactivity. To date, there exists little information to guide intuition when predicting the surface structure of weakly associating liquids at the liquid/vapor interface.

1.2. Sum Frequency Spectroscopy

Vibrational sum frequency spectroscopy (VSFS) is a surface specific technique that provides vibrational spectra of molecules at an interface.[17,24-26] Since the spectra result from a coherent optical response, the spectra also contain information about the orientation of the functional groups which then can be used to deduce the average conformations of molecules at an interface. Although sum frequency generation (SFG) is a complex non-linear optical phenomenon, it is conceptually very simple as shown in Figure 1.1. SFG uses two coherent optical fields overlapped at the interface to produce a third field equal in energy to the sum of two incident energies. Typically one of the incident fields has a fixed visible frequency while the other is tunable in the infrared (IR). Since the incoming fields come from pulsed lasers, the SFG occurs only when two incident fields are spatially and temporally overlapped. The intensity of generated sum frequency (SF) is resonantly enhanced when the frequency of the tunable IR field matches a vibrational frequency of the molecule at the interface. Therefore, tuning the IR frequency and monitoring the intensity of the generated SF field record vibrational spectra of molecules at interfaces. Although the technique employs high energy pulsed lasers, the generated SF signal level is extremely low due to the very low efficiency of the surface non-linear process. The process of up-

conversion, summing the infrared frequency with fixed visible frequency, shifts the collected spectrum to the visible region of the electromagnetic spectrum. Therefore, the technique takes the advantage of higher detector sensitivity in the visible region.

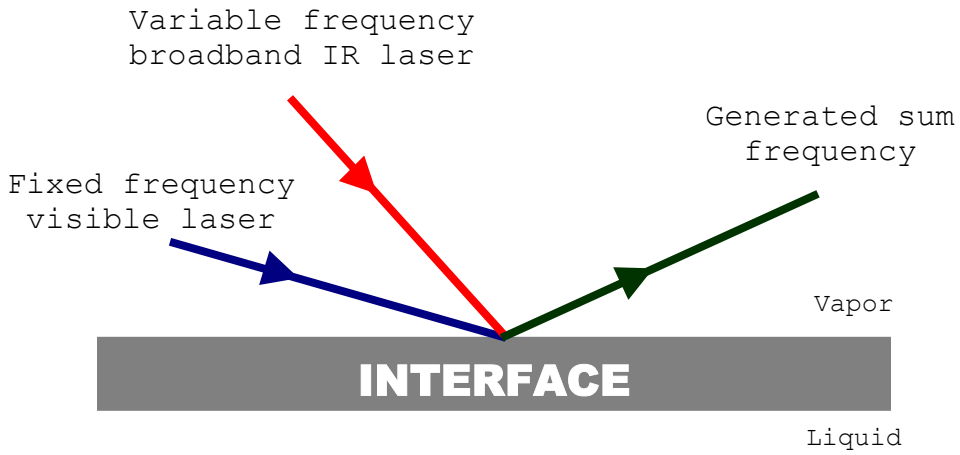

Figure 1.1. Schematic representation of sum frequency generation at a liquid/vapor interface. Colors do not represent the frequency of applied fields and are chosen for clarity.

Initial VSFS systems relied on stimulated Raman scattering to generate the tunable IR light for SF studies.[27] These sources are only used in nanosecond pulsed laser systems to generate a light in a wavelength range of 3000 – 5000 nm (3300 – 2000 cm^{-1}) Although this range covers most of the alkyl vibrational frequencies, many other vibrational frequencies including the frequencies of free and hydrogen bonded O-H and N-H stretches, C=O stretch as well as many other low frequency vibrations of molecules lie outside of this frequency range. With the introduction of solid-state laser systems, a rapid improvement in OPO/OPA (optical parametric oscillator/amplifier) technology in the IR range has been achieved. The wavelength range accessible by these OPO systems depends on the nonlinear crystal employed, and majority of the OPO systems provide continuously tunable IR wavelength from 2000 to 10000 nm (5000 to 1000 cm^{-1}).[28] There are commercial OPO systems that

provide tunability for frequencies beyond 10000 nm (<1000 cm^{-1}), but the generated IR light has very low power for SF studies. Advancements in technology and non-linear crystals may enable future instruments to produce higher power at lower frequencies. Currently, only free-electron lasers such as the ones that are accessible at the Institute of Plasma Physics, Nieuwegein, Netherlands (FELIX), or at LURE, Orsay, France (CLIO), provide such high energy lights for greater wavelength range. Both lasers span a range of 3000 to 40000 nm (3300 to 250 cm^{-1}).[29]

Like linear infrared spectroscopy, VSFS provides a vibrational fingerprint of the molecules but only of those molecules at the interface. Furthermore, VSFS is particularly sensitive to the conformational order of the molecules at the interface. Since SFG is a coherent process, the generated light has an amplitude, direction, polarization and phase associated with the orientation of the vibrational transition moments of the SF active molecular vibrations with respect to the polarizations of the incoming fields. Therefore, analysis of the data provides directional information of these molecular vibrations that then can be used to deduce an average molecular orientation at an interface.

With only ~18 years of history, VSFS is a relatively new technique. Use of VSFS is increasing exponentially with advancements in the technologies of reliable lasers and more efficient detectors. The theoretical basis of the technique was introduced by Bloembergen and Pershan in 1962,[30] but the surface specific application of SFS had to wait until 1986 when Shen and co-workers obtained the first SF spectrum from an monolayer of coumarin dye adsorbed on fused silica.[31] This first spectrum was actually an effective electronic spectrum of the coumarin dye

relying on the sum of two visible fields instead of two fields one in the visible and the other in the infrared. The first examples of the VSFS, using the infrared field, was applied a year later by both Shen[32] and Harris[33]. Once proof of principle was demonstrated, the technique was adopted quickly by many groups worldwide, including our own. The technique is attractive, in part, because of the high interest in interfacial properties, structures, and dynamics. Today, the technique is employed to study many systems ranging from polymer surface analysis[34] to buried interfacial analysis like model studies of water/oil interface.[35] The following paragraphs summarize some of the pioneering work that used SFS to study surfaces.

Since 1987 collaborative and independent studies of the Shen and Somorjai groups have shown a diverse range of application of VSFS on surfaces. [19,24,32,34,36-55] They demonstrated the technique's ability to obtain the molecular orientation of adsorbates at air/solid interfaces in 1987.[31,37] Shen and coworkers have exploited the advantages of VSFS to study structure at a wide variety of aqueous/hydrophobic interfaces. These systems figure prominently in wetting/nonwetting processes and micelle formations.[56] Their study of quartz/water interfaces showed that the orientation of interfacial water molecules depends not only on hydrogen bonding between surface silanol groups and water but also on electrostatic interactions between surface charges (-Si-O-) for pH > 2.[40] Their study implied that surface mediated effects extended 3 to 5 water layers into the aqueous phase. Recently, they have analyzed the surface of a biopolymer blends and demonstrated that the surface of the biopolymer is dominated by a higher portion of the hydrophobic polymer components compared to bulk.[50]

Richmond and coworkers have used VSFS to study the molecular properties of liquid/liquid and vapor/liquid interfaces.[26,35,57-69] This group has concentrated extensively on hydrogen bonding and water structure at both interfaces. Their studies of neat interfaces showed clear deviation from bulk behavior and the presence of water monomers in the organic phase.[61,70] They have also investigated the effect of surfactant adsorption in both systems (liquid/liquid and liquid/vapor) and the dependence of monolayer structure on surface concentration and identity.[59,62-64,67] Their findings challenge chemical intuition by suggesting that in some cases interfacial water molecules align themselves up to 10 nm (~30 water layer) across vapor/water and CCl_4/water interfaces depending on interfacial electric fields. Besides water/oil interfaces, they are currently concentrating on model lipid membranes.[71,72]

A major breakthrough in VSFS methodology has come from Stephenson and coworkers at NIST. In 1998, this group demonstrated the first use of broadband infrared fields to generate a SF response from multiple vibrational transitions simultaneously.[17] This approach dramatically reduces the data acquisition time from hours to less than one second and is the basis for the instrumentation developed in this work. Stephenson and coworkers have used their approach to characterize polymer surfaces and interfaces, as well as model membrane structure and phase transfer analysis.[17,18,73-76]

Studies from Bain and coworkers concentrate on surfactant adsorption[77,78] and phase transitions at liquid/vapor and solid/liquid interfaces.[25,29,77-84] Although not directly related to our specific goals, their work provides a helpful context for our

own research. Experiments highlight the importance of adsorbate conformation and orientation on surface film stability.[84] Stable films result from surfactants that can orient their hydrophobic tails to be in contact with non-polar solid surfaces at solid/water interfaces. These experiments of aqueous solutions in contact with solid surfaces showed unexpected behavior in an adsorbed 1-decanol monolayer consistent with liquid to solid phase transition.[79] The surface induced formation of an ordered solid-like layer of 1-decanol at the interface emphasizes that the properties of solutes in bulk solution cannot be extended to interfacial regions where surface-induced anisotropy exist.

Today VSFS is used to study a wide variety of phenomena including changes in interfacial water structure during protein adsorption,[85] solvation dynamics at the air/water interface,[86] adsorption effects in electrochemistry,[87] restructuring of polymer surfaces after physical contacts,[50] and biosensor activity.[82] Recent interest in atmospheric phenomena has motivated many VSFS studies on atmospherically relevant systems, particularly in acidic and strongly ionic aqueous solutions.[88-91] In some cases, the free OH stretching mode of water is used as a diagnostic for acid-water complexes at the surface, in some, CH_2 symmetric stretch mode is used as an indicator of the surface order. Similar studies have been extended to an ice/air interface.[47]

SFS has also been used to investigate properties of applied material including those used in chromatography,[92] combustion environments[93,94] and tribology[51,95-97]. With such a wide variety of areas for application SFG will likely to continue to grow in popularity as a technique for examining surfaces. Work by both Shen[51] and

Davies[98] as well as our own group has explored the application of the SFS to nanoparticle systems. In addition, Kuhnke et.al.[99] are studying SF microscopy, and Cho[100] and co-workers are investigating the theory of two dimensional spectral generation.

For surface analysis SF is a very valuable technique without a doubt but, as with every major analytical technique, SF also has its drawbacks. SF spectrometers are larger, more complex, less reliable and a much more expensive than a standard linear infrared spectrometers. In addition, operation of a SF instrument requires regular optical optimization. The generation of the tunable infrared light often presents considerable experimental difficulties. Both of the incident beams are high energy pulsed lasers; therefore, extreme care must be taken to avoid excessive heating and damage of the sample. Moreover, not every vibration of a molecule is accessible by SF spectroscopy. This is part due to the SF selection rules requiring both infrared and Raman activity for an SF active vibration and part due to very low efficiency of the SF generation that makes it very difficult to access SF active vibrations with weak IR and Raman activity. As research continues the list of molecular vibrations accessible by SFG is expanding by the advances in tunable IR, high energy pulsed laser technology. The majority of the SF studies are concentrated on fairly well characterized vibrational resonances such C-H and C-D stretches and bends, C-O, C-N, N-O, N-H, O-H, and Si-H stretches.

In addition, SF spectra are difficult to interpret quantitatively. Knowing molecular hyperpolarizabilities makes it possible to determine the molecular orientation by analyzing the spectra collected under different polarization conditions.

Determining the molecular hyperpolarizability associated with a particular vibration and the absolute SF signal level is extremely difficult but still possible with the help of molecular dynamic simulations.[35,49,73,75,88,101,102] Instead, researches try to introduce a local observer for phase information and use that for molecular orientation analysis for each component.[75] This is very difficult for liquid/vapor interfaces. Thus, inevitably SF data are often interpreted qualitatively. However, it should be noted that other surface techniques suffer the similar problems. For example, quantitative interpretation of surface spectra obtained by linear spectroscopic techniques, such as ATR (attenuated total internal reflection) infrared spectroscopy and PM-IRRAS (phase modulated infrared reflection adsorption spectroscopy), are also complicated by contributions from the underlying bulk media.[19] In addition, some of the surface scattering techniques such as X-ray and neutron scattering require an ultra high vacuum systems.

1.2.1. Theory

This section discusses the origin of the SF response. SFG uses two coherent optical fields overlapped on the interface to produce a third field equal in energy to the sum of two incident energies (Figure 1.1). Typically, one of the incident beams has a visible frequency while the other is tunable in the infrared. Tuning the infrared frequency and monitoring the intensity of the generated sum frequency field record vibrational spectra of molecules at surfaces. As a technique SFG is non-invasive and has good spatial, temporal, and spectral resolution.[17,24,57]

The origin of the nonlinear sum frequency response is due to the applied strong electromagnetic field, E, inducing a dipole, μ, to the molecules. The induced dipole can be described in terms of Taylor expansion in field strength:

$$\mu = \mu_0 + \alpha E + \beta E^2 + \gamma E^3 + ... \quad 1.1$$

where μ_0 is the static dipole of the material, α is the polarizability of the molecular electrons, and β *and* γ are known as first and second-order hyperpolarizabilities, respectively. In a condensed phase, the appropriate quantity to consider is the macroscopic polarization. For a bulk material, the induced polarization, P,[102] can than be described:

$$P = \varepsilon_0(\chi^{(1)} E + \chi^{(2)} E^2 + \chi^{(3)} E^3 + ...) \quad 1.2$$

$$P = P^{(1)} + P^{(2)} + P^{(3)} + ... \quad 1.3$$

where $\chi^{(1)}$ is the first, linear, susceptibility, and $\chi^{(2)}$ *and* $\chi^{(3)}$ are the second and third-order (non-linear) susceptibilities, respectively. $\chi^{(1)}$, $\chi^{(2)}$, *and* $\chi^{(3)}$ are the macroscopic averages of α, β, *and* γ, respectively. The first-order susceptibility, $\chi^{(1)}$, is much larger than the second, $\chi^{(2)}$, or third-order, $\chi^{(3)}$; therefore, the nonlinear contribution to the polarization becomes effective only when the applied field is comparable to the field felt by an electron in a molecule. Such a strong field is usually achievable only with lasers. The second order polarizability, $P^{(2)}$, gives rise to either second harmonic generation (SHG) or SFG depending on the frequencies of impinging fields. If the fields are equivalent in energy (or a single incident field), then the result is SHG. If the fields consist of two different frequencies, then the result is SHG and SFG. The process of SHG or SFG will be described below.

Many of the discussions about induced polarizations assume an electric dipole approximation for interaction of light with matter. Within this approximation the effect of the optical magnetic field and multipoles are neglected as well as the contributions from the dipolar fields of neighboring induced dipoles. A majority of the published theoretical and experimental SF studies[17,58,60,101,103,104] neglect these effects and show the validity of these assumptions. More information on the application of SF corrected for multipole and neighbor induced fields can be found in work of Boyd[105] and Braun[80].

Describing the applied field as an oscillating wave,

$$E = E_1 \, Cos \, \omega \, t \tag{1.4}$$

where ω is the frequency of the incident field, the induced polarization from Equation 1.2 may be rewritten as

$$P = \varepsilon_0 (\chi^{(1)} (E_1 \, Cos \, \omega \, t) + \chi^{(2)} (E_1 \, Cos \, \omega \, t)^2 + \chi^{(3)} (E_1 \, Cos \, \omega \, t)^3 + ...) \tag{1.5}$$

which can be rearranged with some trigonometric simplifications as

$$P = \varepsilon_0 (\chi^{(1)} E_1 Cos \, \omega \, t + \frac{\chi^{(2)}}{2} E_1^2 (1 + \, Cos \, 2\omega \, t) + \frac{\chi^{(3)}}{4} E_1^3 (3 Cos \, \omega \, t + Cos \, 3\omega \, t) + ... \tag{1.6}$$

The equation shows that the induced polarization, and hence the emitted light, contains terms that oscillate at two or more times the frequency of the original field, E. If only $P^{(2)}$ is considered:

$$P^{(2)} = \frac{\varepsilon_0 \, \chi^{(2)}}{2} E_1^2 (1 + Cos \, 2\omega \, t) \tag{1.7}$$

it consists of 2 terms:

$$P^{(2)} = \underbrace{\frac{\varepsilon_0 \chi^{(2)}}{2} E_1^2}_{\text{DC Field}} + \underbrace{\frac{\varepsilon_0 \chi^{(2)}}{2} E_1^2 \operatorname{Cos} 2\omega t}_{\text{SHG}} \qquad 1.8$$

Therefore under a single electromagnetic field $P^{(2)}$ term creates a DC field (i.e. no frequency dependence) known as optical rectification and SHG with a frequency equal in energy to the twice of the original frequency. Similar analysis can be made when two fields are applied, namely one in the visible and the other in the infrared. The surface electric field, E, can be described as the sum of the two oscillating incident laser beams:

$$E = E_1 \operatorname{Cos} \omega_{vis} t + E_2 \operatorname{Cos} \omega_{ir} t \qquad 1.9$$

The second order polarization, then, becomes:

$$\begin{aligned} P^{(2)} = \; & \varepsilon_0 \chi^{(2)} \left[(E_1^2 + E_2^2) + E_1^2 \operatorname{Cos} 2\omega_{vis} t + E_2^2 \operatorname{Cos} 2\omega_{ir} t \right. \\ & \left. + \frac{1}{2} E_1 E_2 \operatorname{Cos} (\omega_{vis} - \omega_{ir}) t + \boxed{\frac{1}{2} E_1 E_2 \operatorname{Cos} (\omega_{vis} + \omega_{ir}) t} \right] \end{aligned} \qquad 1.10$$

Therefore, two incident beams give rise to a DC field, SHG for both ω_{vis} and ω_{ir}, difference frequency generation with a frequency equal to the difference between ω_{vis} and ω_{ir}, *and* a SFG response having a frequency equal to the sum of ω_{vis} and ω_{ir}.

The induced second order polarization can simply be expressed without the oscillatory nature of the incident fields as

$$P^{(2)} = \varepsilon_0 \chi^{(2)} E_{vis} E_{ir} \qquad 1.11$$

where $\chi^{(2)}$ is a 3rd rank tensor describing the relationship between the two applied field vector and the resultant vector, $P^{(2)}$.

The nonlinear susceptibility $\chi^{(2)}$ can be expressed, to lowest order, as the sum of a nonresonant term $\chi^{(2)}_{NR}$ and a resonant term $\chi^{(2)}_{R}$:

$$\chi^{(2)} = \chi^{(2)}_{NR} + \chi^{(2)}_{R} \tag{1.12}$$

The former is a characteristic of the materials on either side of the interface and its contribution to the tensor is quite small for nonconducting systems.[19] As mentioned before, $\chi^{(2)}$ is a macroscopic average of the first order molecular hyperpolarizability. Therefore, the relation between the resonant term and hyperpolarizability can be defined as

$$\chi^{(2)}_{R,ijk} = \frac{N}{\varepsilon_0}\sum_{\alpha\beta\gamma}\left\langle R(\psi)\,R(\theta)\,R(\vartheta)\,\beta_{\alpha\beta\gamma}\right\rangle \tag{1.13}$$

where R(ψ)R(θ)R(φ) is the product of the three rotational matrices using all three Euler angles to convert from a molecular to the laboratory-fixed surface coordinate systems. The brackets indicate the orientational average and N is the number of molecules. The $\beta_{\beta\alpha\gamma}$[106] can be expressed as

$$\beta_{\alpha\beta\gamma} = \frac{1}{2\hbar}\,\frac{\mu_{\alpha\beta}T_{\gamma}}{(\omega_{v} - \omega_{ir} - i\Gamma)} \tag{1.14}$$

where ω_{ir} is the frequency of the tunable infrared field, ω_{v} is the frequency of the vibrational resonance, and Γ^{-1} is the relaxation time of the vibrationally excited state, and $\mu_{\alpha\beta}$ *and* T_{γ} are the Raman and infrared transition moments respectively:

$$\mu_{\alpha\beta} = \frac{1}{h}\sum_{s}\left[\frac{\langle g|\mu_{\alpha}|s\rangle\langle s|\mu_{\beta}|v\rangle}{(\omega_{SF} - \omega_{sg})} - \frac{\langle g|\mu_{\beta}|s\rangle\langle s|\mu_{\alpha}|v\rangle}{(\omega_{SF} + \omega_{sg})}\right] \tag{1.15}$$

$$T_{\gamma} = \langle v|\mu_{\gamma}|g\rangle \tag{1.18}$$

where μ is the electric dipole operator, $|i\rangle$ is the Dirac bracket notation for the ith state. g, ν, and s are the ground, excited vibrational and any other (scattering) states, respectively. The following figure shows a pictorial representation of the resonance enhancement process.

The simplified equation of $\chi^{(2)}$ can be written in terms of the vibrational modes of the molecules as

$$\chi_R^{(2)} \alpha \sum_q \frac{N T_{x,q} M_{x,q} \delta\rho}{(\omega_{ir} - \omega_{x,q} + i\Gamma_q)} = \sum_q \frac{A_{R,q}}{(\omega_{ir} - \omega_{x,q} + i\Gamma_q)} \qquad 1.17$$

where N stands for the surface density of the molecules, $T_{x,q}$ is the molecular IR transition dipole moment and $M_{x,q}$ is the molecular Raman transition moment for a specific vibration of molecule X. $\omega_{x,q}$ is the molecular vibrational frequency, Γ_q is the homogeneous half-width of the mode, and δρ is the population difference between the ground and vibrationally excited states for a given mode q. This expression can be simplified by casting A_R simply as the vibrational amplitude of the resonant contribution. The denominator predicts a strong resonance enhancement in the observed sum frequency generation when ω_{ir} approaches ω_x, the frequency of an allowed vibrational transition. The above equation implies that a vibration should be both Raman- and IR-active.

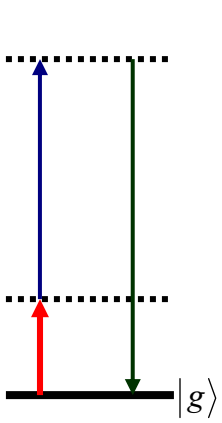

OFF RESONANCE

The incident beam energies are not resonant with any molecular energy level. SFG is minimal.

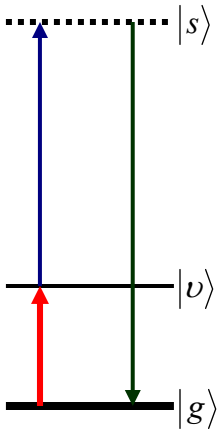

ON RESONANCE

The infrared frequency is resonant with a molecular eigen state. SFG is enhanced.

Figure 1.2. Energy level scheme for off and on resonance SF generation. When the infrared frequency is resonant with a vibrational frequency of the molecule, the generated SF signal is resonantly enhanced. Otherwise, SF signal is negligibly minimal for all of the solvents presented in this study.

The second-order nonlinear susceptibility tensor, $\chi^{(2)}$, contains twenty-seven elements. They completely characterize the nonlinear susceptibility for all combinations of incident and sum frequency polarizations. However, the non-zero components are less than the total number and depend on the symmetry constraints of the system. For example, bulk solution has a centro-symmetric environment meaning that all directions are equivalent to each other and the value of $\chi^{(2)}_{ijk}$ for two opposing directions must therefore be identical:

$$\chi^{(2)}_{ijk} = \chi^{(2)}_{-i-j-k} \qquad 1.18$$

Since $\chi^{(2)}_{ijk}$ is a third rank tensor, the change of sign in the three directions (i,j,k) is simply equal to reversing the system axis, which means $\chi^{(2)}_{ijk}$ must reverse sign.

$$\chi^{(2)}_{ijk} = -\chi^{(2)}_{-i-j-k} \qquad 1.19$$

Equations 1.17 and 1.18 can only be satisfied simultaneously when $\chi^{(2)}_{ijk}$ equals zero. Therefore, in a centrosymmetric medium, such as a bulk phase, SFG is forbidden by symmetry.

However, boundaries between media, such as liquid and vapor, are necessarily non-centrosymmetric due to discontinuities in properties at the interface. If the surface of the liquid is assumed isotropic about the surface normal with C_∞ rotation axis (Figure 1.3), then $z \neq -z$ but $x = -x$ and $y = -y$. Therefore, every component of $\chi^{(2)}_{ijk}$ that has a projection along the Z axis is nonzero. Since x and y are indistinguishable, only 4 components are left from the 27 elements for a liquid/vapor interface: $\chi^{(2)}_{zzz}, \chi^{(2)}_{zii}, \chi^{(2)}_{izi}, \chi^{(2)}_{iiz}$, where the subscripts refer to the polarization directions of sum frequency, visible, and infrared fields, respectively, i = x or y, and z defines surface normal in laboratory fixed frame. It is possible to sample different subsets of these $\chi^{(2)}$ elements by selecting different polarizations of the visible, infrared, and the reflected sum frequency fields:

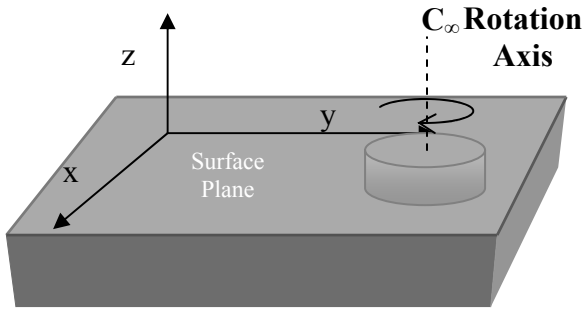

Figure 1.3. An isotropic surface plane about a C_∞ rotation axis.

$$I_{ppp} \alpha \left| \tilde{f}_z f_z f_z \chi^{(2)}_{zzz} + \tilde{f}_z f_i f_i \chi^{(2)}_{zii} + \tilde{f}_i f_z f_i \chi^{(2)}_{izi} + \tilde{f}_i f_i f_z \chi^{(2)}_{iiz} \right|^2 \quad 20$$

$$I_{ssp} \alpha \left| \tilde{f}_i f_i f_z \chi^{(2)}_{iiz} \right|^2 \quad 21$$

$$I_{sps} \alpha \left| \tilde{f}_i f_z f_i \chi^{(2)}_{izi} \right|^2 \quad 22$$

$$I_{pss} \alpha \left| \tilde{f}_z f_i f_i \chi^{(2)}_{zii} \right|^2 \quad 23$$

Once again, subscripts on the sum frequency intensity refer to the polarization of the sum frequency, visible, and infrared fields. The factors $\tilde{f}_{i,z}$ and $f_{i,z}$ represent the nonlinear and linear Fresnel factors governing the transmittance and reflectance of electromagnetic fields at interfaces.[58,106] Non-linear SF Fresnel factors for reflection and transmittance can be represented as

$$\tilde{f}_x^R = -\frac{i\omega_{SF}}{c\varepsilon_0} \frac{\cos\theta_{SF}^T}{n_T \cos\theta_{SF}^I + n_I \cos\theta_{SF}^T} \quad 1.24$$

$$\tilde{f}_y^R \equiv \tilde{f}_y^T = \frac{i\omega_{SF}}{c\varepsilon_0} \frac{1}{n_I \cos\theta_{SF}^I + n_T \cos\theta_{SF}^T} \quad 1.25$$

$$\tilde{f}_z^R = \frac{i\omega_{SF}}{c\varepsilon_0} \frac{\left(n_T / n_{int}\right)^2 \sin\theta_{SF}^T}{n_I \cos\theta_{SF}^T + n_T \cos\theta_{SF}^I} \quad 1.26$$

$$\tilde{f}_x^T = \frac{i\omega_{SF}}{c\varepsilon_0} \frac{\cos\theta_{SF}^I}{n_T \cos\theta_{SF}^I + n_I \cos\theta_{SF}^T} \quad 1.27$$

$$\tilde{f}_z^T = \frac{i\omega_{SF}}{c\varepsilon_0} \frac{\left(n_I / n_{layer}\right)^2 \sin\theta_{SF}^I}{n_I \cos\theta_{SF}^T + n_T \cos\theta_{SF}^I} \quad 1.28$$

where ω_{SF}, c, and ε_0 are present to provide the SF equation with the correct units and i introduces a constant phase term. I and T represent the corresponding term in incident

and transmitting media, respectively. n_{int} is the interfacial refractive index and is assumed to be different from the refractive indices of bulk materials.

Our sum frequency spectrometer is based on a co-propagating geometry of visible and infrared beams and detects the reflected component of the SF signal. Therefore, the resulted SF signal comes from the surface at an angle, θ_{SF}, determined by the incoming angles of the visible, θ_{vis}, and infrared, θ_{ir}, fields. The angle θ_{SF} can be calculated using the conservation of momentum (phase matching) of the beams parallel to the surface of the liquid.

$$n_{SF}\omega_{SF}\theta_{SF} = n_{vis}\omega_{vis}\theta_{vis} + n_{ir}\omega_{ir}\theta_{ir}$$

where n is the wavelength dependent refractive index of the interface. The angles and beam propagations are presented in Figure 1.4.

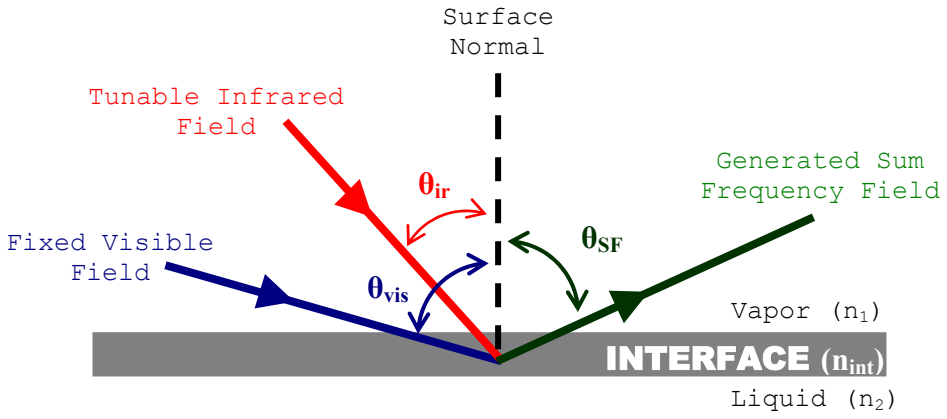

Figure 1.4. The co-propagating geometry of visible and infrared fields generating SF beam. Only the reflected SF beam is shown because the system is set-up only to detect the reflected component. The transmitted SF along with the reflected infrared and visible beams are omitted for clarity. Colors do not represent the frequency of applied fields and are chosen for clarity.

Polarization combinations selectively probe vibrational transitions that are parallel, perpendicular to the surface. Figure 1.5 is given as an example that shows three SFG spectra of same phospholipid monolayer at a D_2O/CCl_4 liquid/liquid interface.[58] The only difference between the spectra is the polarization combinations used for two incoming fields and generated field. As shown in Equation 1.20 and Figure 1.5 a), PPP combination samples all $\chi^{(2)}$ elements and hence all active vibrational transitions appears in spectrum regardless of their orientation (Figure 1.5a). However, other polarization combinations selectively sample either in- or out-of-plane vibrational transitions (See equations 1.21 and 1.22 and Figure 1.5b & c). Comparing in- and out-of-plane spectra from the same interface can identify solute and solvent orientations. In this particular example, the relative intensities of the methylene symmetric stretch (CH_2-SS) and the methyl symmetric stretch (CH_3-SS) allow inferences to be made about alkyl chain conformation in the phospholipid as well.

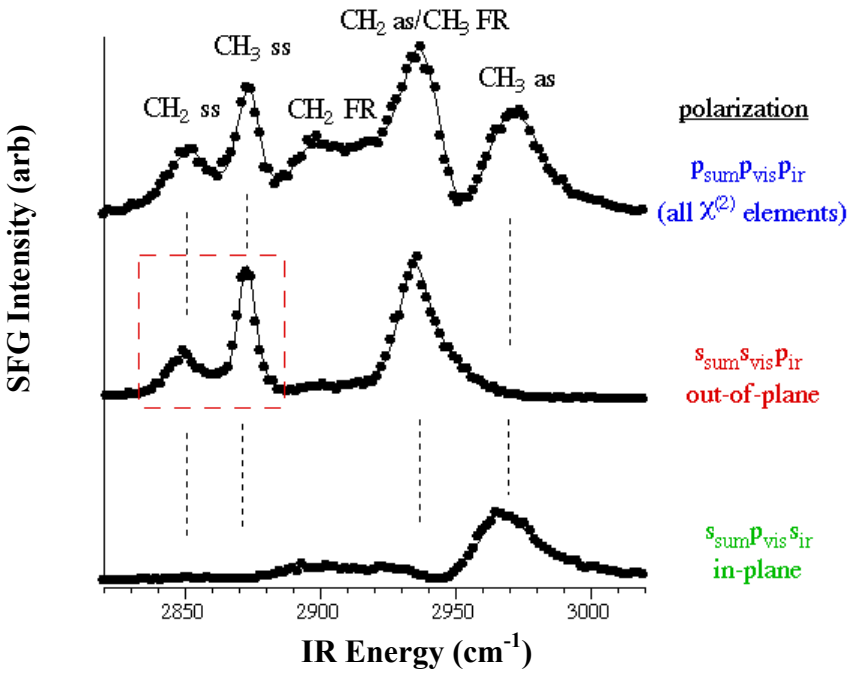

Figure 1.5. SFG spectra of phospholipid monolayer at liq/liq. interface with different polarizations. a) PPP, b) SSP, and c) SPS. The figure is a taken from ref 58 with authors permission.

1.2.2. Walker Group Sum Frequency Spectrometer

The spectra presented in this thesis have been recorded by using the Walker group femtosecond sum frequency spectrometer (WG-SFS). The spectrometer became operational in 2003, and required ~3 years to construct. The spectrometer is unique due to its use of ultrafast IR pulses and continuously variable spectral resolution. Thus far, the spectrometer has been largely used to study the surface structure of liquid/vapor systems as well as monolayer and film structures on liquid surfaces. These were fundamental studies of the effect of the molecular structure as well as the intermolecular interactions between the solvents on the surface organization of common solvents. Throughout this work only the C-H (2800-3000 cm^{-1}) stretching region was studied due to the strong IR and Raman activity of CH_2 and CH_3 groups. Furthermore, features in this region are very sensitive to molecular conformations. The spectrometer, however, has the capability to acquire spectra of the liquids at N-H and C=O stretching regions as well. It is also versatile enough to study both solid/liquid and solid/air interfaces.

1.3. Overview of the Thesis

This thesis presents vibrational studies of liquid surfaces by newly developed vibrational sum frequency spectrometer. The goal of the study is to investigate the effect of the molecular structure and intermolecular forces on the surface organizations of liquids to extend our knowledge on the surfaces and forces that govern them with the perspective outlined in the introduction. Hence the study

represents a mixture of physical chemistry, optical physics, software engineering and electronics. The chapters have been written as rough drafts of manuscripts that will eventually be submitted for publication. Consequently, each chapter contains some redundancy when describing fitting procedures, band assignments, and grounds for interpretation.

The detailed description of our new vibrational sum frequency spectrometer is given in Chapter 2. This next chapter is extended to include a description of how spectral data are processed and analyzed. The following chapters are assembled with respect to groups of studied molecules. Chapter 3 presents the results of vibrational surface studies of linear alkanes. Here, the chain length dependence on surface order is investigated. The alkane length ranges from nine carbon atoms to seventeen carbon atoms. The chapter also includes surface structure comparisons of branched and cyclic alkanes with linear alkanes. The size effect on the end groups of the alkyl chains are introduced in Chapter 4. The surface structure of chloro- and bromoalkanes with chain lengths of 10, 14, and 16 carbon atoms are compared. The haloalkanes are also compared to linear alkanes.

In Chapter 5, stronger intermolecular interactions are investigated. The strength of hydrogen bonding is compared to the strength of dipolar interactions on the surface structure by comparing the surface vibrational spectra of alcohols and ketones. The chapter first examines the neat nonanol and nonanones where –OH or =O group positions on the carbon backbone are shifted toward the center. The results are compared to deduce the effect of a strongly interacting group's position on surface structure. In addition, nine carbon alcohols and ketones are compared to evaluate the

strength of H-bending versus dipolar interactions on surface organizations. Then, the chapter presents an extensive study of alcohol surface structure of 1- and 3-octanol and compares the neat surface spectra to spectra obtained from monolayers of the isomers adsorbed on aqueous solution surfaces.

Chapter 6 presents a bulk solution study on specific and non-specific solvation forces. The study introduces a model for vibrational solvatochromic behavior of strongly interacting solutes such as Indoline. Assuming that the similar forces are governing the interfacial chemistry, we hope to extend the study to liquid/vapor interfaces. Chapter 7 summarizes the overall results and findings of the surface structures of these common liquids. The chapter also discusses the opened horizons in light of these studies and some further applications of the sum frequency technique.

Chapter 2

Experimental

This chapter describes the sum frequency spectrometer employed in this work. After a brief introduction of the spectrometer, the chapter is divided into sections describing the different components of the spectrometer. The function of these components can be described as follows:

i) generation of the laser source

ii) generation of IR light

iii) manipulation of the visible light

1) stretcher

2) delay line

3) time vs frequency domain

iv) generation of SF light

v) delivery of the SF light

vi) detection of SF light

Following a detailed description of these components, the rest of the chapter briefly discusses the interpretation of the sum frequency (SF) spectra regarding assignments of vibrational resonances and data analysis routine as well as importance of the sample stage, cleaning procedure for the equipment, and general maintenance of the instrument.

2.1. Sum Frequency Spectroscopy

2.1.1. The Sum Frequency Spectrometer

As mentioned in the introduction, vibrational sum frequency generation (VSFG) results when two high intensity optical fields, one having a fixed frequency in the visible and the other tunable in the infrared, couple at an interface to produce a third field equal in energy to sum of two incident fields.[17,24,26,38,57] Sum frequency generation (SFG) is enhanced when the infrared frequency becomes resonant with the vibrational frequency of the molecules. Otherwise, the nonresonant SFG of dielectric systems is negligibly small.[19] SFG is a surface specific technique that allows us to acquire vibrational spectra of an interface without interference from the underlying bulk solution.[19,103,104] The efficiency of the process depends upon the visible frequency (ω_{vis}), infrared (IR) frequency (ω_{ir}), and our ability to overlap those beams in time and space as well as our ability to deliver the generated sum frequency (ω_{sf}) to the detector. A schematic representation of the simplified version of the spectrometer is given in Figure 2.1. The components of the spectrometer are grouped according to their function on the spectrometer, and each group will be described in detail in later sections of this chapter.

The generated SF spectrum contains information about the vibrational modes of functional groups that are both IR and Raman active.[17,73] The intensity of the observed modes depends on the cross correlation of the IR and Raman activity as described in the Chapter 1. As a technique, SFG has evolved considerably compared

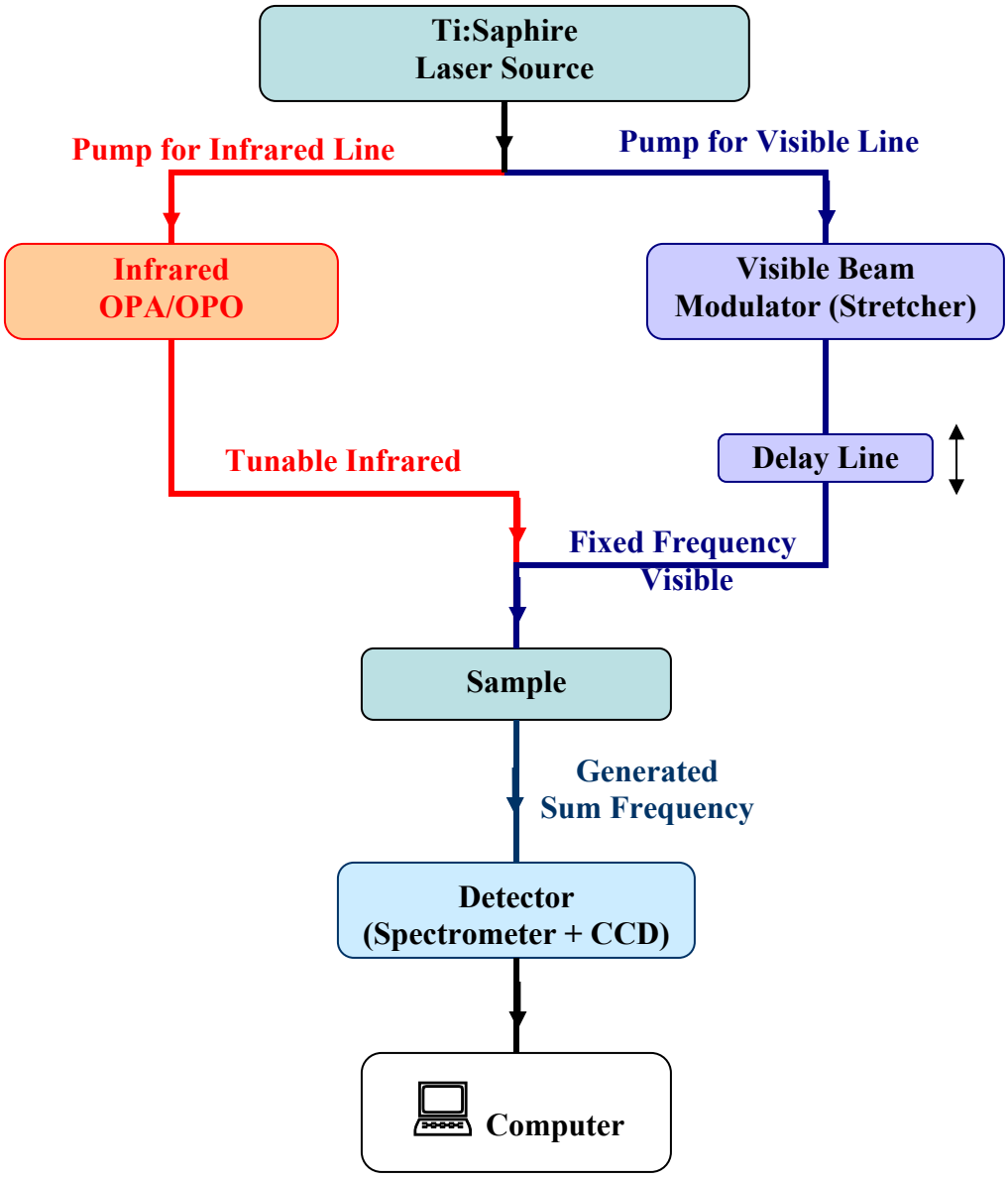

Figure 2.1. A chart diagram of the femtosecond sum frequency spectrometer employed in this work.

over the past 17 years, but the same challenges remain, namely generating the infrared light, ensuring the spatial and temporal overlap of both beams at the interface and maintaining system stability over long of working periods.

The spectrometer used in the experiments described in this thesis is the latest in a new generation of instruments that exploits broadband characteristics of ultrafast

laser techniques.[17,107] The instrument set-up is based on the first broadband design reported by Stephenson and coworkers in 1998.[17] Assembling the Walker research group sum frequency spectrometer required several years. And, given the uniqueness of the instrument, individual components will be discussed in detail. However, before describing the components of the system, a brief experimental set-up overview is valuable. The backbone of the spectrometer is a Ti:Sapphire laser system providing the source for both the IR and visible components of an SF experiment. The Ti:Sapphire laser generates a fixed frequency pulsed laser beam that is then split into two parts. The high energy part of the beam is used to pump an optical parametric amplifier (OPA) with a difference frequency mixer that generates tunable light in mid-IR. The second part of the source laser is used to pump a home-built stretcher to generate narrowband visible light. A delay line is set-up on the visible path to adjust the path traveled by the visible beam from the source to the sample stage so that the path matches the exact same distance traveled by the IR beam, thus, ensuring temporal overlap of both frequencies at the sample. The overlapping visible and IR beams at the interface generate the SF light that is delivered to a monochromator. The monochromater disperses the SF light onto a CCD array according to the colors created during NLO generation. The resulting image is converted to an interfacial vibrational spectrum of the sample. The full experimental details of the SF spectrometer are shown in Figure 2.2. Typical beam energies are detailed in Table 2.1.

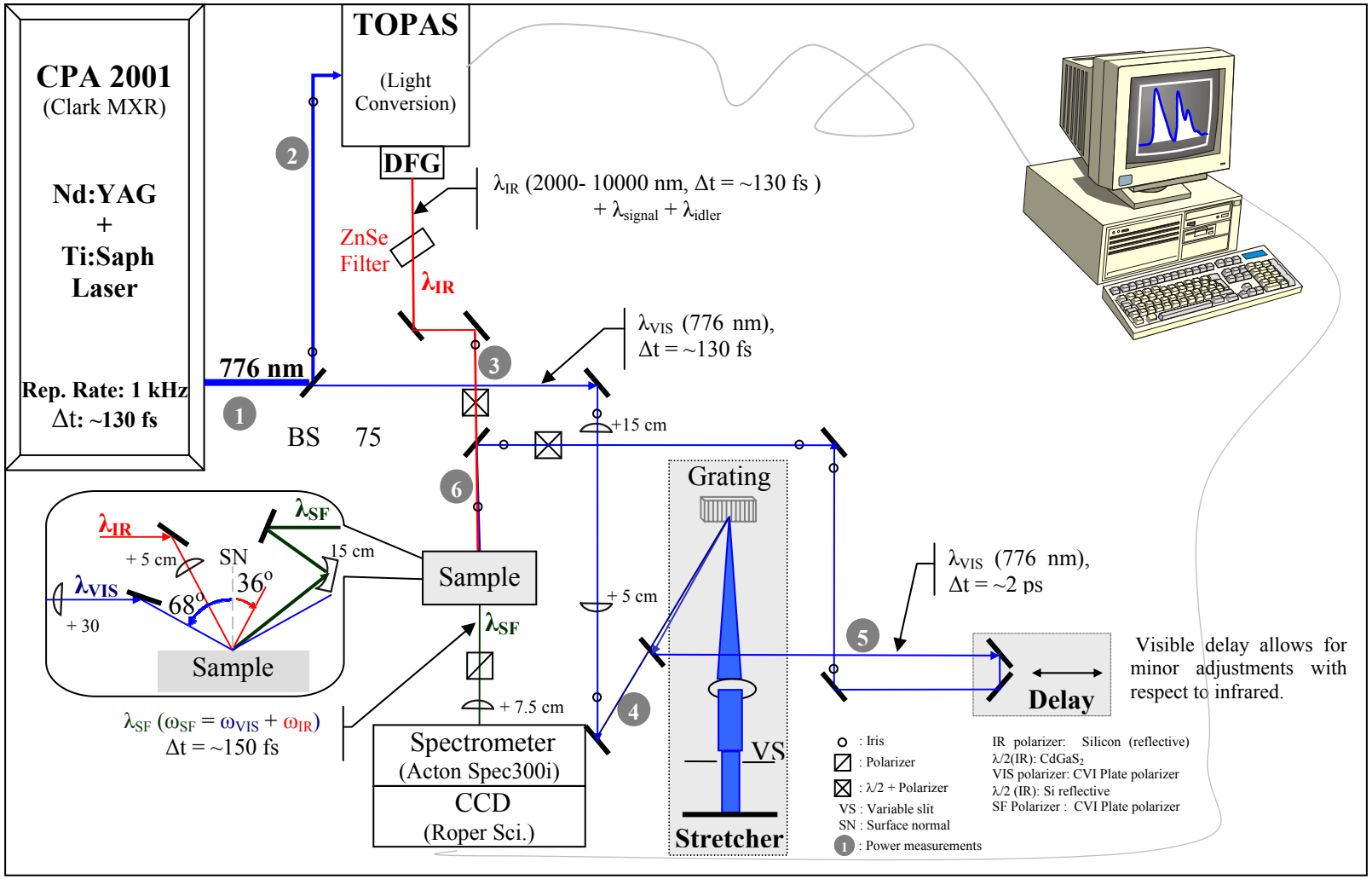

Figure 2.2. Experimental details of the femtosecond sum frequency spectrometer.

Table 2.1. Laser powers and pulsewidths for the femtosecond sum frequency spectrometer shown in Figure 2.2. These reading are typical for a well optimized laser system after 1 hr of warm-up time with a new flashlamp.

Laser Beam	Wavelength (nm)	Pulsewidth (fs)	Measurement Point (Figure 3.2)	Laser Power (mW)
Total CPA 2001 Output	776	~130	❶	770
TOPAS pump (input)	776	~130	❷	516
Infrared power after ZnSe and 2 Au mirrors	3500	~150	❸	6.7
Stretcher pump (input)	776	~130	❹	170
Stretcher output (Slit width of 1.25 mm)	776	~2000	❺	21
Infrared before the last mirror to sample	3500	~150	❻	~5
Visible before the last mirror to sample	776	~2000	❻	~5

Component A: The Laser Source

The laser source is a Clark-MXR CPA 2001 Ti:Sapphire regeneratively amplified laser system. The system is actually a compact combination of four different laser components namely a diode/fiber oscillator combination, a Nd:YAG pump laser and a Ti:Saphire regenerative cavity. Usually these components are in separate boxes and require more hands-on tuning due to sensitivity to environmental conditions. The Clark system is very compact with a single casing containing all of the components to make system performance less sensitive to heat and humidity. However, we still encounter difficulties associated with running a laser system such as beam drifts due to the seasonal changes.

The system operates as follow: continuous wave (CW) light centered at 1550 nm is emitted from a solid-state diode laser. The light is coupled into Erbium doped fiber that self phase modulates and converts the CW light into a series of pulses (80 MHz). These pulses are used to seed the regenerative cavity. The diode/fiber assembly requires very little maintenance. The diagnostics are integrated into the system and can be monitored from an electronic readout in the diode/fiber compartment. Typical values are 170 mW for the output power and 306 mA for the current of the diode laser. The diode laser runs in constant power mode. The light from the fiber couples into an assembly of birefringence filter (BRF) centered in four half waveplates for stable modelocking. Modelocking can be checked via an analog oscilloscope where the typical observation is a steady pulse with an amplitude of 500 mV on 2 μs timescale. If the light is not modelocked, a slight adjustment of 4^{th} phase plate and/or BRF may be needed. Once the beam is modelocked, those low energy

pulses seed the regenerative cavity where they are amplified by the output of a Nd:YAG (neodymium doped yttrium aluminum garnet) pump laser system. The laser system requires very little maintenance except the change of lamp every 200 - 400 hours. The procedure for changing the YAG lamp can be found in the CPA2001 manual. The typical power output of YAG is ~ 7.5 W at 532 nm. The seed beam (at 776 nm) and the pump beam counter propagate through a Ti:Sapphire crystal which is set to its Brewster angle with respect to the beam paths. The Ti:Sapphire crystal lases at the wavelength of seed laser, 776 nm. The amplified beam passes through the crystal multiple times before sufficient gain builds up in the pulse. Once the amplified beam has saturated in energy, the beam is dumped out of the cavity with the help of a Pockels cell. Then the beam is compressed from more than 10 ps to 130 fs with a conversion efficiency of ~55 %. The beam frequency profile of the generated beam is given in Figure 2.3. The half width half maximum (HWHM) of the beam is ~3.6 nm

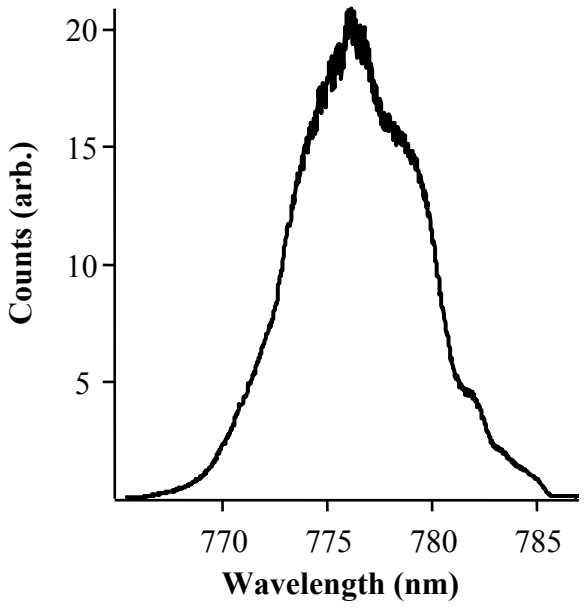

Figure 2.3. Laser beam color profile acquired at ❶ in Figure 2.2 for a optimized system. The laser is delivered to a spectrometer via a multimode fiber.

and centered at 776 nm. This profile can be changed through slight adjustments of the seed steering and 532 nm overlap in the Ti:Sapphire crystal. The generated beam is then delivered both to the IR-OPA and to the stretcher assembly.

Component B: The Infrared Generation Compartment

The IR-OPA is more than just an optical amplifier. It generates and amplifies the required wavelength of the infrared beam. It is called Traveling-wave Optical Parametric Amplifier of Superfluorescence (TOPAS, Light Conversion). Although it is very compact and efficient, maintenance of the TOPAS is extremely difficult. Expertise and care is required even on minor adjustments on the instrument. The biggest difficulty arises from having to vertically align seven passes of a laser through a single crystal (5mm x 5mm x 5mm). The diagram of beam travel inside a TOPAS is given in Figure 2.4.

The 776 nm light used to pump TOPAS is divided into two parts by passing through an 80 % beam splitter (BS) inside of the TOPAS itself (BS1, Figure 2.4). The higher energy part is used later to amplify the generated IR laser beam, therefore it is called amplifier. The lower energy part is split further with another beam splitter (BS2, Figure 2.4) for pre-amplification of the generated IR beam, and for generating IR in a β-barium borate (BBO) crystal. The BBO crystal simultaneously generates two colors, denoted signal (ω_{signal}) and idler (ω_{idler}), simultaneously and the sum of the frequencies of the signal and idler is equal to the frequency of incoming 776 nm beam.

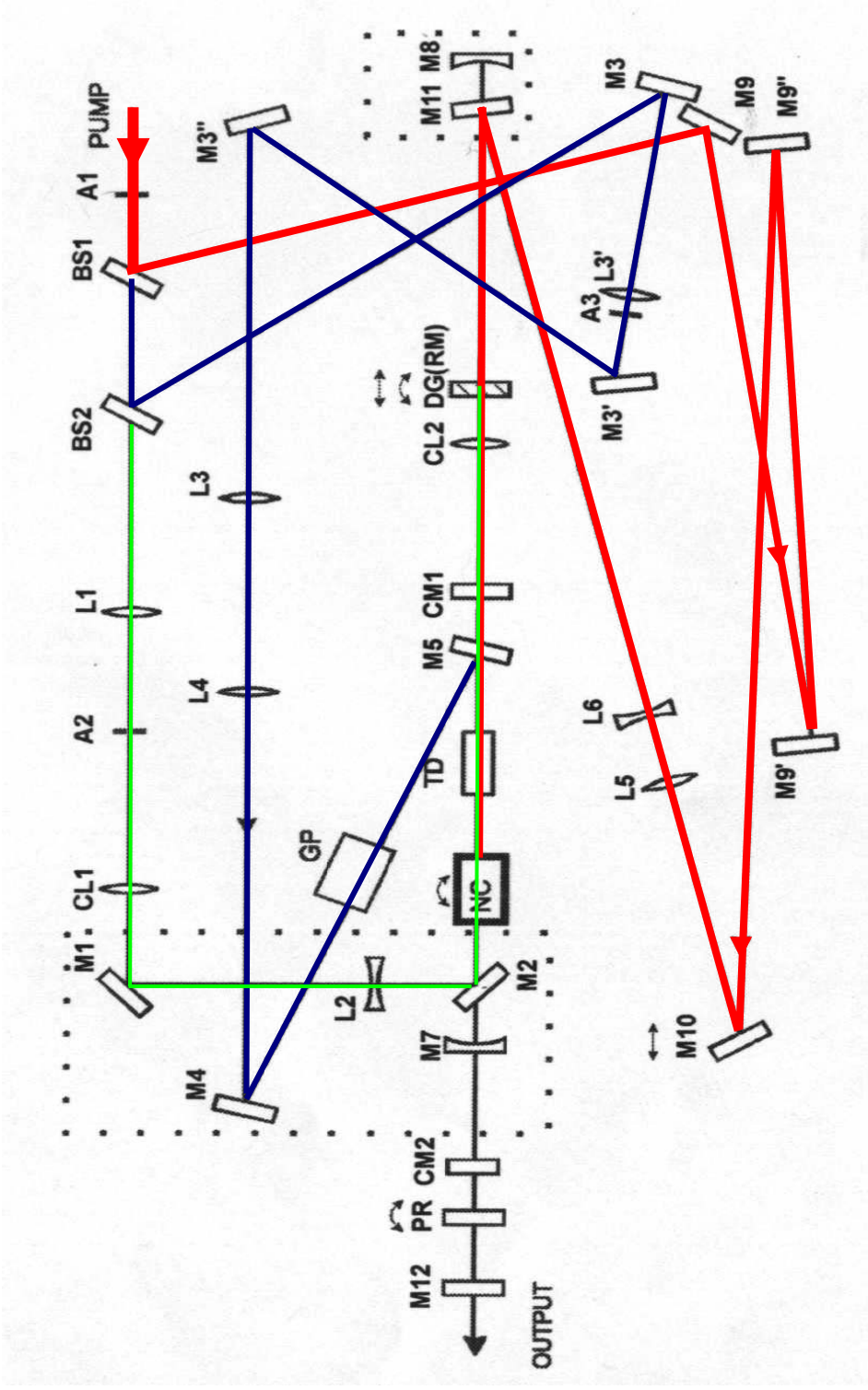

Figure 2.4. Top view of general layout of the TOPAS optical elements where the five passes are represented simultaneously. Red line – Amplifier; Blue Line – Preamplifier; Green – Seed beam. Original figure is reproduced from TOPAS manual.

$$\omega_{signal} + \omega_{idler} = \omega_{pump} \quad (2.1)$$

The frequencies are determined by the angle of the BBO crystal according to phase matching conditions.

The preamplifier beam is matched in time and space in the BBO crystal to amplify ω_{signal} and ω_{idler}. The beams are then amplified further with a strong amplifier field. The energies of the output power of TOPAS with respect to signal color frequencies are given in Table 2.2.

Table 2.2. Power output of TOPAS with respect to of λ_{signal}. Power profile shows the efficiency of the non-linear crystal for generated colors.

λ_{signal} (nm)	Power (mW)
1100	48
1150	90
1200	110
1250	119
1300	122
1350	129
1400	129
1450	130
1500	122
1550	124

Before arriving at the difference frequency (DF) crystal, $AgGaS_2$, the amplified signal and idler beams pass through a time correction plate where the relative timing of the both pulses are equalized. The DF crystal couples ω_{signal} and

ω_{idler} to generate a new frequency which is equal to the difference of the ω_{signal} and ω_{idler}.

$$\omega_{IR} = \omega_{DF} = \omega_{signal} - \omega_{idler} \quad 2.2$$

Therefore, the angle of the BBO crystal effectively tunes the generated IR frequency. The TOPAS can tune the IR frequency from 2800 to 10000 nm. For reasons of sensitivity and stability, most of the experiments in this work are carried out within the region of 3300 to 3800 nm. Falling in this wavelength range are the alkyl C-H stretching bands. The energies of the generated IR beam with respect to frequencies are given in Table 2.3. The generated IR beam passes through a ZnSe filter set at the Brewster angle to separate the signal and idler from the IR beam. Polarization of the IR beam is controlled via a combination of a Silicon transmission polarizer and Cadmium Gallium Sulfide ($CdGaS_4$) half wave plate. The IR beam is focused onto the stage by a 7.5 cm focal length Calcium Fluoride (CaF_2) lens. The beam path alignment of the infrared beam is optimized by using liquid crystal paper (Edmund Sci.) with 25 to 30 ^oC sensitivity.

Table 2.3. Infrared laser power measured at ❻ in Figure 3.2. Although power deviates much in the given range, experiments are carried out between ~3330 and 3570 nm (2800-3000 cm^{-1}) where IR power is fairly constant, ~ 5mW.

λ_{signal} /nm	λ_{IR} /nm	Power /mW
1205.5	2700	2.4
1215.2	2800	3.4
1224.3	2900	3.3
1233.1	3000	3.1
1241.3	3100	3.2
1249.1	3200	4.5
1256.5	3300	4.9
1263.6	3400	4.9
1270.3	3500	5.0
1276.8	3600	5.4
1282.9	3700	5.6
1288.8	3800	5.4

Component C: Modulation of the visible light

i) The Stretcher

Spectral resolution in a SFG spectrum depends on the bandwidth of the incoming fields. Due to the time-energy uncertainty relationship our visible and IR fields have broad bandwidths. If these fields were used for the experiments, the generated signal would contain many unresolved features. It is not possible to get any information out of such a featureless spectrum (Figure 2.5a). One solution to this dilemma involves spectrally narrowing the IR field; however, this solution requires scanning IR frequency across the entire range of interest. This approach can require hours to acquire a single spectrum. Instead, we have chosen to spectrally narrow the visible field and keep the IR field as broad as possible. A broad IR field will excite all of the transitions within the IR window (Figure 2.5b). The narrow bandwidth visible will upconvert the SF signal and resulting spectrum can be dispersed on a CCD. This technique (of using broadband IR) was first demonstrated in 1998.[17] The combination of broadband IR and narrow visible fields combined with a computer-controlled monochromator and CCD detector cuts data collection time from hours to seconds. In our spectrometer, a homebuilt optical stretcher narrows the visible beam bandwidth to ~8 cm^{-1}. The stretcher was modeled after a similar instrument reported in the literature[108] with one important modification. Our stretcher uses a micrometer-controlled slit instead of fixed position razors. The schematic drawing of the stretcher is given in Figure 2.6. This alteration gives us a unique opportunity to optimize the spectral narrowing process and, consequently, the spectral resolution of SFG spectrum. Narrowing the visible field reduces the field's intensity and optimization

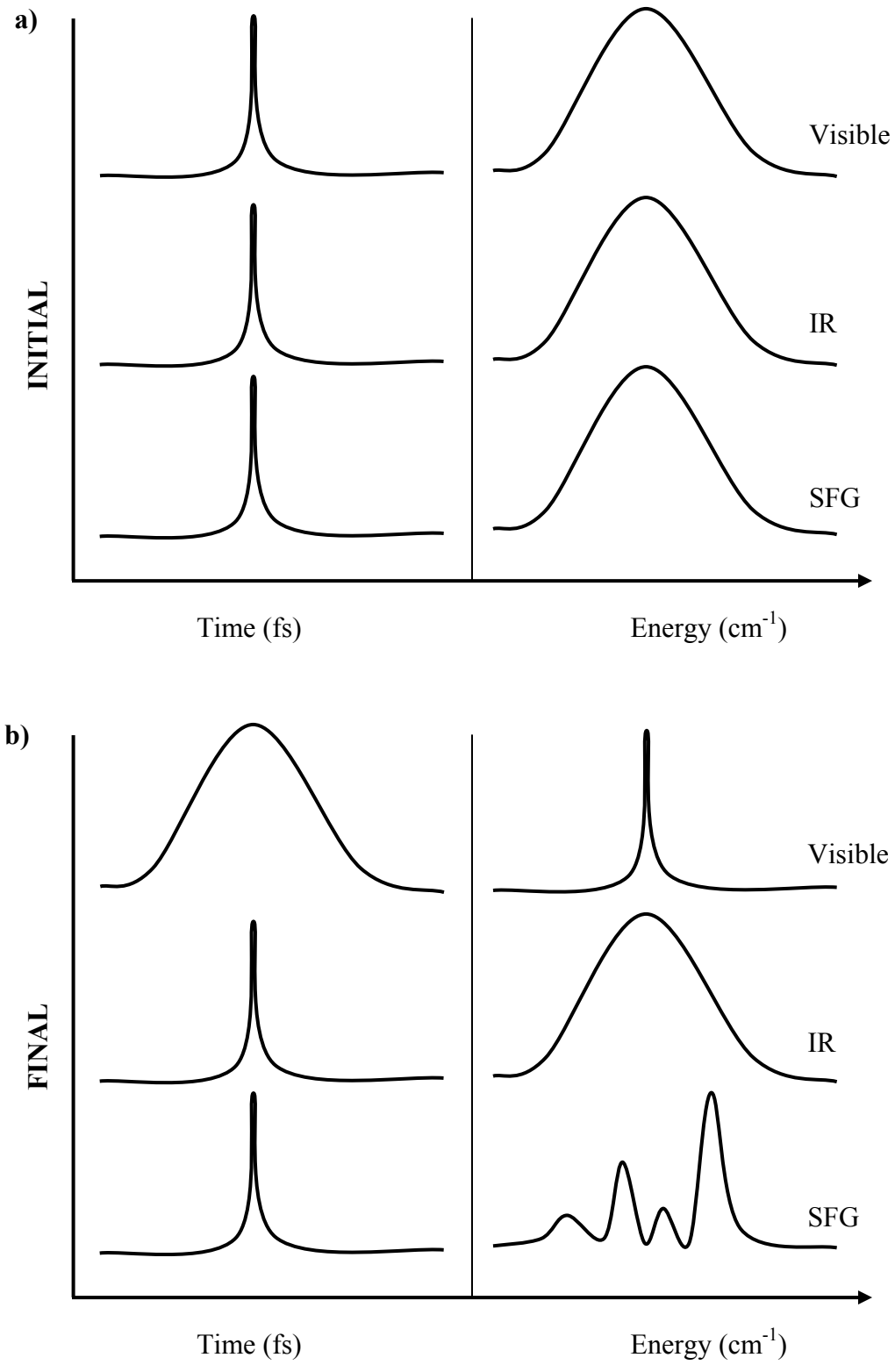

Figure 2.5. Figure shows possible results of a sum frequency field in time and energy domain when a broad infrared field overlaps with a broad visible (a) and a narrow visible (b).

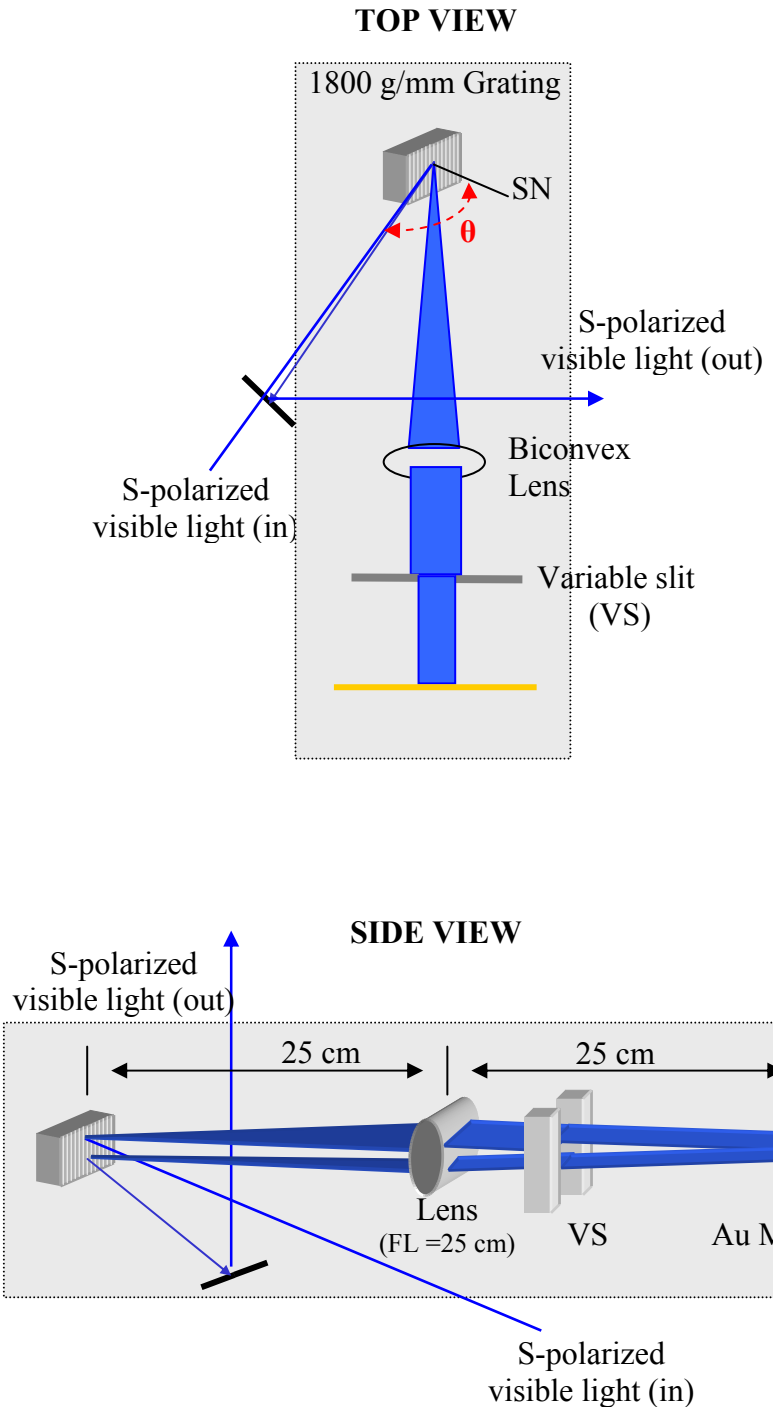

Figure 2.6. Schematic diagram of top and side view of stretcher.

requires balancing spectral resolution with signal intensity. Due to the time-energy uncertainty narrowing the visible field causes a stretch in pulsewidth from 130 fs to 6 ps and brings us an added convenience when overlapping IR and visible beams at the interface in temporal domain. The beam diameter of the visible pulse delivered from the CPA-2001 is considerably larger than the stretcher system can accommodate. The beam diameter is reduced to half by a home-built telescope assembly with 20 and 10 cm focal length lenses. Then the beam is directed to the optical stretcher assembly via a gold mirror. The stretcher consists of a 1800 groves/mm S-polarized grating, a BK7 biconvex spherical lens, micrometer controlled slit, and reflective mirror. The beam path of the visible beam through the stretcher is given in the Figure 2.1 (side view). The 776 nm visible beam is diffracted from the grating toward the end mirror passing through the lens and the slit. The diffracted beam diverges due to the fine color separation provided by the grating. The beam is collimated once it reaches the lens. The collimated beam then passes through a slit that spatially filters the sides of the beam selectively reducing the bandwidth associated with the visible pulse reduced to a value determined by the space between the razors of the slit. The beam is reflected back from the gold mirror, passing through the lens again. This time the lens focuses the modified pulse beam onto the grating to recombine the colors. A height difference between the paths is introduced by a vertical displacement of the lens. The visible beam is then delivered to the delay stage before being sent to the sample where it overlaps with infrared beam spatially and temporally. Pulse width of the manipulated visible beam with slit width opening of the stretcher is given in Table 2.4. Pulse width of the slit is measured by the sum frequency response from GaAs surface as the

visible is delayed with respect to the infrared beam. Range of the delay stage move for a fixed slit width is correlated with the pulse width of the visible beam. Table 2.5 shows the visible beam powers at ❻ (in Figure 2.2) with respect to the slit width of the stretcher. Figure 2.7 shows a sample nonresonant SF response from a clean Au surface collected under PPP polarization conditions with a well optimized spectrometer. The spectrum accumulated for 1s with a 3 mm slit width. The FWHM of the spectrum reaches up to ~120 cm^{-1}, which is correlated with the bandwidth of the IR light. Since the bandwidth of the generated SF depends on the IR bandwidth, a change in the slit opening does not change the bandwith of the generated SF spectrum as illustrated in Figure 2.8. The figure shows overlaid nonresonant SF spectra of clean gold surface acquired under SSP polarization conditions for 1s each. Each spectrum then normalized with respect to maximum intensity.

Table 2.4. Dependence of the visible pulsewidth (fs) with the change in the slit width measured with delay line. Pulse durations are converted to spectral bandwiths by using minimum time-bandwidth product for a Gaussian pulse, $\Delta\omega(Hz)*\Delta t(s) = 0.44$ for FWHM .

ΔDelay (mm)	FWHM (fs)	FWHM (cm^{-1})
	3000	4.9
	2000	7.3
	1000	14.7
620	972	15.1
610	956	15.4
450	705	20.8
340	533	27.5
320	502	29.3
200	292	50.3
190	298	49.3
140	232	63.3
135	220	66.7
120	188	78.0

Table 2.5. Visible beam powers measured at ❻ in Figure 2.2. with respect to the slit width for an optimized system.

Width (mm)	Power(mW)
0	0.3
0.5	1.1
1.0	1.8
1.5	2.5
2.0	3.1
2.5	3.8
3.0	4.3
3.5	5.0

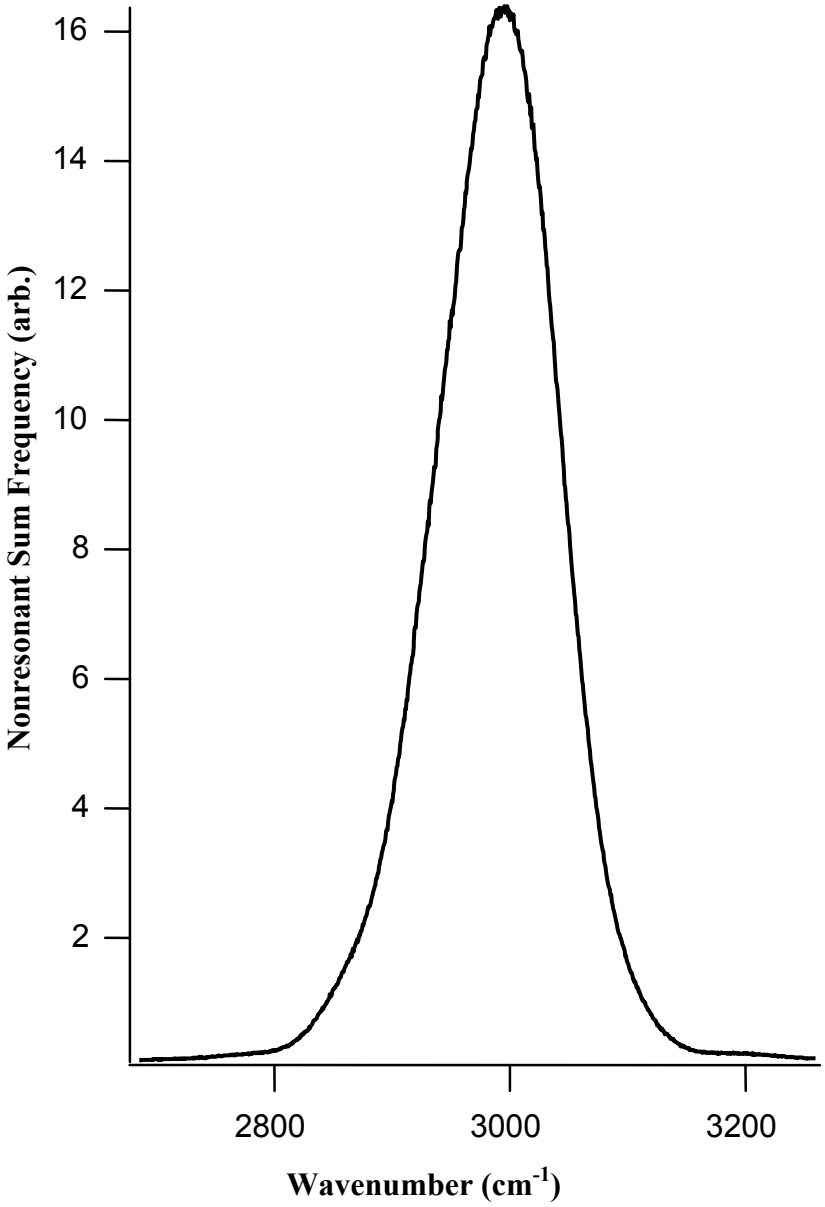

Figure 2.7. Profile of a generated SF light (λ_{IR} = ~3350 nm) from a clean Au surface having ~122 cm^{-1} FWHM. (1 min accumulation under PPP polarization condition with fully open slit of stretcher and a well optimized spectrometer)

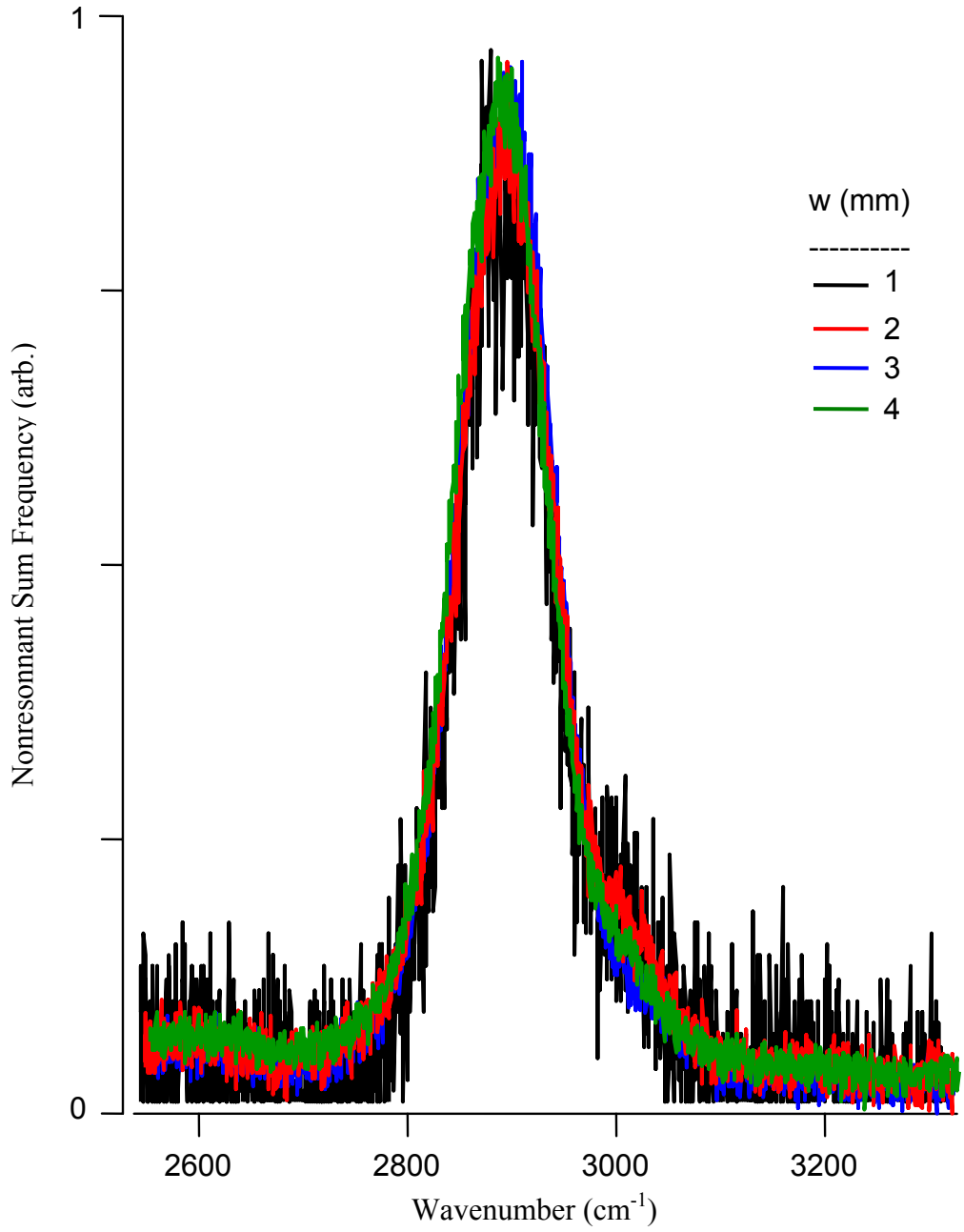

Figure 2.8. Nonresonant SF spectra of a clean Au surface with respect to the slit width (w/mm) of the stretcher aquired under SSP polarization condition. The frequency of the generated SF fields corresponds to the frequency of the IR field. The spectra show that the slit width change does not affect the bandwidth of the generated sum frequency.

ii) Visible Delay

The visible delay consists of two coupled vertically aligned 45 degree mirrors set on a micrometer stage. The main purpose of the delay line is to be able to finely adjust the distance traveled by the visible beam and so that it matches exactly the distance traveled by the IR beam. Generating the SF depends on both the spatial overlap of the visible and infrared beams *and* the temporal overlap of both beams. Since the source beam is a femtosecond (fs) pulsed laser with a repetition rate of 1 kHz, both visible and IR beams are pulsed sources having 1000 pulses per second. This means that between each pulse there is ~1 ms delay, and each pulse is 130 fs wide. We choose to delay the visible beam because of the flexibility on the visible beam path (relative to IR path) as well as the convenience of aligning the visible beam.

Component D: The SF Generation

When two incoming high intensity fields, ω_{vis} and ω_{ir}, overlap at the interface, they generate a sum frequency response. The sum frequency generation is a very low efficiency process as described in Chapter 1. Most of the parameters responsible for SF generation are inherent to the molecular system (such as the Raman and IR crossections, vibrational bandwidth) so that controlling those parameters are almost impossible. However, there are two variables that we can control according to the given equation 1.20 – 1.24 in Chapter 1 Section 2. The simplified equation is as follows:

$$I_{sf} \alpha |\chi^{(2)}|^2 I_{vis} I_{ir} \qquad 2.3$$

As the equation suggests, the power and area of the incoming fields can be optimized for improve SF upconversion efficiency. Due to the instrumental limitations we cannot increase the IR power, and arbitrarily high powers of the visible light will damage the system being studied. Typically, powers and spot size are adjusted to generate largest signal from the system without introducing damage.

The SF experiments are carried out in a geometry shown in Figure 2.9. The visible beam is centered at 776 nm and the bandwidth is determined by the stretcher. Usually the bandwidth is set to ~8 cm^{-1} (with a corresponding pulse duration of 2 ps). The visible light is delivered to the sample stage with an angle of 68^{o} with respect to the surface normal (SN). The beam is focused gently onto the surface with a 30 cm focal length (FL) planoconvex BK7 grade silica lens. The beam diameter is ~0.5 mm on the surface. The visible power is constantly checked with respect to the sample saturation and kept well below the level that causes surface damage. Typical power is in ~2 mW range and corresponds to a power density of ~ 2.5 mW/cm^2. The IR beam is delivered ~4.4 cm above and almost parallel to the visible beam to ensure that the generated SF beam follows the visible beam direction. The IR beam is focused onto the sample with a 5 cm FL planoconvex CaF_2 lens with 36^{o} with respect to SN. The IR beam diameter is ~0.2 mm on the surface with a power of ~4 mW and corresponding power density of ~31 mW/cm^2.

Since the generated SF signal is very weak, we want the minimum number of optics necessary to deliver the signal to the detector in order to minimize the losses. During the set up of the SF delivery path many geometries were tried. Neither of the first two setups lead to observable SF signal. The first successful setup for the

generated SF beam delivery is shown in Figure 2.10. The delivery path of the SF beam from sample stage to monochromator slit is calculated with a visual basic script written in Excel (Appendix A). Given the incoming angles of the visible and IR beams, and the height of the monochromator slit, the script determines the angle of the generated SF frequency as well as the positions and angles of the mirror on the path to deliver the SF beam parallel to the table. The main difficulty with such a setup was making sure that the delivered beam to the monochromator was parallel to the table. Although the calculated position and angle of the delivery mirrors do ensure the parallel delivery, the set-up is highly sensitive to small drifts in incident beam paths requiring recalculations of the SF path and very difficult realignments. Also the SF beam diverges slowly and, due to the long delivery path, requires collimation. We have modified the delivery path by introducing a concave and regular silver mirrors. The new geometry is shown in Figure 2.9. The concave mirror has a FL of 15 cm and collimates the SF beam. The use of two mirrors ensures that the beam path is parallel to the table and less sensitive to the drifts on the SF beam. The beam is then focused onto the slit of the monochromator with a 7 cm FL planoconvex BK7 silica lens. Polarization selection of the SF beam is provided by a CVI BK7 thin film plate polarizer.

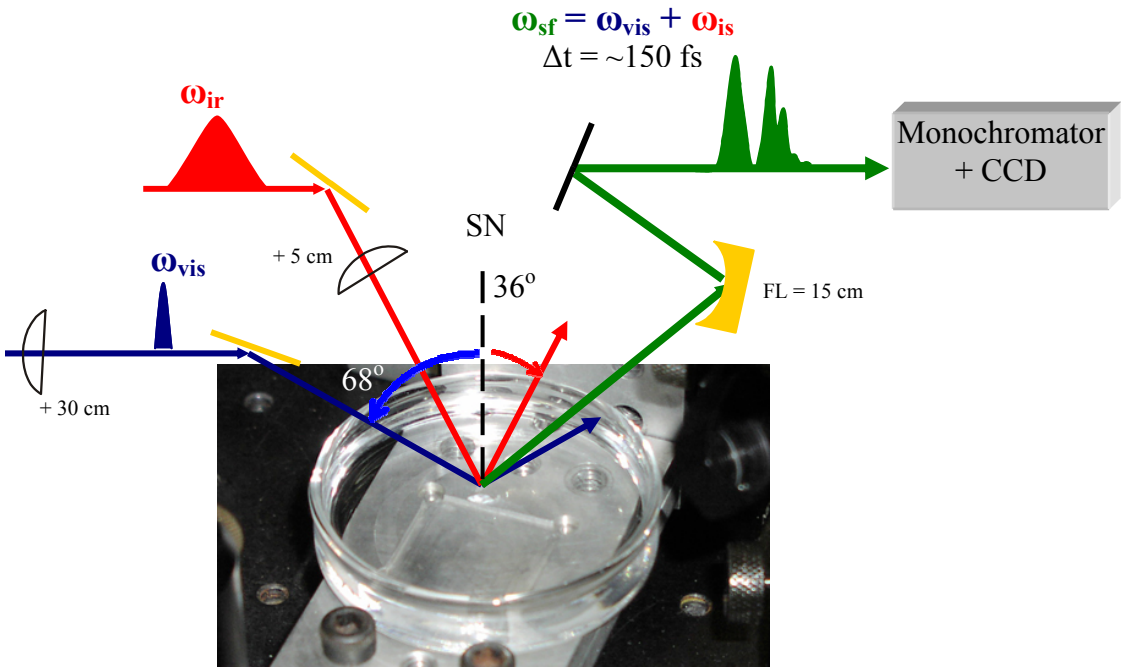

Figure 2.9. The latest SF geometry.

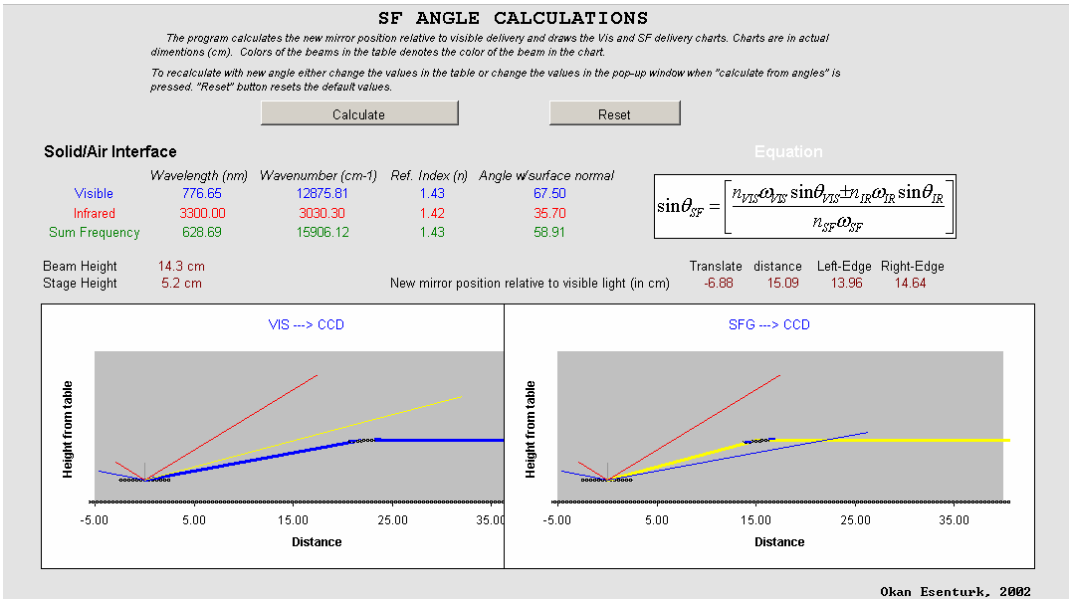

Figure 2.10. A snapshot of SF angle calculation program.

Component E: Detection of SF light

The detection compartment of the SF spectrometer has two main components; a monochromator and a CCD detector. The specifications of the both instruments are given in Table 2.6. Once the beam is focused onto the monochromator slit, a coupled mirror/grating assembly disperses beam onto the CCD detector. The image (Figure 2.11B) is then transferred to the computer and processed for a spectrum of the interface (Figure 2.11C). The processing is done via WinSpec32 software provided by the CCD manufacturer (Roper Sci.). The initial grating on the monochromator was a 2400 groves/mm grating blazed at 500 nm. Although high grooves/mm allows high resolution of the spectrally dispersed image, the efficiency of the grating for the relevant wavelength range (600-650 nm) was too low for SF studies. The grating was replaced with holographic grating with 1800 grooves/mm. The efficiency of the SF delivery to CCD array is increased by ~30 %. The CCD temperature is kept as low as possible, usually -45 ^{o}C. Temperature of the CCD is a diagnostic for the vacuum efficiency of the CCD assembly, if the CCD temperature is above -40 ^{o}C or the controller is not able to lock on to specified temperature, then it requires refurbishing which can be done by sending the CCD back to the manufacturer.

Table 2.6. Roper Scientific (Acton research) Monochromator and CCD specifications.

CCD

Model	Spec-10:100B (Princeton inst.)
Image sensor	Scientific grade1:MPP, back illuminated
CCD format	1340x100 imaging pixels (20x20 μm)
Gains	1/2x, 1x, 2x
CCD read noise	3 e^- rms @20 kHz
System read noise	<5 e^- rms@ 100 kHz
Scan rate	100 kHz
Vertical shift time	10 μs
Spectral rate	65 Hz, full-vertical binning @ 100 kHz digitization.
Dark current	< 0.05 e/p/s @ -50 ^oC
Operating temperature	-45 ^oC
Temperature precision	± 0.04 ^oC
Front window	UV fused silica quartz
Controller Model	ST133

Monochromator

Model	Spectra Pro-300i
Gratings	1) 2400 g/mm, 2) 1800 g/mm, 3) N/A
Focal Length	300 mm
Aperture ratio	f/4
Resolution	0.1 nm@435.8 nm (measured w/1200 gmm grating)
Accuracy	± 0.2 nm

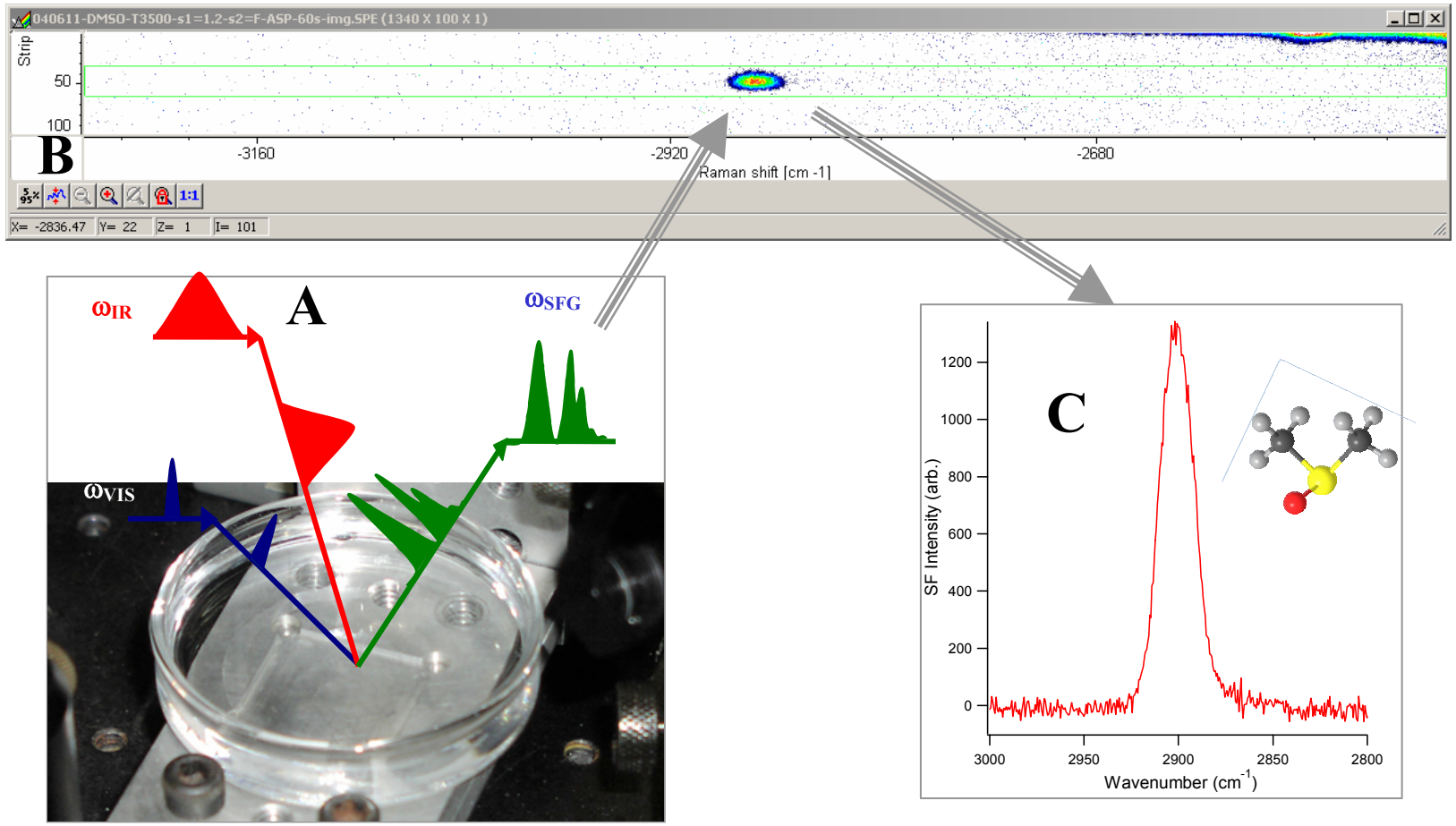

Figure 2.11. Surface vibrational spectra collection from DMSO surface. A) Both ω_{vis} and ω_{ir} overlapped at the liquid surface. B) generated SF(ω_{sf}) is delivered to the CCD (shown as image). C) Region of interest (green rectangle on image B) vertically summed and converted to a spectrum.

Steps for Initial SF Generation

The first step in setting up the SF spectrometer requires ensuring that the visible, IR, and SF paths are well-aligned. To do this, irises are positioned at certain points along the beam paths to be used for fine adjustments as well as for routine diagnostics. With a non reflective white business card, the visible beam path can be optimized. Liquid crystal paper (Edmund Scientific) is used for fine adjustments of the IR beam path. Then the visible and infrared beams are overlapped on a liquid crystal paper located at the sample position. Once spatial overlap is achieved, the visible and IR beam must then be temporally overlapped. Temporal overlap of the visible and IR beams can be achieved by first replacing the liquid crystal paper with a lithium iodate ($LiIO_3$) crystal (Altechna, Lt). $LiIO_3$ crystal has very strong nonresonant SF response, therefore, focusing both beams on the $LiIO_3$ crystal can generate an amount of SF that is visible to the eye. The temporal overlap then is optimized with the delay line while visually observing for maximum SF intensity. However, routine use of $LiIO_3$ crystal has many disadvantages. First, the crystal requires a specific angle with respect to the incoming beams for efficient SF generation. Since the visible and infrared beams have different angles, it very difficult to find an optimum angle for the crystal. Second, the crystal is hygroscopic and therefore must be stored in a special housing stage. The geometry of the housing stage does not allow the SF beam to be reflected to help align the SF path. Each time the stage has to be replaced with the crystal assembly and the returning to the actual experimental geometries is not trivial. After the accidental discovery that a Zinc Selenide (ZnSe) mirror has an equivalently large SF activity we began using the ZnSe

mirror for the routine temporal overlap checking of the visible and infrared beams. The main disadvantage of the ZnSe mirror is that the generated SF beam is so dispersed that it is not possible to use the signal as a guide for SF path alignment. After the temporal and spatial overlap of the visible and IR beam at the sample stage has been achieved, the ZnSe mirror is replaced with Gallium Arsenide (GaAs) coated silicon wafer. Although GaAs has much lower nonresonant SF response (compare to ZnSe or $LiIO_3$), it is strong enough for quick optimization of the SF path once the SF is observed on the CCD. Once the SF beam path is calculated and aligned approximately, the generated SF beam is delivered to the CCD. After the nonresonant SF spectrum of GaAs is observed (and collected over 1s), the SF beam path can be aligned with the help of irises on the parallel side of the path.

2.1.2. Vibrational resonances

The information hidden in SF spectrum of interfacial species is similar to the information gathered by infrared or Raman spectroscopy. An SF spectrum is composed of vibrational information of functional groups that are both infrared and Raman active. The information such as center frequencies, intensities, bandwidths and phases of these vibrations can be obtained by analyzing the surface vibrational spectrum and are valuable for understanding the surface structure.

All of the vibrational sum frequency spectra reported in this thesis are acquired in a region of 2800 to 3000 cm^{-1}, a region in which C-H stretching bands appear. There are two reasons behind the selection of the region. First, the liquid surfaces studied are composed of molecules having long alkyl chains. Second, the C-H stretching modes have large infrared and Raman transition moments. This

uncommon property enhances the observed SF signal, an important consideration given the very low efficiency of SF generation. The features observed in a surface vibrational spectrum have been assigned by comparing the center frequencies with that of bulk solution studies by infrared and Raman spectroscopy of alkanes[11,13,14,109-114] as well as by comparing with results of bulk and surface studies of similar alkanes reported in literature.[18,19,34,48,50,52,58,59,72,73]

A summary of the bulk solution assignments for C-H stretching modes obtained via infrared and Raman spectroscopy are given in Table 2.7 along with reported bulk and surface frequencies of the modes in similar alky structures. The modes are sorted according to corresponding energies.

Table 2.7. C-H stretching mode frequencies from bulk measurements and from reported bulk and interface studies.

Mode	Description	Frequencies /cm^{-1}		
		Bulk* (IR &Raman)	Bulk (Literature)	Interface (Literature)
d^+	Methylene symmetric stretch (CH_2-SS)	2852-54	2846	2850
r^+	Methyl symmetric stretch (CH_3-SS)	2870-75	2870	2875-77
d^+_{FR}	Methylene symmetric stretch (Fermi resonance) (CH_2-FR)	2891-93	2890	~2900
d^-	Methylene asymmetric stretch (CH_2-AS)	2824-31	2915	2925-30
r^+_{FR}	Methyl symmetric stretch (Fermi resonance) (CH_3-FR)	2926-30	2931	2935-37
r^-	Methyl asymmetric stretch (CH_2-AS)	2955-60	2952-62	2964

* bulk results are the range observed in IR and Raman spectra of C_{11} to C_{16} alkanes .

Both CH_2 and CH_3 groups have three distinct vibrational features. The symmetric stretching modes (Figure 2.12) are split either by a Fermi resonance interaction with either an overtone of a symmetric bending mode of the methyl group or a deformation mode overtone of the methylene group. The result is two features in the C-H region: a low energy frequency component labeled as X^+ (d^+ or r^+) and a high energy frequency component labeled as X^+_{FR} (d^+_{FR} or r^+_{FR}). The third frequency is the asymmetric stretch (d^- or r^-) for both functional groups. In addition, the r^- mode consists of in-plane and out-of-plane components (Figure 2.12). The spectra presented in this work do not resolve the individual components of this feature and treat this feature as a single band for two reasons. First, separation of these features is usually observed at low temperatures.[115] Second, the r^- feature is mostly observed only in spectra acquired under SPS polarization conditions where SF signal level is usually very low.

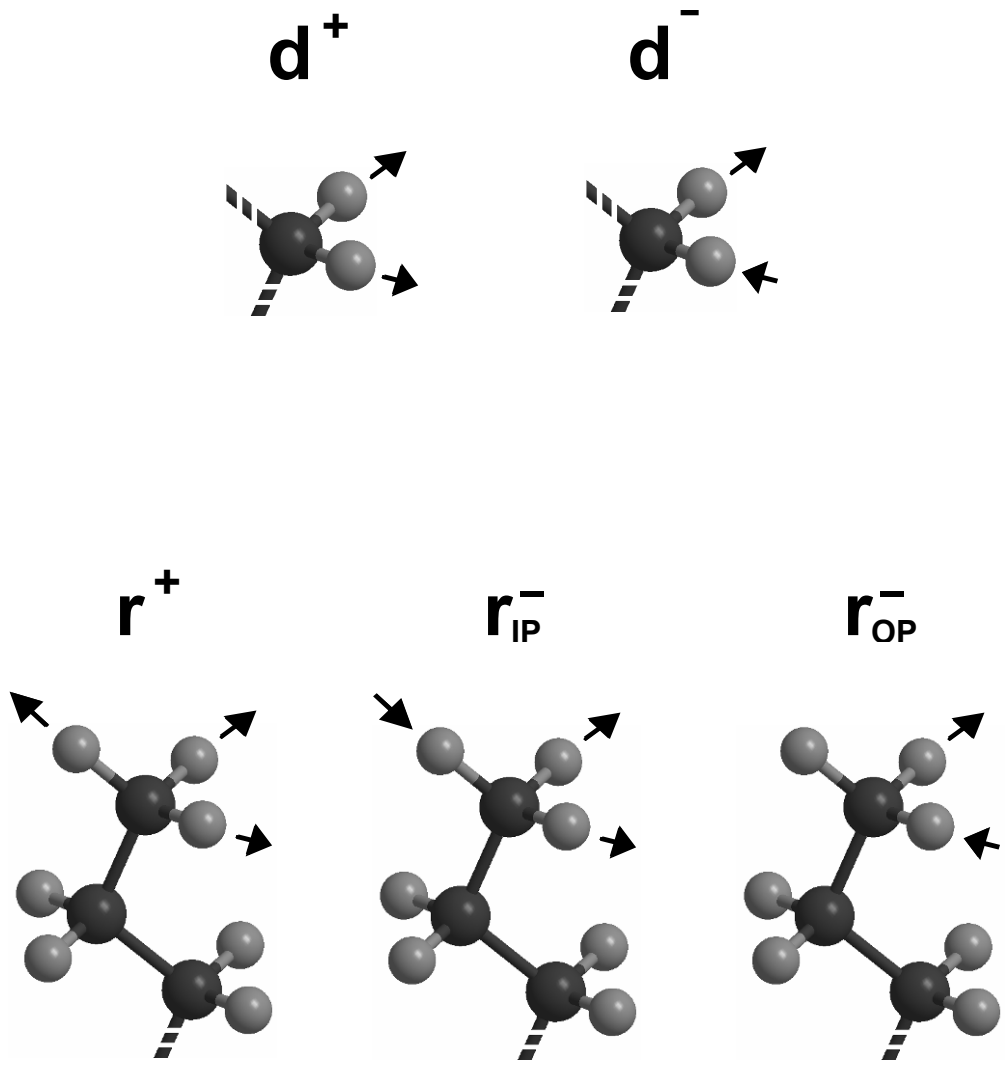

Figure 2.12. Schematic representation of methylene and methyl stretching modes. Arrows indicates the internal displacement vectors of each vibrational mode. d and r refer to the methylene and methyl modes, respectively. + and – refer to symmetric and asymmetric modes. IP = in-plane, OP = out-of-plane.

2.1.3. Surface vibrational spectrum

The SF spectrum of a typical surface acquired under SSP polarization conditions (Figure 2.13) consists of two main regions: a low energy region (below 2900 cm^{-1}) and a high energy region (above 2900 cm^{-1}). The low energy region consists of two symmetric stretch modes, d^+ and r^+, and is fitted usually with two corresponding functions. In the case of unsuccessful attempts to fit with two functions, a multi-component fitting including vibrational phases is considered. The high energy region is fit with up to four functions corresponding to d^+_{FR}, d^-, r^+_{FR}, and

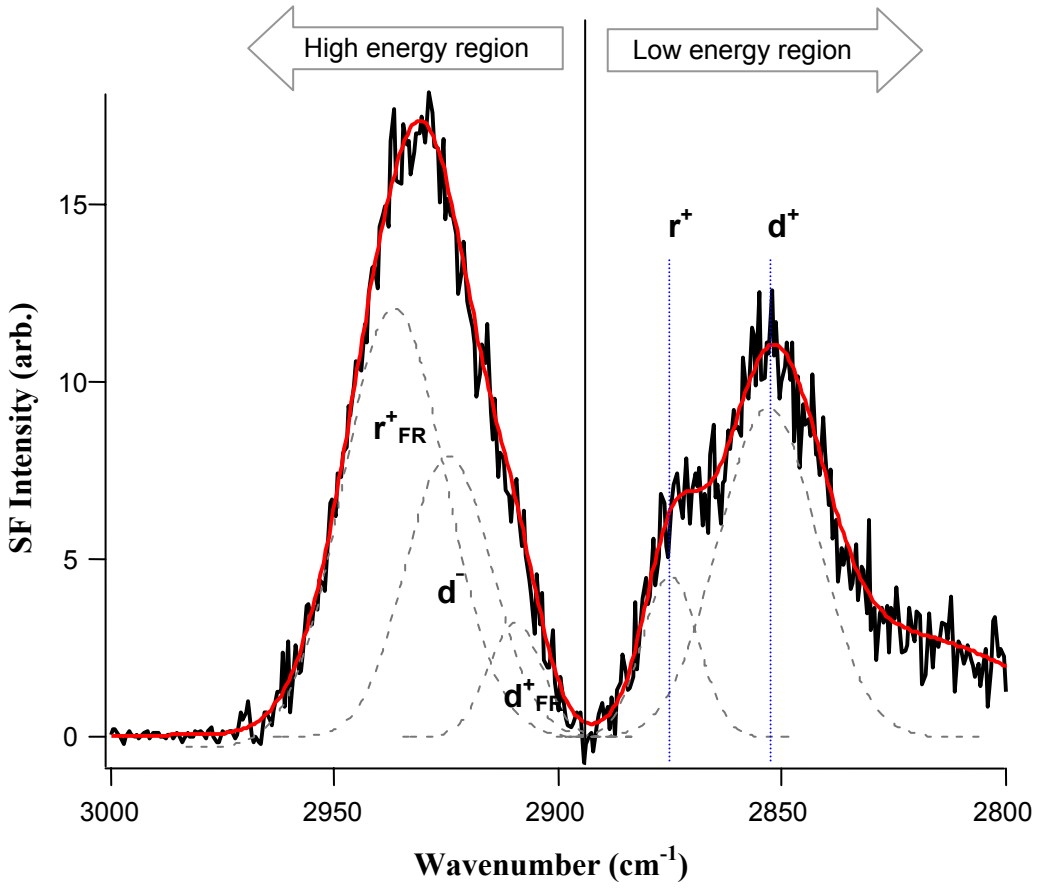

Figure 2.13. Surface vibrational spectrum of hexadecane acquired under SSP polarization condition.

r^- bands. Due to the closeness in their center frequencies (Table 2.7), the results are difficult to interpret quantitatively. Therefore, most of the comparisons of the surface vibrational structure rely on the low energy region rather than high energy region.

2.1.4. Spectra analysis

Although we have a broad infrared beam (80 cm^{-1} FWHM) compared to many infrared sources, the beam is not broad enough to cover the entire region of interest. Due to instrumental limitations, the bandwidth of the infrared beam cannot be extended beyond ~100 cm^{-1} (FWHM). In addition, the infrared beam has a Gaussian power distribution according to nonresonant SF response from a clean gold surface. Therefore observed spectra not only depend on the center position of the broad infrared beam but also the power profile that can selectively amplify the vibrational modes that fall in different parts of the infrared bandwith (Figure 2.14A). This artifact has been eliminated by successive advancement of the center wavelength of the infrared beam such that it provides a constant infrared power within the region of interest when they are summed. Once the spectrum for each infrared center wavelength is collected, then all of the spectra are summed to form surface vibrational spectrum (Figure 2.14B). Then the data are smoothed with 5 cm^{-1} resolution. Since the spectral resolution of the instrument is 8 cm^{-1}, smoothening does not lose any information. Without this acquisition processing it would not be reasonable to compare the relative intensities of observed two (or more) features in the spectrum. Therefore every spectrum shown in this thesis is at least sum of seven spectra collected between 2700 to 3090 cm^{-1} to achieve a constant infrared power between 2800 and 3000 cm^{-1}. Although the effects have not been observed, we do

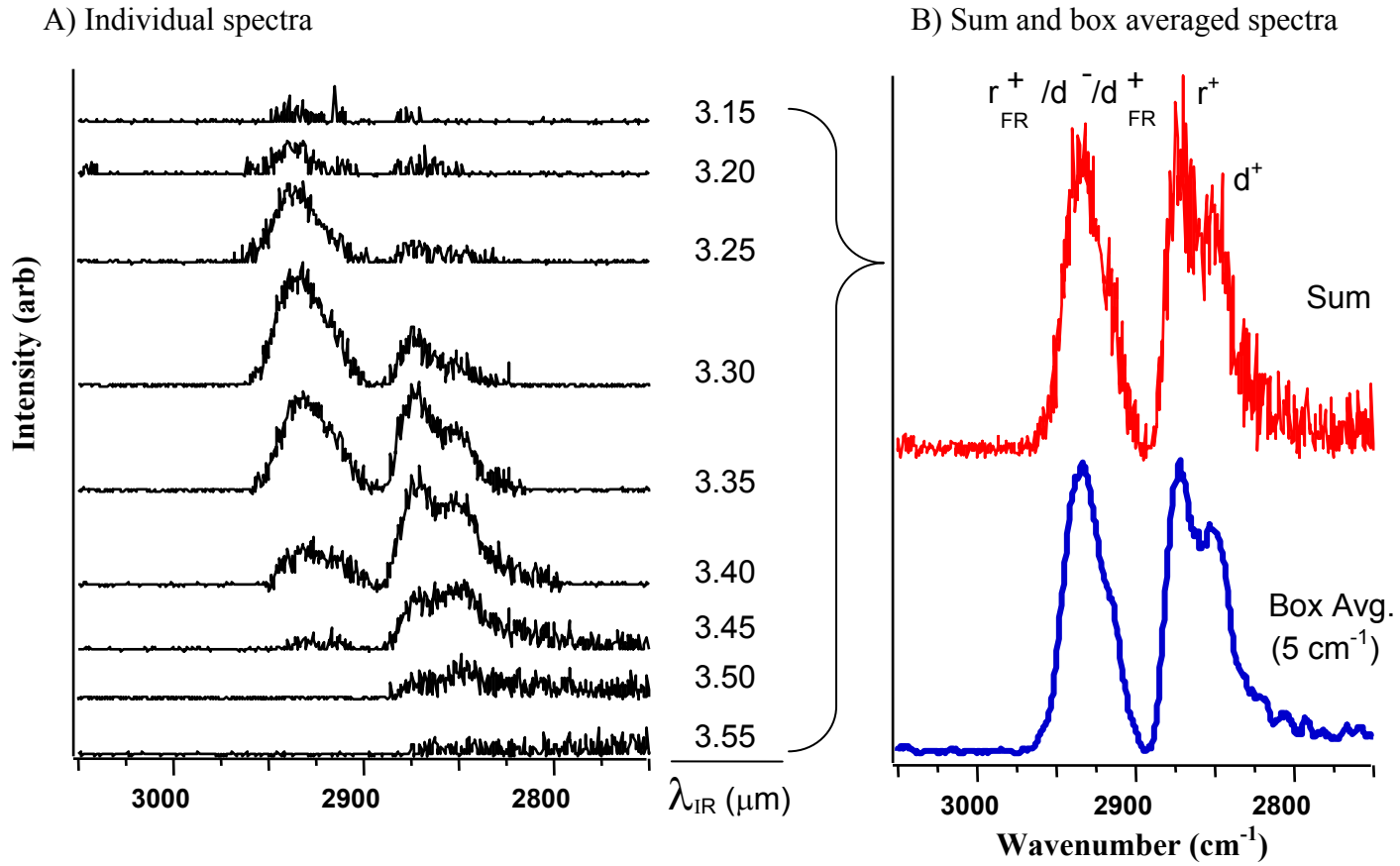

Figure 2.14. A) SF spectra of decane are shown for every λ_{ir}. B) Surface spectra (red) of decane and box averaged spectrum (blue). Once SF spectrum for each infrared wavelength is acquired, all data are summed with respect to wavenumber to form surface spectrum (red). Then the spectrum is smoothed with 5 cm^{-1}. Since spectral resolution of the system is 8 cm^{-1}, smoothening does not loose any information.

recognize the possible influence of the infrared power decay as the center wavelength advances toward lower IR energies.

Once the individual spectra are collected by the spectrometer, all of the data processing is done by Igor routines (Appendix A). The routines read individual spectral data and filters possible cosmic rays by identifying sharp raises (one or two pixel) with respect to nearest neighbors. Then the routines sum all the data pixel-by-pixel and form the sum frequency spectrum. Finally, the routines box average and plot both sum and boxed averaged spectra for visual comparison. Throughout this thesis boxed averaged spectra will be referred as surface vibrational spectra.

Once the surface vibrational spectrum is created, the spectrum is then fitted with a function having multi components where each component corresponds to a possible vibrational band that is given in Table 2.1. If the fit does not reproduce the spectrum, then other possibilities are considered such as destructive or constructive interferences of vibrational features. Since the choice of interference parameters are highly arbitrary, it is used as a last resource and spectrum usually will have signs suggesting interferences. These signs can be either an asymmetric band shape for a feature centered on a vibrational frequency of the molecule or wide bandwidth values (> 25 cm^{-1}) for the feature considered. The high energy feature in surface vibrational spectrum of hexadecane (open red circles, Figure 2.15) is an example of both cases. The high energy feature has a maximum intensity at ~2930 cm^{-1} which is in between the reported methylene asymmetric stretch (2925 cm^{-1}) and methyl Fermi resonance (2935 cm^{-1}). The feature shows a constructive interference for all three features namely, d^{+}_{FR}, d^{-}, r^{+}_{FR}, as shown in the Figure 2.15. In addition, it has a bandwidth of

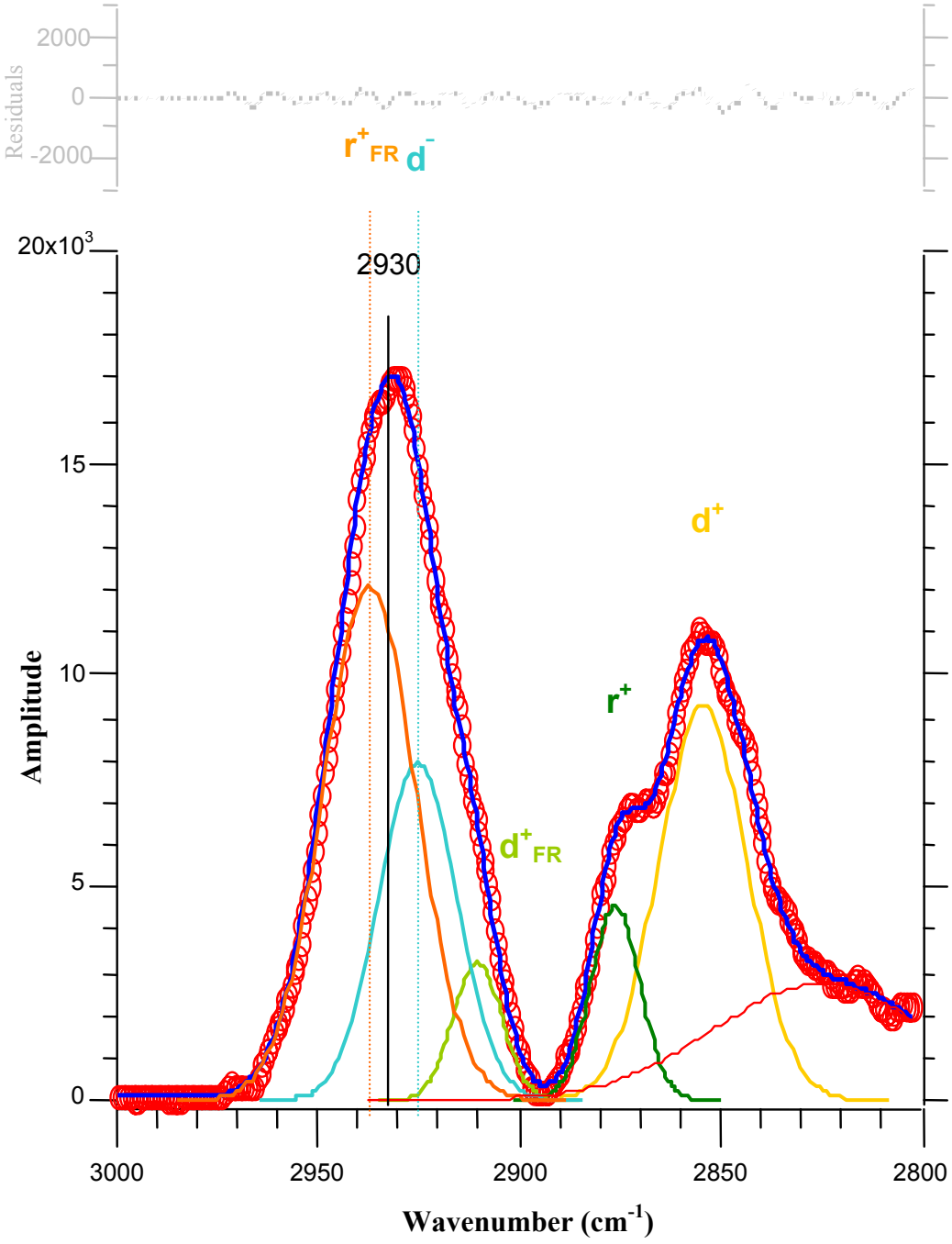

Figure 2.15. Surface vibrational spectra of hexadecane (red circles). The spectra also shows fitted individual functions (gold d^+, green r^+, lime d^+_{FR}, aqua d^-, orange r^+_{FR}) as well as the resulted fit spectrum (blue).

~35 cm^{-1} that is much broader than single vibrational band. The surface vibrational studies showed that a bandwidth corresponding to a single vibrational feature is ~15 cm^{-1} such as the bandwidth (~16 cm^{-1}) of the d^+ band in the SSP spectrum of 1-chlorohexadecane. Our studies showed that a feature can be broaden up to ~25 cm^{-1} (i.e bandwidth of hexadecane d^+ band shown in Figure 2.15) due to environmental effects such as different sampling environments for corresponding vibrational modes. Broader features (than 25 cm^{-1}) suggest constructive or destructive interferences. If the feature has an asymmetric band shape, then first constructive interference possibility is examined for reproducing the surface vibrational spectra. In Figure 2.15, the blue line is the fit result formed from individual components interacting constructively. If this trial fails, then destructive interference is considered to reproduce the spectrum. The surface vibrational spectrum of 5-nonane (Figure 2.16) is a nice example for such a case. Figure 2.16 shows the surface vibrational spectrum, fit spectrum, and r^+ fit functions. The r^+ band (~2875 cm^{-1}) has a band shape with a bandwidth of more than 30 cm^{-1} that looks like slightly flattened from the top. The band shape suggests possible constructive or destructive interferences. Since the r^+ and d^+ features are 25 cm^{-1} apart, it is unlikely that the d^+ modes either constructively or destructively interfere to cause such a band shape, especially when there is comparably weak d^+ intensity. In addition when the center frequencies of the destructively interfering species are not same, the result is a highly asymmetric, narrow band shape with a sharp decline on one side of the band. The next possible feature that might interfere is the d^+_{FR}, which usually has a center frequency at ~ 2905 cm^{-1}, which is even further away from the r^+ band than d^+ band. The only possibility

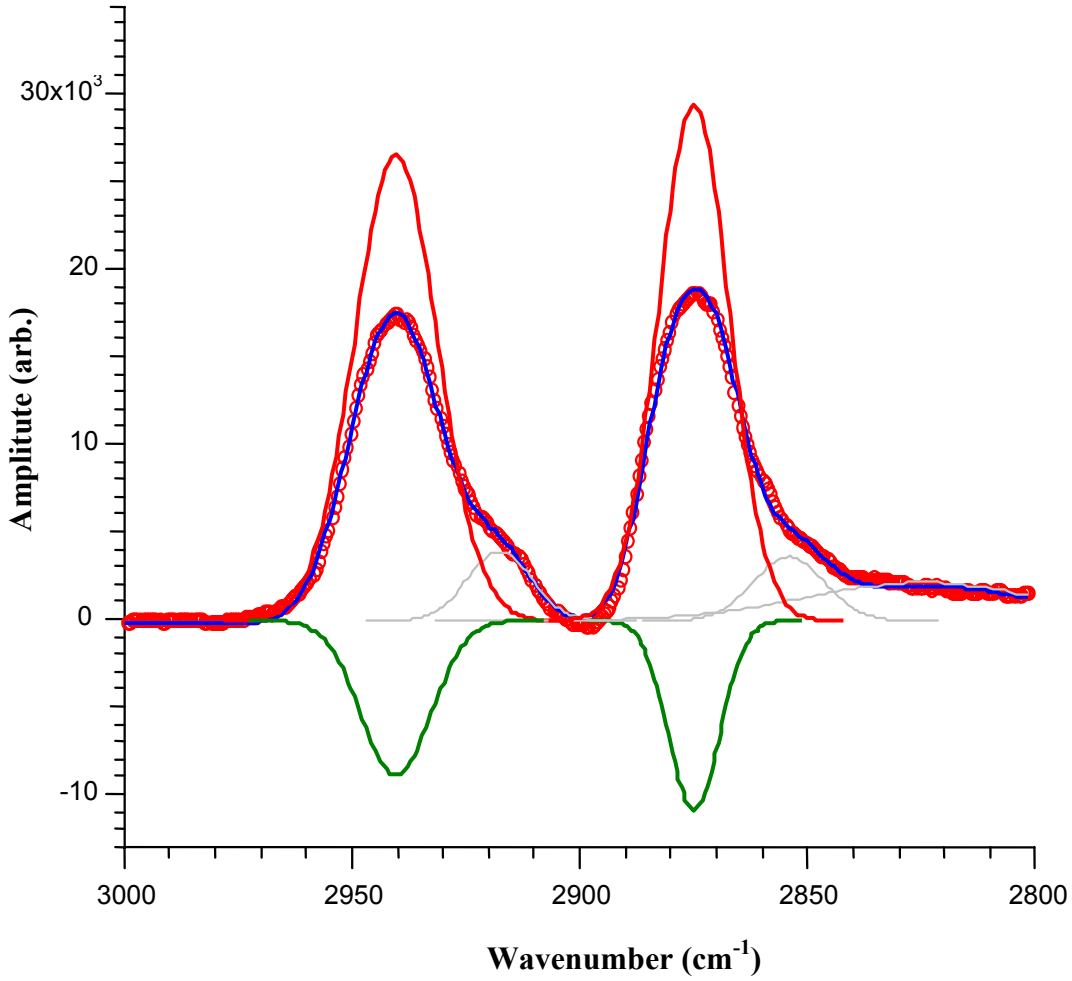

Figure 2.16. Surface vibrational spectra of 5-nonane (red circles). The spectra also shows the multi-component fit function(blue)and destructively interfering r^+ modes in red and green. The other components (d^+, and d^-/d^+_{FR}) are shown in grey.

left is the destructive interference of the r^+ modes having opposite phases, resulting from opposing methyl groups. From the molecular structure, we know that there are two methyl groups that can contribute to the spectrum. The groups are positioned at the opposite end of the molecule thereby increasing possibility of a destructive interference. Using an out of phase contribution we have successfully fit the spectrum including the methyl symmetric stretch region. The results are shown in Figure 2.16 as positive and negative intensities for the destructively interfering features. With the addition of new components to the fit function, three new parameters (center

frequency, bandwidth, and intensity) for each additional band are introduced that increases the parameterization of the fit function, thus ease of the fitting process. Thus, one must have to take special care on fitting process and should not apply such a fitting unless there is a reason. Otherwise, it is very dangerous and, perhaps misleading.

2.2. Samples

The alkanes used in these studies are obtained from the Sigma-Aldrich Chemical Co., and properties are listed in Table 2.8 along with catalog numbers and purities. Since the reported impurities are similar size alkanes, the samples were used without further purification. The experiments were carried out in room temperature ($23 \pm 1\ ^{o}C$), well above the bulk melting point of the alkanes.

Table 2.8. Some properties of the samples used during this work. Surface tension measurements are carried out in our lab except for decalines and consistent with the reported results in references [116,117].

Name	Molecular Formula	Weight (g/mol)	mp/bp (^{o}C)	d (g/ml)	ε^{116}	n^{116}	γ (mN/m)	Purity (%)	Source	Cat. Number
Nonane	C_9H_{20}	128.3	-53/151	0.718	1.97	1.405	22.7±0.1	99+	Aldrich	N2987-1
Decane	$C_{10}H_{22}$	142.3	-30/174	0.73	1.98	1.410	23.7±0.1	99.5	Aldrich	D90-1
Undecane	$C_{11}H_{24}$	156.3	-26/196	0.74	2.00	1.417	24.5±0.1	99+	Aldrich	U407
Dodecane	$C_{12}H_{26}$	170.34	-9.6/215-7	0.749	2.01	1.422	25.2±0.1	99+	Aldrich	D221104
Tridecane	$C_{13}H_{28}$	184.4	-5.5/235	0.755	2.02	1.426	25.8±0.1	99	Sigma	T4508
Tetradecane	$C_{14}H_{30}$	198.4	5.5/252-254	0.763	2.03	1.429	26.4±0.1	99.2	Aldrich	172456
Pentadecane	$C_{15}H_{32}$	212.4	9.9/268-70	0.769	2.04	1.432	27.0±0.1	99+	Aldrich	P3406
Hexadecane	$C_{16}H_{34}$	226.4	18/287	0.773	2.05	1.434	27.2±0.1	99+	Aldrich	H6703
1-Chlorodecane	$C_{10}H_{21}Cl$	176.7	-34/223	0.868	4.58	1.436	28.7±0.1	98	Aldrich	C32909
1-Chlorotetradecane	$C_{14}H_{29}Cl$	232.8	/140(4 mm)	0.865	-	1.446	30.4±0.1	98.6	Aldrich	252239
1-Chlorohexadecane	$C_{16}H_{33}Cl$	260.9	8/149(1mm)	0.865	3.68	1.451	31.0±0.1	98.6	Aldrich	245623
1-Bromodecane	$C_{10}H_{21}Br$	221.2	-30/238	1.066	4.14	1.456	29.6±0.1	98.6	Aldrich	145785
1-Bromotetradecane	$C_{14}H_{29}Br$	277.3	5-7/181	0.932	3.84	1.461	31.3±0.1	98.8	Aldrich	195332
1-Bromohexadecane	$C_{16}H_{33}Br$	305.3	17.3/190	0.999	3.76	1.461	31.8±0.1	99.4	Aldrich	234451
1-Nonanol	$C_9H_{19}OH$	144.26	-6/214	0.828	8.83	1.434	25.1±0.1	98	Aldrich	131210
3-Nonanol	$C_9H_{19}OH$	144.26	-/192	0.824	4.49	1.429	-	95	Aldrich	74295
5-Nonanol	$C_9H_{19}OH$	144.26	-/195	0.821	3.54	1.429	-	95	Aldrich	74308
1-Nonanone	$C_9H_{18}O$	-	-	-	-	1.427	24.2±0.1	-	Aldrich	-
3-Nonanone	$C_9H_{18}O$	142.24	-/187-8	0.821	-	1.421	24.5±0.1	98	Aldrich	259519
5-Nonanone	$C_9H_{18}O$	142.24	-6/185-7	0.821	-	1.420	26.3±0.1	98	Aldrich	136948
Heptamethylnonane		226.9	-/240	0.793	2.05	1.439	24.0±0.1	98	Aldrich	128511
Cis-Decahydronaphthalene		138.25	-43/192-4	0.896	2.22	1.481	31.6[117]	99	Aldrich	110469
Trans-decahydronaphthalene		138.3	-32/186-88	0.87	2.18	1.470	42.92[116]	99	Aldrich	110477
Dimethylsulfoxide(DMSO)	C_2H_6SO	78.13	-	-	47.24	-	-	-	Fisher	D128

Chapter 3

Alkanes

Alkane terminated surface structure influences every aspect of daily life from linens (polymers) to household cleaning to the membranes that define cells in our body. In each instance, the properties of these alkane structures are of considerable interest because structure often correlates closely with the function. To understand interfacial processes that occur on an alkane surface one needs to identify the structure of these surfaces. Recent studies carried out in our group and in other groups have shown that even small changes in molecular structure may lead to big changes in alkane surface structure and interfacial properties,[6,7,118,119] although the bulk properties of liquid alkanes are very similar. Bulk properties such as density, dielectric constant, and interfacial tension of the alkanes have been studied extensively,[8-12,14] however, surface properties of these simple liquids remain poorly understood. Numerous surface studies of alkanes using various methods like surface IR such as PMIRRAS, scattering techniques such as X-ray and neutron scattering and nonlinear optical techniques such as SFG have probed different properties of alkane interfaces.[3,4,19,20,120-124] The majority of the studies have investigated how the surface of a particular system changes with environmental factors (such as temperature) rather than systematically investigate how surface structure depends on molecular structure. For example, the bulk properties of decane and hexadecane are similar. What about their surface properties? How does a change in chain length affect surface structure and order? With studies outlined in Chapter 1 we have begun to address

such questions and increase our knowledge about surface structure correlation with molecular structure. Chapters 3, 4, and 5 present the results and analysis of vibrational spectra for groups of molecules that are related by either molecular structure or by the types of intermolecular interactions. The goal is to understand how shape and forces control the structure of liquid surfaces.

In this chapter we present the results from vibrational studies of medium length alkane systems in order to address the effect of chain length on the alkane surface structure. The carbon length ranges from nine atoms to seventeen atoms and all are liquids at room temperature. The lower and upper limits of chain lengths studied are determined by the experimental constraints. The lower limit is determined by the vapor pressure of the liquids when it becomes too high. The liquid evaporates too quickly and we can not acquire an equilibrium vibrational spectrum of the surface. The upper limit of the liquids is determined by the melting point of the molecules where heptadecane (17 carbon atoms) is the longest linear alkane that is a liquid at room temperature. Once the experimental sample stage is redesigned to accommodate temperature dependent studies, it may be possible to acquire the vibrational spectra of shorter and longer chains and compare to the spectra of systems reported in this thesis. However, our studies of simple liquid alkanes have already led to results that force us to rethink picture of liquid alkane surface structure developed from X-ray scattering and molecular dynamic simulations.

In addition to linear alkanes one sample study is performed on surface of a highly branched alkane, heptamethylnonane, and the results are compared with its

linear isomer, hexadecane. An additional study compares surface structure of two 10 carbon fused ring isomers.

3.1. Chain length dependence of linear alkanes

The molecular structures of the studied linear alkanes are shown in Figure 3.1. These molecules consist of only CH_2 and CH_3 groups. Again, the only difference between these linear alkanes is the chain length. Selected properties such as density, refractive index, melting and boiling points as well as surface tension and purity are given in Table 2.8.

Figure 3.2 shows the collection of surface vibrational spectra of nine consecutive linear alkanes starting with nonane and finishing with heptadecane. The spectra are acquired under SSP polarization conditions. The three letter combination of polarizations refers to the polarizations of the sum frequency (SF), visible, and infrared fields, respectively. This combination of polarizations samples only those vibrational modes that have their infrared transition moments aligned perpendicular to the surface. Features fall into two regions of the spectra. The low energy region (below 2900 cm^{-1}) contains information of symmetric stretch modes as presented in Chapter 2. Therefore, the region is fitted with two functions corresponding to a methylene symmetric stretch (CH_2-SS, d^+, 2852 ± 2 cm^{-1}) and a methyl symmetric stretch (CH_3-SS, r^+, 2876 ± 1 cm^{-1}). The high energy region is fitted with up to four corresponding to a methylene Fermi resonance (CH_2-FR, d^+_{FR}, 2907 ± 3 cm^{-1}), a methylene asymmetric stretch (CH_2-AS, d^-, 2923 ± 2 cm^{-1}), a methyl Fermi resonance (CH_3-FR, r^+_{FR}, 2937 ± 3 cm^{-1} cm^{-1}), and a methyl asymmetric stretch (CH_3-AS, r^-, 2962 ± 3 cm^{-1}). However, due to very low intensity in the r^- band region, the

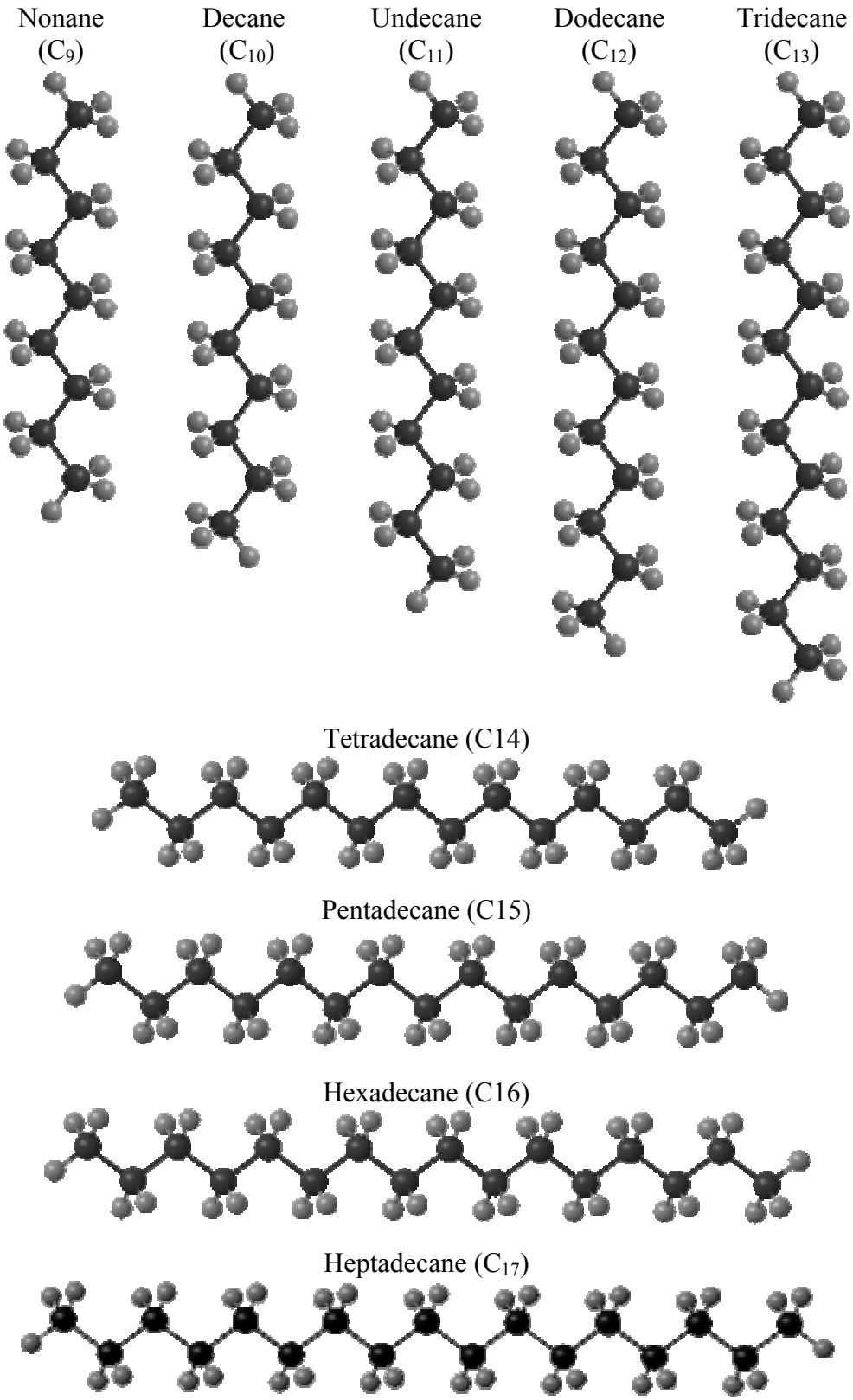

Figure 3.1. Molecular structures of the alkanes

r^- band is dropped from the fitting routine. All these assignments are based on the previous infrared, Raman, and SF studies of alkyl structures. [11,14,19,34,50,58,59,72,73,110-114]

The surface vibrational spectra of these alkanes acquired under SPS polarization conditions are shown in Figure 3.3. This polarization combination samples only those modes that have infrared transition moments aligned in the plane of the surface. The spectra also have two regions. The higher region is dominated by a feature around ~2960 cm^{-1} and the other is around 2900 cm^{-1}. The former is associated with the r^- mode since its center frequency is reported at ~2960 cm^{-1} (Table 2.7). The latter is comparably broader and usually lower in intensity. It is usually assigned to d^+_{FR} combination but the reported basis for this assignment is always very vague. Due to low signal level and broadness of the feature it has not been fit to the functions. Vibrational sum frequency spectroscopy is very sensitive to molecular geometry and samples average orientations of molecules at the interface (equations 1.13 and 2.3). Therefore, comparisons of the features observed in SSP and SPS spectra of these liquid surfaces can be used to infer the orientation of the functional groups and, consequently, the average molecular conformation and relative order of the structures. Specifically, the ratio of r^+/d^+ intensities is used frequently as a measure of conformational order at surfaces containing alkyl chains. For example, *n*-decane in its *all-trans* conformation possesses inversion symmetry along the carbon chain meaning that the r^+ and d^+ modes are SF inactive. In principle the r^+ and d^+ modes can contribute to a SF spectrum only when this inversion symmetry is broken by gauche defects along the chain or when the two ends of the molecule are subjected to different forces. Thus, larger r^+/d^+ ratios are associated with higher order and

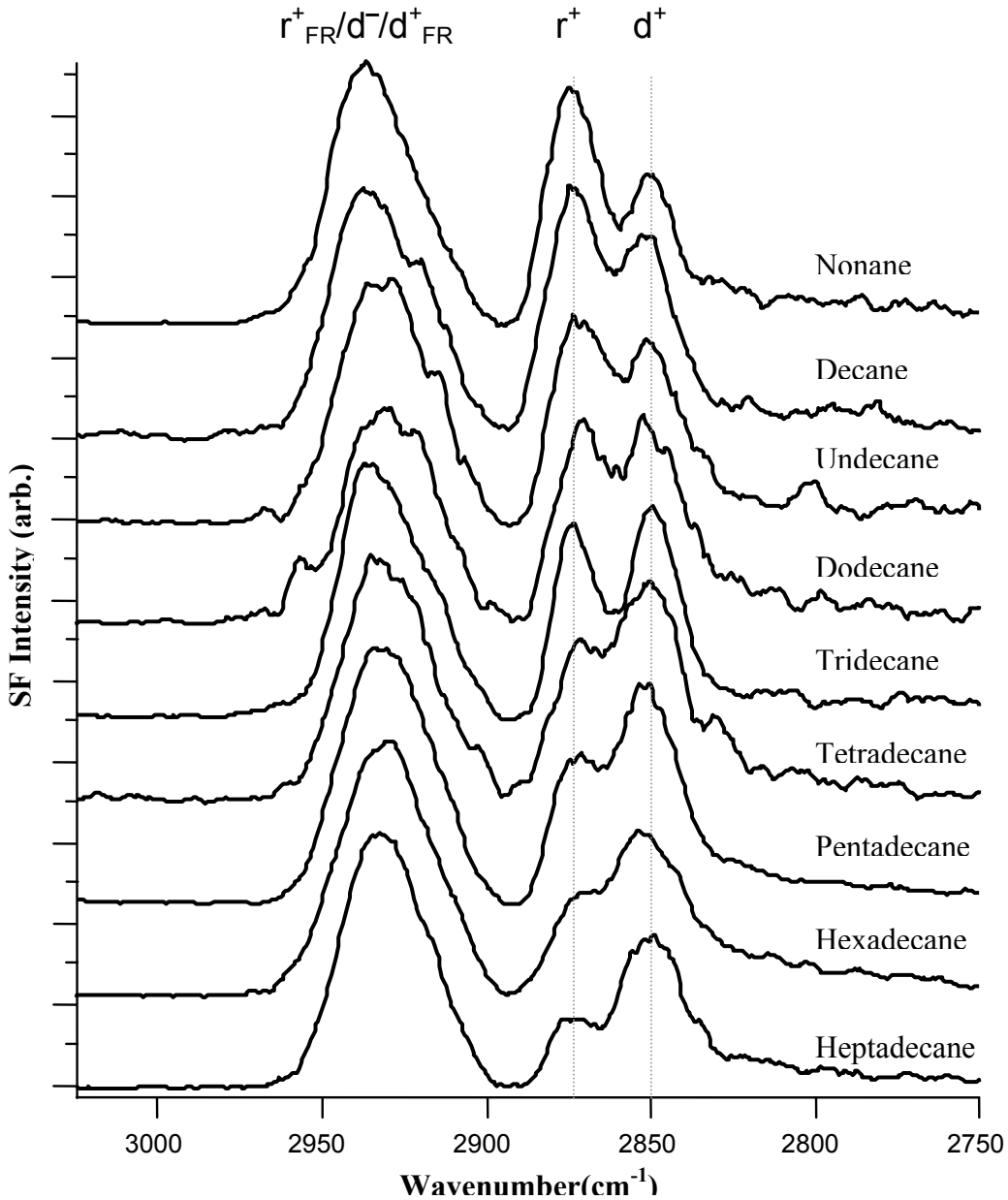

Figure 3.2. SSP spectra of alkanes with increasing chain length from top to bottom.

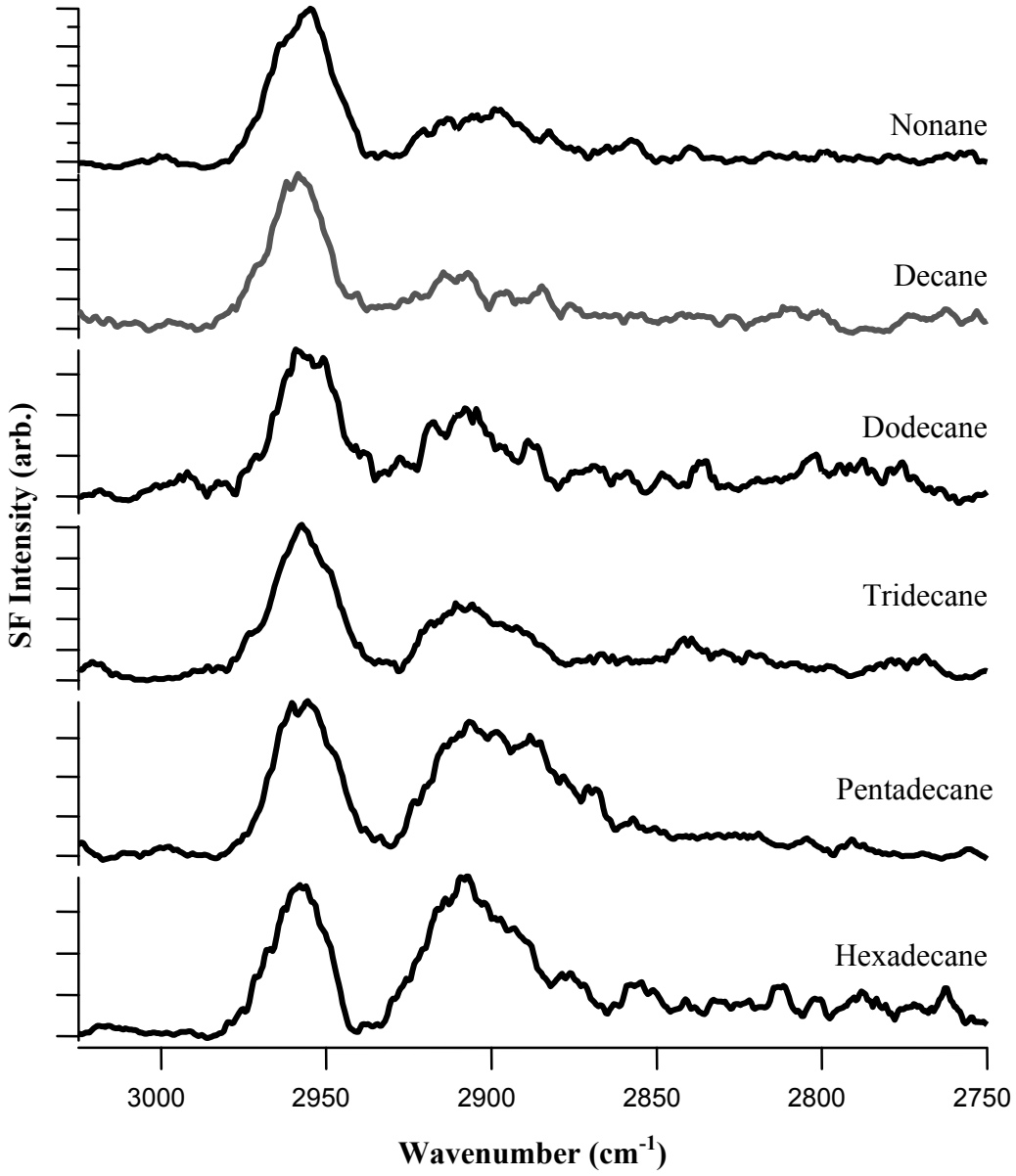

Figure 3.3. SPS spectra of selected alkanes.

smaller r^+/d^+ ratios are associated with lower order. The r^+/d^+ ratio calculated from SF spectra of the alkane liquid/vapor interface are listed in Table 3.1. The procedure of fitting these bands is described in Chapter 2, section 1.4.

Table 3.1. r^+/d^+ values for alkanes. The ratio is calculated by the area of the bands resulted from the fitting.

Molecule	**r^+/d^+**
Nonane (C_9)	1.40 ±0.25
Decane (C_{10})	1.04 ±0.42
Undecane (C_{11})	0.81 ±0.11
Dodecane (C_{12})	0.78 ±0.04
Tridecane (C_{13})	0.68 ±0.03
Tetradecane (C_{14})	0.45 ±0.04
Pentadecane (C_{15})	0.47 ±0.01
Hexadecane (C_{16})	0.31 ±0.03
Heptadecane (C_{17})	0.35 ±0.09

Before comparing the surface vibrational spectra of the alkanes, one should consider previous studies of similar systems and the models currently used to describe alkane surface structure. There are very few neat liquid/vapor alkane system studies because of the difficulties associated with such a system. One of the biggest challenges is finding a suitable technique to study systems lacking strong intermolecular interactions. In general, surface studies rely on the surface scattering techniques such as X-ray and neutron scattering that require a clear difference between the surface and the bulk for analysis. Due to its inherent surface specificity

SFG is a very suitable technique for systems with low order and can reveal properties of a surface that go undetected by scattering techniques. For example, X-ray scattering studies of the room temperature hexadecane liquid/vapor interface carried out by Ocko and coworkers show no diffraction patterns, leading them to conclude that at room temperature this surface possesses no order and interfacial structure is very similar to the bulk solution.[3] In contrast, vibrational sum frequency spectra of hexadecane acquired at room temperature by both our group and Shen's group[19] show a very pronounced feature assigned to a methyl symmetric stretch. With fourteen methylene groups and only two methyl groups, one would not anticipate such a strong methyl response *unless* existed surface structure having a non-statistical number of methyl groups aligned perpendicular to the interfacial plane. This apparent discrepancy between X-ray and vibrational data simply reflects differences in the properties probed by the two techniques. Long chain alkanes *can* posess surface structure (e.g. methyl groups oriented towards the vapor phase) without having any long-range order (e.g. beneath the terminal methyl groups, the solvent structure is randomized).

In general, the alkane surface studies are limited to long chain alkane/vapor interfaces.[3,4,121,124] Phase transitions studies of alkane ranging in chain length from 16 to 50 carbon atoms show unusual behavior known as surface freezing.[3] Surface freezing happens when a monolayer of the alkane freezes before the bulk solution freezes. The frozen alkane layer is reported to be a highly ordered film extending for 1 molecular layer with no or very few gauche defects. The molecular orientation is reported as perpendicular to the surface plane. The overall structure is a rotator II

phase. The range of temperatures where observed surface freezing depends on the chain length and shows a maximum of 3 ^{o}C and a minimum of 1 ^{o}C above the bulk freezing point. Surface freezing is not observed for chains having less than 16 carbon atoms or more than ~50 carbon atoms. Clearly, surface freezing is a chain length dependent property. Long chain alcohol studies showed that this property transfers to the systems having strong intermolecular interactions such as linear alcohols. In these strongly associating systems the surface freezing is observed only for chains having even number of carbon atoms of between 16 and 28.[125] Again, this shows that surface freezing is highly correlated with chain length and molecular structure. The depth of the frozen layer above the bulk is reported as two monolayer thickness due to the strong hydrogen bonding interaction between top two adjacent layers.

The surface vibrational spectra of alkanes ranging from nonane to heptadecane acquired under SSP polarization conditions show substantial differences. The nonane spectra contain very significant intensity in CH_3-SS band, resulting an r^+/d^+ ratio of ~1.4. This result is surprising given that the molecular structure has only two methyl groups compared to seven methylene groups (Figure 3.1). This high ratio suggests relatively strong ordering at the interface. The maximum intensity of the high energy feature in the nonane spectrum is at ~2935 cm^{-1} implying a strong contribution from r^+_{FR} (2937 cm^{-1}) to the feature than the d^- mode. This is expected given the observed strong intensity of the r^+ band. The strong and narrow r^+ band also implies a net perpendicular orientation of the methyl groups. A significant r^- band in the SPS spectrum supports the picture. When the CH_3 group is perpendicular to the surface, the transition moment of the r^+ mode is also perpendicular to the surface and

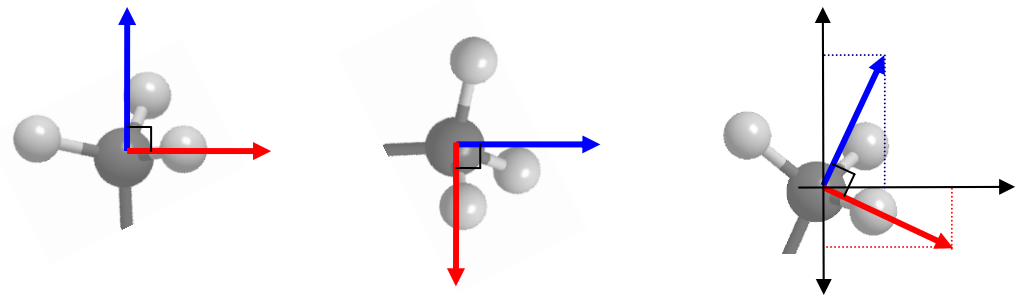

Figure 3.4. Schematic representation of r^+ and r^- transition moments and their projection onto yz plane.

the transition moment of the r^- mode is parallel to the surface (Figure 3.4). Since the SSP polarization condition only samples the modes having net perpendicular projections, the r^- mode would not appear in an SSP spectrum but would appear in an SPS spectrum as observed in the case of nonane. If the methyl group is tilted then both transition moments will have projections in both planes, and both should contribute in both polarization spectra. The same arguments can in principle be made for the d^+ and d^- modes, too. However, there are too many methylene groups complicating such an analysis. The observation of the r^+ band along with the d^+ band in the SSP spectrum and the r^- band in the SPS spectrum also suggests that the molecules at the liquid/vapor interface do contain at least one and probably more gauche defects. Otherwise, the contribution from one methyl group to an r^+ band would interfere destructively with the contribution from the other methyl group, resulting in an asymmetrical or nonexistent r^+ band in the spectrum regardless of the orientation of the molecule. Figure 3.5a illustrates the case for nonane and decane molecules having their carbon backbone structure aligned perpendicular to the surface plane. For both molecules the vector sum of the perpendicular projections of the r^+ mode transition moments cancel each other and, therefore, become SF inactive for

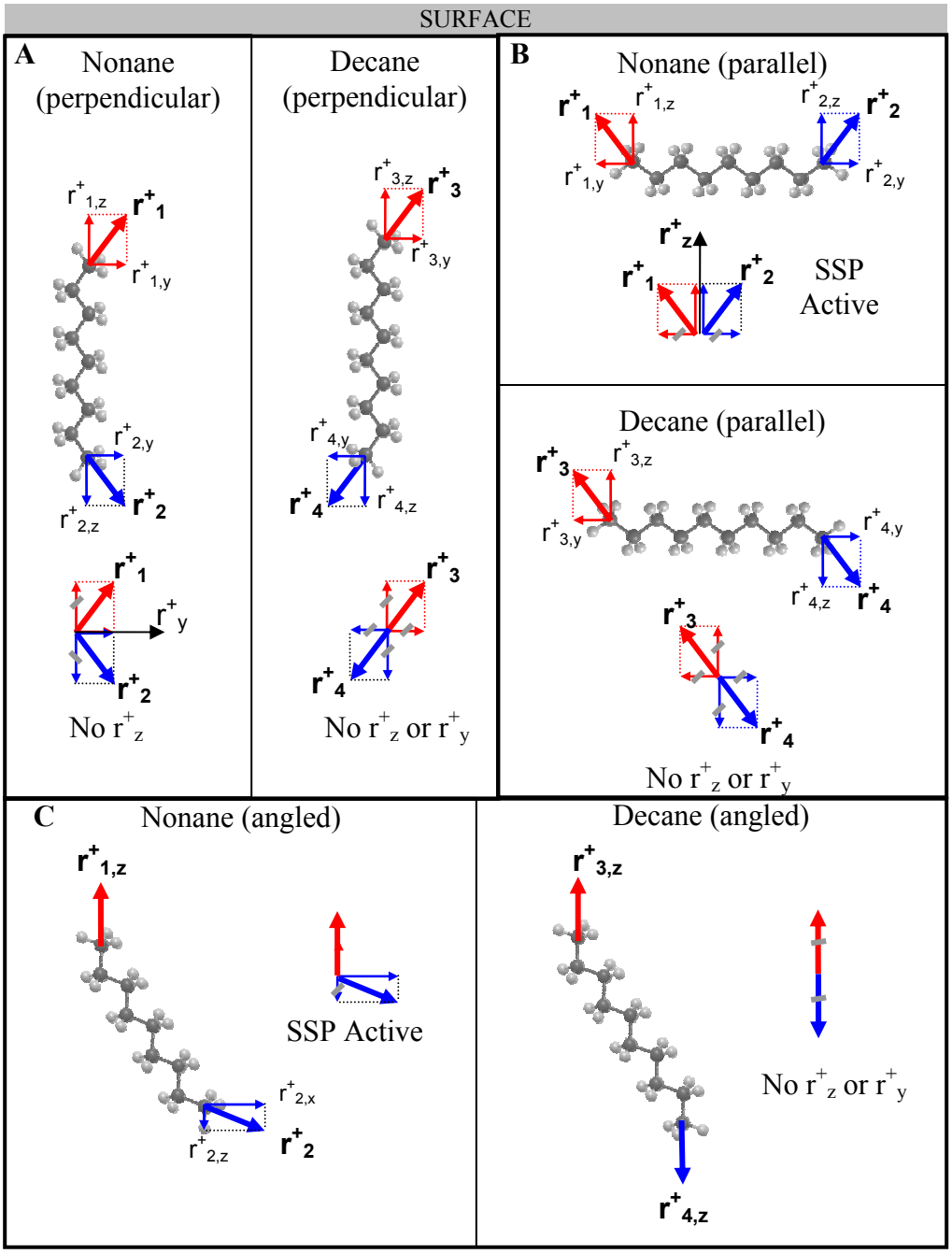

Figure 3.5. Schematic fully stretched nonane and decane r^+ vector sums of both end CH_3 groups for a) perpendicular, b) parallel, and c) angled with respect to surface plane.

SSP polarization. This structure is inconsistent with observed results. Figure 3.5b illustrates the case for the same molecules, this time having a planar orientation at the surface. In this case, the averaged vector sum of the induced polarization results

two different predictions. The perpendicular projections for nonane add up while those for decane cancel suggesting a weak r^+ band in the SSP spectrum of nonane and no band for the corresponding SSP spectrum of decane. In addition, a dynamic surface would introduce rotational freedom around the backbone, resulting in a cancelation of vectors when an ensemble of molecules is considered. Figure 3.5c shows the case of a tilted geometry so that one of the methyl groups is perpendicular to the surface. Although the vector sum of nonane suggests a net component contributing to the r^+ band in SSP spectra, the contribution from one is canceled by the other for decane assuming similar strengths for the transition moment of both end of the molecule. The spectra do not support this geometry either. Therefore, the system must have some gauche defects in order to have a reasonably strong r^+ contribution in SSP spectra (and r^- contribution in SPS spectra) of linear alkanes. The extent of the gauche defects can be determined by the relative intensities of r+ and d+ bands on the SSP spectra of alkanes as discussed earlier.

The surface vibrational spectrum of decane under the SSP polarization combination shows similar features with different intensity distribution. Although the r^+ band intensity is still higher than the d^+ band intensity, the resulting an r^+/d^+ ratio of 1.0 is smaller than the ratio for nonane. Low energy (right) side of the high energy region (> 2900 cm^{-1}) of the spectrum has a definite rise in intensity corresponding to increased contribution of d^- and d^+_{FR} as expected. These trends are followed by undecane. The r^+ band maximum intensity is slightly less than that of d^+ band resulting in an r^+/d^+ ratio of ~0.81. The shoulder on the feature at high energy region becomes more apparent causing the peak position of the feature to shift slightly

toward the d^- band. The r^+ and d^+ bands in surface spectrum of dodecane with same polarization combination show relatively the same intensity maxima, resulting in a band area ratio, r^+/d^+, of ~0.78 due to the broader bandwidth of d^+ band. The high energy feature becomes considerably broader, as expected, with additional intensity gained on CH_2 vibrational modes. The tridecane spectrum is very similar to the dodecane and has better resolution compared to the others. The tridecane surface spectrum follows the trend of relative intensity increase in the d^+ band. The d^+ band becomes slightly higher than the r^+ band resulting in an r^+/d^+ ratio of ~0.68. In between tridecane and tetradecane slightly larger changes occur. The d^+ band intensity becomes much higher than the r^+ band intensity resulting in an r^+/d^+ ratio of ~0.45. The peak center of the high energy feature continues to shift toward the d^- band frequency. The higher intensity of d^+ becomes apparent in the surface spectrum of pentadecane. The ratio of area underlying the r^+ and d^+ band is ~0.47. The ratio is close to that of tetradecane due to a slight increase in the bandwidth of the r^+ band. The features observed in hexadecane and heptadecane surface spectrum follow the trend of changes observed between nonane and pentadecane. The hexadecane SSP spectrum shows slightly lower r^+/d^+ ratio as ~0.31 compared to ~0.35 of heptadecane.

The changes observed in the surface vibrational spectrum of nonane to heptadecane shows a systematic behavior. The r^+/d^+ ratios have been plotted with respect to chain length of the alkanes in Figure 3.6. The change in r^+/d^+ ratio with respect to chain length is certainly not linear. The exponential fitting of the data shows very strong correlation between r^+/d^+ ratio and chain length, but we have not assigned any physical meaning to the exponent and amplitude of the fit function. We

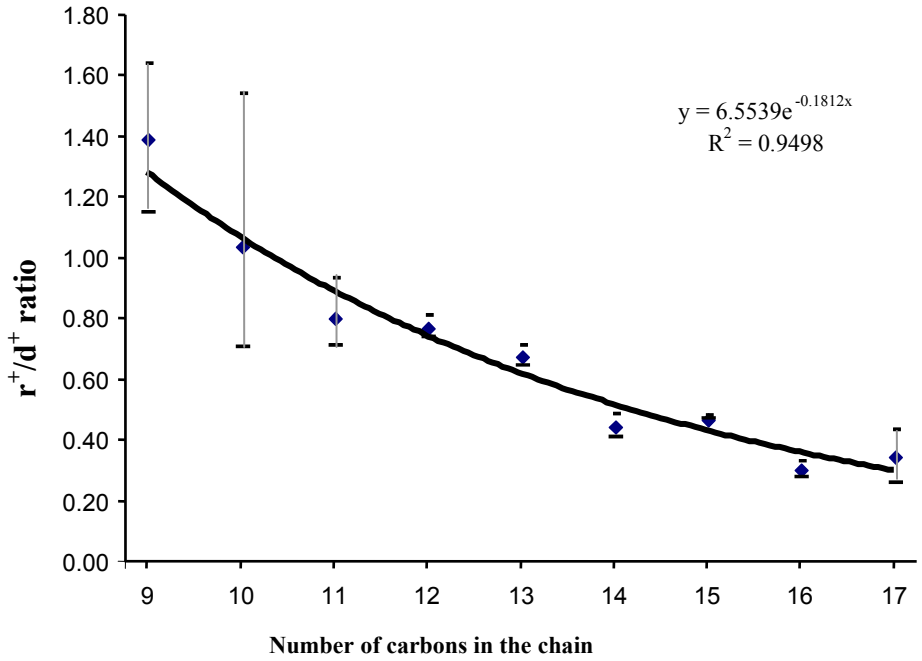

Figure 3.6. plot of r^+/d^+ with respect to chain length.

can say, however that the r^+/d^+ ratio results from the changes in intensities of the r^+ and d^+ bands. The d^+ band can only be observed if the molecule possesses some degree of gauche defects. Therefore, the exponent of the fit function is presumably correlated with the number of gauche defects on the molecules at the interface. With a suggested surface geometry such that the molecules have one methyl group at the surface side and the other oriented randomly toward the bulk solution, only surface methyl groups will contribute to the observed r^+ band intensity. Therefore, the r^+ band intensity is expected to be similar for each of the nine alkanes. The slight decrease in the r^+ band intensity with respect to chain length might occur due to the larger surface area of the longer chain alkanes that creates more free volume for the surface methyl groups to orient. This effect results in a broader angular distribution of the surface

methyl group, causing also slight broadening of the r^+ band with respect to chain length increase as observed.

Although there is a suggestive odd-even effect for the r^+/d^+ ratio with respect to the chain length, due to large error bars on the ratio for shorter chains it is very difficult to make this claim with certainty. For the chain lengths between 13 and 17, there is a clear evidence of oscillating behavior on the r^+/d^+ ratio. The large error bar of the shorter chains is associated with difficulty in reproducing the surface spectrum due to the evaporation of the sample during the data collection. With a sampling stage that reduces the evaporation rate of the sample, we might be able to decrease the error bars on the r^+/d^+ ratio for shorter chain lengths.

In summary, the simple model analysis of the r^+ and r^- contributions to the SSP and SPS spectra suggest a molecular orientation of the alkanes having a net methyl transition moment perpendicular to the surface with a wide distribution of θ, angles between the surface and the line between two ends of the molecules (Figure 3.7). The constraint on the angular distribution is such that the second methyl group that resides toward bulk (bulk CH_3) has an isotropic distribution so that ensemble contribution of bulk CH_3 groups to r^+ cancels each other and they do not contribute to the SSP spectra of the alkanes. This structure assumes a significant amount of gauche defects which can be observed by d^+ band intensity in the SSP spectrum, and consequently by the r^+/d^+ ratio. This assumption is necessary because methylene groups can only contribute to a spectrum when the local inversion symmetry is broken by a gauche defect (Equations 1.18 and 1.19 in Chapter 1). The r^+/d^+ ratio for alkanes ranges from 1.4 of nonane to 0.35 of heptadecane. An exponential decay on

the r^+/d^+ ratio is observed with chain length. The decay is a result of both an increase in gauche defects and an increase in the angular distribution of surface methyl groups as the chain length increases.

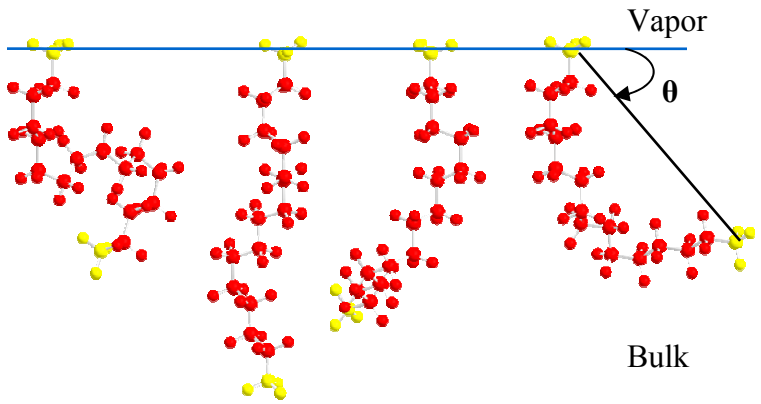

Figure 3.7. Simple representation of angular distribution of the second methyl group positioned toward the bulk. The methyl groups are yellow and methylene groups are red. The angle θ is defined as the angle between the surface plane and the second methyl group.

3.2. Linear versus branched

In addition to linear alkanes we have performed a sample study on a highly branched alkane, heptamethylnonane. The molecule is an isomer of hexadecane (Figure 3.8). The molecule consists of 9 methyl (CH_3), 3 methylene (CH_2) and 1 CH groups, compared to 2 CH_3, 14 CH_2 of hexadecane. Due to the comparably higher number of methyl groups in the heptamethylnonane structure, the surface vibrational spectra for both polarization combinations are expected to be dominated by the CH_3 vibrational bands. The Figure 3.9 shows the vibrational spectra of heptamethylnonane surface under both polarization conditions, SSP and SPS, together with the surface spectra of hexadecane.

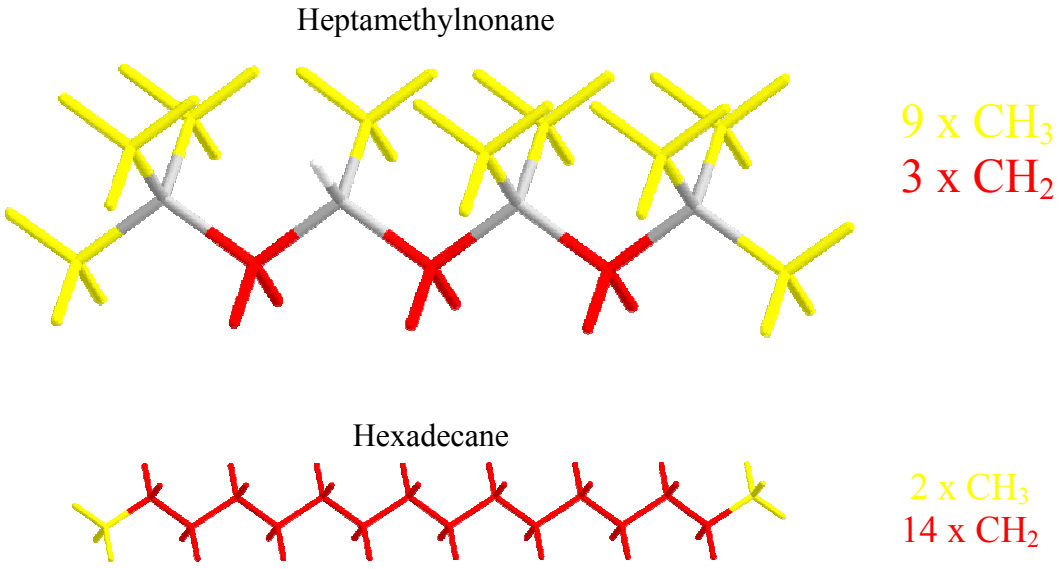

Figure 3.8. Molecular structure of Heptamethylnonane. Hexadecane molecular structure is given for comparison.

As expected, the spectra of heptamethylnonane is very different from that of hexadecane and dominated mainly by the methyl vibrational bands. The SSP spectrum has three features. The first feature is positioned on the low energy side of the spectrum. It is strong, *and* centered at ~2865 cm^{-1} with a full-width-half-maximum (FWHM) of ~25 cm^{-1}. This feature is assigned the methyl symmetric stretch mode (r^{+}) according to the surface vibrational frequencies reported in Table 2.7. The second, middle, feature is also strong. The feature is centered at 2905 cm^{-1} with a FWHM of ~20 cm^{-1} and assigned to the methylene asymmetric stretch (d^{+}). The last feature is comparably lower in intensity but still a reasonably strong feature that is positioned at ~2957 cm^{-1} with a FWHM of ~ 17 cm^{-1}. This high energy feature is assigned to the asymmetric stretch mode (r^{-}) of the methyl groups.

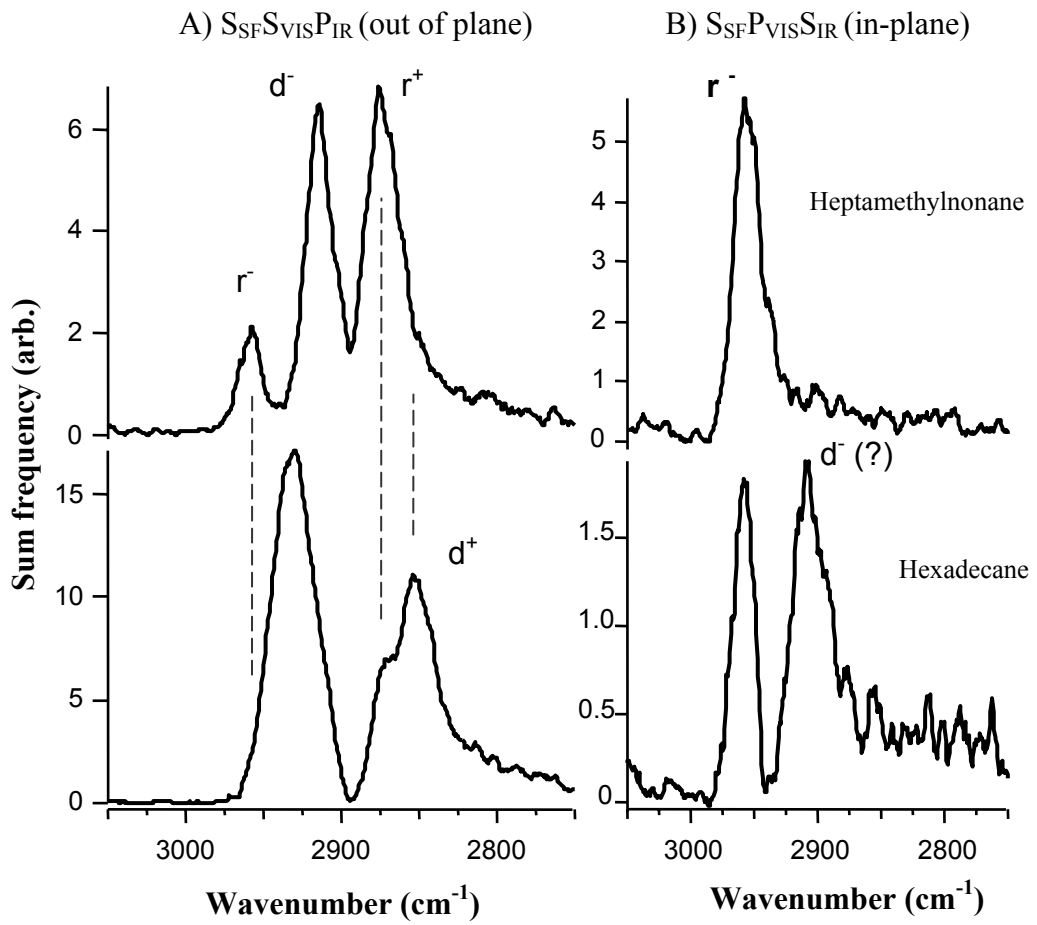

Figure 3.9. Surface vibrational spectra of Heptamethylnonane under both A) SSP and B) SPS polarization condition together with surface vibrational spectra of hexadecane for comparison.

The surface vibrational spectrum of heptamethylnonane under SSP polarization condition (Figure 3.9A) is very different than the SSP spectrum of hexadecane. The first striking difference is the loss of intensity at the d+ band region of the heptamethylnonane spectrum compared to the same region of hexadecane spectrum. This is mainly due to the fewer methylene (3) groups existing in heptamethylnonane compared to methylene groups (14) of hexadecane. The other reason might be the way in which the methylene groups of the heptamethylnonane are oriented at the surface. Since the sum frequency cares about the orientation of the functional groups at the surface, their angular distribution with respect to surface

plane will be very important on their contribution to the sum frequency spectrum. The very low intensity on the d^+ band region suggests that the molecules are oriented themselves such that the CH_2 groups are parallel to the surface plane (Figure 3.10). Another striking difference between the SSP spectra of the heptamethylnonane and hexadecane is the strong appearance of the d^- band on spectrum of heptamethylnonane. The d^- transition moment is perpendicular to the d^+ transition moment. Therefore, if the d^+ moment is aligned parallel to the surface plane then d^- is expected to be perpendicular to the surface and contribute strongly to the SSP spectra as observed. Therefore, the strong and sharp d^- band supports the suggested picture of CH_2 groups having a parallel orientation at the surface (Figure 3.10). The third difference between the SSP spectra of heptamethylnonane and hexadecane is the relatively strong contribution of the r^- band in SSP spectrum of heptamethylnonane. This is due to the high branching of methyl groups by which some of r^- transition moment that is oriented perpendicular to the surface plane thus contributing to the SPS spectrum.

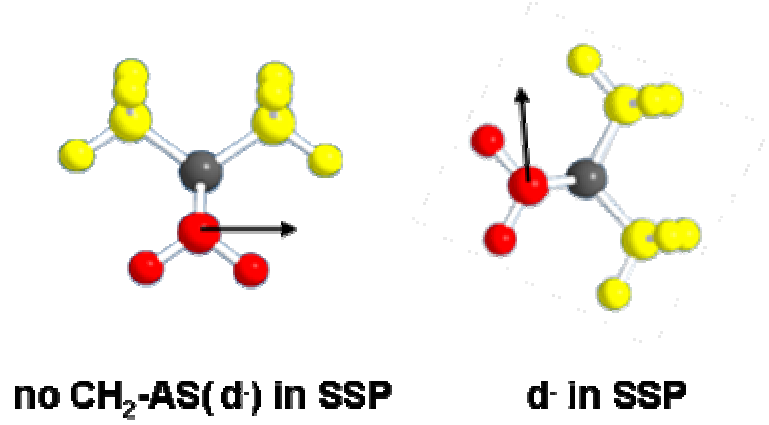

Figure 3.10. Orientational representation of heptamethylnonane (side view).

The r^- band in SPS spectrum (Figure 3.9B) of heptamethylnonane is sharp and strong similar to hexadecane feature. However, a feature around ~2910 cm^{-1}, possibly a d^- band, is missing in the heptamethylnonane spectrum. Comparing the d^- band in SSP and SPS spectra of heptamethylnonane shows that CH_2 groups are not tilted with respect to the surface as suggested.

In summary, the observed features in heptamethylnonane surface vibrational spectra suggest a possible molecular structure that is oriented such that the CH_2 groups are parallel to the surface and CH_3 groups are angled. Observation of r^- band both in SSP and SPS spectra supports the picture. A systematic isotopic labeling of CH_3 groups might enable us to identify the angle of the CH_3 groups with respect to the surface plane.

3.3. Surprising result from a molecule with inversion symmetry

Figure 3.11 shows the surface vibrational spectra and trans- and cis-decahydronaphthalene (decalin) acquired under SSP and SPS polarization conditions. The molecular structures are given in Figure 3.12. The trans-decalin possesses inversion symmetry whereas cis-decalin does not. Therefore, trans-decalin should not be an SF active molecule regardless of its orientation at the surface. Cis-decalin may be SF active depending on its orientation at the interface. The SSP and SPS spectra of both species are very similar. The only difference is the appearance of a stronger feature at ~2915 cm^{-1} on cis-decalin SSP spectra possibly due to a stronger C-H response. This result is expected because the two C-H groups in the cis-decalin are oriented ~90^o with respect to each other. Regardless of the molecular orientation, either one or the other or a combination of both will have an out-of-plane projection.

What is not expected are the similar surface spectra of trans-decalin. According to the SF selection rules, this molecule should be SF active. One cause of surface activity could be impurities. However, the fact that the features are very similar to cis-decalin raises doubts about the impurities. The other reason might be a surface induced symmetry break. Although this is a new phenomenon that needs to be investigated extensively, there are already some reported surface vibrational studies of molecules having inversion symmetry, such as the highly symmetric molecule, benzene.[126] Isotopic labeling of the certain groups may enable us to assign the bands in the spectra of centro-symmetric molecules and clarify the origins of the SF response of trans-decalin.

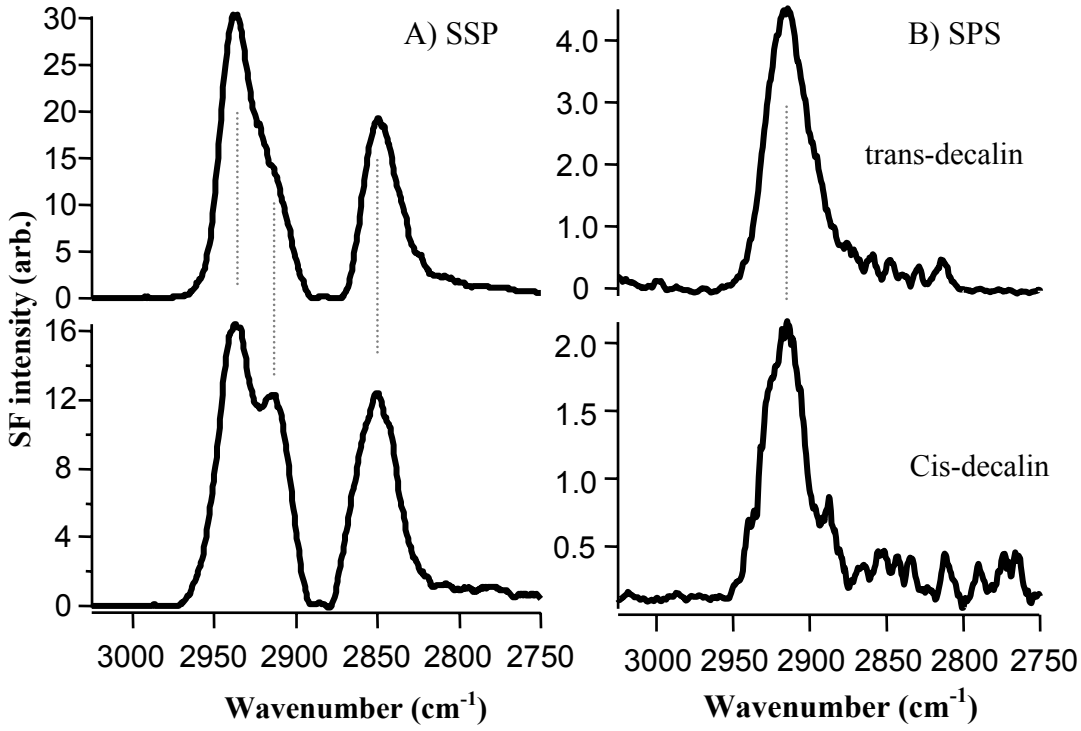

Figure 3.11. Surface vibrational spectra of cis- and trans-decahydronaphtalene (decalin) acquired under A) SSP and B) SPS polarization conditions.

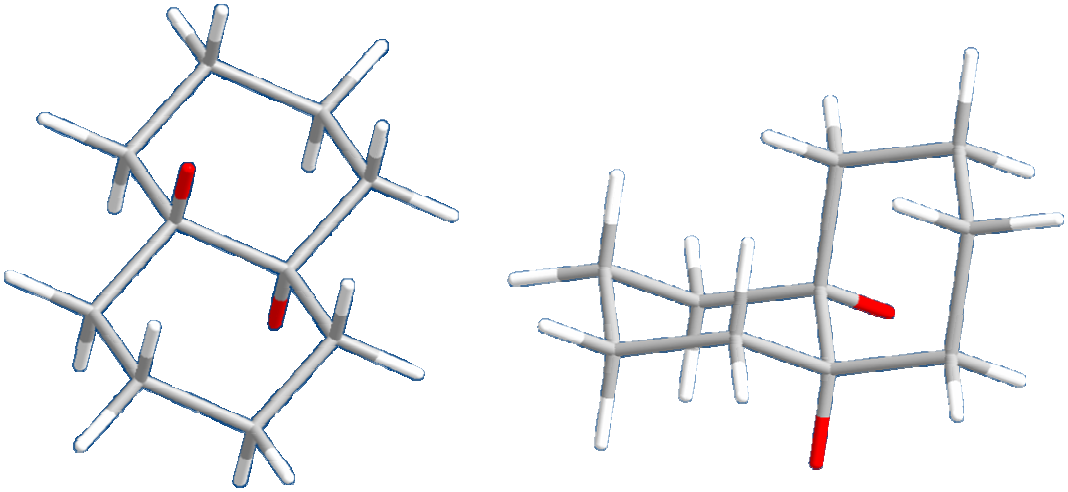

Trans-decalin Cis-decalin

Figure 3.12. Molecular structures of trans- and cis-decalin. Gray is Carbon, white is H of a CH_2 group, and red is H of a CH group.

Chapter 4

Haloalkanes

This chapter compares the surface vibrational spectra of haloalkanes and alkanes having different chain lengths. Chains consist of 10, 14, and 16 carbons and halogen substituents are either chlorine or bromine (Figure 4.1). Briefly, the 1-chloro- and 1-bromo-hexadecane spectra show dramatic reduction in the intensity of vibrational bands assigned to methyl group. Results are interpreted in terms of the surface activity of halogenated end groups. The goal of the current work is to examine what effect - if any chain length has on the surface structure of these different solvents at the liquid/vapor interface. The data are separated into two categories: i) surface structure is examined with respect to alkyl chains having different lengths but same end groups (e.g. 1-chlorodecane vs 1-chlorotetradecane vs 1-chlorohexadecane) and ii) the surface structure of liquids having the same chain lengths is examined as a function of the end group identity (e.g. neat- vs 1-chloro- vs 1-bromo-hexadecane).

4.1. Chloroalkane surface structures

4.1.1. Chloroalkanes

Figure 4.2 shows the surface vibrational spectra of 1-chlorodecane ($Cl\text{-}C_{10}$), 1-chlorotetradecane ($Cl\text{-}C_{14}$), and 1-chlorohexadecane ($Cl\text{-}C_{16}$) acquired under the

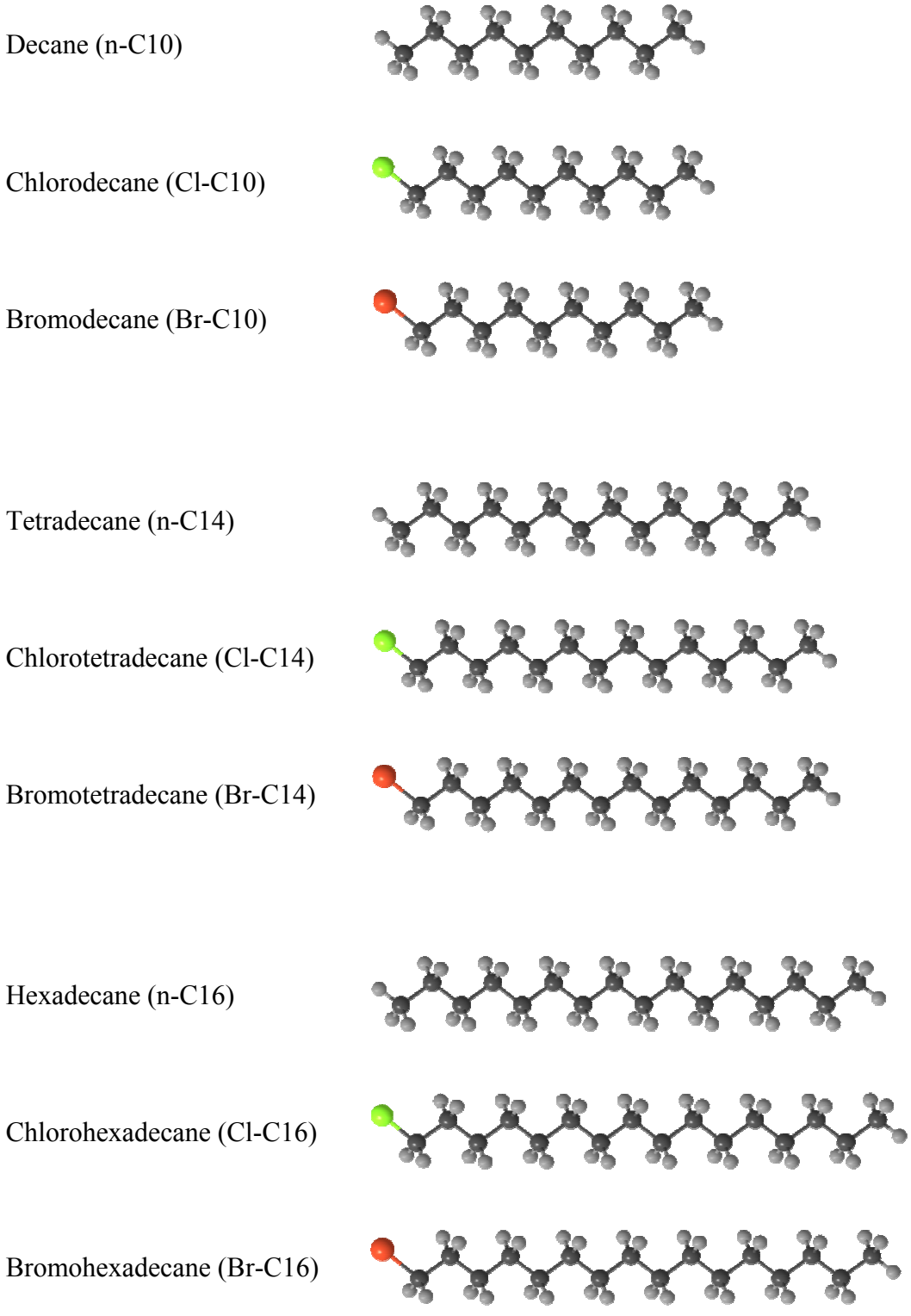

Figure 4.1. Molecular structures of haloalkanes. Linear alkane molecular structures are given for comparison reasons.

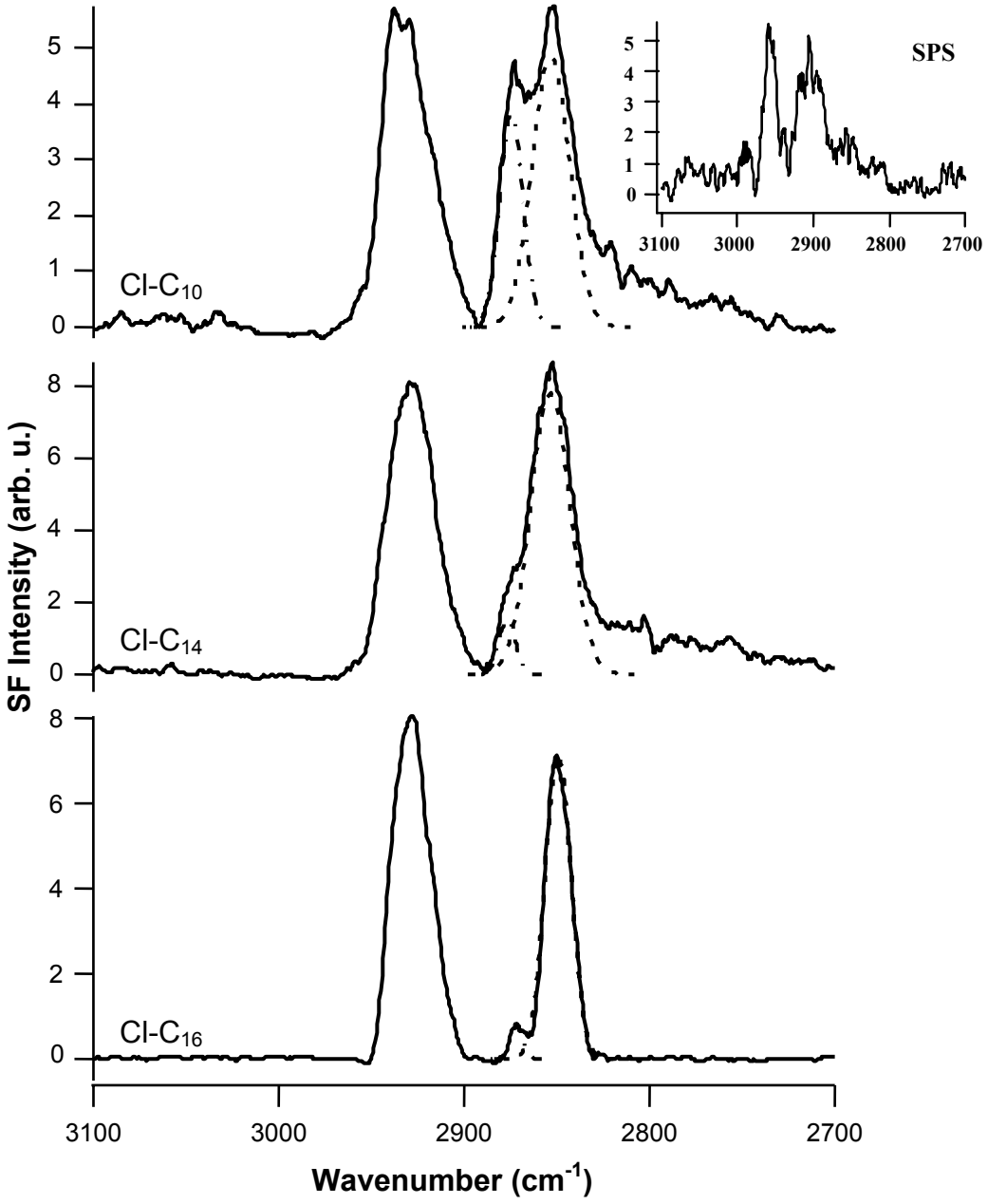

Figure 4.2. Surface vibrational spectra of chloroalkanes acquired under SSP polarization combination. Cl-C_{10} is 1-chlorodecane, Cl-C_{14} is 1-chlorotetradecane, and Cl-C_{16} is 1-chlorohexadecane. The inset figure is the surface vibrational spectrum of 1-chlorodecane acquired under SPS polarization combination.

SSP polarization combination. This combination of polarizations refers to an S polarized sum frequency field, an S polarized visible field, and a P polarized IR field. The SSP polarization combination samples those vibrational modes that have their IR transition moments aligned perpendicular to the surface. The inset is the spectrum of Cl-C_{10} acquired under the SPS polarization combination and reflects those vibrational modes that have their IR transition moments aligned parallel to the surface. Features observed in these SSP spectra can be grouped into two regions. The low energy region is fitted with two vibrational modes that are assigned to a methylene symmetric stretch (CH_2-SS, d^+, 2850 cm^{-1}) and a methyl symmetric stretch (CH_3-SS, r^+, 2870 cm^{-1}), respectively. The high energy region (>2900 cm^{-1}) is fitted with up to four vibrational bands corresponding to a methylene Fermi resonance (CH_2-FR, d^+_{FR}, 2905 cm^{-1}), a methylene asymmetric stretch (CH_2-AS, d^-, 2925 cm^{-1}), a methyl Fermi resonance (CH_3-FR, r^-, 2935 cm^{-1}), and a doubly degenerate methyl asymmetric stretch (CH_3-AS, r^-, 2962 cm^{-1}). These assignments are all based on previous IR, Raman and SFG studies of alkyl vibrational structure.[34,109,113,114,127,128] In general r^- appears only in spectra acquired under SPS polarization conditions, signifying an average upright orientation of surface methyl groups. Due to the ambiguity associated with fitting the high energy feature centered at ~2930 cm^{-1} with 3(or 4) possible contributions, a quantitative comparison of specific vibrational bands in this region of spectra is difficult. Instead, much of the analysis presented below relies on comparing the relative intensities in the low energy region, namely the r^+/d^+ ratio as a measure of conformational order at surfaces containing alkyl chains as mentioned in Chapter 2.

The 1-chlorodecane (Cl-C_{10}) spectrum (top, Figure 4.2) shows strong features at ~2853 and ~2874 cm^{-1} that are assigned to the d^+ and r^+ bands respectively. The intensity ratio of r^+ to d^+ (r^+/d^+) is 0.45 ± 0.07. The narrow bandwidth of the r^+ band (~15 cm^{-1} FWHM) suggests a relatively homogeneous distribution of the CH_3 groups at the interface, implying that the methyl groups that contribute to the SF spectrum share a similar chemical environment. The d^+ band is considerably broader with a FWHM of ~23 cm^{-1}. The bandwidth likely reflects the contribution from the CH_2 groups sampling an inhomogeneous environment due to gauche defects along the chain. We note that the halogenated end group of Cl-C_{10} consists of a -CH_2 that can also contribute to the intensity of d^+ band. The symmetric band shape of the d^+ band suggests that within the resolution of the experiments, the symmetric stretch of the terminal -CH_2 group has center frequency comparable to that of the CH_2 groups of the rest of the chain. Furthermore, the symmetric band shape also implies an absence of interferences from adjacent, SF active vibrational modes. Spectra of longer chains support this interpretation. The high energy feature of the Cl-C_{10} spectrum contains significant CH_3-FR intensity causing the maximum intensity in the high energy region (~2933 cm^{-1}) to fall in between the d^- (~2925 cm^{-1}) and r^+_{FR} (~2935 cm^{-1}) bands. This pattern is expected given the considerable intensity observed for the r^+ band at the low energy region. The fitting results are tabulated in Table 4.1.

The relative intensities of the r^+ and d^+ bands in the 1-chlorotetradecane (Cl-C_{14}) spectrum (middle, Figure 4.2) are quite different from those in the Cl-C_{10} spectrum. The fitting results are tabulated in Table 4.2. The intensity of the r^+ band of Cl-C_{14} decreases by approximately a factor of three, while the intensity of the d^+ band

Table 4.1. The 1-chlorodecane SSP spectrum fitting results.

Feature	Position (cm^{-1})	Width (cm^{-1})
d^+	2853 ± 1	23 ± 1
r^+	2874 ± 1	14 ± 1
d^+_{FR}/d^-	2920 ± 7	28 ± 9
r^+_{FR}	2935 ± 3	20 ± 2

increases slightly. The r^+/d^+ value decreases from 0.45 ± 0.07 (Cl-C_{10}) to 0.15 ± 0.10 (Cl-C_{14}). Accompanying these changes is a significant change in the shape and maximum intensity in the high energy region of the spectrum. This feature loses considerable intensity on the high frequency, r^+_{FR} side causing a shift in the maximum intensity from ~2933 to ~2926 cm^{-1}. This behavior is consistent with the idea that the methyl end group plays less of a role in determining the surface structure at the Cl-C_{14} liquid/vapor interface compared to that of Cl-C_{10}.

Table 4.2. The 1-chlorotetradecane SSP spectrum fitting results.

Feature	Position (cm^{-1})	Width (cm^{-1})
d^+	2853 ± 1	22 ± 1
r^+	2875 ± 2	15 ± 1
d^+_{FR}/d^-	2921 ± 5	27 ± 5
r^+_{FR}	2936 ± 2	20 ± 2

Changes in the overall appearance between Cl-C_{10} to Cl-C_{14} spectra became even more pronounced in the Cl-C_{16} spectrum. The fitting results are tabulated in Table 4.3. Again, the r^+ band loss intensity so that it now appears as a very small

feature on the high frequency side of a very strong d^+ band. The r^+/d^+ value for the Cl-C_{16} is only 0.07±0.05 and the high energy feature becomes even narrower as additional intensity is lost in the r^+_{FR} band. Based on the findings of X-ray scattering studies[3,19], we assume that most of the chain is disordered with the "bulk" -CH_3 group and -CH_2 groups (beyond a certain persistence length) randomized ensuring that they do not contribute to the SF spectrum. Here the term "bulk" CH_3 group refers to the CH_3 group of the molecules that have their CH_2Cl side aligned towards the vapor phase and the CH_3 end oriented into bulk solution.

Table 4.3. The 1-chlorohexadecane SSP spectrum fitting results.

Feature	**Position (cm^{-1})**	**Width (cm^{-1})**
d^+	2850 ± 1	17 ± 1
r^+	2873 ± 2	11 ± 3
d^+_{FR}/d^-	2920 ± 5	22 ± 4
r^+_{FR}	2934 ± 2	16 ± 1

The following assumptions have been used during the analysis of the spectral data:

- the CH_2Cl groups interact through dipole-dipole interactions that are on the order of kT.

- the dipole-dipole interactions are more easily accomodated at the surface than the bulk solution due to steric hindrances in later from the long alkyl chains.

- the dipole-dipole interactions between the surface CH_2Cl groups allow the rest of the molecule to pack more efficiently, reducing gauche defects along the chain.

- the dipole-dipole interactions cause the surface CH_2Cl groups to organize better and form correlated interactions that can require shielding from each other.

- the dipole interactions between the dipoles and correlated regions are strongest for Cl-C_{10} and weakest for Cl-C_{16} due to the radius of gyration considerations.

The systematic drop in r^+ band intensity as chain length increases from 10 to 16 could arise from two sources. First, an increase in chain length would increase the surface area per molecule resulting fewer methyl groups at the surface reducing the observed relative intensity of the r^+ band. A second cause for the reduction in the number of surface methyl groups would be replacement of -CH_3 groups with an increasing fraction of -CH_2Cl end groups. These two pictures assume that the average orientation (and angular distribution) of these surface methyl groups does not change significantly. Furthermore, both cases assume that only those methyl groups oriented toward the vapor phase contribute to a SF spectrum and a randomized distribution of "bulk" methyl groups is assumed.[3] If these assumptions prove unfounded, then the "bulk" methyl groups could also contribute to the r^+ band intensity. This situation would lead to the "bulk" methyl group vibrational modes that are 180^o out of phase with respect to those of surface CH_3 and CH_2 groups oriented toward the vapor phase. Such a condition should lead to the observed r^+ and d^+ features that have asymmetric band shapes as well as diminished intensity due to destructive interference effects.

These effects would be most pronounced for the shorter alkanes where there exists stronger correlation between the two end group orientations. The spectra shown in Figure 4.2 simply do not support this picture. Instead the r^+ and d^+ bands are quite symmetric and, contrary to the prediction of destructive interference, the r^+ band is strongest in the Cl-C_{10} spectrum and weakest in the Cl-C_{16}.

To determine the average projection of the -CH_3 transition moment, the r^+ and r^- contributions to the SSP and SPS spectra can be compared. The SPS spectrum of Cl-C_{10} (inset in Figure 4.2) is representative of all chloroalkanes. The SF signal level in every SPS spectrum is relatively much lower than that of the SSP spectrum. The IR transition moments of the r^+ and r^- modes are perpendicular to each other. Therefore, the r^+ band intensity observed in an SSP spectrum should correlate with the r^- band in the SPS polarized spectrum. Moreover, if the CH_3 pseudo-C_3 symmetry axis is angled with respect to the surface normal, the r^+ and r^- bands should be observed (with different intensities) under both polarization conditions.[18] The persistent absence of the r^- band in SSP spectra (as well as the absence of the r^+ band in SPS spectrum) means that the decrease in the r^+ band intensity with increasing chain length cannot be assigned to changes in a net methyl group orientation. In addition, the bandwidth of the r^+ stays reasonably constant confirming that the angular distribution of the methyl groups at the interface is not changing. This situation leaves only the reduction in number density of CH_3 end-groups at the surface as the source of the reduced r^+ band intensity as chain length increases. The number of methyl groups could change either because the number of molecules per area changes with the chain length, and/or the

relative fraction of the $-CH_3$ (X_{Me}) and the $-CH_2Cl$ (X_{Cl}, where $X_{Me} + X_{Cl} = 1$) groups at the surface change with chain length.

An increase in the chain length should decrease the number of molecules per area due to an increase in the radius of gyration and, consequently, the volume and surface area occupied per molecule.[129] However, a decrease in the number of molecules at the liquid/vapor interface cannot by itself explain the observed behavior. For example, if one assumes that X_{Me} (and X_{Cl}) remain constant as chain length increases, then the r^+ and d^+ bands should decrease in intensity together, although not necessarily by the same amount due to the several sources that can contribute to the intensity of the d^+ band in the SF spectrum. In addition, the bandwidth of the d^+ band should reflect the source of contributions; the gauche defects and/or the terminal CH_2Cl group. The narrower bandwidth of d^+ band in the Cl-C_{16} spectrum implies that the primary contributions are from the terminal $-CH_2$ groups. The broad d^+ bandwidths in the Cl-C_{10} and Cl-C_{14} spectra indicate contributions from the $-CH_2$ groups associated with the gauche defects along the chain. We might expect the d^+ bandwidth to become broader as the chain gets longer since longer chains can support more gauche defects as observed for the linear alkanes in Chapter 3. However, the chloroalkane spectra show the opposite behavior. The bandwidth of the d^+ band decreases from 25 cm^{-1} for Cl-C_{10} to 16 cm^{-1} for Cl-C_{16}. Thus, the change in number density of the surface molecules due to increasing chain length cannot explain the observed differences in the r^+/d^+, forcing us to consider the dependence of the X_{Me} on the chain length to explain the observed behavior.

The observed decrease in the r^+ band intensity (and r^+/d^+ value) with respect to an increase in chain length can be understood if X_{Me} decreases for longer chains. The decrease in the X_{Me} could result from changes in surface energy minimization associated with shielding interactions between the "correlated dipole".[130,131] Due to the moderate dipole that exists in the haloalkanes (~2D), especially for the chloroalkanes, dipole-dipole interactions may play important role in haloalkane surface organizations. The dipolar interactions between surface molecules can cause formation of correlated dipoles that may require shielding from others correlated dipoles (Figure 4.3). Stronger dipole-dipole interactions will require more shielding. As the alkyl chain length increases dipole-dipole interactions weaken because the C-Cl dipoles of chloroalkanes move further from each other with increase in the surface area per molecule. Since the dipole interactions fall off $1/r^3$, these interactions would be comparably weaker for longer chains. Since the shielding is provided by the $-CH_3$ groups, fewer methyl groups will be required for the longer chains thereby reducing the X_{Me}. This picture is supported by the observed relative drop in the r^+ band intensity with respect to the d^+ band. We note that the loss in the X_{Me} reduces the entropy of the surface (thereby raising surface free energy) but this effect is offset by a more favorable enthalpic contribution due to the enhanced interactions of the $-CH_2Cl$ polar end groups. Furthermore, chains residing in the first few solvent layers can greater conformational entropy once the large halogen head groups of the top layer are out of the way. These observations suggest that the halogenated side of the haloalkane molecules does not prefer to be solvated but rather the halogenated end use the steric freedom found at the liquid/vapor interface to improve its dipolar

interactions and raise slightly the entropy of the underlying bulk liquid. This picture is supported by the surface tensions of haloalkanes that is very close to the alkanes (Table 2.7).

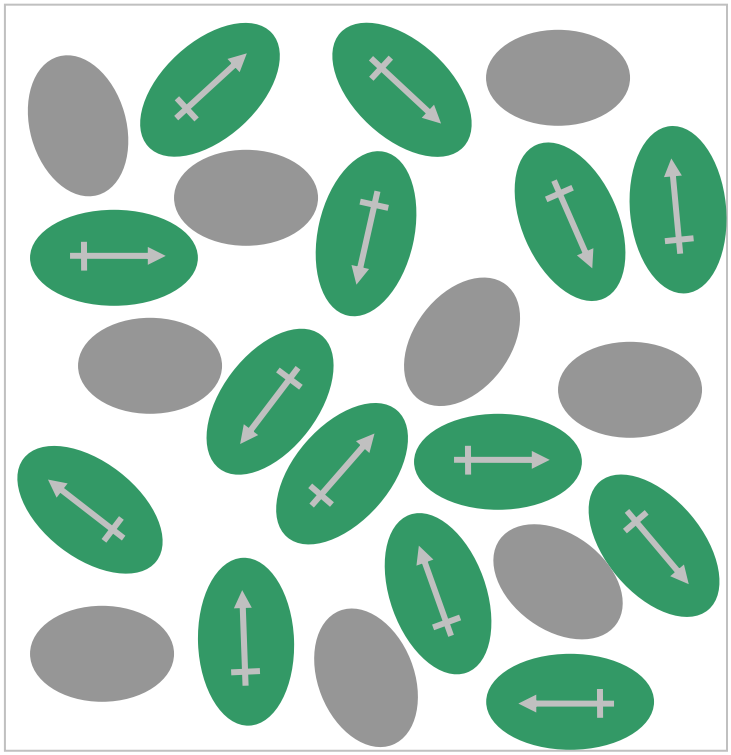

Figure 4.3. Schematic picture suggesting the role of highly polarizable CH_3 groups shielding the repulsive dipolar interactions. The green oval shapes representing the CH_2Cl having a dipole represented by an arrow. The gray ovals represent the polarizable CH_3 groups. This picture is speculative and represents one surface structure that could account for observed spectral behavior.

In summary, the decrease in the X_{Me} number can explain the observed drop in the intensity of the r^+ band (and r^+/d^+) in surface vibrational spectra of haloalkanes as the chain length increases. Since the main contribution to the band broadening of the d^+ band is thought to originate from the $-CH_2$ groups of methyl terminated molecules, we infer that a narrowing on the bandwidth of the d^+ band can also be correlated to a decrease in the number of molecules having $-CH_3$ side up. In addition, the narrowing

is associated with an increase in the number of molecules having the CH_2Cl end oriented towards the vapor phase.

4.1.2. Bromoalkanes

Figure 4.4 shows the surface vibrational spectra of 1-bromoalkanes for chain lengths of 10, 14, and 16 under the SSP polarization condition. The inset is the SPS polarized spectrum of Br-C_{10}. Similar to the chloroalkane spectra, the low energy region in the spectra are fitted with two vibrational bands at 2850 cm^{-1} and 2872 cm^{-1} center frequencies and are assigned to the methylene symmetric stretch (CH_2-SS, d^+) and the methyl symmetric stretch (CH_3-SS, r^+), respectively. Again the poorly resolved high energy feature has been fit with up to four contributions corresponding to a methylene Fermi-resonance (CH_2-FR, d^+_{FR}) at 2905 cm^{-1}, a methylene asymmetric stretch (CH_2-AS, d^-) at 2925 cm^{-1}, a methyl Fermi resonance (CH_3-FR, r^+_{FR}) at 2935 cm^{-1}, and an asymmetric stretch (CH_3-AS, r^-) at 2961 cm^{-1}. The r^- band appears prominently only in the SPS spectra. Its contribution to the SSP spectra is vanishingly small. The fitting results of 1-bromodecane, 1-bromotetradecane, and 1-bromohexadecane are tabulated in Table 4.4, 4.5 and 4.6, respectively.

Table 4.4. The 1-bromodecane SSP spectrum fitting results.

Feature	Position (cm^{-1})	Width (cm^{-1})
d^+	2851 ± 2	25 ± 2
r^+	2873 ± 2	20 ± 3
d^+_{FR}/d^-	2920 ± 3	24 ± 4
r^+_{FR}	2936 ± 1	20 ± 1

Table 4.5. The 1-bromoteradecane SSP spectrum fitting results.

Feature	Position (cm^{-1})	Width (cm^{-1})
d^+	2851 ± 1	21 ± 1
r^+	2874 ± 1	13 ± 1
d^+_{FR}/d^-	2924 ± 4	27 ± 4
r^+_{FR}	2936 ± 1	19 ± 1

Table 4.6. The 1-bromohexadecane SSP spectrum fitting results.

Feature	Position (cm^{-1})	Width (cm^{-1})
d^+	2850 ± 1	23 ± 1
r^+	2873 ± 2	13 ± 3
d^+_{FR}/d^-	2924 ± 5	33 ± 4
r^+_{FR}	2933 ± 2	19 ± 1

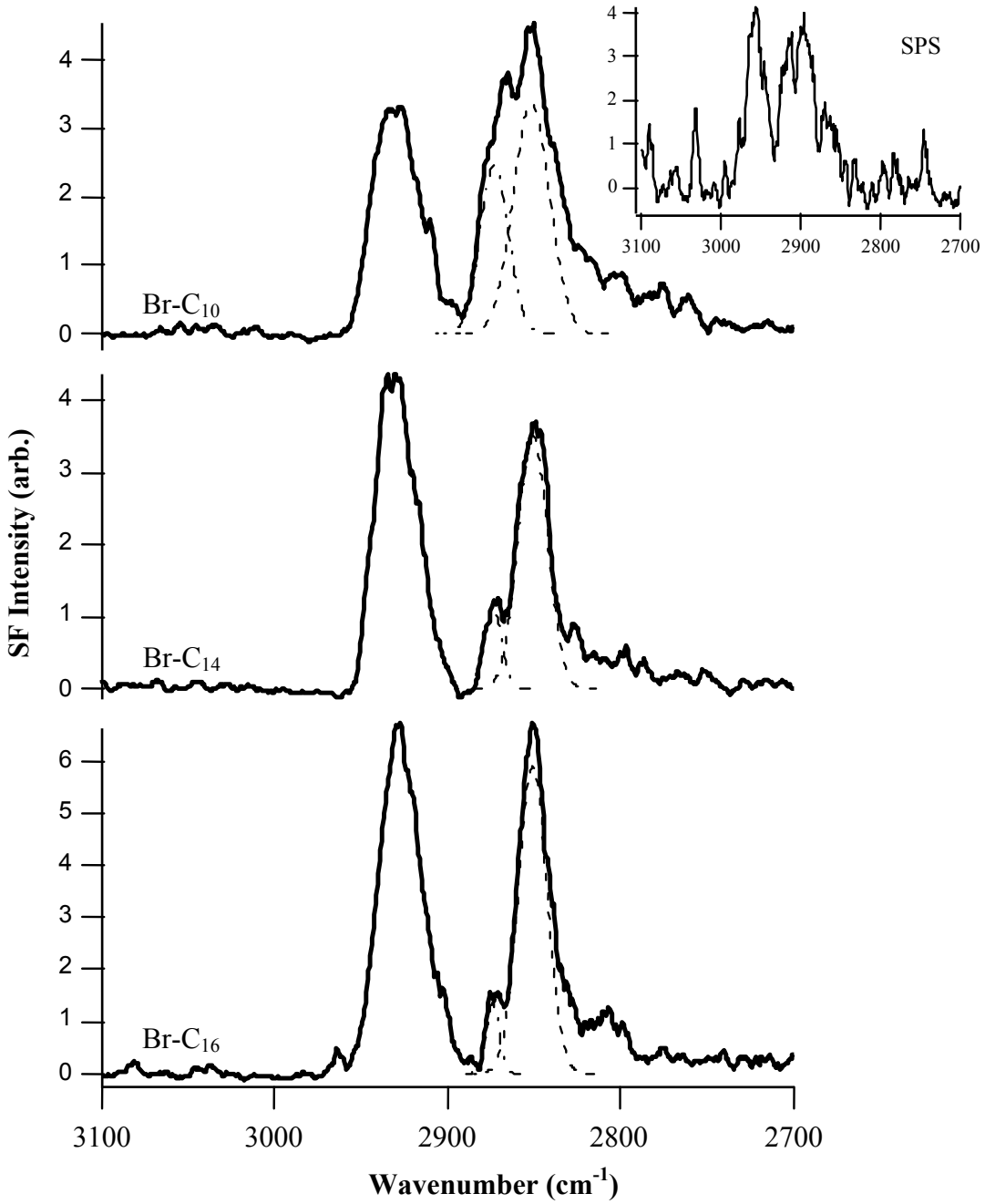

Figure 4.4. Surface vibrational spectra of bromoalkanes acquired under SSP polarization combination. Br-C_{10} is 1-bromodecane, Br-C_{14} is 1-bomotetradecane, and Br-C_{16} is 1-bromohexadecane. The inset figure is the surface vibrational spectrum of 1-bromodecane acquired under SPS polarization combination.

The bromoalkane spectra show very similar behavior to those of the corresponding chloroalkanes except that the signal to noise levels are consistently lower. For the bromoalkanes this effect is most probably due to the relatively larger size of the bromo group causing a decrease in the number of molecules per area, and, consequently, a decrease in the observed SF signal. Trends observed for the chloroalkanes with respect to the chain length are qualitatively the same for the bromoalkanes, namely the r^+ band intensity decreases, and the bandwidth of the d^+ band becomes narrower as the chain length increases. The bromodecane (Br-C_{10}) (top, Figure 4.4) shows significant intensity in the r^+ band with respect to the intensity in the d^+ band with an r^+/d^+ ratio of 0.55 ± 0.05. The r^+ bandwidth is broader (20 cm^{-1}) than in the Cl-C_{10} spectrum (15 cm^{-1}) suggesting that the environment of CH_3 end groups at the Br-C_{10} surfaces are less homogeneous than that of the Cl-C_{10}. However, the d^+ bandwidth is same as that (~23 cm^{-1}) in Cl-C_{10} spectrum implying that the methylene groups contributing to the SF intensities share similar environments, and the overall surface conformational order of the two species is likely quite similar. The high energy feature of the Br-C_{10} spectrum contains significant CH_3-FR intensity causing the peak of the feature (~2932 cm^{-1}) to be centered between d^- and r^+_{FR} as expected based on the observed intensity of the r^+ band in the low energy region.

The overall intensity distribution in the Br-C_{14} spectrum (middle, Figure 4.4) is significantly different from that of the Br-C_{10}. The intensity of the r^+ band decreases significantly compared to that of the Br-C_{10}. The d^+ bandwidth and the width of the high energy feature is considerably narrower (30 cm^{-1}) suggesting a more

homogeneous conformation for surface molecules compared to the case of Br-C_{10}. The main reason behind the narrowing of the high energy feature is due to the decrease in the CH_3-FR contribution as it was in the chloroalkane case. Therefore, the high energy feature is centered close to the CH_2-AS center frequency. The r^+/d^+ ratio decreases to a value of 0.20 ± 0.05. This approximately three fold decrease is similar to that observed for the chloroalkanes.

Again changes between the Br-C_{10} and Br-C_{14} spectra become more pronounced for the Br-C_{16} spectrum (bottom, Figure 4.4). The r^+ band intensity diminishes even more, the relative intensity of the d^+ band is noticeably increased, and the r^+/d^+ value is 0.15 ± 0.05. The high energy feature of the spectrum again loses intensity on the high frequency side, presumably due to the diminished r^+_{FR} band intensity.

All of the assumptions made for the chloroalkane systems are also relevant for the bromoalkane systems such as the dipole-dipole interactions between two -CH_2Br being on the order of kT, dipolar interactions being more favored at the surface than the bulk due to steric considerations, interactions between the dipoles and the correlated dipoles decreasing with the chain length. The overall similarities and subtle differences between bromo- and chloroalkane results can be understood using pictures developed for the chloroalkane systems. First, the decrease in surface concentration with increasing chain length will cause a decrease on the overall observed spectral intensity. As discussed in the chloroalkane case, this effect should have a minimal impact on the r^+/d^+ ratio. The other factor contributing to a reduced r^+/d^+ ratio is the relative fraction of surface active CH_3 groups (X_{Me}) with respect to

the CH_2Br groups at the liquid/vapor interface. The dipole screening picture predicts that as the surface area per molecule increases the dipole-dipole interactions will become weaker and the correlated dipoles will require less shielding from each other. Less shielding will lead to a decrease in the relative number of surface methyl groups, X_{Me}, preferentially decreasing the r^+ band intensity and increasing the d^+ band intensity due to additional CH_2Cl groups. These changes will lead to a chain length dependence of r^+/d^+ ratio and a d^+ band that narrows as chain length increases. If the number of gauche defects stays approximately same or even decreases as chain length increases as suggested by the bandwidth considerations, and X_{Me} diminishes as chain length increases, then one must conclude that the main contribution to the gauche defect part of d^+ band occurs from the methyl terminated molecules. As the surface methyl groups are replaced by the bromomethyl groups, the contribution to the d^+ band intensity from bulk $-CH_2$ groups significantly decrease. This result sharpens the d^+ band as observed in the Br-C_{16} spectrum compared to the Br-C_{10} spectrum. As the relative number of the CH_2Br (X_{Br}) increases with the increase in chain length halogenated end group will dominate the observed d^+ band intensity of the spectrum. The surface free energy considerations are valid for the bromoalkanes, too.

As in the chloroalkane systems, as the chain length increases the relative number of the $-CH_3$ end groups appears to decrease along with an increase in the relative number of $-CH_2Br$ end groups. Although the change causes a reduction in the surface entropy, the enthalpic contribution will compensate for this rise in free energy with an increase in the number of dipolar interactions.

4.2 End group effect

To this point, results have focused on the effect of chain length on the surface structure of haloalkanes where the endgroup does not vary. Observed changes in the spectra cannot be explained simply by considering molecular size and corresponding surface area per molecule. Energetic factors, namely dipolar interactions, must be considered in order to understand the reorganization of surface structure as chain length increases. Although a reduction in the X_{Me} creates an entropically less favored surface structure, the corresponding relative increase in the CH_2(Cl or Br) polar end groups improves the enthalpic contribution to the surface free energy. These observations suggest that the halogenated side of the haloalkane molecules does not prefer to be solvated but rather prefer the steric freedom found at the liquid/vapor interface for better dipole-dipole interactions. The surface vibrational spectra of the (halo)alkane systems with the same chain length but varying end groups supports conclusions.

This section compares the effect of the end groups for alkanes having equivalent chain length in order to determine how the size and interactions between the end groups influence the surface structure at the liquid/vapor interfaces by comparing the r^+/d^+ ratios. The r^+/d^+ value is used as a common measure of the order of a surface layer in many studies as discussed in Chapter 3.[72] In most cases it is highly sensitive and it provides a qualitative measure of the order so long as the d^+ band contribution is solely from the CH_2 groups of the gauche defect sites. Table 4.7 shows the calculated r^+/d^+ values from SSP spectra as a function of chain length. Two observations in the change of r^+/d^+ values with respect to end groups are worth

Table 4.7. r+/d+ ratio of haloalkanes.

	Chain length (n)		
	10	**14**	**16**
Cl-C_n	0.45 ±0.07	0.15 ±0.10	0.07 ±0.05
Br-C_n	0.55 ±0.05	0.20 ±0.05	0.15 ±0.05
n-C_n	1.00 ±0.50	0.50 ±0.05	0.30 ±0.03

noting: First, the r^+/d^+ drops dramatically for haloalkanes compared to *n*-alkanes (see also Figure 4.5). Without independent measurements of surface concentrations and molecular conformations, the magnitude of the decrease in the r^+/d^+ values of the haloalkanes compared to the *n*-alkanes cannot be interpreted quantitatively. Therefore, it is not possible to use the r^+/d^+ ratio as an absolute quantitative measure of a system's conformational order. We can only make qualitative comparisons of the r^+/d^+ values of *n*-alkanes and haloalkanes. The second striking change in the r^+/d^+ values listed in Table 4.7 is that the r^+/d^+ values of the bromoalkanes are consistently higher compared to those of the chloroalkanes. The latter can be explained by the size difference between the CH_2Cl and CH_2Br end groups. Due to the larger size of the CH_2Br groups, the packing of the bromoalkane molecules at the interface will not be as efficient as the packing of the chloroalkanes. The result is additional free surface area that can be occupied by CH_3 groups, leading to a small increase in the r^+ band intensity and r^+/d^+ values compare to the chloroalkanes. In addition the absolute number of the CH_2Br end groups at the surface should be slightly lower than for the CH_2Cl systems because of size considerations. As a result, the d^+ band intensity in the bromoalkane spectra should have a lower intensity relative to the chloroalkanes

resulting a slightly higher r^+/d^+ ratio.

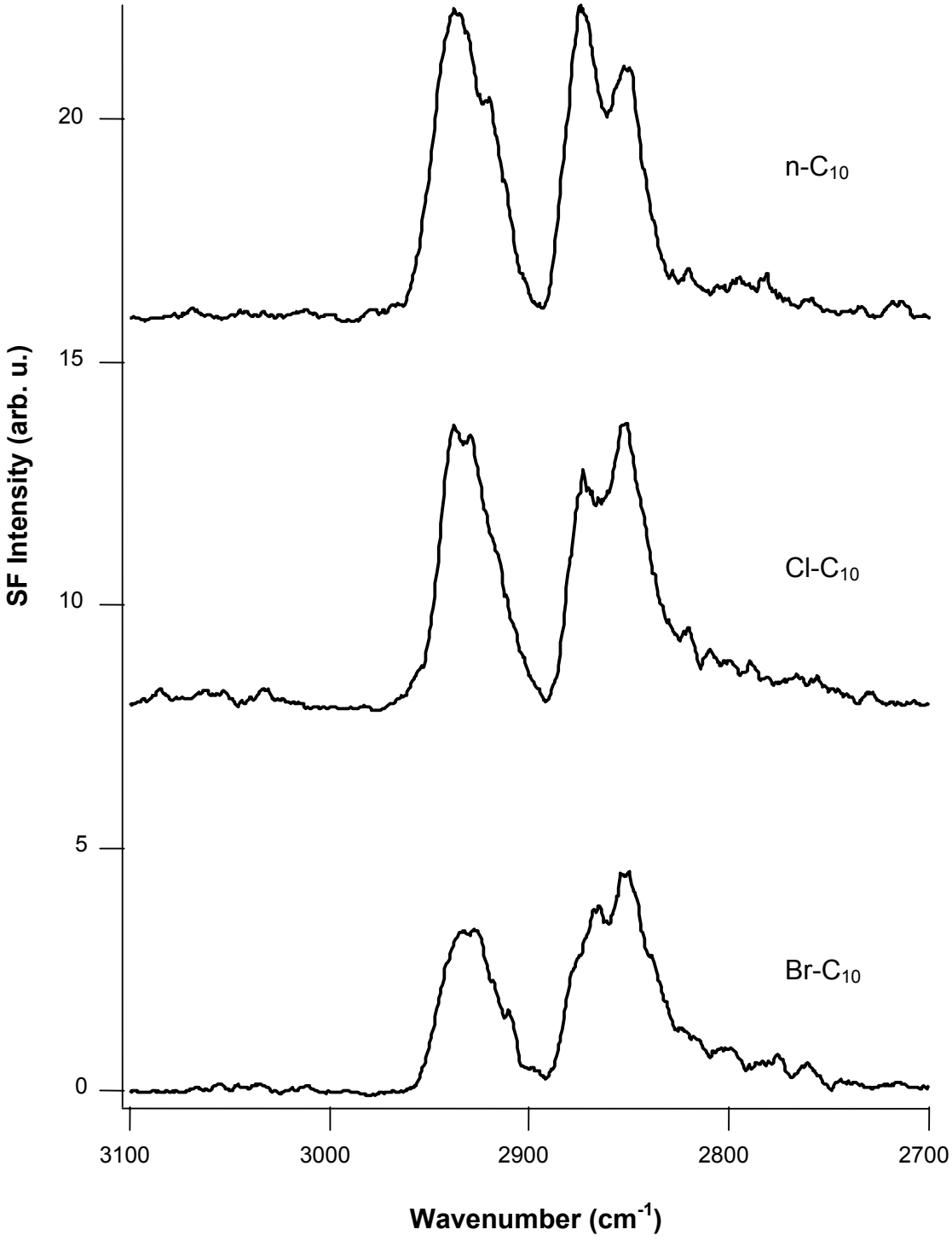

Figure 4.5. Surface vibrational spectra of neat, chloro-, and bromo-alkanes acquired under SSP polarization combinations. The spectra are reproduced for comparison reason.

For a given chain length, the r^+/d^+ ratios decrease by a factor of ~2-4 when the terminal hydrogen is replaced by a Cl or Br. This behavior cannot be explained simply by considering changes in the end group size. Although the number of molecules in a given area of haloalkanes should be less than that for regular alkanes, a reduction in the surface concentration would decrease the signal levels of all of the vibrational bands according to Equation 1.17 and 1.20-23. However, this effect should impact both features in a similar manner so that the r^+/d^+ values of the haloalkanes should behave like the n-alkane systems.

Simple statistical considerations cannot explain the amount of the observed decrease. For example, if the surface of a chloroalkane consists of a 1:1 mixture of CH_3 and CH_2Cl end groups, the CH_3 amount decreases ~3 times compare to n-alkanes. Therefore, the signal level of the r^+ ratio should decrease by a factor of 9 compared to a same length *n*-alkane. This only considers the decrease in the r^+ intensity. If the intensity in d^+ band increases due to the surface CH_2Cl groups, the decrease in r^+/d^+ ratio is expected to be an order of magnitude more. The decrease of ~2-4 fold in r^+/d^+ ratio is much smaller than the expected amount even for the longest chains. If, however, dipole-dipole interactions are sufficiently strong, chains will pack more efficiently, reducing the number of gauche defects and, consequently, intensity in the d^+ band. Although the d^+ band intensity gains contribution from the CH_2Cl end groups, it loses intensity from the loss of many $-CH_2$ group associated with gauche defects. This effect becomes more evident for longer chains where much narrower bandwidth is observed for the d^+ band. A narrower bandwidth will reduce the d^+ band intensity areand increase the r^+/d^+ value.

In summary, the main reason behind the drop in the r^+/d^+ value changing form *n*-alkanes to haloalkanes is the surface active end group change from -CH_3 to CH_2Cl. The amount of change depends on the interaction strength of the dipoles that scales inversely with chain lengths. There are more –CH_3 end groups at the surface for short chains than for long chains. There is a very small difference in the r^+/d^+ values of the chloroalkanes and bromoalkanes. Bromoalkane values are slightly higher than chloroalkane ones because of the extra CH_3 groups at the surface occupying the free surface created by inefficient packing due to their bigger size.

Chapter 5

Alcohols and Ketones

Solvents having similar bulk solution properties can create very different environments at surfaces simply because they have different molecular shapes.[6,7,118] Although a great deal is known about the bulk properties of the solvents, very little is known about their surface structure and properties. At surfaces, a solvent's packing efficiency as well as its functionality can lead to nonintuitive surface structure and organization. This study focuses on the different surface structures created by some simple alcohols and ketones. In addition, this work also aims to understand how hydrogen bonding differs from simple dipolar interactions in its ability to control surface structure. Here, we have investigated the surface structure of 1- and 3-octanols, 1-, 3-, and 5-nonanol, *and* 1-, 3-, and 5-nonanone. In addition, monolayer structures of octanols formed at the liquid/vapor interface of aqueous solutions have been compared with the surface structure of neat octanols. The following chapter divided into sections according to carbon length of the molecules.

5.1. C_9 Molecules – Nonanols and Nonanones

The surface vibrational spectra of the nine carbon alcohols (nonanols) and ketones (nonanones) have been acquired by vibrational sum frequency spectroscopy (VSFS). The functional group (-OH or =O) varied in its placement between 1, 3 and 5 positions (Figure 5.1).The vibrational spectra of the solvents were collected under two different polarization combinations, SSP and SPS where the three letter

1-nonanol	3-nonanol	5-nonanol
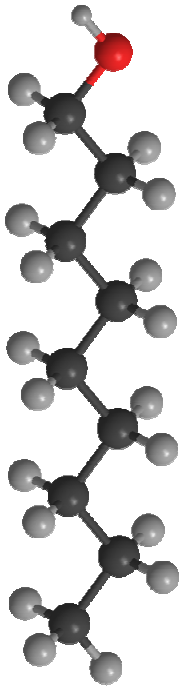	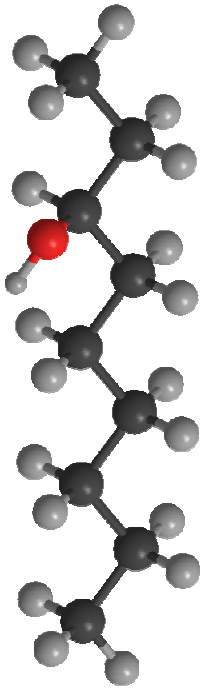	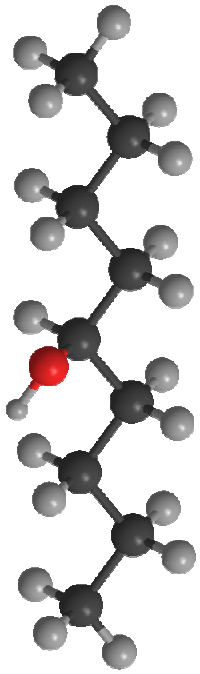
1-nonanone	3-nonanone	5-nonanone
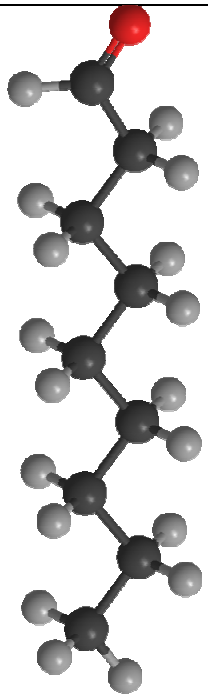	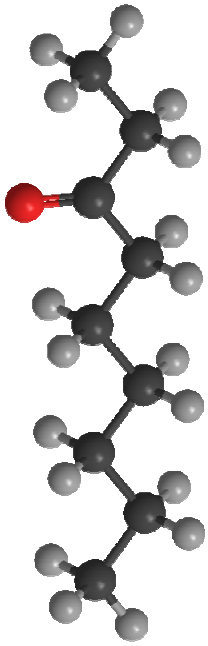	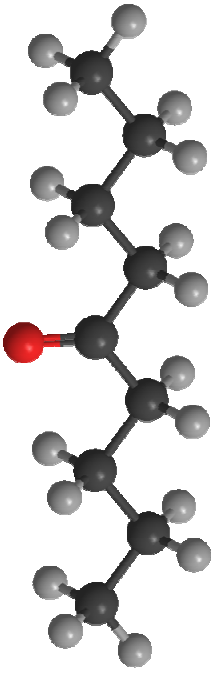

Figure 5.1. Molecular structures of nonanols and nonanones

combination denotes the polarizations of the sum frequency, visible, and IR, respectively. Comparison within the family of isomers will enable us to determine the effects of geometry on the surface structure. Differences in surface structure between equivalent nonanol and nonanone spectra (e.g. 3-nonanol and 3-nonanone) result from the differences in intermolecular interactions. In addition to the relatively weak chain-chain interactions common to both systems, the nonanols can interact through hydrogen bonding as well as dipolar interactions. Nonanones can interact only through dipolar forces. The hydrogen bonding is strongly directional whereas simple dipolar interactions do not depend as strongly on orientation. Comparison of different surface vibrational responses will enable us to determine relative importance of hydrogen bonding vs dipole-dipole forces in determining the surface structure.

A useful exercise before interpreting the results is to consider the possible molecular structures that can be adopted by these linear and branched solvents at liquid/vapor interfaces. Specifically, we want to focus on the impact these geometries will have on the methyl (r^+) and methylene (d^+) symmetric stretch bands commonly observed in the surface vibrational spectrum. We assume that these alcohols and ketones can adopt up to four different molecular structures. First, the chain of the solvent may adopt a "fully-stretched" geometry meaning that the carbon backbone of the structure is in an all-trans conformation (Figure 5.2). The molecule can adopt two limiting orientations at the surface: parallel (Figure 5.2a) or perpendicular (Figure 5.2b) to the surface. If the fully stretched molecule lies parallel to the surface then contributions are highly influenced by the angular distributions of the transition moments of CH_2 groups.[57,72] In case of a molecule parallel to the liquid/vapor

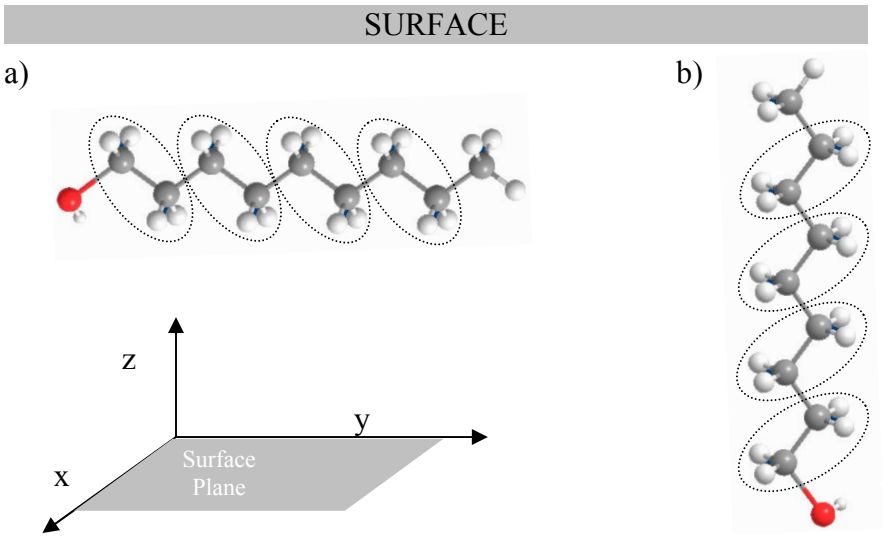

Figure 5.2. Possible orientations of a fully-stretched surface molecule; a) parallel to the surface and b) perpendicular to the surface. The dashed lines show the local inversion symmetry in every second carbon on the backbone of the both structures.

interface, contributions from one CH_2 group cancels contribution from the adjacent CH_2 group, including the terminal CH_2 group, due to the local inversion symmetry. Should the highly electronegative oxygen atom break the inversion symmetry between the last two methylene groups, then they may contribute to the d^+ band. However, the expected contributions should be very weak due to the angled positions of those groups. In addition, the CH_3 groups of the molecules that lie flat on the surface will also have their CH_3 pseudo-C_3 symmetry axis angled with respect to the surface normal (Figure 5.2a) making both symmetric and asymmetric methyl stretches active for SSP and SPS polarization combinations. Therefore, these features (r^+ and r^-) are both expected to be observed in both SSP and SPS spectra.

The backbone of the molecules may also be perpendicular to the surface and oriented toward the vapor phase. Without a reference it is very difficult to identify which end is oriented toward the vapor phase (thereby the phase of the contributing

vibrations) unless there exists a significant destructive interference between the modes.[73,75] As in the case for the molecules oriented parallel to the surface, the all-trans for the molecules oriented parallel to the surface, the all-trans conformation precludes the existence of gauche defects meaning that d^+ from the alkyl chain is forbidden by local symmetry (dashed lines in Figure 5.2b). However, the terminal CH_2 group and its immediate neighbor may contribute to the d^+ feature if the inversion symmetry is broken due to the highly electronegative oxygen atom. The contributions to the SSP spectra are expected to be very weak first because of the out of phase orientations of these two groups and second because of the orientation of their transition moments with respect to the surface (Figure 5.2b). An all-trans chain perpendicular to the surface will have methyl transition moment perpendicular to the surface resulting in a strong, sharp r^+ band.

At the 1-nonanol and 1-nonanone liquid/vapor interfaces, surface structure may represent a mixture from both ends of the molecules meaning that some of the molecules could be oriented with their CH_3 end aligned toward the vapor phase and some molecules point their CH_2OH or CH_2O toward the vapor phase. In that case, there are two types of CH_3 groups at the interface; the CH_3 groups with their transition moments oriented toward the vapor phase, and CH_3 groups with transition moments oriented toward the bulk solution. These CH_3 groups will be referred as surface CH_3 and bulk CH_3 groups, respectively. The contribution of these CH_3 groups to the r^+ feature will destructively interfere; thereby reducing observed intensity and, possibly, distorting the band shape.

A second possible surface structure that nonanol and nonanone solvents can adopt is a "partially extended" geometry that includes some significant segment of the chain in an all-trans conformation fallowed by a disordered, randomized segment. A similar structure has been proposed for alkane systems (Figure 3.7). Due to the anisotropy that exists at the liquid/vapor interface we expect some degree of ordering amongst the molecules at the surface. The extent of the order will depend on the interaction between the chains as well as the structure of the chain molecules.[132] If the surface induced polar ordering falls off at distances considerably shorter than the length of the molecules, the end of the molecule oriented toward the bulk solution will be randomized and uncorrelated with respect to the surface aligned segments. The SF response can only be observed from the aligned portion (referred as the persistence length) but not from the randomized portion. The persistence-length will depend sensitively on the molecular structure and strength of the intermolecular interactions. Gauche defects occurring within the persistence length enable those CH_2 groups to become SF active and contribute to the observed d^+ band causing a broadening in the feature (>15 cm^{-1}) as has been reported from the comparison of Cl-C_{10} and Cl-C_{16} spectra in Chapter 4. These CH_2 groups will be referred as gauche CH_2 throughout the text. As was the case for the fully stretched structures, the contribution of the any surface CH_3 groups to the r^+ band will be strong and the resulting r^+ band should have a symmetric, narrow bandwidth. Due to the disorder beyond the persistence length, bulk CH_3 groups should not contribute to the feature.[19]

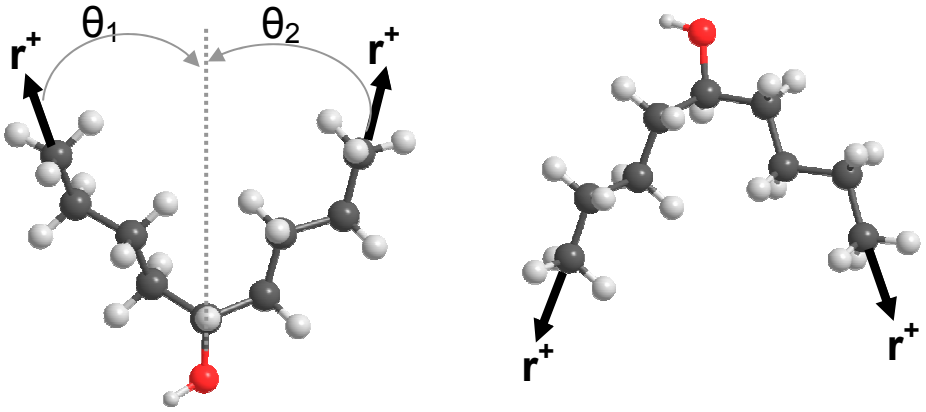

Figure 5.3. Possible a)V and b) /\ shaped molecular geometries.

A third possible geometry of the surface molecules is a V-shaped molecular structure where the length of the arms are determined by the position of the –OH (or =O) group oriented toward the bulk phase (Figure 5.3). This geometry is possible only for the branched alcohols and ketones used in this work. Such a conformation is common for strongly interacting systems such as branched alcohols on water surfaces (e.g. the 3-octanol/water, Chapter 5.2.2). The arms of the V-shaped geometries at surfaces can be treated as two separate (but correlated) alkyl chains. Due to the short arm lengths (minimum of 2 and maximum of 6 carbons), the possibility of having gauche defects on each branch is reduced significantly relative to the linear isomers. Therefore, contributions to the d^+ band from the gauche CH_2 groups are expected to be small. Given that the functional group placement occurs at the 3 or 5 positions, there will always be an odd number of CH_2 groups on each arm of the chain meaning that these unbalanced CH_2 groups can, in principle, contribute to the d^+ band intensity. Since those two CH_2 groups will sample very similar environments, the observed d^+ band should have a narrow bandwidth and the intensity of the band will depend on the orientation of those CH_2 groups. Again, broken symmetry due to the

electronegative oxygen atom may enable the adjacent CH_2 groups to also contribute to the d^+ band intensity causing spectral broadening. The net transition moments of the CH_3 groups are necessarily angled with respect to the surface normal and should give rise to in-plane and out-of-plane components for both r^+ and r^- bands under SSP and SPS polarization conditions.

The last possible surface molecular structure is a tent (/\) shaped structure which may be observed either if the –OH or =O functional groups orient themselves toward the vapor phase (Figure 5.3b). We expect this structure to be very unlikely given the large surface free energy associated with non-interacting surface dipoles. However, should molecules adopt this structure at the surface, we expect the d^+ and r^+ responses to be similar to that of V-shaped molecular structures. Differences may arise from the different environments sampled by the functional groups causing shifts in the center frequencies of the vibrational features compared to V-shaped molecular structures.

5.1.1. Nonanols

The surface vibrational spectra of nonanols collected under the SSP polarization combination are shown in Figure 5.4. The SPS spectra of alcohols are given in Figure 5.5. The SSP spectra consist of two main regions. The low energy region (below ~2900 cm^{-1}) contains information from the symmetric stretches of methyl (r^+) and methylene (d^+) groups. The high energy region contains information about Fermi resonances and asymmetric stretches of methyl and methylene groups. The spectra look very different demonstrating that the position of the –OH leads to significant changes in the surface structure. Due to uncertainties associated with data

acquisition, the absolute intensity of a feature in one spectrum cannot be compared quantitatively to the intensity of the same feature in the spectrum of a different isomer. However, comparisons of intensity ratios (r^+/d^+ from one spectrum vs. that of the other) are valid and will be used where appropriate.

The SPS spectra of alcohols are similar to each other. Due to the low reflectivity and weak responses associated with the SPS polarization combinations of fields, the signal levels are considerably lower than SSP spectra. The SPS spectra are dominated by the asymmetric stretch of the methyl group (r^-) at high energy side of the spectrum. A consistent decrease in intensity near 2900 cm^{-1} region with respect to the shift in the hydroxyl group position spectrum is also observed. The feature is assumed to be as Fermi resonance of methylene groups. The intensities observed in the methylene and methyl symmetric stretch regions are comparable to the noise, thus allowing us to say that neither r^+ nor d^+ bands contributes to the spectrum.

The ratio of intensities of the r^+ and d^+ bands, r^+/d^+, observed in the SSP spectra is used frequently as a measure of conformational order at surfaces containing alkyl chains. For example, a linear alkyl chain with an even number of carbon atoms extended in an *all-trans* conformation possesses inversion symmetry along the carbon backbone meaning that r^+ and d^+ are SF inactive (Figure 5.6). In principle r^+ and d^+ can contribute a SF spectrum only when this symmetry is broken with gauche defects.

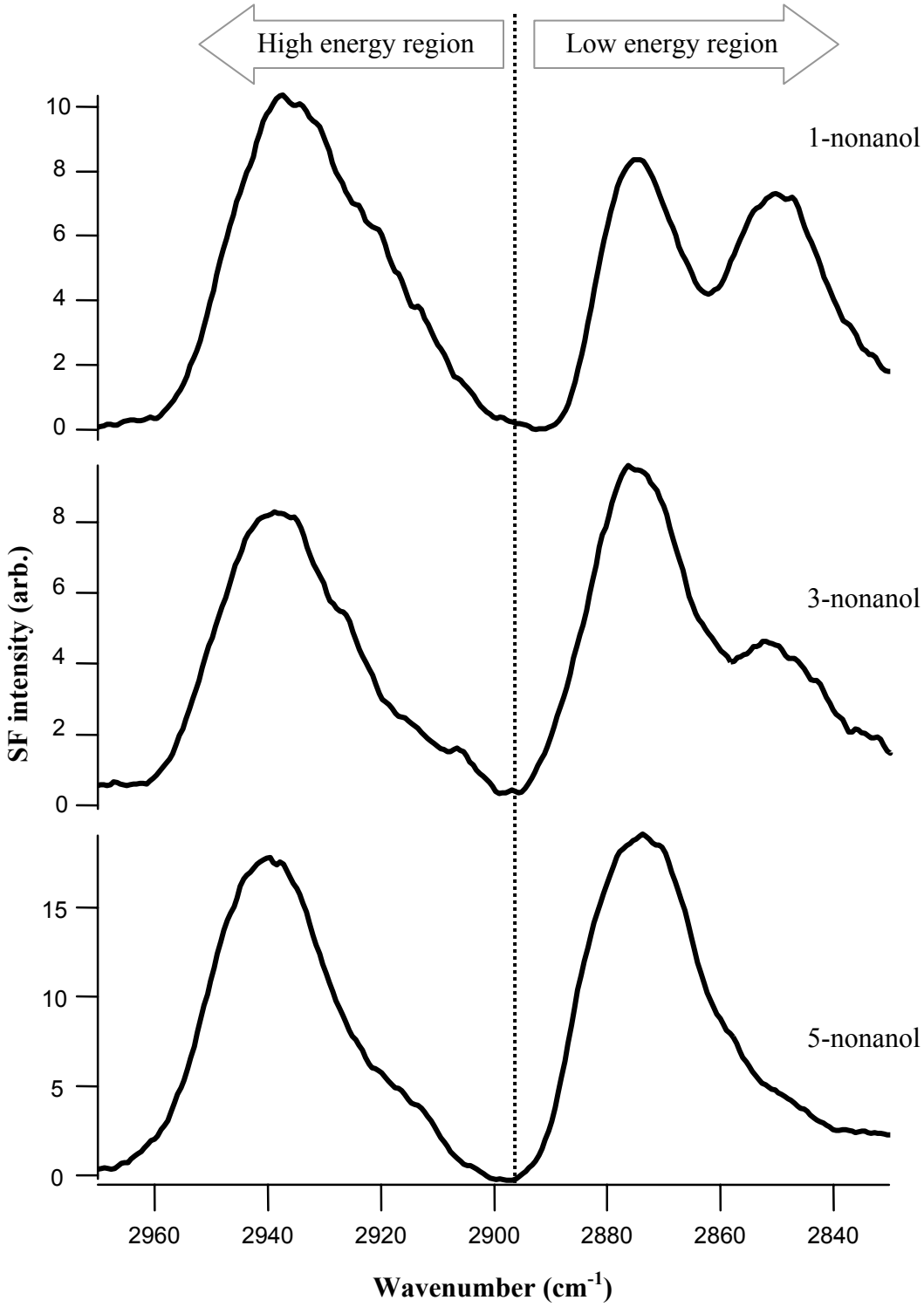

Figure 5.4. Surface vibrational spectra of 1-, 3- and 5-nonanol under SSP polarization conditions

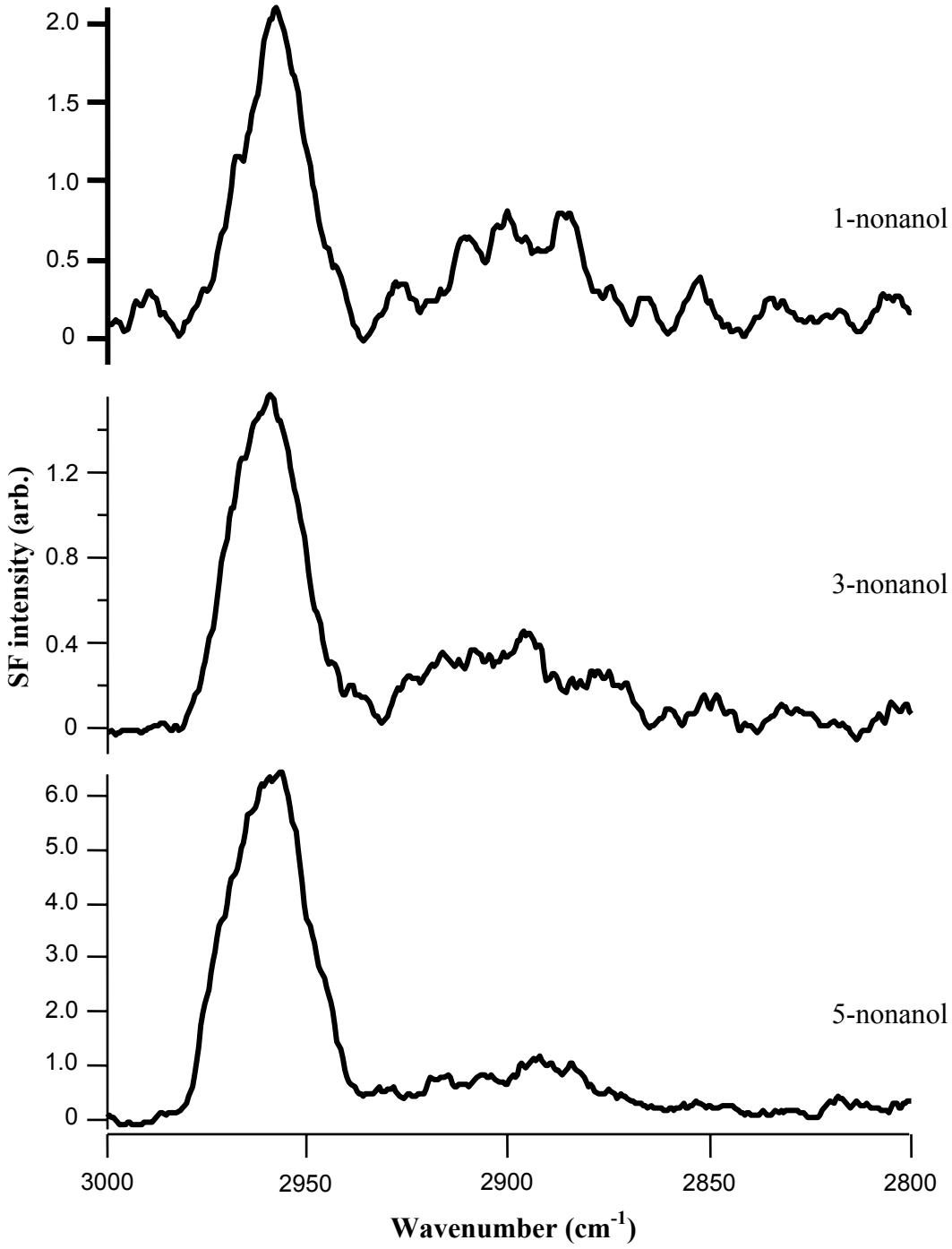

Figure 5.5. Surface vibrational spectra of 1-, 3- and 5-nonanol under SPS polarization conditions.

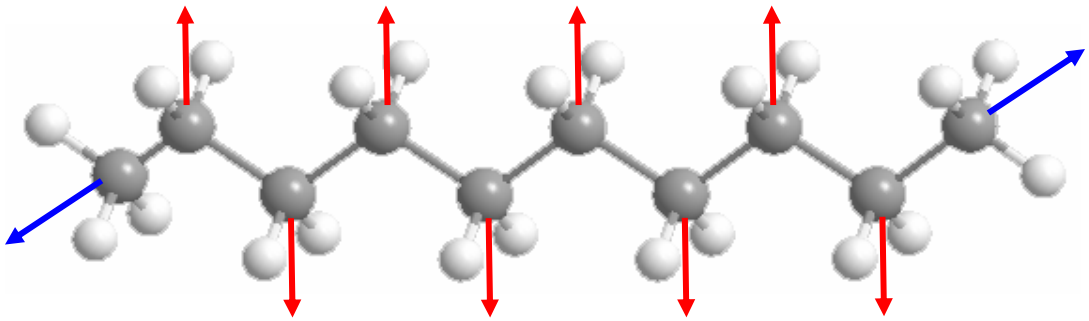

Figure 5.6. A linear alkyl chain with even number of carbon atoms extended in an all-trans conformation showing the local inversion symmetry for transition moments of CH_2 and CH_3 symmetric stretch vibrations.

However, if the chain consists of an odd number of carbon atoms, the molecular inversion symmetry is broken but local inversion symmetry exists between all CH_2 groups except the last one. Therefore, those terminal CH_2 groups and the CH_3 groups becomes SF active and can contribute to the d^+ and r^+ bands, respectively. The r^+/d^+ values of the nonanols are given in Table 5.1. These values increase systematically and significantly, resulting in a ~10 fold increase with respect to functional group placement and the largest r^+/d^+ ratio is observed for the symmetric 5-nonanol. The increase is attributed to the increase in surface order as the hydroxyl group position shifts toward the center of the molecules.

Table 5.1. r+/d+ ratio of alcohols and ketones.

	-OH or =O position on the carbon backbone		
Isomers	**1**	**3**	**5**
Octanol	0.6 ±0.5	1.4 ±0.5	
Nonanol	0.8 ±0.2	2.4 ±0.3	8.8 ±0.7
Nonanone	0.7 ±0.5	2.7 ±0.5	4.6 ±2.1

1-nonanol

The low energy region of 1-nonanol SSP spectrum (top, Figure 5.4) is fit with two functions corresponding to a methylene symmetric stretch (CH_2-SS, d+, 2851 cm^{-1}, 21 cm^{-1} FWHM) and a methyl symmetric stretch (CH3-SS, r^+, 2875 cm^{-1}, 15 cm^{-1} FWHM). The high energy region of the spectrum is fit with up to four vibrational functions corresponding to a methylene Fermi resonance (CH_2-FR, d^+_{FR}, 2911 cm^{-1}, 16 cm^{-1} FWHM), a methylene asymmetric stretch (CH_2, d^-, 2921 cm^{-1}, 15 cm^{-1} FWHM), a methyl Fermi resonance (CH_3-FR, r^+_{FR}, 2937 cm^{-1}, 22 cm^{-1} FWHM), and a methyl asymmetric stretch (CH_3-AS, r^-, N/A cm^{-1}, N/A FWHM). All of these assignments are based on previous bulk and surface studies of alkyl vibrational structures.[9,50,80,110,111,127,133,134] Typical contribution of the CH_3-AS to a SSP spectrum is vanishingly small. The fit results are tabulated in Table 5.2. The SPS spectrum (top, Figure 5.5) shows a relatively strong r^- band at ~2960 cm^{-1} along with very weak intensity in CH_2-FR region (~2900 cm^{-1}). The intensities at the C-H symmetric stretch region (2880-2840 cm^{-1}) for CH_3-SS and CH_2-SS are within the noise level. No other feature can be assigned with confidence.

Table 5.2. The 1-nonanol SSP spectrum fitting results.

Feature	**Position (cm^{-1})**	**Width (cm^{-1})**
d^+	2851 ± 1	21 ± 1
r^+	2875± 1	15 ± 1
d^+_{FR}	2911± 7	16 ± 5
d^-	2921± 3	14 ± 3
r^+_{FR}	2937 ± 1	22 ± 1

Of the nonanols, 1-nonanol shows the most significant d^+ band (and correspondingly the smallest r^+/d^+ ratio, 0.8 ± 0.2) implying the lowest degree of conformational order. Given the position of hydroxyl group and water/1-alcohol interface studies,[118,119,125] this result is surprising. 1-nonanol consists of 1 CH_3 group, 7 CH_2 groups and 1 terminal CH_2OH group (Figure 5.1). Depending on the molecular orientation and conformation at the surface either all or some of these groups may contribute to the observed spectrum. The 1-nonanol spectrum acquired under SSP polarization conditions is very similar to that of nonane spectrum shown in Chapter 3 suggesting that the surface of 1-nonanol is populated primarily by methyl groups and that the chains are considerably disordered. Assuming that the highly electronegative oxygen breaks the local inversion symmetry between the CH_2 groups attached to the 1st and 2nd carbon atoms of the molecule, contributions to the d^+ band can come from 3 sources; the CH_2 groups of the terminal CH_2OH, the extra CH_2 group if the chain is fully stretched and the CH_2 groups that becomes SF active due to gauche defects along the chain.

$$I(d^+) = I(d^+_{CH2OH}) + I(d^+_{extra} \text{ or } d^+_{gauche})$$

Here d^+_{extra} and d^+_{gauche} are mutually exclusive because if gauche defects exists, the extra CH_2 is no longer unique. Although isolating the contributions from these sources is very difficult, a qualitative comparison of their contributions can be estimated from comparing the 1-nonanol spectrum with spectra of 3- and 5-nonanol. The d^+ band in 1-nonanol spectrum has a bandwidth of 24 cm^{-1}. As has been shown in Ch 4, the band broadening of the d^+ band originates from gauche defects along the chain. The underlying intensity of the broad d^+ feature implies the relative amount of

the gauche CH_2 groups. The symmetric band shape of the d^+ band also suggest that the center frequency of the transition moment corresponding to the terminal CH_2 symmetric stretch is similar in energy to that of gauche CH_2 groups as the case for the haloalkane systems. The difference in the center frequencies of those bands is lower than our spectral resolution of the instrument.

The observed r^+ band likely results from surface active CH_3 groups. The narrow bandwidth (15 cm^{-1}) and symmetric band shape suggests a very homogeneous environment for those groups. Although it is not possible to quantify the absolute coverage, the relative intensity in r^+ implies that the methyl terminus of the 1-nonanol dominates the surface structure at the liquid/vapor interface. Again, surface tension studies support this premise. The surface tension of neat 1-nonanol (25.1 mN/m) is very similar to that of nonane (24.2 mN/m) meaning that both solvents have comparably low surface free energies. If the surface contained a significant number of free dipoles, we would expect a much higher surface tension. For reference, water has a surface tension of 72 mN/m (at 25 ^oC) and both vibrational SF studies and simulations have estimated that ~25% of all surface -OH groups are free.[135,136] The strong intensity in the r^+ feature also implies a net perpendicular orientation of those CH_3 groups with respect to the surface. The absence of the r^- band near ~2960 cm^{-1} supports this conclusion. The broad, incompletely resolved feature above ~2900 cm^{-1} shows signs of a strong r^+_{FR}, and weak d^- and d^+_{FR} as expected, although we note that there are high error bars associated with fitting this high energy feature with three separate bands each having three adjustable parameters (frequency, bandwidth, and intensity).

Using the different molecular structures discussed previously, the surface molecular structure of 1-nonanol can be evaluated based on the vibrational signatures in the surface spectra acquired with different polarization combinations, SSP and SPS. Out of the four molecular geometries, only two are applicable to 1-nonanol system: fully-stretched and partially-extended. Having the functional group at the 1st carbon makes V and tent (/\) geometries unlikely. The possibility that the 1-nonanol adopts a fully-stretched molecular structure can be dismissed for the following reasons: in the case of a fully stretched structure at the surfaces there will be no contribution to the d^+ band from gauche CH_2 groups and the band shape should be quite sharp. However, the observed d^+ feature of 1-nonanol at SSP spectrum is strong and rather broad (~24 cm^{-1} bandwidth). The fact that the d^+ band is broad implies that there is a significant contribution from gauche CH_2 groups. Based on the r^+ intensity and narrow and symmetric band shape, we assume that the chains do not adopt mixed orientations with some fraction of molecules having surface CH_3 groups and some having bulk CH_3 groups. If this molecular arrangement were present at the interface, the bulk CH_3 groups of a fully stretched structure could destructively interfere with the surface CH_3 groups due to the phase differences. This interaction would reduce the intensity and alter the band shape. In addition, due to the different sampling environments broadening in the bandwidth of the r^+ band may occur.

As mentioned before, a partially-extended ensemble of molecules at the liquid/vapor interface would have a broad d^+ band due to the contributions from the gauche CH_2 groups. Furthermore, in the case of molecular structures that have CH_3 groups aligned toward vapor phase, a sharp r^+ band would be observed. Any bulk

CH_3 group is expected to be highly disordered and unlikely to contribute to the r^+ band. The observed broad (~21 cm^{-1}) d^+ band and the sharp (15 cm^{-1}), symmetric r^+ band, both of which show no sign of destructive interference, support a partially-extended surface structure. The results suggest that the 1-nonanol/vapor interface is composed of chains having a persistence-length that is less than ~13 Å (the length of a fully extended chain) and the surface composition expected to be dominated by CH_3 groups.

3-Nonanol

Although 3-nonanol and 1-nonanol are isomers, the observed SSP spectrum of 3-nonanol (middle, Figure 5.4) differs significantly from its linear counterpart. The SPS spectra of the two isomers look very similar (middle, Figure 5.5). 3-nonanol consists of 2 CH_3 groups, 6 CH_2 groups and 1 CHOH group (Figure 5.1). From the standpoint of analyzing vibrational SF spectra, there are now two CH_3 groups that can contribute to an r^+ band. This situation may result in an increase in the observed intensity in this feature. The SSP spectrum is fit with parameters similar to those of 1-nonanol except for an additional band associated with the isolated CH stretch near 2900 cm^{-1}. The results of the fit are given in Table 5.3. The low energy region is fit with two functions corresponding to a d^+ band at 2851 cm^{-1} (~21 FWHM) and an r^+ band at 2875 cm^{-1} (~19 FWHM). Again, the high energy region is fit up to three functions corresponding to a d^+_{FR} (2907 cm^{-1}, ~12 cm^{-1} FWHM), d^- (2925 cm^{-1}, ~22 cm^{-1} FWHM), and r^+_{FR} (~2941 cm^{-1}, ~21 cm^{-1} FWHM). The 4th function corresponding to r^- band was not used given the absence of intensity in the SSP spectrum near ~2960 cm^{-1}. The SPS spectrum of 3-nonanol is similar to that of 1-

nonanol (top, Figure 5.4). The spectrum shows a relatively strong but asymmetric band assigned to r^- band and very weak, featureless intensity near 2900 cm^{-1} region. Due to the very low signal to noise level, the r^+ and d^+ bands cannot be identified.

Table 5.3. The 3-nonanol SSP spectrum fitting results.

Feature	Position (cm^{-1})	Width (cm^{-1})
d^+	2851 ± 1	21 ± 6
r^+	2875 ± 1	19 ± 1
d^+_{FR}/C-H (?)	2907 ± 1	11 ± 1
d^-	2925 ± 3	22 ± 5
r^+_{FR}	2940 ± 2	21 ± 1

The SSP spectrum shows considerably weaker d^+ band intensity, and correspondingly larger r^+/d^+ ratio, 2.4 ± 0.3, relative to the 1-nonanol SSP spectrum. The loss of intensity in the d^+ band can be attributed either to the loss of terminal CH_2 group that existed in 1-nonanol or to a drop in the number of gauche defects or some combination of both sources. The high energy region of the spectrum (above ~2900 cm^{-1}) is similar to the 1-nonanol spectrum. Again, the absence of the r^- band in the SSP spectrum signifies a net perpendicular orientation of the surface CH_3 groups. We also observe a loss in intensity of the CH_2 features. In addition, a more pronounced band at ~2907 cm^{-1} is observed and assigned tentatively to C-H stretch of the CHOH group. A band at this frequency usually corresponds to d^+_{FR} mode. However, there is no reason to expect an increase in the intensity of d^+_{FR} when all the other CH_2 modes, d^+ and d^- lost intensity compared to those of 1-nonanol. 3-nonanol also gained an

extra vibrational mode, C-H stretched, compare to 1-nonanol. In addition, the maximum intensity of the feature in the high energy region is shifted toward the r^+_{FR} band as expected.

The location of the -OH group in 3-octanol makes all four different surface structures possible candidates as the geometry that can be adopted by 3-nonanol at the liquid/vapor interface. These surface geometries include V or /\ shaped molecular structures. Again the fully-stretched option is dismissed for reasons already outlined in the case of 1-nonanol, namely the broadness of the observed d^+ band in SSP spectrum, and the strong symmetric r^+ band. The observed features in the SSP spectrum of 3-nonanol support a partially-extended system of 3-nonanols at the surface. There are some gauche defects presumably along the six carbon chain because partial disorder causing the d^+ band to broaden. The r^+ band is strong and symmetric. The feature does not show signs of destructive interference from CH_3 groups aligned in opposing directions.

Two observables argue against the V and /\ shaped surface molecular structures: The first is the relatively large width of the d^+ band. If the 3-nonanol adopts either bent geometries, we would expect CH_2 groups to contribute to the d^+ band according to the projection of CH_2 transition moments along the surface normal. Furthermore, the long arm (6 carbon lengths) should have no or very few gauche defects meaning that the extra CH_2 on the arm will contribute to the d^+ band in a similar manner expected for the extra CH_2 group of the short arm. Both of these contributions would give rise to a sharp, symmetric d^+ band that has significant intensity. The fact that the d^+ band in the 3-nonanol spectrum is broader (and weaker)

than in the 1-nonanol spectrum suggests that the surface molecular structure is partially extended. The second observation that makes the V and /\ shaped geometries unlikely is the absence of r^- band in SSP spectra. For an adopted bent geometry, either up or down, the transition moments of the CH_3 groups are expected to be angled with respect to the surface meaning that both r^+ and r^- bands should be observed in SSP and SPS spectra. For example, the SSP spectra (Figure 5.12, section 5.2.2) of 3-octanols adsorbed to an aqueous/vapor interface show both features quite clearly. The absence of these features in the neat 3-nonanol spectrum supports the partially extended geometry for 3-nonanol molecules at the liquid/vapor interface. One end pointing toward the vapor phase and the other end randomized in solution. As mentioned in Chapter 1 and 2, due to the difficulty associated with identifying the absolute phase contribution, it is very difficult to identify which end is pointing toward the vapor phase.

5-nonanol

The 5-nonanol SSP spectrum (bottom, Figure 5.4) is considerably different from the spectra of both 1- and 3-nonanols. The SPS spectrum of 5-nonanol is similar to the others except there is no observed intensity around 2900 cm^{-1} (bottom, Figure 5.5). The spectrum shows relatively strong r^- band at ~ 2960 cm^{-1}. The 5-nonanol molecules differ from 3-nonanol molecules only in the placement of the alcohol functional group. The -OH group is positioned on the middle carbon instead of the 3rd carbon of the alkyl backbone. As with 3-nonanol, the molecule has 2 CH_3, 6 CH_2 and 1 CHOH groups (see Figure 5.1). In the SSP spectrum of 5-nonanol the d^+ band has very little intensity and appears as a shoulder on the low frequency side of a very

strong r^+ band. In addition, the bandwidth and the shape of the r^+ band changes significantly. The shape of the r^+ band signifies a destructive interference of surface CH_3 groups with bulk CH_3 groups. The overall width of the high energy feature (>2900 cm^{-1}) narrows significantly as expected due to the drop in intensity of the d^+ band. A slight shoulder on high energy side of this feature suggests a weak contribution from the CH_3-AS (r^-) but, in fact, it is very small. The results of fitting the SSP spectrum of 5-nonanol are given in Table 5.4. The d^+ feature is fit with a band having center frequency at ~2853 cm^{-1} and ~18 cm^{-1} FWHM. The r^+ feature appears very broad with a flattened top suggesting contributions from two different CH_3 groups. After many unsuccessful attempts to fit the feature with two functions having same phase, we have successfully fit the feature with two r^+ bands having the same center frequency at ~2874 cm^{-1} but with opposite phases. The resultant bandwidths are ~18 and ~13 cm^{-1}.

Table 5.4. The 5-nonanol SSP spectrum fitting results.

Feature	**Position (cm^{-1})**	**Width (cm^{-1})**
d^+	2853 ± 1	21 ± 1
r^+_1	2874 ± 4	18 ± 1
r^+_2	2874 ± 2	13 ± 1
d^+_{FR}/d^-	2917 ± 3	17 ± 1
$r^+_{FR,\,1}$	2940 ± 1	22 ± 2
$r^+_{FR,\,2}$	2940 ± 2	18 ± 3

The observed features are consistent with a structure that is either fully-stretched or very close to a fully-stretched molecular structure of 5-nonanol at the

liquid/vapor surface. The small number of gauche defects along with destructive interference of the two r^+ bands support the picture as does the asymmetric band shape of the r^+ band.. Starting with the premise that the trend observed between 1-nonanol and 3-nonanol should continue with 5-nonanol, molecular structures of either up (V) or down (/\) bent geometries are not anticipated. Due to the anticipated high conformational order, the proposed surface structure of 5-nonanol may be observed by X-ray scattering experiments. The structure is unusual and unexpected; however, it follows the trend observed between 1- and 3-octanols. The ordered surface structure may be imagined as a fully stretched molecular geometry of molecules interacting at the center through strong dipole-dipole and hydrogen bonding interactions.

Order at the liquid/vapor interfaces of nonanols increases as the OH group position advances toward the center of the nine carbon chain. The surface molecular structure changes from a partially extended molecular geometry for 1-nonanol to an almost fully extended molecular structure of 5-nonanol. The surface of 1-nonanol having primarily CH_3 groups and disordered chains show clear differences with 3- and 5-nonanol surface structure where surface is covered mostly with CH_3 groups.

5.1.2. Nonanones

The surface vibrational spectra of nonanones under SSP polarization conditions are shown in Figure 5.7. SPS spectra of these ketones are shown in Figure 5.8. As in the alcohols, the absolute intensity of a given feature in one spectrum cannot be compared to the same feature in different spectrum. Again, however, the intensity ratio, r^+/d^+, can be compared where appropriate. Both SSP and SPS spectra of nonanone isomers closely resemble to those of the corresponding nonanol isomers. Thus, the zeroth order interpretation is that dipolar forces but not hydrogen bonding are responsible for overall geometry adopted by molecules at surfaces. However, subtle differences do exist between the nonanone and nonanol isomers. The signal/noise level in the nonanone spectra are reduced slightly compared to those of alcohols. Additionally, low frequency features on the SSP spectra of nonanone isomers are not resolved as well as the ones of the nonanol isomers. These observations suggest that the functional groups of nonanols do adopt a better defined surface structure with narrower distributions compared to the nonanones. Thus, average surface structures of these strongly interacting molecules may be determined by dipolar interactions but the hydrogen bonding may restrict the distribution of orientations.

Again, the surface vibrational spectra of nonanone isomers under SSP polarization conditions are broken into two main regions: the low energy region (below ~2900 cm^{-1}) contains information from methylene and methyl symmetric stretches. The high energy region (above ~2900 cm^{-1}) contains information of Fermi

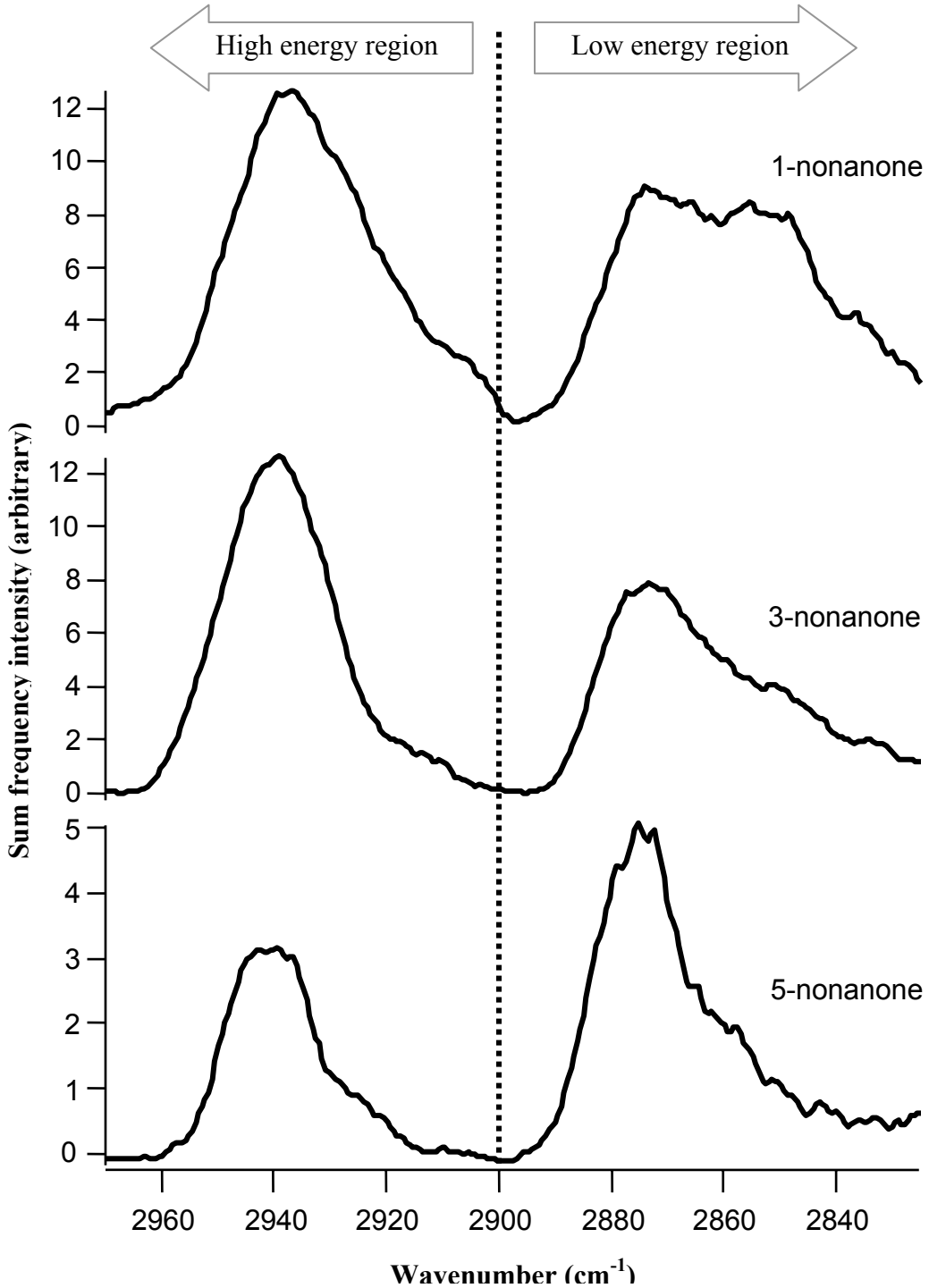

Figure 5.7. Surface vibrational spectra of 1-, 3- and 5-nonanone under SSP polarization conditions.

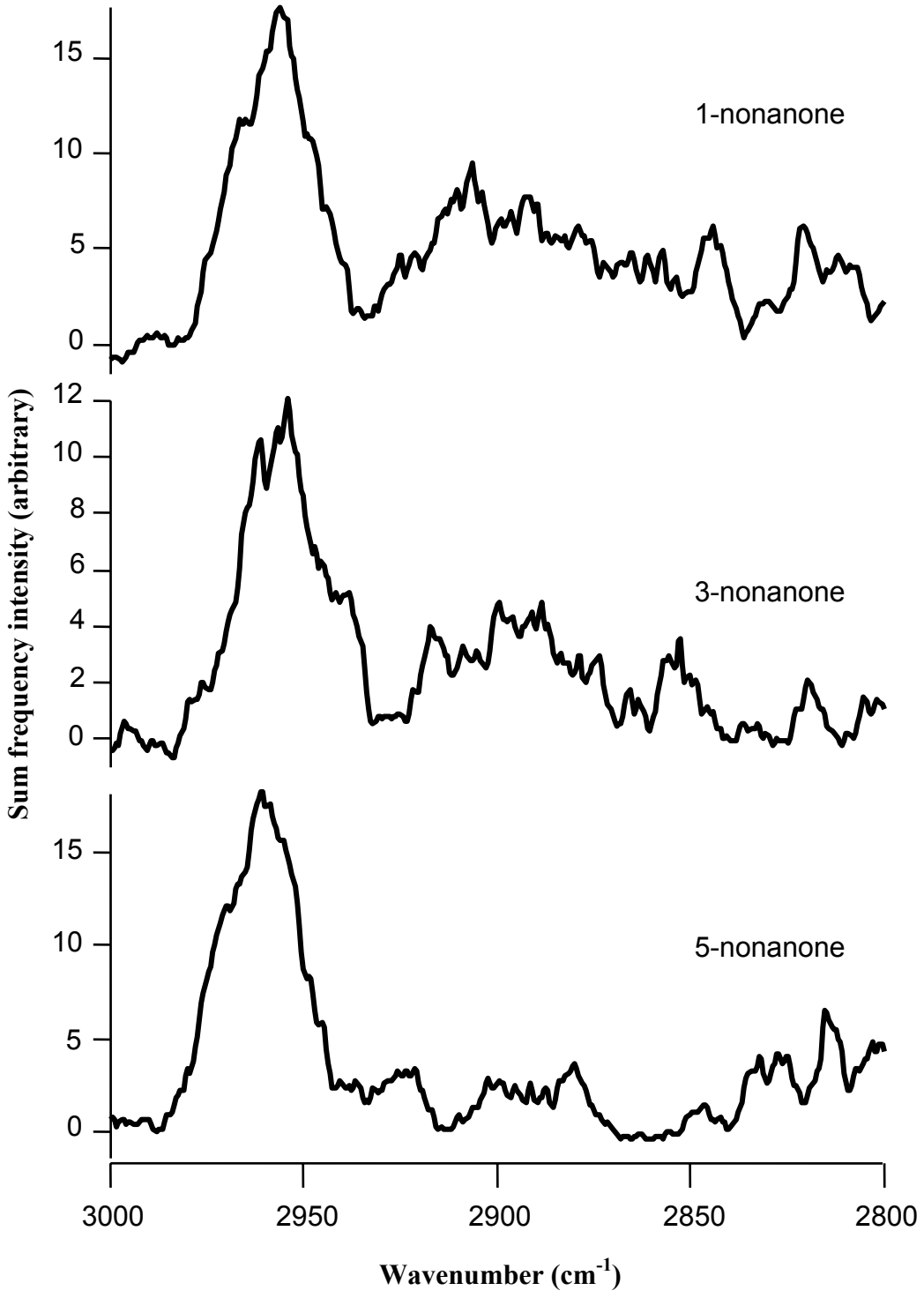

Figure 5.8. Surface vibrational spectra of 1-, 3- and 5-nonanone under SPS polarization conditions.

resonances and asymmetric stretches of methylene and methyl groups. The center frequency that results from fitting will be given in the descriptions of individual systems. The observed spectra of nonanone isomers are significantly different from each other showing the importance of the =O group position on the carbon backbone for the surface order. The SPS spectra of nonanone isomers are similar to each other. Again, the signal to noise levels the spectra are considerably lower than the corresponding SSP spectra due to the reasons stated during the alcohol discussion. The SPS spectra are dominated by the r^- feature at ~2960 cm^{-1}. In addition, a decrease in intensity in ~2900 cm^{-1} region is observed with a shift in =O group position.

1-nonanone

Of the nonanones, 1-nonanone is the only one that has the =O group at its terminus. The surface vibrational spectra of 1-nonanone are acquired under both polarization, SSP and SPS, conditions. The SSP spectrum of 1-nonanone (top, Figure 5.7) consists of two main regions. The low energy region of 1-nonanone SSP spectrum is fitted with two functions corresponding to a methylene symmetric stretch (CH_2-SS, d^+, 2852 cm^{-1}, 25 cm^{-1} FWHM) and a methyl symmetric stretch (CH3-SS, r^+, 2874 cm^{-1}, 18 cm^{-1} FWHM). The high energy region of the spectrum is fit with up to four vibrational functions corresponding a methylene Fermi resonance (CH_2-FR, d^+_{FR}, 2906 cm^{-1}, 10 cm^{-1} FWHM), a methylene asymmetric stretch (CH_2, d^-, 2921 cm^{-1}, 21 cm^{-1} FWHM), a methyl Fermi resonance (CH_3-FR, r^+_{FR}, 2938 cm^{-1}, 23 cm^{-1} FWHM), and a methyl asymmetric stretch (CH_3-AS, r^-, N/A cm^{-1}, N/A FWHM). We are unable to identify any intensity associated with the r^- feature in the SSP spectrum. The fit parameters are tabulated on Table 5.5. The 1-nonanone SPS spectrum (top,

Figure 5.8) is very similar to its alcohol counterpart. The spectrum is dominated by the r^- at ~2960 cm^{-1}. A very weak and broad band at ~2900 cm^{-1} is also observed. Due to the low signal-to-noise level it is very difficult to make any definitive assignments.

The 1-nonanone consists of 1 CH_3 group, 7 CH_2 groups and 1 terminal CHO group. All or some of these groups may contribute to an observed spectrum depending on the molecular orientation and conformation of the molecule at the surface. The 1-nonanone SSP spectrum is very similar to both 1-nonanol and nonane SSP spectra, again, implying that the surfaces of this solvent is occupied primarily by methyl groups. The similar surface tensions of nonanone and nonanol (25.1 mN/m for 1-nonanone vs 24.2 mN/m for 1-nonanol and 22.7 mN/m for nonane) support this picture.

Table 5.5. The 1-nonanone SSP spectrum fitting results.

Feature	**Position (cm^{-1})**	**Width (cm^{-1})**
d^+	2852 ± 1	25 ± 2
r^+	2874 ± 1	18 ± 2
d^+_{FR}	2906 ± 2	10 ± 2
d^-	2921 ± 1	21 ± 2
r^+_{FR}	2938 ± 1	23 ± 2

Assuming that the =O group breaks the inversion symmetry between the 1st and 2nd carbon, the intensity of the d^+ band in the SSP spectrum of 1-nonanone can come from two sources; the extra CH_2 group if the chain is fully stretched and the CH_2 groups that becomes SF active due to gauche defects along the chain.

$$I(d^+) = I(d^+_{extra} \text{ or } d^+_{gauche})$$

The extra CH_2 and gauche CH_2 are mutually exclusive because the extra CH_2 becomes a part of the gauche CH_2 population when there are gauche defects along the chain. Although it is very difficult to isolate the contributions of these sources, a qualitative comparison of the 1-nonanone spectrum with 3- and 5-nonanone spectra allows us to determine the dominant component. The d^+ band in 1-nonanone SSP spectrum has a bandwidth of 25 cm^{-1}. Usually, gauche CH_2 contributions cause the observed d^+ band to broaden. The symmetric band shape of the feature suggest that the center frequencies of the components contributing to the d^+, gauche and extra CH_2, are similar to each other and the difference between these frequencies are less than the spectral resolution of our instrument.

The observed r^+ band has a comparable intensity to the d^+ band with a linewidth of ~18 cm^{-1}. The r^+ feature is still sharp enough to consider the contributing CH_3 groups to be sampling a similar environment. In addition, the sharp and symmetric band shape suggests that there is no destructive interference from any bulk CH_3 groups. The relative intensities of the both features and the broadness of the d^+ band suggest that the surface of the 1-nonanone is occupied primarily by CH_3 groups. The high energy feature shows the dominance of the r^+_{FR} band by having the maximum intensity of the feature at ~2935 cm^{-1}, very close to the vibrational frequency of the r^+_{FR}. In addition, absence of the r^- band in the SSP spectrum (and the absence of the r^+ band in the SPS spectrum) along with a strong r^- band in SPS spectrum of 1-nonanone suggest that surface methyl groups have a net transition moment parallel to the surface normal.

Amongst the suggested molecular geometries, only the partially-extended molecular structure is consistent with the observed broad d^+ band and the net alignment of CH_3 groups and symmetric band shape. The rest of the molecular structures can be dismissed by arguments similar to those given in the presentation of the 1-nonanol discussion. One striking difference between 1-nonanone and 1-nonanol is that r^+ and d^+ features of 1-nonanone are not resolved as well as 1-nonanol. This observation suggests that the 1-nonanone/vapor interface has a broader distribution of molecular conformations compare to 1-nonanol.

3-nonanone

As with the alcohol isomers, the SSP spectrum of 3-nonanone (middle, Figure 5.7) is significantly different from that of 1-nonanone. Compared to 1-nonanone, the 3-nonanone molecular structure has one additional CH_3, one less CH_2 group and no CH group. The SSP spectrum of 3-nonanone is fit in similar manner as 1-nonanone. The fit results are given in Table 5.6. The low energy region of the spectrum is fit with three functions corresponding to a d^+ band (2851 cm^{-1}, 15 cm^{-1} FWHM) and two constructively interfering r^+ bands (2868 cm^{-1} with 19 cm^{-1} FWHM, and 2878 cm^{-1} with 13 cm^{-1}). Both d^+ and r^+ bands are broader compare to 3-nonanol. As usual, the high energy region is fit with three functions corresponding to a combination band of d^+_{FR}/d^- (2925 cm^{-1}, 16 cm^{-1} FWHM), and two r^+_{FR} band (2934 cm^{-1} and 2944 cm^{-1} with 18 cm^{-1} FWHM for both). No r^- feature is observed. The SPS spectrum of 3-nonanone (middle, Figure 5.8) is similar to that of 1-nonanone. The spectrum consists of a r^- band having moderate intensity at ~2960 cm^{-1} and a weak, very broad band at ~2900 cm^{-1}.

Table 5.6. The 3-nonanone SSP spectrum fitting results.

Feature	Position (cm^{-1})	Width (cm^{-1})
d^+	2851 ± 2	15 ± 3
r^+_1	2868 ± 2	19 ± 2
r^+_2	2878 ± 2	13 ± 3
d^+_{FR}/d^-	2925 ± 1	16 ± 2
$r^+_{FR,\,1}$	2934 ± 4	18 ± 3
$r^+_{FR,\,2}$	2944 ± 3	18 ± 2

The d^+ band intensity in 3-nonanone SSP spectrum is considerably decreased compared to that of 1-nonanone. The relative intensity of the r^+ band is increased with respect to the d^+ band resulting in a significantly higher r^+/d^+ ratio, ~ 2.7. Due to increase in the number of methyl groups, an increase in the r^+ band intensity relative to the d^+ band is expected. However, the amount of the increase cannot be estimated due to the unknown surface coverage and orientation. The high energy feature (> 2900 cm^{-1}) in the SSP spectrum is narrower compared to the 1-nonanone case as expected due to the loss of intensity in the d^+ band as well as the increase in the methyl density on the surface. The peak position of the high energy feature is shifted toward the r^+_{FR} compared to the 1-nonanone spectrum. As is the case comparing the features 1-nonanone to that of the 1-nonanol, the 3-nonanone features are not resolved as well as those in the 3-nonanol spectrum suggesting a broader distribution of molecular conformations at the interface.

Given the position of the =O group in the C_3 position, all four geometries are possible candidates for 3-nonanone at the liquid/vapor interface. However, only the

partial extended structure is supported by the observed features. The fully-stretched molecular structure can be dismissed with the same arguments presented in 3-nonanol case, namely a broad d^+ band in the SSP spectrum due to the gauche defects. If the geometry were a fully-stretched, there would not be any gauche defects and a narrow band d^+ would be expected, if any. Both the up and down bent molecular structures can be dismissed due to the width of the observed d^+ band – again, a narrow band would be expected – and the absence of the r^- band in the SSP spectrum as well as the absence of the r^+ band in SPS spectrum. Therefore, the inferred surface structure adopted by 3-nonane at the liquid/vapor interface is a partially-extended geometry where the structure has a persistence length of order at the vapor side.

5-nonanones

The surface vibrational spectra of 5-nonanone have been acquired in both SSP and SPS polarizations. The SSP spectra of 5-nonanone (bottom, Figure 5.7) consists of two main regions. The low energy region of the spectrum is fit with two vibrational features corresponding to a d^+ (2858 cm^{-1}, 29 cm^{-1} FWHM) and an r^+ (2876 cm^{-1}, 17 cm^{-1} FWHM). The high energy region is fit with a combination of bands corresponding to a combination of d^+_{FR} and d^- (2915 cm^{-1}, 12 cm^{-1} FWHM), and a r^+_{FR} (2940 cm^{-1}, 18 cm^{-1} FWHM). There is no sign of r^- feature. All the fit results are given in Table 5.7. The only feature observed in the SPS spectrum (bottom, Figure 5.8) is an r^- band at ~2960 cm^{-1}.

Table 5.7. The 5-nonanone SSP spectrum fitting results.

Feature	Position (cm^{-1})	Width (cm^{-1})
d^+	2858 ± 5	29 ± 6
r^+	2876 ± 1	17 ± 1
d^+_{FR}/d^-	2915 ± 3	12 ± 2
$r^+_{FR,}$	2940 ± 2	18 ± 2

The 5-nonanone molecule is composed of exactly the same functional groups as 3-nonanones (see Figure 5.1). The only difference is that the =O group is symmetrically positioned in the 5th, center, position. Although the observed SSP spectrum is very different than both 1- and 3-nonanone, the spectrum follow the trend established by changing the carbonyl fraction to the 1 and 3 position. The intensity of the d^+ band decreases even further compared to that of 3-nonanone indicating a decrease in the gauche defects amount along the 5-nonanone chain. The resulted r^+/d^+ ratio, ~4.6, is comparably lower than for the analogous alcohol, 5-nonanol (~8.8). However, this value is still much higher than that of 1-nonanone, 0.7. In addition, the bandwidth and the shape of the r^+ band changes significantly. Results of 5-nonanol suggest that the bulk-CH_3 groups destructively interfere with the surface CH_3 groups. The similar destructive interference may also apply to the 5-nonanone surface. However, it was possible to fit a single r^+ mode and fitting with two destructively interfering r^+ modes is avoided for reasons discussed in section 2.1.4 of Chapter 2. Similar to 3-nonanone, the overall width of the high energy feature narrows significantly compared to 1-nonanone as expected given the drop in intensity of the

d^+ band intensity. There is no sign of the r^- band indicating a net perpendicular orientation for the CH_3 groups with respect to the surface.

As in the 5-nonanol case, the observed features indicate that the surface molecules adopt either a fully-stretched structure or a structure which is very close to the fully-stretched molecular structure at the 5-nonanone/vapor interface. The very low occurrence of gauche defects and high r^+/d^+ ratio support the picture. In addition the asymmetric band shape of the r^+ band supports the proposed structure. Although not as well ordered as surfaces of 5-nonanol, the surface structure of 5-nonanone may be possible to observe with X-ray scattering experiments.

In summary, we have compared 1-, 3-, and 5-nonanone's surface vibrational spectra in order to observe the effect of the position of the =O group on the carbon backbone. Comparison of the observed features indicate that the order in surface structure increases with the shift in the =O group toward the bulk solution. The shifted =O groups and corresponding strong dipolar interaction between chains extends the surface induced order of the chain. The surface molecular structure is changed from a partially extended molecule to an almost fully stretched molecule as the source of interchain interactions moves towards the center of the chain. Similar to 1-nonanol, 1-octanol, and 1-haloalkanes, the surface of 1-nonanone is a mixture of dominating CH_3 and CH_2O. The surface structure then becomes fully covered by CH_3 groups for 3- and 5-nonanones.

5.2. C_8 Molecules - Octanols

The surface vibrational spectra of eight carbon alcohols have been acquired both at neat liquid/vapor and aqueous/vapor interfaces by vibrational sum frequency spectrometer. The vibrational spectra of alcohols were acquired in two different polarization conditions, SSP and SPS. Again, the three latter combinations denote the polarizations of the sum, visible and infrared frequencies. The molecular structures of 1- and 3-octanol vary from each other by the placement of the hydroxyl group (Figure 5.9). The difference in hydroxyl group position on the molecular structure will enable us to determine the effect of the hydrogen bonding as well as the geometry on the surface structure. In this section, we present the findings from neat 1- and 3-octanol at theliquid/air interfaces and monolayers of 1-and 3-octanol at aqueous/air interfaces.

5.2.1. Neat Octanol Surfaces

Surface tensions of 1- and 3-octanol are 27 mN/m and 31 mN/m, respectively. These surface tensions are much closer to the surface tensions of neat alkanes (22 -24 mN/m for alkanes ranging in length from 8 to 21 carbons) than to the surface tension of water (72 mN/m). This suggests that the surface of octanols do not consist of many free or dangling OH bonds. In addition slightly higher surface tension of 3-octanol suggests a rougher surface structure than the surface structure of linear isomer.

One might associate a lower surface tension of 1-octanol with a higher degree of conformational order at the liquid/vapor interface. However, the surface vibrational studies of 1- and 3-octanol show the opposite behavior. The surface vibrational spectra of the 1- and 3-octanol are acquired under SSP and SPS polarization conditions and are presented in Figure 5.10 and Figure 5.11. The SSP spectra consist

of two regions. The low energy region (below 2900 cm^{-1}) contains information of symmetric stretch contributions and the high energy region (above 2900 cm^{-1}) contains information of Fermi resonances and asymmetric stretches of the methylene and methyl groups. Since the high energy feature is not well resolved, the discussion will primarily focus on the low energy region of the spectrum.

1-octanol

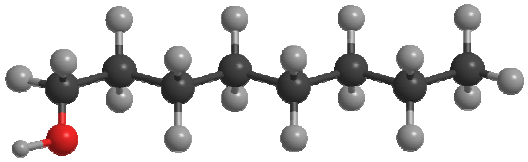

3-octanol

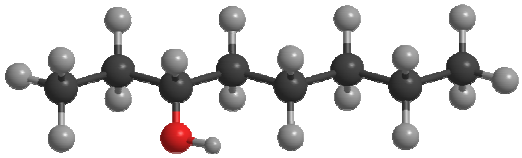

Figure 5.9. Molecular structures of 1- and 3-octanols.

The low energy features of the spectra is fitted with a methylene symmetric stretch (d^+, ~2850 cm^{-1}, ~15 cm^{-1} FWHM) and a methyl symmetric stretch (d^+, ~2875 cm^{-1}, ~15 cm^{-1} FWHM). The considerable differences between the spectra of 1- and 3-octanol signify the importance of the hydroxyl group position on the molecular structure. The relative order at the neat liquid/vapor interfaces of 1- and 3-octanol can be deduced by comparing the r^+ and d^+ bands in the SSP spectra. In addition, a common strategy for assessing conformational order in alkyl monolayers involves comparing the relative area under the r^+ and d^+ features in the SF spectra.

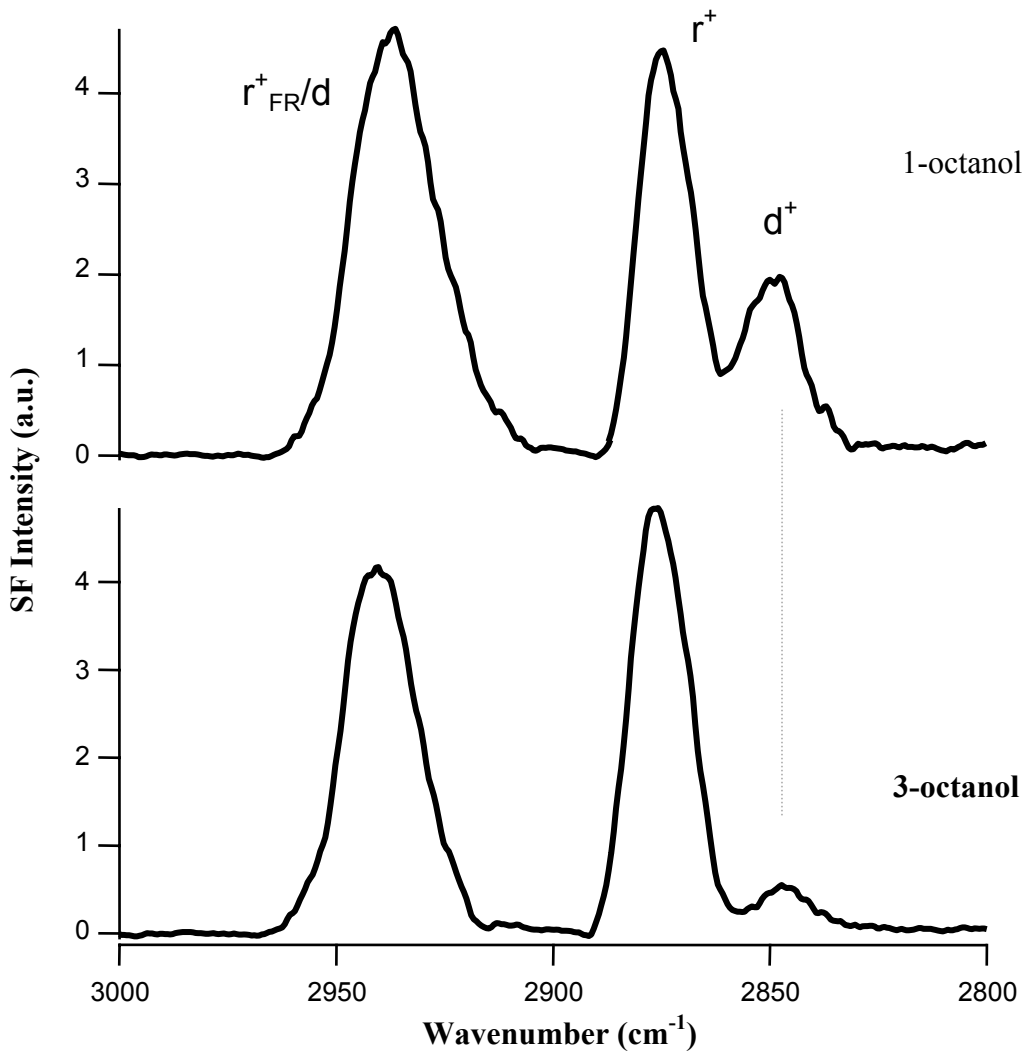

Figure 5.10. SSP spectra of neat 1-octanol and 3-octanol at liquid/vapor interface.

Given that the d^+ band is symmetry forbidden in long, extended alkyl chains, a large r^+/d^+ ratio implies a well-ordered monolayer consisting of surfactants in primarily all-trans conformations. Conversely, a small r^+/d^+ ratio suggests varying degrees of conformational disorder brought about by gauche defects within the adsorbed surfactants. While not rigorously correct – ordered alkyl chains having an odd number of methylene groups in an all-trans conformation can give rise to a weak d^+

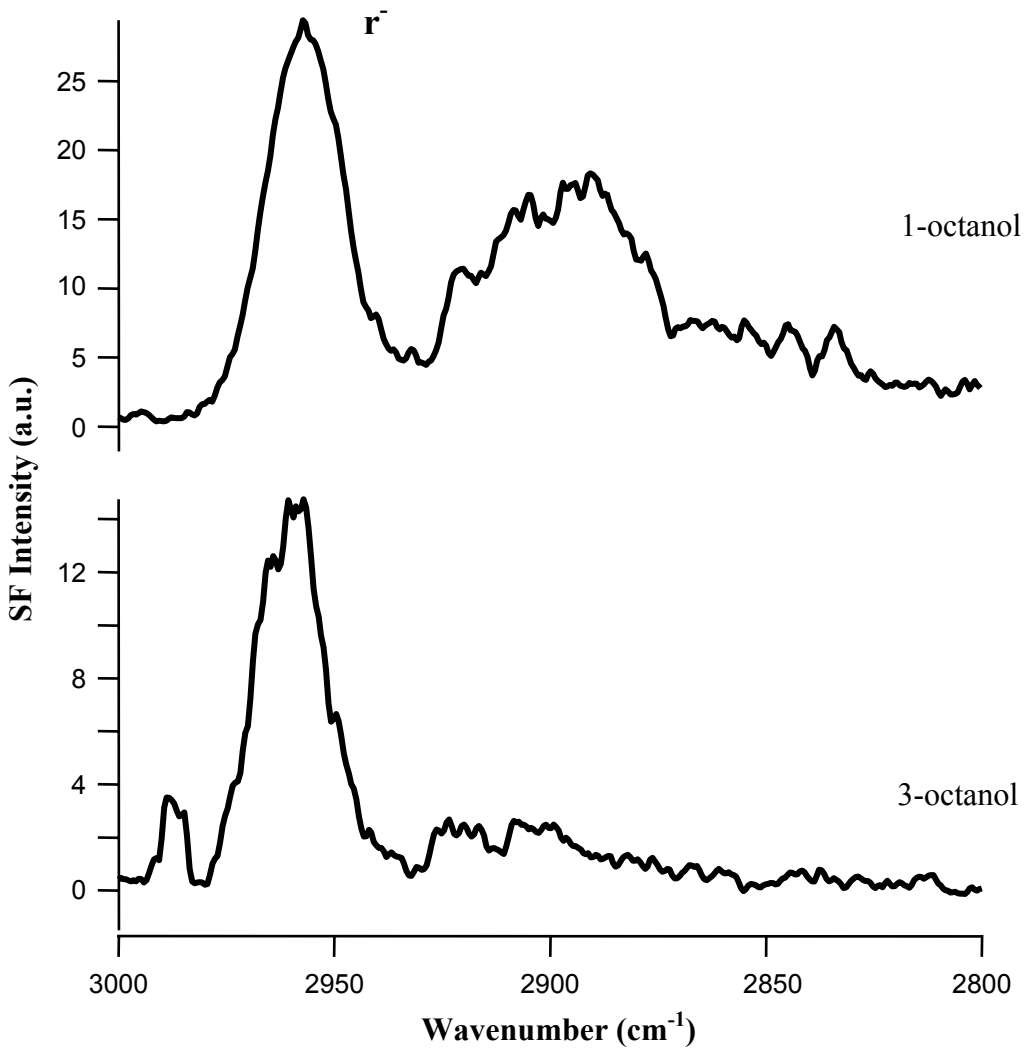

Figure 5.11. SPS spectra of neat 1-octanol and 3-octanol at liquid/vapor.

signature – this analysis nevertheless proves useful when evaluating the 1-octanol and 3-octanol spectra presented in this chapter. The r^+/d^+ ratio of 1- and 3-octanol from neat liquid/vapor interface are listed in Table 5.1. The higher r^+/d^+ ratio of 3-octanol (~1.4) compared to the ratio of 1-octanol (0.6) implies that the surface of 3-octanol is significantly more ordered than the surface of 1-octanol.

The relatively weak d^+ band in 1-octanol SSP spectrum coupled with the strong r^+ response suggests that 1-octanol molecules at vapor/liquid interface adopt an

orientation such that the methyl groups are primarily parallel to the surface normal. The presence of a very weak r^+ band in the 1-octanol SPS spectrum supports the presence of small tilt angle of CH_3. Despite the isolated CH_2 group in the 3-octanol the d^+ response is considerably weaker in the 3-octanol SSP spectrum relative to that in the 1-octanol spectrum. This observation suggests that either no gauche defects exist and the extra CH_2 groups are parallel to the surface or the molecule has defects such that all of CH_2 groups are oriented parallel to the surface. The second choice is highly unlikely given that this is a short chain and there is an asymmetry induced by OH group. The strong r^+ intensity with no r^- in the neat 3-octanol SSP spectrum supports the first possibility and implies that the CH_3 groups are oriented perpendicular to the surface with almost no tilt angle. The absence of an r^- band in the 3-octanol SSP spectrum and its presence in the SPS spectrum further supports this.

5.2.2. Octanol Monolayers on Aqueous Solutions

Despite having similar bulk properties, the 1-octanol and 3-octanol isomers behave very differently at interfaces. Second harmonic generation studies carried out in our group have shown that when 1-octanol is in contact with water, it creates an alkane-like region that extends for the length of a single, extended octanol molecule (~1.2 nm). In contrast, 3 octanol creates an interface that is much more abrupt and interfacial polarity converges to the bulk alcohol limit in less than 5 Å.

At 25° C, saturated aqueous solutions of 1-octanol and 3-octanol have concentrations of 4.2 mMolar ($X_{1\text{-oct}} = 7.5 \times 10^{-5}$) and 9.6 mMolar ($X_{3\text{-oct}} = 1.7 \times 10^{-4}$), respectively. The ~2-fold difference in solubility reflects the difference in having to solvate a single C_7 alkyl chain vs. a pair of C_2 and C_5 chains. Despite the

lower bulk concentration, saturated solutions of 1-octanol form dense monolayers having a terminal surface coverage of $4.5 \pm 0.4 \times 10^{14}$ /cm^2 (22 ± 2 Å^2/molecule) as determined by surface tension measurements. The corresponding terminal coverage for the aqueous/3-octanol system is $2.0 \pm 0.2 \times 10^{14}$/cm^2 ($49 \pm 5$ Å^2/molecule).

Structure within these monolayers can be examined by comparing the surface vibrational spectra of octanol monolayers acquired by VSFS. Within the dipole approximation, VSFS experiments probe the vibrational structure of surface species without contributions from the underlying liquid. Figure 5.12 shows SF spectra of 1-octanol and 3-octanol monolayers adsorbed to the water/vapor interface from saturated aqueous solutions. Spectra were acquired under SSP polarization conditions meaning that only those vibrational modes having a net out-of-plane projection of their infrared transition moment contribute intensity to the spectrum. Assignments are based on previous reports from surface and bulk solution studies of neutral, alkyl systems as reported in Table 2.7. Of particular importance are the two bands centered at ~2847 cm^{-1} and 2873 cm^{-1}. These two features correspond to the CH_2 symmetric stretch (d^+) and CH_3 symmetric stretch (r^+), respectively.

The SF spectrum of 1-octanol (top, Figure 5.12) adsorbed to the water/vapor interface shows a very large r^+/d^+ ratio (> 50, integrated area) consistent with the idea that the linear alcohol creates highly ordered, dense monolayers at the water/vapor interface. Such behavior is common in Langmuir films consisting of longer chains. Not surprisingly, monolayers of 3-octanol adsorbed to the water/vapor interface evince a smaller r^+/d^+ ratio suggesting a lower degree of conformational order in the adsorbed surfactants. This result is expected for several reasons. First, steric

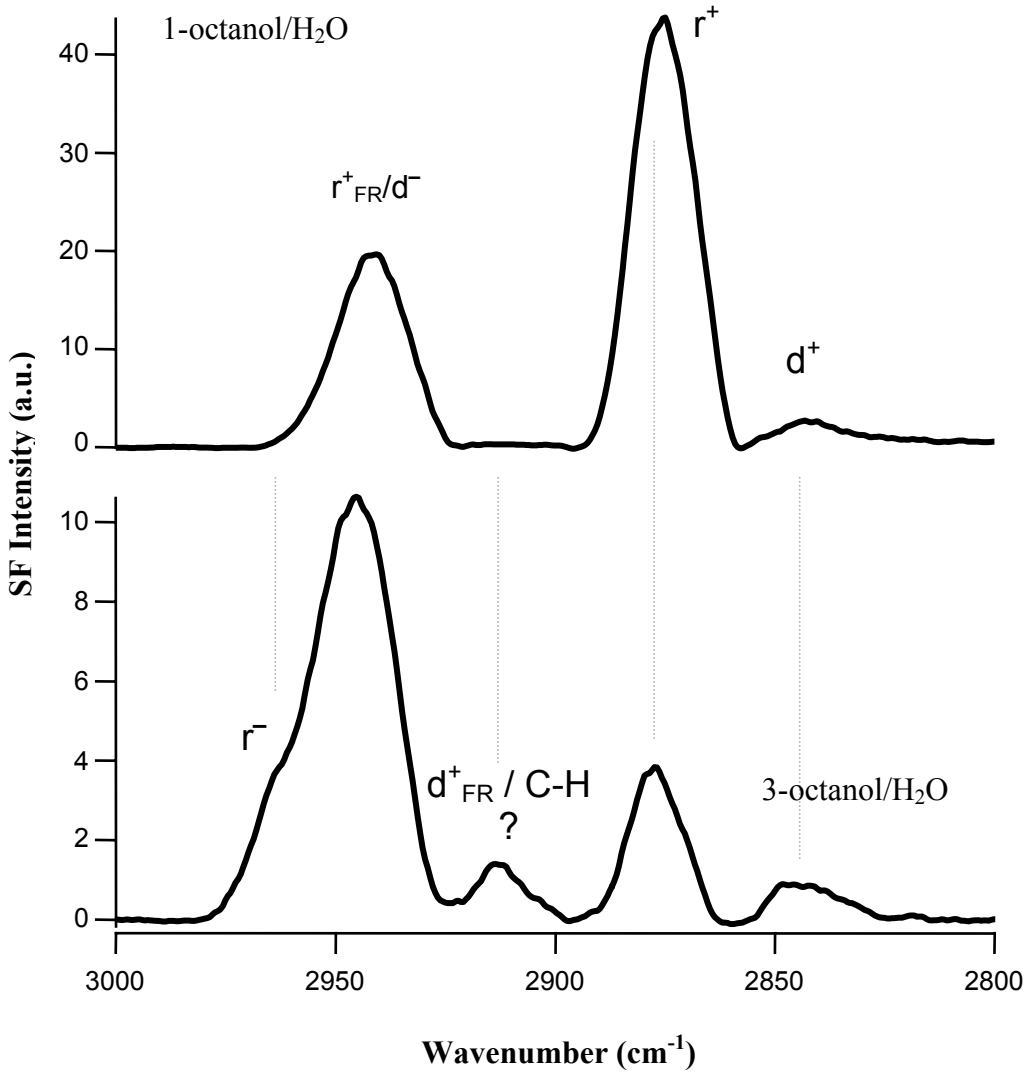

Figure 5.12. SSP spectra of 1-octanol and 3-octanol adsorbed to liquid/vapor interface of saturated aqueous solutions.

considerations keep the 3-octanol surfactants from packing as efficiently as their linear counterparts as evidenced by the smaller terminal surface concentrations in the 3-octanol monolayer. Second, the methylene group at the 2-position is decoupled from the rest of the alkyl chain making its vibrations SF active regardless of chain conformation. One curious aspect of the spectrum is the surprising intensity in a band at 2941 cm^{-1}. This feature is usually assigned to a Fermi resonance interaction between an overtone of the CH_3 symmetric bend with r^+. Even in the limit of

complete state mixing, one would not expect the nominal overtone (at 2941 cm^{-1}) to be stronger than the fundamental (at 2970 cm^{-1}). In principle, the 2941 cm^{-1} band could contain contributions from neighboring modes (such as the methylene asymmetric stretch, d^-, centered ~2925 cm^{-1}), but the narrow bandwidth of the feature (FWHM = 17 cm^{-1}) makes this possibility unlikely. In fact, the high frequency shoulder observed at 2957 cm^{-1} likely arises from the methyl asymmetric stretch (r^-) and shows that features separated in frequency by 15 cm^{-1} are readily distinguishable from each other.

Spectra of these same systems acquired using an SPS polarization combination supports these contrasting pictures of monolayer structure. (Figure 5.13) The SPS polarization combination samples only those vibrations that have their infrared transition moments aligned parallel to the surface. For both the 1 octanol and 3 octanol monolayer films, the SPS spectra are dominated by the methyl asymmetric stretch (r^-) and the 1-octanol monolayer shows a very weak band corresponding to the methyl symmetric stretch. The appearance of both r^+ and r^- in the same spectrum necessarily requires that the 1-octanol chains be tilted relative to the surface normal, a result that is consistent with previous studies that report tilt angles of 8-18° for similar, neutral systems.[80]

In summary, both 1-octanol and unexpectedly 3-octanol is well ordered at the air/neat-liquid interface. A higher surface order observed for 3-octanol is difficult to reconcile given its asymmetric shape and anticipated strong, intermolecular hydrogen bonding interactions,. Monolayers of 1-octanol and 3-octanol adsorbed to the air/water interface have easily identifiable vibrational signatures that reflect

chain/chain interactions constrained by hydrogen bonding between the alcohol functional group and the underlying aqueous subphase. These observations emphasize the difficulty in trying to predict the properties of liquid surfaces.

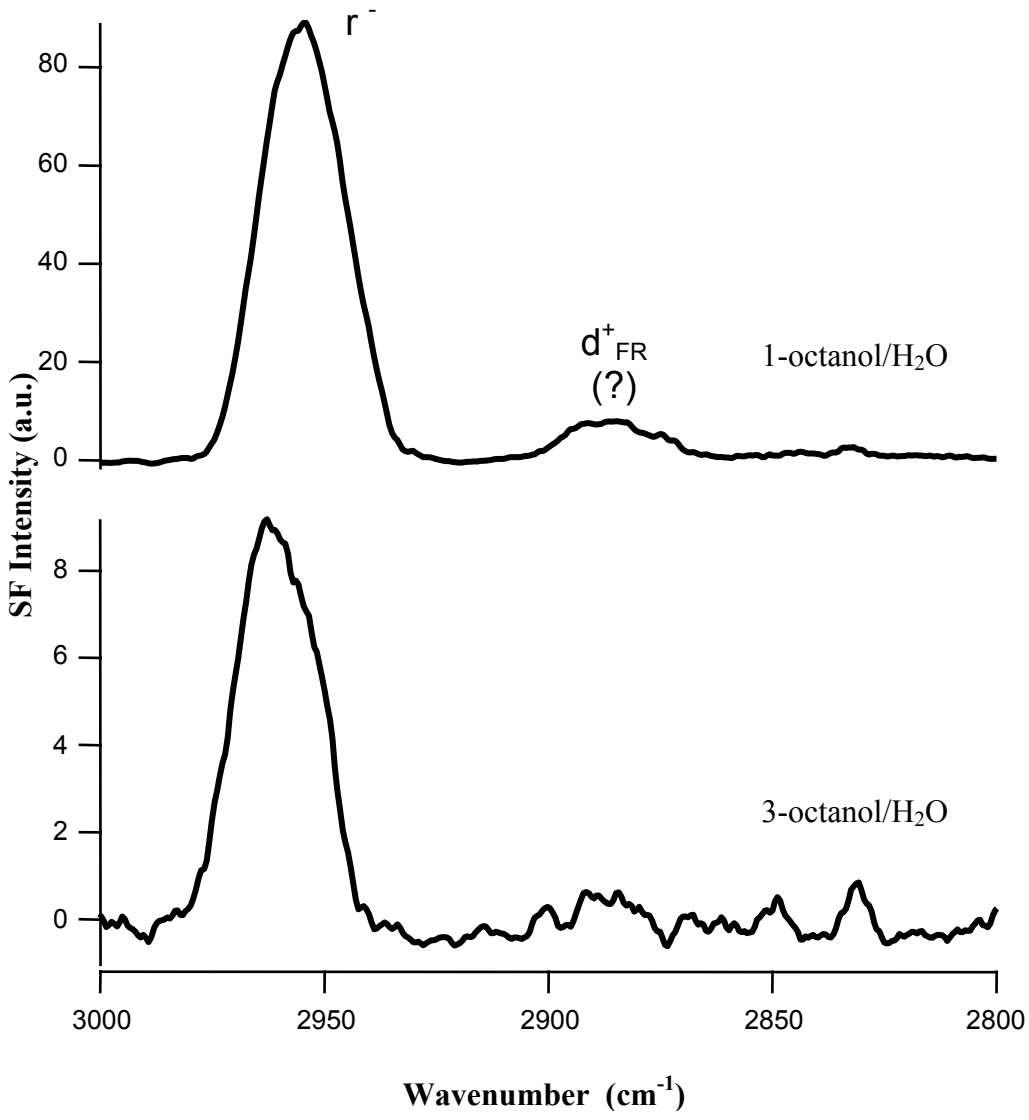

Figure 5.13. SPS spectra of 1-octanol and 3-octanol adsorbed to liquid/vapor interface of saturated aqueous solutions.

5.3. Surface structure of cyclooctanols on aqueous/vapor interface

In addition to the linear alcohols, we have investigated the surface structure of of 1-cyclooctanol and 1,2-cyclooctanediol at aqueous/vapor interfaces via VSFS. The molecular structures are given in Figure 5.15. The surface vibrational spectra of those alcohols acquired under SSP and SPS polarization conditions are presented in Figure 5.15 and Figure 5.16. The SSP spectra of the cyclooctanols are significantly different despite the fact that only difference is a second hydroxyl group on the ring structure.

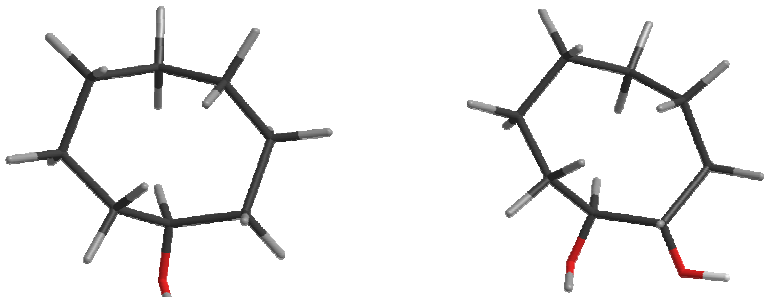

1-cyclooctanol 1,2-cyclooctanediol

Figure 5.14. Molecular structures of 1-cyclooctanol and 1,2-cyclooctanediol.

The SSP of cyclooctanols are assigned to four bands, namely methylene symmetric stretch (d^+), Fermi resonance (d^+_{FR}), and asymmetric stretch (d^-) and C-H stretch. The center frequencies of the features are given in Table 5.8.

Table 5.8. Center frequencies of the vibrational bands observed in surface vibrational spectra of cyclooctanols.

	d^+	**d^+_{FR}**	**d^-**	**C-H**
1-cyclooctanol/H2O	2850	2913	2927	2964
1,2-cyclo-octanediol/H2O	2851	2911	2936	2960

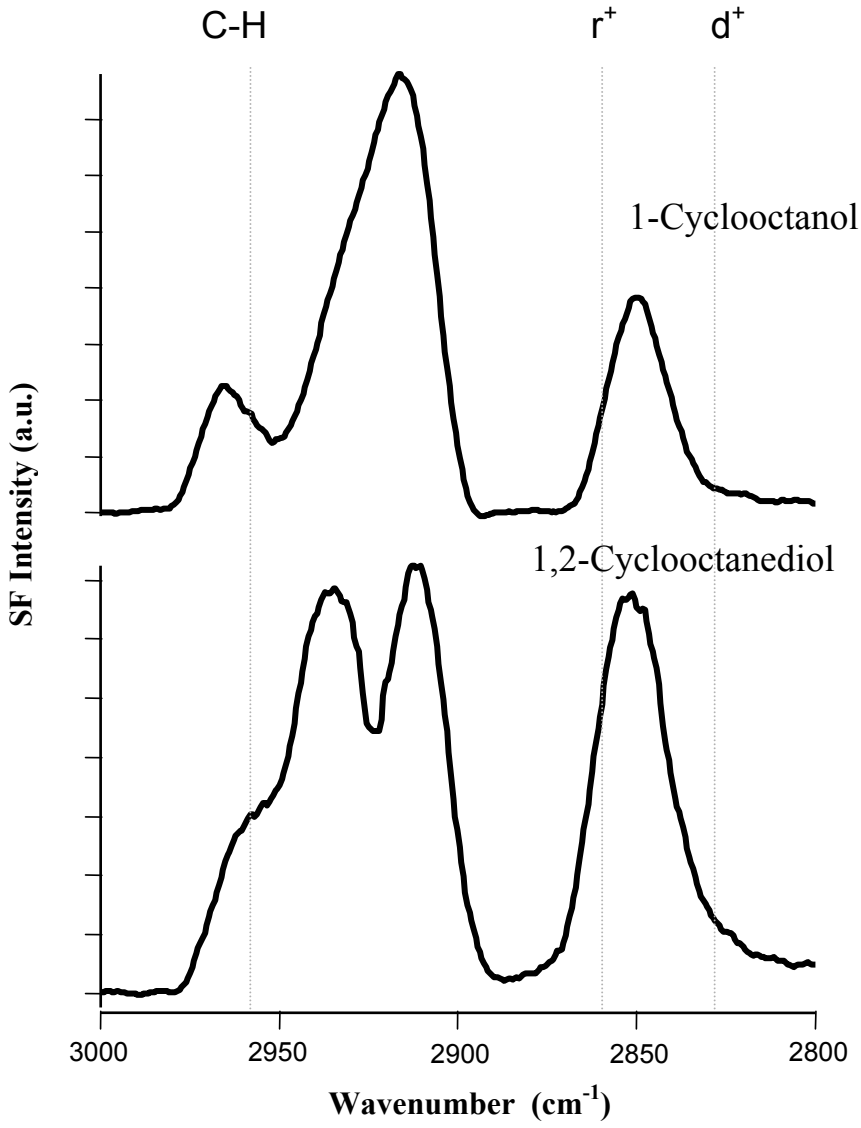

Figure 5.15. Surface vibrational spectra of cyclooctanols acquired under SSP polarization conditions.

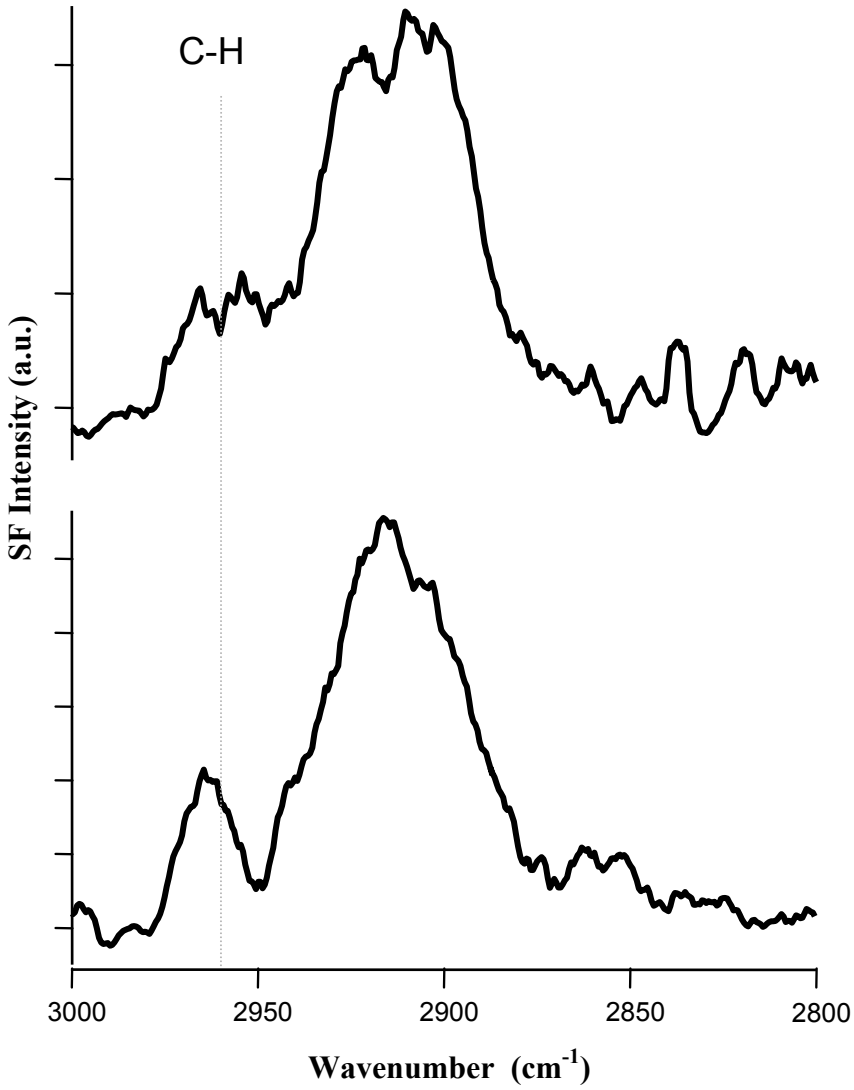

Figure 5.16. Surface vibrational spectra of cyclooctanols acquired under SPS polarization conditions.

Due to known multiple stable conformations of cyclooctanols in solution determining the surface structure of 1-cyclooctanol and cis-1,2-cyclooctanediol films on water is difficult. H-bonding interactions with the aqueous subphase should anchor the hydroxyl group(s) of the adsorbed cyclooctanols down toward water. The C-H band observed at 2964 cm^{-1}, assigned in the absence of CH_3 groups, in SSP spectrum suggest a tilt of the overall ring structure. The presence of a significant d^- band in the

SSP spectrum of both solutes supports this conclusion. The second hydrogen bonding interaction of 1,2-cyclooctanediol leads to a smaller overall tilt angle compared to 1-cyclooctanol. The changes in d- and d+ support this finding. With the second -OH in a cis-configuration relative to the first -OH, one of the C-H of 1,2-cyclooctanediol aligns almost parallel with the surface and does not contributes to the SSP spectrum. The stronger C-H response in the SPS spectrum of 1,2-cyclooctanediol relative to the 1-cyclooctanol data supports this finding. Although quantify the tilt angle without firm assignments is difficult, simple considerations suggest an angle less than 45^{o} of the ring plane with respect to surface normal for both molecules.

The study requires further investigation both with additional cyclooctanols varying in their position of OH groups such as 1,5-cyclooctanediol, and with the isotopic labeling of the studied structures.

Chapter 6

Indoline

To this point we have investigated the surface structure of solvent molecules. The study can be extended toward the effect of solvent structure on solute's behavior at liquid/vapor interfaces where interfacial solvation will control adsorption, wetting and chemical reactivity. In order to better understand interfacial solvation, we first wanted to understand how intermolecular forces controll solvation in bulk solution. This chapter describes our efforts to quantify intermolecular interactions, especially hydrogen bonding, between Indoline – an aromatic heterocycle – and a wide variety of polar and nonpolar solvents.

Electronic and vibrational spectra of the poly-cyclic, heterocycle indoline have been used to explore both specific and nonspecific solvation forces in a wide variety of solvents. Excitation of indoline to its first excited state shows little sensitivity to solvent dielectric properties, but excitation wavelengths are dependent on a solvent's ability to accept and/or donate hydrogen bonds. In contrast, emission spectra of indoline in different solvents demonstrate classic dependence on solvent polarity in accord with nonspecific solvation mechanisms. The frequency associated with the single NH stretch, ω_{NH}, also depends sensitively on specific solvation forces. In different solvents ω_{NH} can vary by more than 100 cm^{-1} depending on the opportunities that exist for hydrogen bond formation. In order to predict the strength of specific solvent-solute interactions, a semi-empirical scale is developed based on a ω_{NH} and each solvent's ability to accept hydrogen bonds. This scale was tested with a

second solute, indole, and accurately predicted ω_{NH} of indole in different solvents (and in the gas phase) to within 10 cm^{-1} in most cases.

6.1. Introduction

In the most general sense, dipolar solvation describes the noncovalent interactions between a polar solute and its environment.[137] The solvating environment is usually a liquid, and molecular contributions to solvation can be described in terms of forces (charge-dipole, dipole-dipole, dipole-induced dipole, etc.) or in terms of directionality. In this latter classification, nonspecific solvation refers to a solute dipole inside of a well-defined cavity interacting with a structureless, dielectric continuum, while specific solvation refers to localized, highly anisotropic interactions between the solute and its surroundings. Hydrogen bonding stands out as an example of specific solvation. Both nonspecific and specific solvation can impact a number of solute properties including conformation, reactivity, diffusion and photophysical behaviour, and numerous studies have used variations in these properties to identify the strength and type of solvent-solute interactions.[138-148]

To characterize solvation a number of scales have emerged. These include empirical measures of solvent polarity such as $E_T(30)$[149] and π^*[150] scales as well as model-dependent measures of local dielectric properties such as the Onsager[151] and Kirkwood[152] descriptions of dipolar solvation. Empirical scales enjoy wide usage due to their ease of application and general utility. These scales typically involve measuring an observable (such as a transition energy, fluorescence lifetime, etc.) of a given solute or family of solutes solvated by a particular solvent and then comparing the result to similar quantities from standard, reference solvents. In contrast, solute

identity is inconsequential in dielectric models, where the solute is treated simply as a dipole in a solute cavity buried inside of a structureless continuum.

Both empirical and model-dependent solvation descriptions of solvent polarity necessarily address only non-specific solvation forces.[143,149,150,153-155] Specific solvation interactions have proven more difficult to treat in a systematic, comprehensive manner. The π* scale attempts to account for hydrogen bonding interactions by including additional parameters, but these parameters tend to correlate only within a given family of solvents (such as alcohols or ketones or ethers) and do not transfer from family to family.[150] *Ab initio* methods have enjoyed considerable success in predicting the strength of hydrogen bonding interactions between a solute and a small number of solvent species, but these studies are limited to small system sizes and have not been applied to specific solvation forces in any general way.[145,156-163]

In the work described below, we use a single solute to probe both non-specific and specific solvation forces in a wide variety of solvents ranging from nonpolar to polar and including solvents that can serve either as hydrogen bond donors (HBDs) and/or hydrogen bond acceptors (HBAs). The solute is indoline, a simple, poly-cyclic heterocycle composed of a benzene ring attached to a pyrroline at carbons 1 and 2. (Figure 6.1) Here the nitrogen lone pair participates in the conjugated electronic structure of the benzene ring making electron donation to and back-donation from the benzene ring possible. A close relative of the biologically relevant, natural chromophore indole, indoline stands out as an attractive probe of nonspecific and specific solvation forces for several reasons.

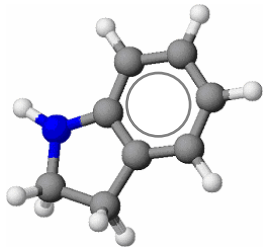

Figure 6.1. Structure of indoline.

First, the electronic and vibrational spectra of the solute are relatively simple and interpreting solvent/solute interactions from solvatochromic spectral shifts is straightforward. Second, unlike indole, indoline is photochemically stable in solution.[164] Finally, different functionalities make indoline sensitive to both nonspecific and specific solvation forces, enabling experiments to identify both isotropic and directional solvent/solute interactions with the same probe.

Electronic excitation and emission of indoline in various solvents illustrate the solute's sensitivity to different types of solvation mechanism. Excitation spectra of indoline are insensitive to long-range, nonspecific solvation forces (as characterized by solvent polarity), but excitation to the first excited state *is* very sensitive to a solvent's ability to either accept and/or donate hydrogen bonds. In contrast, emission spectra of indoline in these same solvents demonstrate classic sensitivity to nonspecific solvation forces. A solvent's hydrogen bonding capabilities make only subtle contributions to the indoline's overall solvatochromic emission behaviour. The NH stretching frequency of indoline (ω_{NH}) also serves as a very sensitive indicator of specific solvation forces. We have measured ω_{NH} in a wide variety of solvents and, not surprisingly, we have found the vibrational frequency of this feature to be quite sensitive to hydrogen bonding opportunities. In an effort to predict the strength of

solute/solvent hydrogen bonding, we have developed a semi-empirical scale that accurately predicts ω_{NH} vibrational frequencies in all types of solvents and accurately (to within 10 cm^{-1}) extrapolates to the gas phase ω_{NH} limit. This scale is readily applicable to other probes having solvent-sensitive, vibrational signatures and requires only modest computational capabilities that can be found in standard, *ab initio* packages.

6.2. Experimental

All solvents were purchased from Aldrich or Fisher and used as received. Solvents were chosen based on their optical transparency between 3200 and 3500 cm^{-1} (for IR measurements) and between 260 and 400 nm (for absorbance and fluorescence measurements). All reported spectral data have been collected with a background correction. Indoline was purchased from Aldrich and used as received.

UV spectra were acquired with a HP 8452A Diode Array Spectrometer with 1 cm quartz cells. Fluorescence spectra were acquired with a Spex-Fluorolog Spectrofluorometer. In all cases both sample and blank spectra were recorded in the same cell. Infrared spectra were acquired with a Nicolet Magna-IR 560 Spectrometer with a demountable liquid cell (Reflex) having CaF_2 windows and 25 μm spacer. Infrared absorbance measurements with protic solvents were acquired from solutions suspended in KBr pellets in order to maintain optical transperancy across the spectral region of interest.

All calculations have been carried out for gas phase species by using GAMESS[165] with 6-31G* basis set on a Pentium III 667 MHz with 532 MB RAM.

Prior to single point calculations, solvents were optimised under standard conditions. Mulliken population analysis has been done, and total atomic population has been used for each active center (O, N). For more than one strong center an average of those Mulliken charges was used.

6.3. Results and discussion

Due to its structure, indoline is sensitive to both long-range and short-range solvation forces. Here long-range refers to electrostatic interactions such as nonspecific dipole-dipole and polarization interactions while short-range refers to localized, directional interactions such as those arising from hydrogen bonding. The effect of these different interactions on indoline can be probed by different optical methods.

A. Indoline as a probe of long and short range solvation forces – electronic structure

The sensitivity of indoline to specific and nonspecific solvation forces can be seen in the solute's electronic excitation and emission behaviour. Figure 6.2 shows both the excitation and emission maxima (λ_{max}) of indoline in a variety of solvents plotted as a function of solvent polarity as characterized by the Onsager function, f(ε):

$$f(\varepsilon) = \frac{2(\varepsilon - 1)}{(2\varepsilon + 1)} \qquad 6\text{-}1$$

where, ε is the solvent static dielectric constant. Solvents were chosen to represent a wide range of polarities and hydrogen bonding capabilities. Plotting λ_{max} as a function of different empirical solvent polarity scales did not prove any more (or less) instructive than using f(ε) as the measure of polarity. One advantage of f(ε) over the

other scales is that it is independent from the size and the shape of the solute.[166,167]

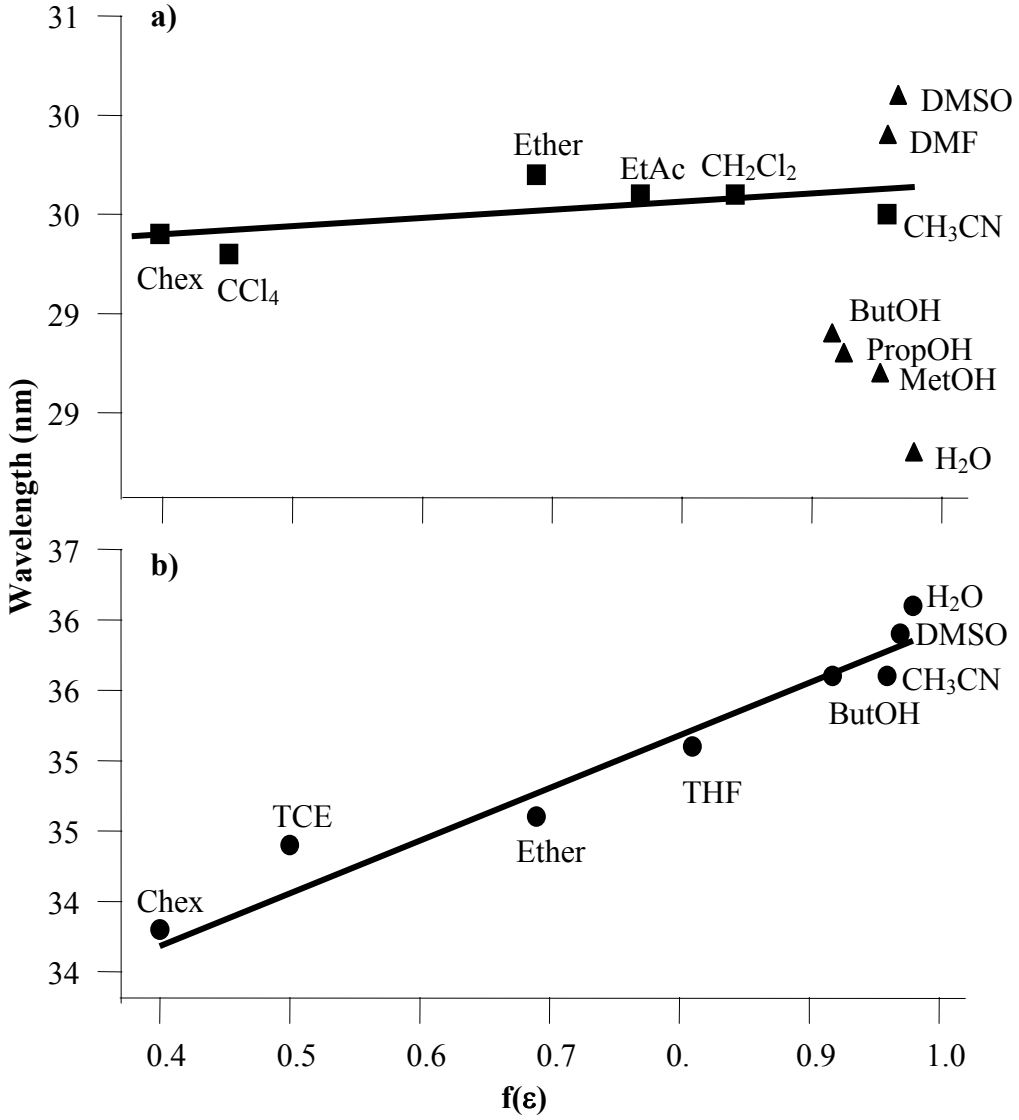

Figure 6.2. Excitation and emission maxima of indoline in a variety of solvents. Figure 2a) Squares denote excitation maxima in non-hydrogen bonding solvents. Triangles denote excitation maxima in hydrogen bonding solvents (both HBA and HBD). Figure 2b) Circles denote emission maxima in all solvents, regardless of their respective hydrogen bonding capabilities. Data are plotted versus each solvent's Onsager polarity as described in the text.

Indoline's insensitivity to solvent polarity can be seen in the invariance of excitation maxima across a wide range of aprotic solvents (Figure 6.2a). In solvents ranging from cyclohexane to acetonitrile λ_{max} varies by less than 2 nm. However, once indoline is solvated by a solvent capable of hydrogen bonding, its excitation

maximum shifts either to shorter or longer wavelengths depending on the dominant type of solute-solvent hydrogen bonding. Protic solvents such as alcohols and water can serve as both hydrogen bond donors (HBDs) and hydrogen bond acceptors (HBAs). These solvents cause indoline's absorption spectrum to blue shift due to their ability to stabilize indoline's HOMO with respect to its LUMO (Figure 6.3). This behaviour of indoline is consistent with an electronic structure that localizes the HOMO primarily on the nitrogen lone pair. The structure is common in aromatic amines.[168] Thus, solute-solvent interactions with the HBD solvents preferentially lower the energy of indoline's ground electronic state and increase the energy required to reorganize electron density in the first excited electronic state localized primarily on the aromatic ring.

In contrast, the hydrogen bonding interactions between indoline with aprotic, HBA solvents (i.e. DMSO or DMF) cause a red shift in the excitation spectrum with respect to non-hydrogen bonding solvents. This result arises from diminished stabilization of indoline's HOMO (Figure 6.3). This behaviour is most easily understood using aniline as a model. The lowest energy excited state of aniline requires charge transfer from the nitrogen to the conjugated ring.[168] Pratt and co-workers showed that $S_1 \leftarrow S_0$ excitation increases the dipole moment of aniline from 1.129 D to 2.801 D. Using the excitation and emission wavelengths of indoline in common solvents, we calculated a ratio of excited state to ground state dipole, μ_e/μ_g, of 2.05. Reported solvatochromic behaviour of aniline also shows similar blue shifts with HBD solvents and red shifts with HBA solvents.[169]

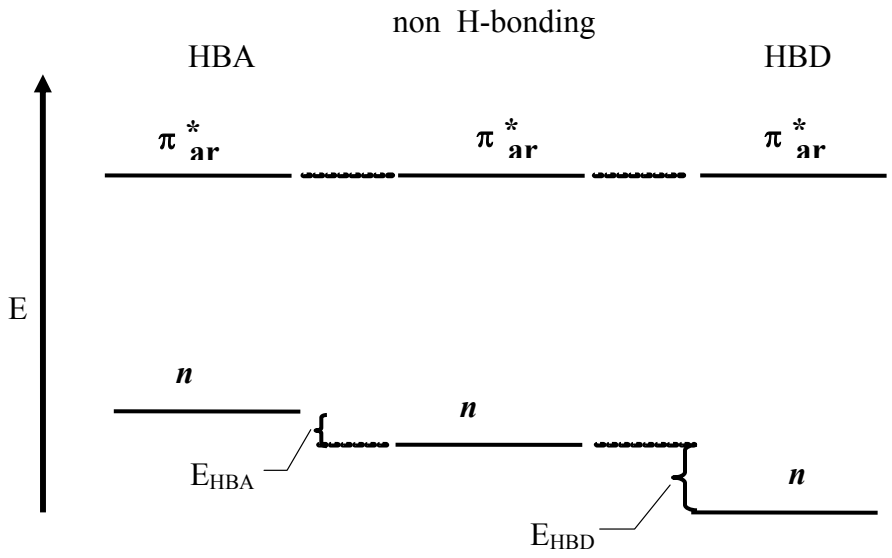

Figure 6.3. A schematic diagram illustrating the effects of hydrogen bond donating and hydrogen bond accepting solvents on the electronic excitation energy of indoline. The center of the diagram (non H-bonding) depicts the excitation energy of indoline in a solvent that cannot interact through hydrogen bonds. In hydrogen bond accepting solvents (such as DMSO) solvent-solute interactions through the NH bond raise the energy of the indoline HOMO relative to the non HB case thus red-shifting indoline's excitation energy. In contrast, hydrogen bond donating solvents (such as water) can lower the energy of indoline's HOMO by forming hydrogen bonds with indoline's amino lone pair. This effect increases the energy needed to excite indoline to its first excited electronic state.

If indoline excitation leads to a significant transfer of electron density from the nitrogen lone-pair to the aromatic ring, the excited state should be less sensitive to localized directional forces such as hydrogen bonding and more sensitive to long-range, nonspecific solvation forces. Such solvatochromic behaviour typically appears as a direct correlation between a solute's transition energy (or wavelength) and solvent polarity. In fact, this behaviour is observed in the emission spectra of indoline in different solvents. Figure 6.2b plots the emission maxima of indoline versus solvent polarity as characterized by the Onsager function. Unlike the excitation spectra, emission behaviour of indoline is dominated by a ~25 nm monotonic, red shift as solvent polarity varies from that of cyclohexane to that of polar solvents such

as water and DMSO. In the high polarity limit subtle effects due to hydrogen bonding differences between solvents are observed. In this case interaction with water manifests itself as a red shift instead of a blue shift due to indoline's reduced electron density on the nitrogen in the S_1 excited state. This observation implies that indoline in its excited state functions better as a HBD than a HBA.

To summarize the solvatochromic behaviour of indoline excitation and emission in different solvents, we observe the following:

- Dipolar or long-range interactions do not affect indoline's transition energy to the first excited electronic state.

- Protic solvents lead to a blue shift in indoline's excitation energy. This effect likely results from the solvent's ability to stabilize indoline's HOMO relative to its LUMO through specific, directional hydrogen bonding to the amine lone pair.

- Aprotic solvents that can function as HBAs cause indoline's excitation energy to red shift, presumably by destabilizing indoline's HOMO relative to its LUMO.

- Emission spectra of indoline in different solvents are dominated by each solvent's long-range dielectric properties rather than solvents' HBD or HBA abilities. Such sensitivity to nonspecific solvation forces implies that indoline in its excited state interacts with surrounding solvent less through the amine lone pair and more through delocalised electron density on the aromatic ring.

B. Indoline as a probe of local solvation forces – vibrational structure

Electronic excitation and emission spectra show that localized directional interactions play an important role in indoline's solvation. Based on indoline's electronic structure and the solvatochromic behaviour of indoline's electronic excitation and emission spectra, these interactions depend sensitively on the nitrogen lone-pair and the N-H functional group. Consequently, the vibrational frequency of the N-H stretch should also serve as a sensitive probe of specific solvation forces. A recent study of Gai and co-worker showed the advantage of using CN vibrational stretch as a local probe to observe the local environmental changes of the amino acids in proteins upon binding and folding under different solvents.[140]

We have measured the N-H stretching frequency (ω_{NH}, energy of maximum IR absorption) in 20 different solvents. Figure 6.4 shows the 3500-3100 cm^{-1} region for indoline in cyclohexane as well as the spectrum of neat, liquid indoline for comparison. In cyclohexane, a narrow, isolated band at 3407 cm^{-1} (15 cm^{-1} FWHM) is assigned to the NH stretch of the isolated indoline monomer. The spectrum of neat indoline is dominated by a feature at 3375 cm^{-1} (Figure 6.4b) corresponding to the hydrogen-bonded N-H stretch of dimer indoline. The low-energy shoulder of the 3375 cm^{-1} band and the broad feature centered ~ 3296 cm^{-1} likely arise from hydrogen-bonded indoline clusters. Since we are interested in using the indoline's electronic and vibrational transitions to characterize solute- solvent interactions, we focus our attention on the N-H stretch (either isolated or hydrogen-bonded to the solvent) rather than solute clusters. Indoline concentrations were kept low to inhibit dimer formation in bulk solution.

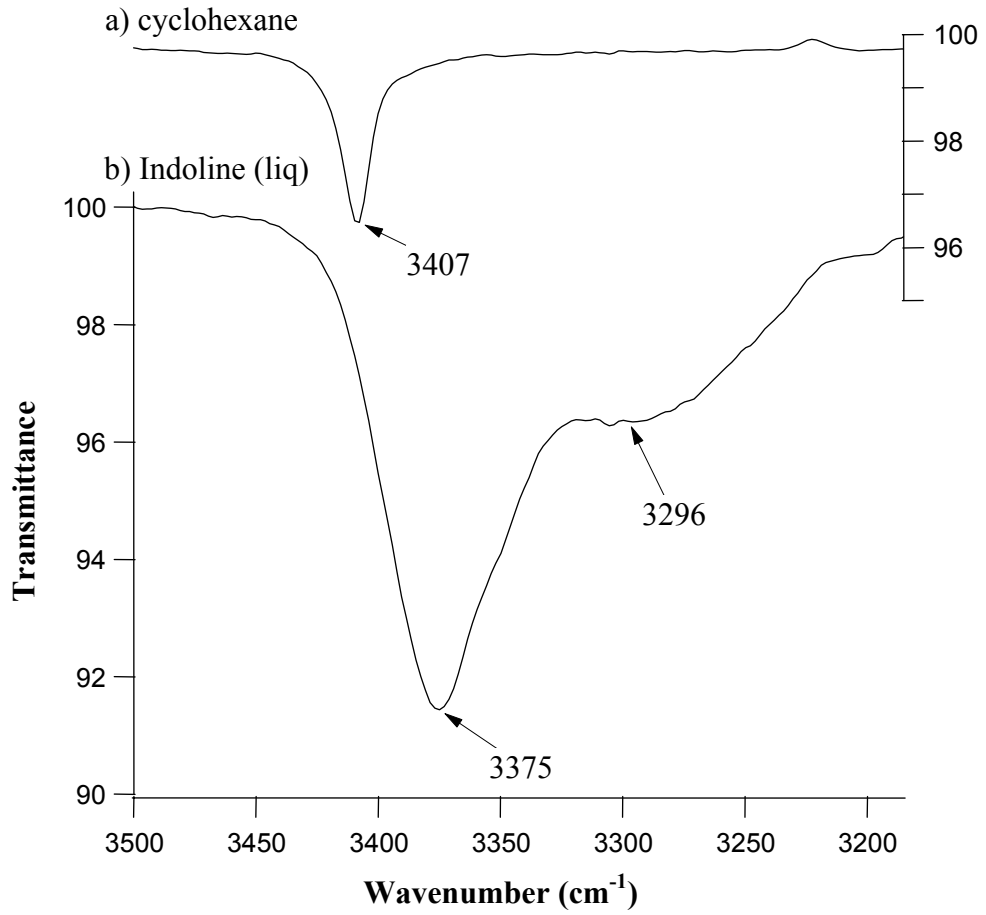

Figure 6.4. FTIR spectra of indoline solvated in a) cyclohexane and b) bulk indoline (liq).

Figure 6.5 shows ω_{NH} plotted against Onsager polarity scale, f(ε), in 20 solvents, covering a wide range of polarity and hydrogen bonding capabilities. As with the electronic excitation data in Figure 6.2, ω_{NH} shows no clear dependence on the solvent polarity. This observation is not unexpected given that polarity does not depend directly on specific solvation forces. Nevertheless, presenting the data in this manner does illustrate the tremendous sensitivity of ω_{NH} to different solvation environments. In non-hydrogen bonding solvents the free N-H stretch shows up at ~3405 ± 10 cm^{-1}. In hydrogen bonding solvents ω_{NH} shifts to lower energies with the largest shift being 110 cm^{-1} in water with respect to cyclohexane (134 cm^{-1} with

respect to the gas phase vibrational frequency[170]). Unlike electronic excitation spectra, shifts in ω_{NH} do not reflect differences in solvent hydrogen bonding capabilities. Both protic and aprotic hydrogen bonding solvents lead to large red shifts in ω_{NH}. The red shift in HBA solvents is expected because hydrogen bonding lengthens the N-H bond of indoline. Given the electronic solvatochromism of indoline in protic solvents, one might (naively) expect a blue shift of ω_{NH} in alcohols and water due to indoline's apparent preference for these solvents to function as HBDs.[159,171] However, protic solvents function as both HBDs and HBAs and ω_{NH} reflects only the strength of the hydrogen bond between the NH group of indoline and an electron lone pair on an adjacent solvent. In other words, with ω_{NH} as the observable, protic and aprotic hydrogen bonding solvents behave similarly.

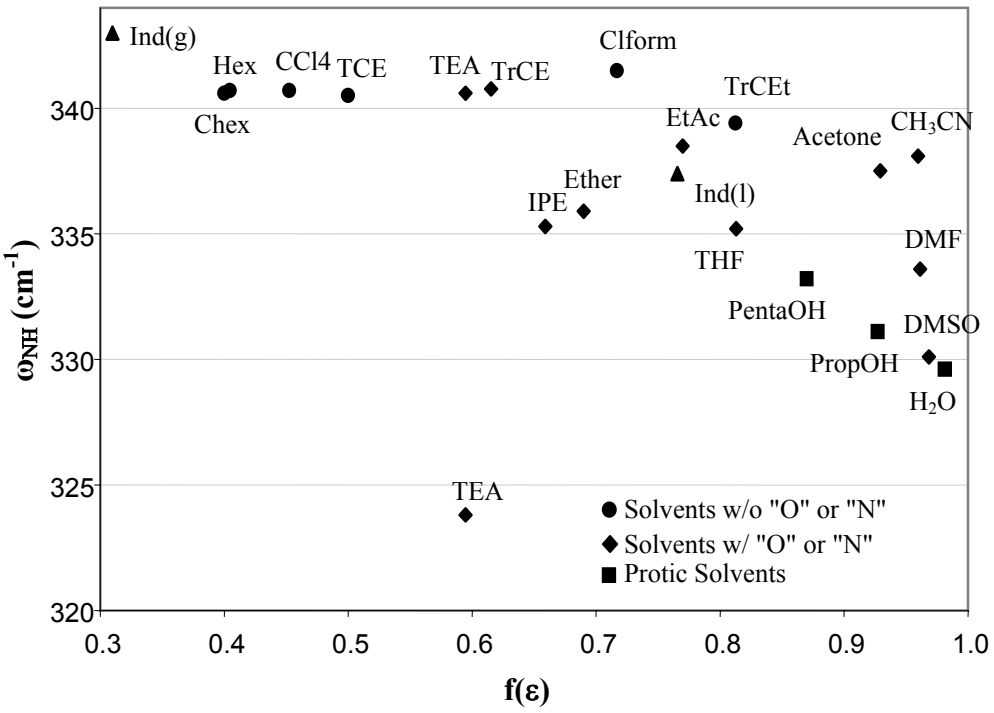

Figure 6.5. Vibrational excitation frequencies (ω_{NH}) of indoline in different solvents plotted versus Onsager polarity. The gas phase value of ω_{NH} should appear at a f(ε) = 0 but appears at 0.31 in order to be included on the plot. f(ε) for indoline(liq) is estimated to be 0.766 based on its similarity to n-Ethyl aniline (ε = 0.59).

We note that of solvents tested, triethylamine (TEA) showed anomalous behaviour. TEA is a tertiary amine that can function as a HBA but not as a HBD. In this respect, it is similar to DMSO. The vibrational spectrum of indoline in TEA contains two features in the N-H stretch region: 3406 and 3238 cm^{-1}. The first feature arises from the isolated indoline N-H stretch as in cyclohexane. We cannot definitively assign the second, low energy feature. This feature appears at too low a frequency to be identified as hydrogen bonding between indoline and the tertiary amine solvent. Spectra are corrected by a neat solvent background subtraction, and a concentration dependence of indoline has also been observed, thus the low frequency, 3238 cm^{-1} feature is inextricably correlated with the presence of indoline in solution. Based on a charge population analysis described below, the strength of the hydrogen bonding of indoline with TEA should be less than that with DMSO. However, the low frequency vibrational band of indoline in TEA is 63 cm^{-1} lower in energy than the corresponding N-H feature in DMSO. The predicted shift of hydrogen-bonded indoline in TEA is 50 cm^{-1} compared to the observed 192 cm^{-1} relative to the gas phase. The water content in the TEA is not labelled, and the solvent may have more water than anticipated. It is possible that this feature arises from some complex formed by (trace) water, TEA, and indoline. ω_{NH} in water, however, is still only 3296 cm^{-1}, a 58 cm^{-1} higher in energy than the observed feature in TEA. Finally, we acknowledge that in the vibrational spectrum of neat indoline there exists appreciable intensity between 3200 & 3250 cm^{-1} suggesting that large solvent clusters can lead to spectral shifts in excess of 140 cm^{-1}.

Observed results for the local interactions can be summarized as follows:

- The ω_{NH} vs. f(ε) data show no characteristic trend although there are some correlations that could represent solvent specific functional group behaviour.

- In alkane and haloalkane solvents the sharp N-H band is characteristic of isolated N-H within a narrow window from 3394 to 3415 cm^{-1}.

- In solvents containing carbonyl and ether oxygens the N-H stretch peak shows up in the region of 3350 to 3385 cm^{-1}.

- For protic solvents ω_{NH} appears below 3350 cm^{-1} as is also the case for strong HBA solvents such as DMF and DMSO.

C. Indoline as a probe of local solvation – dielectric enrichment

Dielectric enrichment refers to a distribution of solvent around a solute that does not reflect the bulk composition of a binary solvent mixture. Given the window of λ_{max} in indoline excitation and emission spectra as well as the range of energies spanned by ω_{NH}, indoline stands out as an attractive candidate for probing dielectric enrichment in a wide variety of binary solvent mixtures. In order to test the relative interactions between different solvents and indoline, electronic and vibrational spectra of indoline were studied in two different binary solvent systems, DMSO-THF and DMSO-water. DMSO-THF is a system well-suited to study the role of hydrogen bond accepting. Both solvents are aprotic but can function as HBA by virtue of the oxygen lone pairs. Disparities in the strength of solute-solvent hydrogen bonding are evidenced by the frequency of ω_{NH} in THF (3352 cm^{-1}) and in DMSO (3301 cm^{-1}), respectively. In Figure 6.6a observed ω_{NH} frequencies for different DMSO-THF

mixtures are plotted against mole fraction of DMSO. Data show that in these solvent mixtures, indoline samples an environment that does not reflect the bulk solvent composition. Specifically, the data shows that DMSO dominates indoline solvation above a DMSO mole fraction of ~0.25.

The DMSO-water system can differentiate a solvent's HBA properties versus HBD abilities from the shifts in electronic excitation maxima. Since the HBD property of water is dominant in the electronic excitation studies, one might expect to observe a dominant behaviour of water in DMSO-water mixtures. However, in Figure 6.6b we observe the opposite behaviour. With DMSO mole fractions of ~0.25, indoline appears to be solvated preferentially by DMSO instead of water. Several explanations can rationalize indoline's preferentialsolvation by DMSO in DMSO-water mixtures. One possibility is that hydrogen bonding between DMSO and water inhibits water's ability to donate hydrogen bonds to indoline thus forcing water to function primarily as a HBA like DMSO. Bagchi and co-workers have shown that solvent-solvent interactions play an important role in determining solvation behaviour in addition to solute-solvent interactions.[172] Another possibility is that indoline is a hydrophobic solute. Thus, the rest of the indoline may enhance local DMSO concentration relative to bulk solution composition.

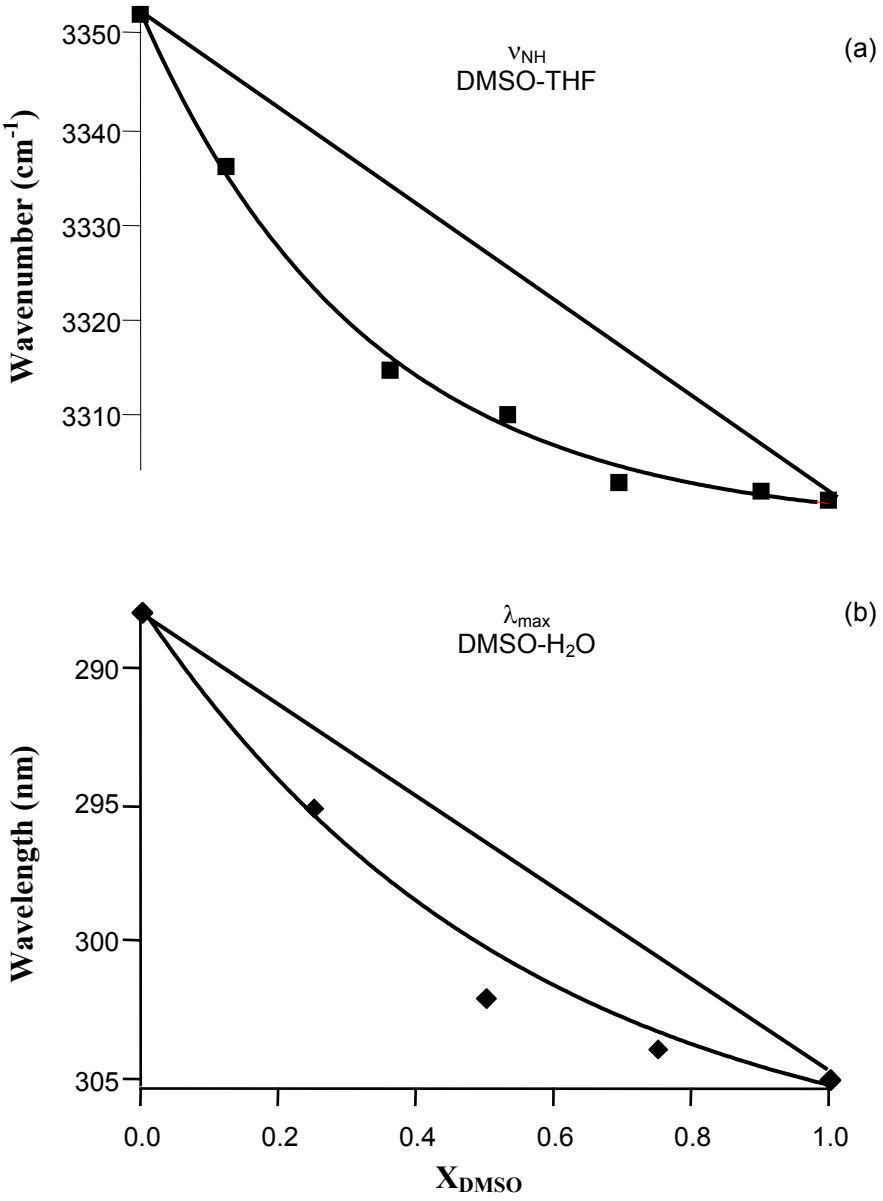

Figure 6.6. a) Plot of ω_{NH} in binary solvent mixtures of DMSO and THF having different bulk solution compositions. The straight line denotes ideal behaviour. Systematic deviation from ideal behaviour demonstrates indoline's preferential solvation by DMSO. b) Plot of λ_{max} for indoline electronic excitation in binary solvent mixtures of DMSO and water having different bulk solution compositions. The straight line denotes ideal behaviour. Although less pronounced than in the vibrational DMSO/THF studies shown in 5a), data show systematic variation indicating that indoline is preferentially solvated by DMSO relative to water.

D. Predicting the strength of specific solvation forces – vibrational solvatochromism

Given the sensitivity of indoline to different solvation forces, a model that could predict the spectral position of ω_{NH} in different solvents would be helpful in estimating the strength of local solvent-solute interactions. Figure 6.5 clearly shows that solvent polarity (as characterized by $f(\varepsilon)$) is inadequate by itself. Traditional scales of solvent polarity typically consider solvatochromic shifts of a solute's electronic transition energy in different solvents. Common examples include $E_T(30)$, Z and π^*.[143,149,150] However, these models fail to predict observed solvent sensitivity of the indoline ω_{NH} frequency in different solvents. Even π^* with α and β parameters accounting the solvent's ability to function as a HBD or HBA does not account for the observed behaviour of ω_{NH} in different solvents. Previous treatments of carbonyl vibrational excitation demonstrated that if solvents were grouped into families, their solvating properties fit to different types of linear functions including $f(\varepsilon)$.[173,174] Simplified molecular orbital treatments can account for the influence of a polar solvent but did not include local, directional solvent-solute interactions.

The inability of these models to describe the behaviour of indoline in different solvents has motivated us to develop a predictive scale for vibrational transition energies that is both accurate and general for all solvents. Ideally, the scaling of ω_{NH} should be determined by as few parameters as possible and the model should extrapolate back to the zero solvent (gas phase) value of ω_{NH}. In terms of determining ω_{NH} the main effect of solute-solvent interactions is hydrogen bonding to the hydrogen of the indoline molecule. Solvents with higher electron density on the HBA atom (O and N) will have stronger interactions. This correlation suggests

parameterizing the shift of ω_{NH} according to electron density on the solvent atom responsible for accepting a hydrogen bond from indoline. Using calculated Mulliken charges of HBA atoms in solvent molecules presents an easy, simple, and independent solution to the problem of defining localized solute-solvent interactions. We have carried out isolated gas phase calculations for each solvent molecule with 6-31G* basis set using GAMESS. The results are reported in Table 6.1. Although Mulliken charges are not an exact, quantitative measure of electron density, they *can* provide reasonably accurate relative electron densities for solvents with respect to each other provided that the applied level of calculation is the same for all solvents.

Accounting for localized solute-solvent interactions based on the Mulliken charges, ω_{NH} should obey the linear behaviour estimated by many models:[139,150,154,173,174]

$$\nu_{NH,s} = \nu^{o}_{NH,g} - c\, f(M,\varepsilon) \qquad 6\text{-}2a$$

$$f(M,\varepsilon) = \left|M - 1\right|^{3}\, 2(\varepsilon - 1)/(2\varepsilon + 1) \qquad 6\text{-}2b$$

where $\omega^{o}_{NH,g}$ is the gas phase vibrational position of the N-H stretch, and c is a constant defines the correlation between the new scale f(M, ε) and the vibrational energy (and includes the cavity radius for the dipole interactions, and the solute cavity radius is assumed to be the same for all solvents). In this model lower and upper limits of f(M, ε) are 0 (for non-interacting, gas-phase) and 8 (for a –1 charged solvent with f(ε)=1), respectively.

Table 6.1. Properties of various solvents used in this work. ε is a solvent's static dielectric constant; f(ε) is a solvent's Onsager polarity as calculated by Eq. 1; MC is a solvent's Mulliken charge on atoms that can accept hydrogen bonds; and f(M, ε) is the solvation variable describing the strength of specific solvent-solute interactions as described in the text.

Solvents	**ε**	**f(ε)**	**M[a]**	**f(M,ε)**
Acetonitrile	36.60	0.96	-0.454	2.95
Acetone	20.70	0.93	-0.516	3.24
Carbon tetrachloride	2.24	0.45	-	0.45
Chloroform	4.80	0.72	-	0.72
Cyclohexane	2.00	0.40	-	0.40
Dimethyl sulfoxide	47.20	0.97	-0.784	5.50
Ether	4.34	0.69	-0.617	2.92
Ethyl acetate (Avg)	6.02	0.77	-0.589	3.09
Hexane	2.02	0.40	-	0.40
Diisopropyl ether	3.90	0.66	-0.649	2.96
N-N-Dimethyl-formamide (Avg N+O)	38.30	0.96	-0.593	3.89
Pentanol	11.00	0.87	-0.744	4.61
Propanol	20.10	0.93	-0.739	4.88
Tetrachlorolethane	7.50	0.81	-	0.81
Tetrachloroethylene	2.50	0.50	-	0.50
Tetrahydrofuran	7.52	0.81	-0.643	3.61
Trichloroethane	3.40	0.62	-	0.62
Triethylamine	3.20	0.60	-0.567	2.29
Water	80.00	0.98	-0.868	6.40

[a] Mulliken atomic charges for O or N in solvent molecule. Average values are given where applies.

Figure 6.7 shows the plot of vibrational absorption maxima with respect to the new scale, f(M,ε) and a linear least squares fit of the data. Although the fit is not perfect, it does predict the vibrational N-H stretch of indoline to within 10 cm^{-1} for a wide variety of solvents that range from nonpolar to polar and from hydrogen bond donating to hydrogen bond accepting. Presumably, the fit may be improved by calculating the Mulliken charges of liquid solvents instead of using solvent gas phase values. Also the parameterisation of the cavity radius might improve the predictions, especially for non-hydrogen bonding solvents.

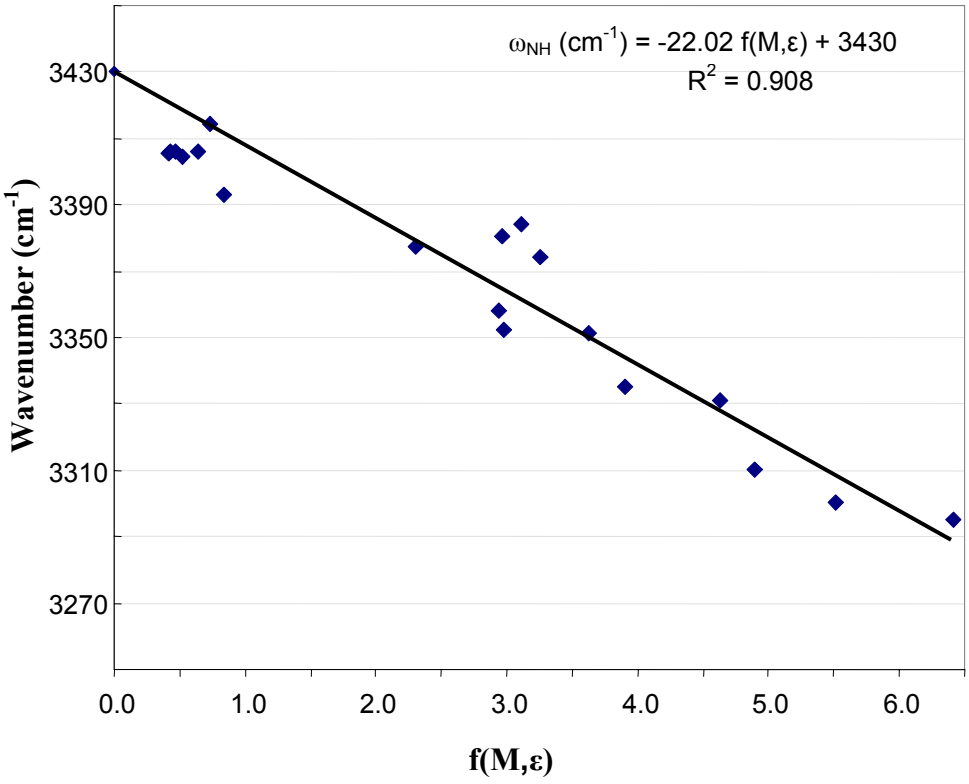

Figure 6.7. Plot of ω_{NH} of indoline versus the parameterised solvation variable f(M,ε), calculated to account for specific solvation forces.

An attractive aspect of this model is that it can be easily applied, and, it predicts solvent-sensitive spectral features better than other parametric models. Applying the model requires several steps:

- Obtain or measure gas phase vibrational transition energy, a quantity that is often available in databases.

- Calculate f(M, ε) from dielectric constants and Mulliken charges for a small number of solvents, preferably for slightly polar and very polar solvents.

- Measure the vibrational spectra of the solute in these solvents.

- Graph and fit the points to a linear function by a least squares technique.

- Predict the vibrational excitation energy of the solute in a solvent of interest using calculated f(M, ε) of the solvent and the fit.

If the gas phase vibrational frequency is not available, one can use a nonpolar solvent with no Mulliken charge (e.g. saturated alkane) instead of the gas phase value and then predict the gas phase ω_{NH} frequency. Once it applied to indoline, it predicts $\omega_{NH,g}$ as 3420 cm^{-1} compared to the measured gas phase value of 3430 cm^{-1} with a correlation of 0.920.

We have tested the generality of this model for a similar solute by using N-H stretch of indole with two different solvents: trichloroethane and DMF. Table 6.2 shows the absolute deviations of the estimated N-H stretching frequencies for four different solvents from their experimental results and Figure 6.8 shows the least squares fit along with their experimental values. The model actually behaves better for indole than for indoline with these randomly selected solvents. The correlation of the fit is 0.9996, and the fit predicts the N-H stretch to within 10 cm^{-1} for most of the tested solvents. In addition, using ω_{NH} for the seven solvents listed in Table 6.1, we can

successfully predict the gas phase value of indole to within 10 cm^{-1} with a correlation coefficient of 0.995. This uncertainty is less than 0.3% of the frequency range spanned by indole's ω_{NH} in the seven different solvents.

Table 6.2. Identifying the strength of solvent-solute interactions using ω_{NH} of indole. The empirical scale was created using the gas phase value of ω_{NH} as well as ω_{NH} in trichloroethane and DMF. (See Figure 7). Using the resulting fit, ω_{NH} could be estimated in other solvents. Estimated and experimental values of indole ω_{NH} show remarkably good correlation across a window of 350 cm^{-1}.

	f(M,ε)	**ω_{NH} (cm^{-1})**
Indole (gas)[a]	0	3530
Trichloroethane	0.81	3470
N-N-Dimethyl-formamide	3.89	3262

Estimated N-H stretch		**ω_{est}(cm^{-1})**	**ω_{exp} (cm^{-1})**	**$\Delta\omega$ (cm^{-1})**
Cyclohexane	0.4	3502	3494	8
Dimethyl sulfoxide	5.5	3150	3176	26
Hexane	0.4	3502	3497	5
Diisopropyl ether	3.0	3325	3317	8
Tetrachloroethylene	0.5	3495	3489	6
Tetrahydrofuran	3.6	3281	3304	23

[a] N-H vibrational stretch of indole (gas) is taken from NIST database.[170]

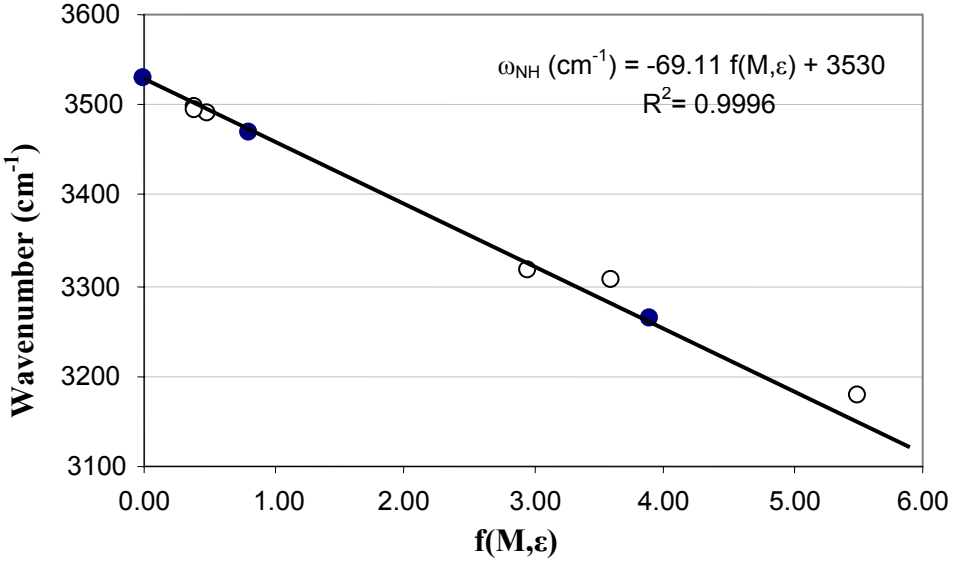

Figure 6.8. Plot of ω_{NH} of indole versus the parameterised solvation variable f(M,ε). Solid circles represent experimental data used in generating the linear fit. Open circles represent data acquired subsequent to calculating the empirical fit. Deviations between actual and predicted vibrational frequencies in several solvents appear in Table 6.2.

In summary, we have developed and applied a model in order to predict the vibrational frequency of a functional group for this family of molecules in a variety of solvents ranging from non-polar to polar and hydrogen bonding solvents. The main advantage of this model over others is that there is no need to identify a particular family of solvents in order to predict the position of the vibrational feature. The fit requires empirical data of only a modest number of solvents, and required parameters can easily be obtained or calculated. Although its applicability for other strongly interacting functional groups such as O-H has not been tested we believe this approach holds great promise for identifying and predicting specific solvation forces.

Chapter 7

Summary and Outlook

This thesis has presented detailed study of how molecular structure affects the surface structure of common liquids. The study has been carried out with a newly developed vibrational sum frequency spectrometer.The results form the analysis of the surface vibrational spectra challenge the chemical intuition and shows that the common knowledge gained from bulk solution studies may not be extended to the surface.

7.1. Summary

The vibrational sum frequency spectroscopy (VSFS) is sensitive only to the interfacial region. Due to its inherent property of detecting molecular vibrations, it is very sensitive to the interfacial molecular forces and resulting molecular conformations. The studies presented in this thesis have used VSFS to examine the surface structure of common liquids at liquid/vapor interfaces. The goal of this work is to correlate molecular structure and intermolecular forces with surface structure sdopted by the molecules at liquid surfaces. The molecular structures of studied liquids are systematically varied both in shape and intermolecular interactions. Changes in surface structure are observed in the vibrational spectra acquired with newly built VSFS.

A detailed description of the instrument as well as the procedure for sum frequency generation and detection are given in Chapter 2. Chapter 3 presented the

surface vibrational studies of linear alkanes ranging in length from 9 to 17 carbon atoms. In contrast to X-ray studies of medium to long chain alkanes, the studies of liquid alkanes at room temperature have shown surprising order. The results have implied an odd-even effect on surface s of alkyl chains ranging in length between 10 and 17 carbon atoms.

The structures are further varied by replacing one terminal methyl group of linear alkanes with 10, 14, and 16 carbon atoms with chloro- or bromomethyl group. The study has aimed to investigate the effect of end group size as well as weakly and moderately interacting dipoles exist in bromo- and chloromethyl groups, respectively, on the surface structure. The studies showed a mixed surface layer primarily occupied by the halogenated end group of the molecules. In addition, the relative amount of methyl terminated end with respect to the halogenated end decrease with increase in chain length of the molecule. These results are attributed to the dipole-dipole interactions and are indicative of a higher surface activity of the halogenated ends compared to the unsubstituted ends.

Chapter 5 has presented additional experiments investigating effect of stronger interactions on surface structure of 1-, 3-, and 5-nonanol and their ketone analog namely 1-, 3-, and 5-nonanones. The results of both alcohol and ketone surfaces showed an increasing surface order as the OH or =O group advances toward the center of the molecule. The results are surprising when linear and branched alcohol/water studies are considered where branched alcohols show a higher disorder molecular structure due to strong hydrogen bonding interactions. Another surprising result is that the surface order observed for ketones are close to the order observed for

alcohols. This implies the importance of simple dipolar interactions compare to highly directional hydrogen bonding in determining the surface structure. The vibrational studies of 1- and 3-octanol liquid surfaces support the observation of a higher order for branched alcohols at liquid/vapor interfaces. The studies are extended to films of octanols on aqueous/vapor interfaces. The 1-octanol film on water showed much higher surface order than 3-octanol films. The increased order in 1-octanol and decreased order in 3-octanol compared to neat surfaces are attributed to the strong hydrogen bonding interactions with underlying water molecules.

Chapter 7 has presented a model study carried out in bulk solution to quantify the interaction between a solute and polar or nonpolar solvent molecule. In this study an aromatic, hetereocyclic molecule, Indoline, is used as a probe for both specific and nonspecific interactions between the solute, Indoline, and variety of solvent molecules. An empirical formula based on semi-empirical parametrization of solvent interaction strength have been proposed. The formula have been tested successfully on a similar molecule, indole. We aim to extend the study to the liquid surfaces in order to better understand interactions between a solute and solvent molecules at liquid/vapor interfaces where interfacial solvation controls adsorption, wetting and chemical reactivity of systems.

7.2. Outlook

The studies can be extended in two directions: improvement on the existing instrument set-up and further investigation of surface structures. Although the SF spectrometer is fully functional and can be used to acquire spectra of many other liquid surfaces of interest, some improvements may increase its sensitivity as well as

applicability. For example, a temperature and pressure controlled sampling stage would enable us to further investigate the systems with high vapor pressure or high melting point.

On the science front, there are many outlined studies in this thesis that each of them can be extended further. A systematic investigation of branched alkanes may address steric effect on surface structures. In addition, the spectra of trans-decalin raised a question of whether or not surface breaks the inversion symmetry exists in a molecule. Isotopic labeling studies of the decalin as well as studies on other symmetric molecules may address the origin of the observed SF activity.

To this point we have investigated the surface structure of pure solvents. The study can be extended toward understanding of solvent structure effect on solute's behavior in interfacial region. Bulk solution studies of indoline suggested that Indoline may be a good candidate to observed solvent specific and nonspecific interactions with solute molecules at interfaces.

Appendix A

A.1. Excel procedure for SF angle and mirror position calculations

The procedure calculates the SF angle with respect to the incoming angles of visible and infrared beam and also the positional changes of the last mirror with respect to the visible light delivery to the monochromator slit. The calculation equations do include the refractive index; therefore, it can be used to calculate angle of reflection inside of prisms. However, mirror positions and angle will be wrong because of the diffraction from the side of the prism. CaF_2 refractive index values with respect to wavelengths are included in the program. Although program provides option for other type of prisms, their refractive index is not provided within the program.

```
'Refractive Index Sheet is password protected with "SFG-RefInd"

Public opt As Integer
Public VisAngle, IRAngle, SFAngle As Double
Public VisWnbr, IRWnbr As Double 'VIS and IR Wavenumber
Public nmat As Single ' =0  air, =1 CaF2, =2 silica, =3 LiF, =4 BaF
Public Avis, Air, Asf As Double
Public nvis, nir, nsf As Single
Public wvis, Wir, Wsf As Single
Public mc As Single 'mirror center positions for translation calculation

Public Const Pi = 3.141592654
Public Const Hs = 5.2 ' stage height
Public Const Hb = 14.3 'beam height from table
Public Const Hbs = Hb - Hs
Public fname As String

Sub From_Angles()

   frmMain.Show
   fname = ActiveSheet.Name

   Select Case nmat
   Case 0 'without prism
      nvis = 1
      nir = 1
      nsf = 1
   Case 1      'CaF2

'Ref Index of Vis
```

```
        VisL = 10000000 / VisWnbr
        For i = 1 To 7
           Rng = "B" & (65 + i)
           L1 = Sheets("RefInd").Range(Rng).Value
           Rng = "B" & (65 + i + 1)
           L2 = Sheets("RefInd").Range(Rng).Value
           If L1 <= VisL And VisL <= L2 Then
              If VisL = L1 Then
                 Rng = "C" & (65 + i)
                 nvis = Sheets("RefInd").Range(Rng).Value
              ElseIf VisL = L2 Then
                 Rng = "C" & (65 + i + 1)
                 nvis = Sheets("RefInd").Range(Rng).Value
              Else
                 Rng = "C" & (65 + i)
                 n1 = Sheets("RefInd").Range(Rng).Value
                 Rng = "C" & (65 + i + 1)
                 n2 = Sheets("RefInd").Range(Rng).Value
                 nvis = (n1 + n2) / 2
              End If
           End If
        Next i

'Ref Index of IR
        IRL = 10000000 / IRWnbr
        For i = 1 To 48
           Rng = "B" & (72 + i)
           L1 = Sheets("RefInd").Range(Rng).Value
           Rng = "B" & (72 + i + 1)
           L2 = Sheets("RefInd").Range(Rng).Value
           If L1 <= IRL And IRL <= L2 Then
              If IRL = L1 Then
                 Rng = "C" & (72 + i)
                 nir = Sheets("RefInd").Range(Rng).Value
              ElseIf IRL = L2 Then
                 Rng = "C" & (72 + i + 1)
                 nir = Sheets("RefInd").Range(Rng).Value
              Else
                 Rng = "C" & (72 + i)
                 n1 = Sheets("RefInd").Range(Rng).Value
                 Rng = "C" & (72 + i + 1)
                 n2 = Sheets("RefInd").Range(Rng).Value
                 nir = (n1 + n2) / 2
              End If
           End If
        Next i
```

```
'Ref index of SF
        SFWnbr = VisWnbr + IRWnbr
        ISF = 10000000 / SFWnbr
        For i = 1 To 13
           Rng = "B" & (59 + i)
           L1 = Sheets("RefInd").Range(Rng).Value
           Rng = "B" & (59 + i + 1)
           L2 = Sheets("RefInd").Range(Rng).Value
           If L1 <= ISF And ISF <= L2 Then
              If ISF = L1 Then
                 Rng = "C" & (59 + i)
                 nir = Sheets("RefInd").Range(Rng).Value
              ElseIf ISF = L2 Then
                 Rng = "C" & (59 + i + 1)
                 nir = Sheets("RefInd").Range(Rng).Value
              Else
                 Rng = "C" & (59 + i)
                 n1 = Sheets("RefInd").Range(Rng).Value
                 Rng = "C" & (59 + i + 1)
                 n2 = Sheets("RefInd").Range(Rng).Value
                 nsf = (n1 + n2) / 2
              End If
           End If
        Next i

     Case 2      'Silica

'Ref Index of Vis
        VisL = 10000000 / VisWnbr
        For i = 1 To 13
           Rng = "B" & (9 + i)
           L1 = Sheets("RefInd").Range(Rng).Value
           Rng = "B" & (9 + i + 1)
           L2 = Sheets("RefInd").Range(Rng).Value
           If L1 <= VisL And VisL <= L2 Then
              If VisL = L1 Then
                 Rng = "C" & (9 + i)
                 nvis = Sheets("RefInd").Range(Rng).Value
              ElseIf VisL = L2 Then
                 Rng = "C" & (9 + i + 1)
                 nvis = Sheets("RefInd").Range(Rng).Value
              Else
                 Rng = "C" & (9 + i)
                 n1 = Sheets("RefInd").Range(Rng).Value
                 Rng = "C" & (9 + i + 1)
```

```
            n2 = Sheets("RefInd").Range(Rng).Value
            nvis = (n1 + n2) / 2
          End If
        End If
      Next i

'Ref Index of IR
      IRL = 10000000 / IRWnbr
      If IRL > 3370 Then
        msg = "Requested wavelength is beyond the transmission range of silica."
        msg = msg & Chr(13) & "Please check the wavelength and try again."
        MsgBox msg, vbCritical, "Error"
        End
      Else
      For i = 1 To 17
        Rng = "B" & (21 + i)
        L1 = Sheets("RefInd").Range(Rng).Value
        Rng = "B" & (21 + i + 1)
        L2 = Sheets("RefInd").Range(Rng).Value
        If L1 <= IRL And IRL <= L2 Then
          If IRL = L1 Then
            Rng = "C" & (21 + i)
            nir = Sheets("RefInd").Range(Rng).Value
          ElseIf IRL = L2 Then
            Rng = "C" & (21 + i + 1)
            nir = Sheets("RefInd").Range(Rng).Value
          Else
            Rng = "C" & (21 + i)
            n1 = Sheets("RefInd").Range(Rng).Value
            Rng = "C" & (21 + i + 1)
            n2 = Sheets("RefInd").Range(Rng).Value
            nir = (n1 + n2) / 2
          End If
        End If
      Next i
      End If
'Ref index of SF
      SFWnbr = VisWnbr + IRWnbr
      ISF = 10000000 / SFWnbr
      For i = 1 To 15
        Rng = "B" & (7 + i)
        L1 = Sheets("RefInd").Range(Rng).Value
        Rng = "B" & (7 + i + 1)
        L2 = Sheets("RefInd").Range(Rng).Value
        If L1 <= ISF And ISF <= L2 Then
          If ISF = L1 Then
```

```
                Rng = "C" & (7 + i)
                nir = Sheets("RefInd").Range(Rng).Value
            ElseIf ISF = L2 Then
                Rng = "C" & (7 + i + 1)
                nir = Sheets("RefInd").Range(Rng).Value
            Else
                Rng = "C" & (7 + i)
                n1 = Sheets("RefInd").Range(Rng).Value
                Rng = "C" & (7 + i + 1)
                n2 = Sheets("RefInd").Range(Rng).Value
                nsf = (n1 + n2) / 2
            End If
        End If
    Next i

    Case Else
        nvis = 1
        nir = 1
        nsf = 1
    End Select

    Range("D12").Value = nvis
    Range("D13").Value = nvis
    Range("D14").Value = nvis

    wvis = VisWnbr
    Wir = IRWnbr
    Wsf = wvis + Wir

'transfer data to excel

    Range("B12").Value = Format(10000000 / wvis, "##00.00")
    Range("B13").Value = Format(10000000 / Wir, "##00.00")
    Range("B14").Value = Format(10000000 / Wsf, "##00.00")

    Range("C12").Value = Format(wvis, "##00.00")
    Range("C13").Value = Format(Wir, "##00.00")
    Range("C14").Value = Format(Wsf, "##00.00")

    Range("D12").Value = nvis
    Range("D13").Value = nir
    Range("D14").Value = nsf

    Avis = (VisAngle * Pi / 180)
    If IRAngle < 0 Then IRAngle = 180 - Air
    Air = (IRAngle * Pi / 180)
```

```
    X = (nvis * wvis * Sin(Avis) + nir * Wir * Sin(Air)) / (nsf * Wsf)
    Asf = Atn(X / Sqr(1 - X ^ 2))

    SFAngle = Asf * 180 / Pi

    Range("E12").Value = Format(VisAngle, "##00.00")
    Range("E13").Value = Format(IRAngle, "##00.00")
    Range("E14").Value = Format(SFAngle, "##00.00")

    Calculate4Vis
    Calculate4SF

End Sub

Sub Calculate4Vis()

Dim Xt1, Xt2, Yt1, Yt2 As Single  'Table coordinates
Dim Xs1, Xs2, Ys1, Ys2 As Single  'Table coordinates
Dim Xn1, Xn2, Yn1, Yn2 As Single  'Surface normal coordinates
Dim Xiv1, Xiv2, Yiv1, Yiv2 As Single  'Incoming visible
Dim Xrv1, Xrv2, Xrv3, Yrv1, Yrv2, Yrv3 As Single 'Reflected visible
Dim Xir1, Xir2, Yir1, Yir2 As Single 'Incoming IR coordinates
Dim Xrir1, Xrir2, Yrir1, Yrir2 As Single  'Reflected IR coordinates
Dim Xsf1, Xsf2, Ysf1, Ysf2 As Single  'SF coordinates

'chart....

    fname = ActiveSheet.Name
    cname = " Vis2CCD"

    n = ActiveSheet.ChartObjects.Count

    If n < 1 Then
       Charts.Add
       ActiveChart.Location Where:=xlLocationAsObject, Name:=fname

          With ActiveSheet.ChartObjects(1)
           .Top = 225
           .Left = 1
           .Height = 200
           .Width = 400
       End With
    End If

'table
```

```
Xt1 = -10
Yt1 = 0
Xt2 = 60
Yt2 = 0

   Range("AB30").Value = "Table"
   Range("AB31").Value = Xt1
   Range("AB32").Value = Xt2
   Range("AB34").Value = Yt1
   Range("AB35").Value = Yt2

'beginning of chart settings
   If n < 1 Then
      ActiveChart.ChartType = xlXYScatterLines
      ActiveChart.SeriesCollection.NewSeries
      ActiveChart.SeriesCollection(1).XValues = "=" & fname & "!R31C28:R32C28"
      ActiveChart.SeriesCollection(1).Values = "=" & fname & "!R34C28:R35C28"
      ActiveChart.SeriesCollection(1).Name = "=" & fname & "!R30C28"

      With ActiveChart
       '.Name = cname
       .HasTitle = True
       .ChartTitle.Characters.Text = "VIS ---> CCD"
       .ChartTitle.Font.Name = "Arial"
       .ChartTitle.Font.Size = 10
       .ChartTitle.Font.Color = RGB(0, 0, 255)
       .Axes(xlCategory, xlPrimary).HasTitle = True
       .Axes(xlCategory, xlPrimary).AxisTitle.Characters.Text = "Distance"
       .Axes(xlValue, xlPrimary).HasTitle = True
       .Axes(xlValue, xlPrimary).AxisTitle.Characters.Text = "Height from table"
       .Axes(xlCategory, xlPrimary).CategoryType = xlAutomatic
       .HasAxis(xlCategory, xlPrimary) = True
       .HasAxis(xlValue, xlPrimary) = False
       .Axes(xlCategory, xlPrimary).CategoryType = xlAutomatic
      End With

      ActiveChart.PlotArea.Select
      With Selection.Border
         .Weight = xlThin
         .LineStyle = xlNone
      End With
      'Selection.Interior.ColorIndex = xlNone

'x-scale

      With ActiveChart.Axes(xlCategory)
```

```
            .HasMajorGridlines = False
            .HasMinorGridlines = False
        End With

       If ActiveChart.HasAxis(xlCategory, xlPrimary) = True Then
            With ActiveChart.Axes(xlCategory)
                .MinimumScale = -5
                .MaximumScale = 40
                .MinorUnitIsAuto = True
                .MajorUnitIsAuto = True
                .Crosses = xlCustom
                .CrossesAt = -5
                .ReversePlotOrder = False
                .ScaleType = xlLinear
                .DisplayUnit = xlNone
            End With
        End If

'y-scale

        With ActiveChart.Axes(xlValue)
            .HasMajorGridlines = False
            .HasMinorGridlines = False
        End With

        If ActiveChart.HasAxis(xlValue, xlPrimary) = True Then
            With ActiveChart.Axes(xlValue)
                .MinimumScale = 0
                .MaximumScale = 20
                .MinorUnitIsAuto = True
                .MajorUnitIsAuto = True
                .ReversePlotOrder = False
                .ScaleType = xlLinear
                .DisplayUnit = xlNone
            End With
        End If

        ActiveChart.HasLegend = False
        ActiveChart.ApplyDataLabels                    Type:=xlDataLabelsShowNone,
LegendKey:=False
    End If
'end of chart setting

'surface
Xs1 = -2.5
Ys1 = Hs
```

```
Xs2 = 2.5
Ys2 = Hs

   Range("AC30").Value = "Sample"
   Range("AC31").Value = Xs1
   Range("AC32").Value = Xs2
   Range("AC34").Value = Ys1
   Range("AC35").Value = Ys2

   If n < 1 Then
      ActiveChart.SeriesCollection.NewSeries
      ActiveChart.SeriesCollection(2).XValues = "=" & fname & "!R31C29:R32C29"
      ActiveChart.SeriesCollection(2).Values = "=" & fname & "!R34C29:R35C29"
      ActiveChart.SeriesCollection(2).Name = "=" & fname & "!R30C29"
   End If
'surface normal
Xn1 = 0
Yn1 = Hs
Xn2 = 0
Yn2 = Hs + 5

   Range("AD30").Value = "Normal"
   Range("AD31").Value = Xn1
   Range("AD32").Value = Xn2
   Range("AD34").Value = Yn1
   Range("AD35").Value = Yn2

   If n < 1 Then
      ActiveChart.SeriesCollection.NewSeries
      ActiveChart.SeriesCollection(3).XValues = "=" & fname & "!R31C30:R32C30"
      ActiveChart.SeriesCollection(3).Values = "=" & fname & "!R34C30:R35C30"
      ActiveChart.SeriesCollection(3).Name = "=" & fname & "!R30C30"
   End If

'incident beam
   Range("AE29").Value = "Incident Beams"

'VISIBLE

Xiv1 = Xn1 - (5 * Sin(Avis))
Xiv2 = Xn1
Yiv1 = Hs + (5 * Cos(Avis))
Yiv2 = Hs

    Range("AE30").Value = "VIS"
   Range("AE31").Value = Xiv1
```

```
    Range("AE32").Value = Xiv2
    Range("AE34").Value = Yiv1
    Range("AE35").Value = Yiv2

    If n < 1 Then
        ActiveChart.SeriesCollection.NewSeries
        ActiveChart.SeriesCollection(4).XValues = "=" & fname & "!R31C31:R32C31"
        ActiveChart.SeriesCollection(4).Values = "=" & fname & "!R34C31:R35C31"
        ActiveChart.SeriesCollection(4).Name = "=" & fname & "!R30C31"
    End If

'IR

Xir1 = Xn1 - (5 * Sin(Air))
Xir2 = Xn1
Yir1 = Hs + (5 * Cos(Air))
Yir2 = Hs


    Range("AF30").Value = "IR"
    Range("AF31").Value = Xir1
    Range("AF32").Value = Xir2
    Range("AF34").Value = Yir1
    Range("AF35").Value = Yir2

    If n < 1 Then
        ActiveChart.SeriesCollection.NewSeries
        ActiveChart.SeriesCollection(5).XValues = "=" & fname & "!R31C32:R32C32"
        ActiveChart.SeriesCollection(5).Values = "=" & fname & "!R34C32:R35C32"
        ActiveChart.SeriesCollection(5).Name = "=" & fname & "!R30C32"
    End If

'Reflected Visible

Xrv1 = Xn1
Xrv2 = Xn1 + (Hbs * Tan(Avis))
Xrv3 = Xrv2 + 30
Yrv1 = Hs
Yrv2 = Yrv1 + Hbs
Yrv3 = Yrv2

    mc = Xrv2 ' stores center of mirror for tanslation calculation

    Range("AG29").Value = "Reflected Beams"
    Range("AG30").Value = "VIS"
    Range("AG31").Value = Xrv1
```

```
    Range("AG32").Value = Xrv2
    Range("AG33").Value = Xrv3
    Range("AG34").Value = Yrv1
    Range("AG35").Value = Yrv2
    Range("AG36").Value = Yrv3

    If n < 1 Then
        ActiveChart.SeriesCollection.NewSeries
        ActiveChart.SeriesCollection(6).XValues = "=" & fname & "!R31C33:R33C33"
        ActiveChart.SeriesCollection(6).Values = "=" & fname & "!R34C33:R36C33"
        ActiveChart.SeriesCollection(6).Name = "=" & fname & "!R30C33"
    End If

'IR

Xrir1 = Xn1
Xrir2 = Xn1 + (30 * Sin(Air))
Yrir1 = Hs
Yrir2 = Hs + (30 * Cos(Air))

    Range("AH30").Value = "IR"
    Range("AH31").Value = Xrir1
    Range("AH32").Value = Xrir2
    Range("AH34").Value = Yrir1
    Range("AH35").Value = Yrir2

    If n < 1 Then
        ActiveChart.SeriesCollection.NewSeries
        ActiveChart.SeriesCollection(7).XValues = "=" & fname & "!R31C34:R32C34"
        ActiveChart.SeriesCollection(7).Values = "=" & fname & "!R34C34:R35C34"
        ActiveChart.SeriesCollection(7).Name = "=" & fname & "!R30C34"
    End If

'Mirror
Dim Xm1, Xm2, Ym1, Ym2 As Single

    Call CalcMirrorPos(Avis, Xm1, Xm2, Ym1, Ym2)

    Range("AI30").Value = "Mirror"
    Range("AI31").Value = Xm1
    Range("AI32").Value = Xm2
    Range("AI34").Value = Ym1
    Range("AI35").Value = Ym2

    If n < 1 Then
        ActiveChart.SeriesCollection.NewSeries
```

```
        ActiveChart.SeriesCollection(8).XValues = "=" & fname & "!R31C35:R32C35"
        ActiveChart.SeriesCollection(8).Values = "=" & fname & "!R34C35:R35C35"
        ActiveChart.SeriesCollection(8).Name = "=" & fname & "!R30C35"
    End If

'SFG

    Xsf1 = 0
    Ysf1 = Hs
    Asfg = Pi / 2 - Asf

    Xsf2 = Xrv2
    Ysf2 = Ysf1 + Xsf2 / Tan(Asf)


    Do Until Xsf2 >= Xm2

        Xsf2 = Xsf2 + 0.1
        Ysf2 = Ysf1 + Xsf2 / Tan(Asf)

        If Ysf2 >= Ym2 Then
            If Format(Ysf2, "##0.0") = Format(Ym2, "##0.0") Then
                hitmirror = 1
            Else
                hitmirror = 0
            End If
            Exit Do
        End If
    Loop

    Xsf3 = 10 + Xsf2  ' 10 is an arbitrary number

    If hitmirror = 1 Then
        Ysf3 = Ysf2 + (Xsf3 - Xsf2) * Tan(Asf)
    Else
        Ysf3 = Ysf1 + Xsf3 / Tan(Asf)
    End If


    Range("AJ30").Value = "SFG"
    Range("AJ31").Value = Xsf1
    Range("AJ32").Value = Xsf2
    Range("AJ33").Value = Xsf3
    Range("AJ34").Value = Ysf1
    Range("AJ35").Value = Ysf2
    Range("AJ36").Value = Ysf3
```

```
    If n < 1 Then
       ActiveChart.SeriesCollection.NewSeries
       ActiveChart.SeriesCollection(9).XValues = "=" & fname & "!R31C36:R33C36"
       ActiveChart.SeriesCollection(9).Values = "=" & fname & "!R34C36:R36C36"
       ActiveChart.SeriesCollection(9).Name = "=" & fname & "!R30C36"
    End If

'Set styles in chart
    If n < 1 Then
       Call Setstyles

          ActiveChart.SeriesCollection(4).Select
       With Selection.Border
          .ColorIndex = 5
          .Weight = xlThin
          .LineStyle = xlContinuous
       End With
       With Selection
          .MarkerBackgroundColorIndex = xlNone
          .MarkerForegroundColorIndex = xlAutomatic
          .MarkerStyle = xlNone
          .Smooth = False
          .MarkerSize = 7
          .Shadow = False
       End With

       ActiveChart.SeriesCollection(6).Select
       With Selection.Border
          .ColorIndex = 5
          .Weight = xlThick
          .LineStyle = xlContinuous
       End With
       With Selection
          .MarkerBackgroundColorIndex = xlAutomatic
          .MarkerForegroundColorIndex = xlAutomatic
          .MarkerStyle = xlNone
          .Smooth = False
          .MarkerSize = 7
          .Shadow = False
       End With

       ActiveChart.SeriesCollection(9).Select
       With Selection.Border
          .ColorIndex = 6
          .Weight = xlThin
```

```
            .LineStyle = xlContinuous
        End With
        With Selection
            .MarkerBackgroundColorIndex = xlNone
            .MarkerForegroundColorIndex = xlAutomatic
            .MarkerStyle = xlNone
            .Smooth = False
            .MarkerSize = 5
            .Shadow = False
        End With
    End If

End Sub
Sub Calculate4SF()

Dim Xt1, Xt2, Yt1, Yt2 As Single  'Table coordinates
Dim Xs1, Xs2, Ys1, Ys2 As Single  'Table coordinates
Dim Xn1, Xn2, Yn1, Yn2 As Single  'Surface normal coordinates
Dim Xiv1, Xiv2, Yiv1, Yiv2 As Single  'Incoming visible
Dim Xrv1, Xrv2, Xrv3, Yrv1, Yrv2, Yrv3 As Single 'Reflected visible
Dim Xir1, Xir2, Yir1, Yir2 As Single 'Incoming IR coordinates
Dim Xrir1, Xrir2, Yrir1, Yrir2 As Single  'Reflected IR coordinates
Dim Xsf1, Xsf2, Ysf1, Ysf2 As Single  'SF coordinates


'chart....

    fname = ActiveSheet.Name
    cname = " Vis2CCD"


    n = ActiveSheet.ChartObjects.Count

    If n < 2 Then
        Charts.Add
        ActiveChart.Location Where:=xlLocationAsObject, Name:=fname


        With ActiveSheet.ChartObjects(2)
            .Top = 225
            .Left = 350
            .Height = 200
            .Width = 400
        End With
    End If
```

```
'table
Xt1 = -10
Yt1 = 0
Xt2 = 60
Yt2 = 0

    Range("AB40").Value = "Table"
    Range("AB41").Value = Xt1
    Range("AB42").Value = Xt2
    Range("AB44").Value = Yt1
    Range("AB45").Value = Yt2

'beginning of chart settings
    If n < 2 Then
        ActiveChart.ChartType = xlXYScatterLines
        ActiveChart.SeriesCollection.NewSeries
        ActiveChart.SeriesCollection(1).XValues = "=" & fname & "!R41C28:R42C28"
        ActiveChart.SeriesCollection(1).Values = "=" & fname & "!R44C28:R45C28"
        ActiveChart.SeriesCollection(1).Name = "=" & fname & "!R40C28"

        With ActiveChart
          '.Name = cname
          .HasTitle = True
          .ChartTitle.Characters.Text = "SFG ---> CCD"
          .ChartTitle.Font.Name = "Arial"
          .ChartTitle.Font.Size = 10
          .ChartTitle.Font.Color = RGB(0, 0, 255)
          .Axes(xlCategory, xlPrimary).HasTitle = True
          .Axes(xlCategory, xlPrimary).AxisTitle.Characters.Text = "Distance"
          .Axes(xlValue, xlPrimary).HasTitle = True
          .Axes(xlValue, xlPrimary).AxisTitle.Characters.Text = "Height from table"
          .Axes(xlCategory, xlPrimary).CategoryType = xlAutomatic
          .HasAxis(xlCategory, xlPrimary) = True
          .HasAxis(xlValue, xlPrimary) = False
          .Axes(xlCategory, xlPrimary).CategoryType = xlAutomatic
        End With

        ActiveChart.PlotArea.Select
        With Selection.Border
            .Weight = xlThin
            .LineStyle = xlNone
        End With
        'Selection.Interior.ColorIndex = xlNone


'x-scale
```

```
        With ActiveChart.Axes(xlCategory)
           .HasMajorGridlines = False
           .HasMinorGridlines = False
        End With


        If ActiveChart.HasAxis(xlCategory, xlPrimary) = True Then
           With ActiveChart.Axes(xlCategory)
              .MinimumScale = -5
              .MaximumScale = 40
              .MinorUnitIsAuto = True
              .MajorUnitIsAuto = True
              .Crosses = xlCustom
              .CrossesAt = -5
              .ReversePlotOrder = False
              .ScaleType = xlLinear
              .DisplayUnit = xlNone
           End With
        End If

'y-scale

        With ActiveChart.Axes(xlValue)
           .HasMajorGridlines = False
           .HasMinorGridlines = False
        End With

        If ActiveChart.HasAxis(xlValue, xlPrimary) = True Then
           With ActiveChart.Axes(xlValue)
              .MinimumScale = 0
              .MaximumScale = 20
              .MinorUnitIsAuto = True
              .MajorUnitIsAuto = True
              .ReversePlotOrder = False
              .ScaleType = xlLinear
              .DisplayUnit = xlNone
           End With
        End If

        ActiveChart.HasLegend = False
        ActiveChart.ApplyDataLabels                    Type:=xlDataLabelsShowNone,
LegendKey:=False
     End If
'end of chart setting
```

```
'surface
Xs1 = -2.5
Ys1 = Hs
Xs2 = 2.5
Ys2 = Hs

   Range("AC40").Value = "Sample"
   Range("AC41").Value = Xs1
   Range("AC42").Value = Xs2
   Range("AC44").Value = Ys1
   Range("AC45").Value = Ys2

   If n < 2 Then
      ActiveChart.SeriesCollection.NewSeries
      ActiveChart.SeriesCollection(2).XValues = "=" & fname & "!R41C29:R42C29"
      ActiveChart.SeriesCollection(2).Values = "=" & fname & "!R44C29:R45C29"
      ActiveChart.SeriesCollection(2).Name = "=" & fname & "!R40C29"
   End If

'surface normal
Xn1 = 0
Yn1 = Hs
Xn2 = 0
Yn2 = Hs + 5

   Range("AD40").Value = "Normal"
   Range("AD41").Value = Xn1
   Range("AD42").Value = Xn2
   Range("AD44").Value = Yn1
   Range("AD45").Value = Yn2

   If n < 2 Then
      ActiveChart.SeriesCollection.NewSeries
      ActiveChart.SeriesCollection(3).XValues = "=" & fname & "!R41C30:R42C30"
      ActiveChart.SeriesCollection(3).Values = "=" & fname & "!R44C30:R45C30"
      ActiveChart.SeriesCollection(3).Name = "=" & fname & "!R40C30"
   End If

'incident beam
   Range("AE29").Value = "Incident Beams"

'VISIBLE

Xiv1 = Xn1 - (5 * Sin(Avis))
Xiv2 = Xn1
Yiv1 = Hs + (5 * Cos(Avis))
```

```
Yiv2 = Hs

   Range("AE40").Value = "VIS"
   Range("AE41").Value = Xiv1
   Range("AE42").Value = Xiv2
   Range("AE44").Value = Yiv1
   Range("AE45").Value = Yiv2

   If n < 2 Then
      ActiveChart.SeriesCollection.NewSeries
      ActiveChart.SeriesCollection(4).XValues = "=" & fname & "!R41C31:R42C31"
      ActiveChart.SeriesCollection(4).Values = "=" & fname & "!R44C31:R45C31"
      ActiveChart.SeriesCollection(4).Name = "=" & fname & "!R40C31"
   End If

'IR

Xir1 = Xn1 - (5 * Sin(Air))
Xir2 = Xn1
Yir1 = Hs + (5 * Cos(Air))
Yir2 = Hs

   Range("AF40").Value = "IR"
   Range("AF41").Value = Xir1
   Range("AF42").Value = Xir2
   Range("AF44").Value = Yir1
   Range("AF45").Value = Yir2

   If n < 2 Then
      ActiveChart.SeriesCollection.NewSeries
      ActiveChart.SeriesCollection(5).XValues = "=" & fname & "!R41C32:R42C32"
      ActiveChart.SeriesCollection(5).Values = "=" & fname & "!R44C32:R45C32"
      ActiveChart.SeriesCollection(5).Name = "=" & fname & "!R40C32"
   End If

'SFG

Xsf1 = Xn1
Xsf2 = Xn1 + (Hbs * Tan(Asf))
Xsf3 = Xsf2 + 30
Ysf1 = Hs
Ysf2 = Ysf1 + Hbs
Ysf3 = Ysf2

   Range("AG39").Value = "Reflected Beams"
   Range("AG40").Value = "SF"
```

```
    Range("AG41").Value = Xsf1
    Range("AG42").Value = Xsf2
    Range("AG43").Value = Xsf3
    Range("AG44").Value = Ysf1
    Range("AG45").Value = Ysf2
    Range("AG46").Value = Ysf3

    If n < 2 Then
        ActiveChart.SeriesCollection.NewSeries
        ActiveChart.SeriesCollection(6).XValues = "=" & fname & "!R41C33:R43C33"
        ActiveChart.SeriesCollection(6).Values = "=" & fname & "!R44C33:R46C33"
        ActiveChart.SeriesCollection(6).Name = "=" & fname & "!R40C33"
    End If

'IR

Xrir1 = Xn1
Xrir2 = Xn1 + (30 * Sin(Air))
Yrir1 = Hs
Yrir2 = Hs + (30 * Cos(Air))

    Range("AH40").Value = "IR"
    Range("AH41").Value = Xrir1
    Range("AH42").Value = Xrir2
    Range("AH44").Value = Yrir1
    Range("AH45").Value = Yrir2

    If n < 2 Then
        ActiveChart.SeriesCollection.NewSeries
        ActiveChart.SeriesCollection(7).XValues = "=" & fname & "!R41C34:R42C34"
        ActiveChart.SeriesCollection(7).Values = "=" & fname & "!R44C34:R45C34"
        ActiveChart.SeriesCollection(7).Name = "=" & fname & "!R40C34"
    End If

'Mirror
Dim Xm1, Xm2, Ym1, Ym2 As Single

    Call CalcMirrorPos(Asf, Xm1, Xm2, Ym1, Ym2)

    Range("AI40").Value = "Mirror"
    Range("AI41").Value = Xm1
    Range("AI42").Value = Xm2
    Range("AI44").Value = Ym1
    Range("AI45").Value = Ym2

    If n < 2 Then
```

```
        ActiveChart.SeriesCollection.NewSeries
        ActiveChart.SeriesCollection(8).XValues = "=" & fname & "!R41C35:R42C35"
        ActiveChart.SeriesCollection(8).Values = "=" & fname & "!R44C35:R45C35"
        ActiveChart.SeriesCollection(8).Name = "=" & fname & "!R40C35"
    End If

'VIS

    Xrv1 = 0
    Yrv1 = Hs


    Xrv2 = Xsf2
    Yrv2 = Yrv1 + Xrv2 / Tan(Avis)

    Do Until Xrv2 >= Xm2

        Xrv2 = Xrv2 + 0.1
        Yrv2 = Yrv1 + Xrv2 / Tan(Avis)

        If Yrv2 >= Ym2 Then
            If Format(Yrv2, "##0.0") = Format(Ym2, "##0.0") Then
                hitmirror = 1
            Else
                hitmirror = 0
            End If
            Exit Do
        End If
    Loop

    Xrv3 = 10 + Xrv2  ' 10 is an arbitrary number

    If hitmirror = 1 Then
        Yrv3 = Yrv2 + (Xrv3 - Xrv2) * Tan(Avis)
    Else
        Yrv3 = Yrv1 + Xrv3 / Tan(Avis)
    End If

    Range("AJ40").Value = "VIS"
    Range("AJ41").Value = Xrv1
    Range("AJ42").Value = Xrv2
    Range("AJ43").Value = Xrv3
    Range("AJ44").Value = Yrv1
    Range("AJ45").Value = Yrv2
    Range("AJ46").Value = Yrv3
```

```
    If n < 2 Then
       ActiveChart.SeriesCollection.NewSeries
       ActiveChart.SeriesCollection(9).XValues = "=" & fname & "!R41C36:R43C36"
       ActiveChart.SeriesCollection(9).Values = "=" & fname & "!R44C36:R46C36"
       ActiveChart.SeriesCollection(9).Name = "=" & fname & "!R40C36"
    End If

'Set styles in chart
    If n < 2 Then
       Call Setstyles

       ActiveChart.SeriesCollection(4).Select
       With Selection.Border
          .ColorIndex = 5
          .Weight = xlThin
          .LineStyle = xlContinuous
       End With
       With Selection
          .MarkerBackgroundColorIndex = xlNone
          .MarkerForegroundColorIndex = xlAutomatic
          .MarkerStyle = xlNone
          .Smooth = False
          .MarkerSize = 7
          .Shadow = False
       End With

       ActiveChart.SeriesCollection(6).Select
       With Selection.Border
          .ColorIndex = 6
          .Weight = xlThick
          .LineStyle = xlContinuous
       End With
       With Selection
          .MarkerBackgroundColorIndex = xlAutomatic
          .MarkerForegroundColorIndex = xlAutomatic
          .MarkerStyle = xlNone
          .Smooth = False
          .MarkerSize = 7
          .Shadow = False
       End With

       ActiveChart.SeriesCollection(9).Select
       With Selection.Border
          .ColorIndex = 5
          .Weight = xlThin
          .LineStyle = xlContinuous
```

```
        End With
        With Selection
            .MarkerBackgroundColorIndex = xlNone
            .MarkerForegroundColorIndex = xlAutomatic
            .MarkerStyle = xlNone
            .Smooth = False
            .MarkerSize = 5
            .Shadow = False
        End With
    End If

' mirror translation amount and heights of two edges

    Range("D16:J17").Font.ColorIndex = 42
    Range("G17:J17").Font.ColorIndex = 2
    Range("G17:J17").HorizontalAlignment = xlCenter
    Range("G17:J17").VerticalAlignment = xlCenter

    Range("D17").Value = "New mirror position relative to visible light (in cm)"
    Range("G16").Value = "Translate"
    Range("H16").Value = "distance"
    Range("I16").Value = "Left-Edge"
    Range("J16").Value = "Right-Edge"
    mc = Xsf2 - mc
    Sheets(fname).Activate
    Range("G17").Value = Format(mc, "##0.00")
    Range("H17").Value = Format(Xsf2, "##0.00")
    Range("I17").Value = Format(Ym1, "##0.00")
    Range("J17").Value = Format(Ym2, "##0.00")

    Range("A1").Select

End Sub
Sub CalcMirrorPos(Ain, x1, x2, y1, y2 As Single)
Dim Am, Asn As Single ' angle of mirror with visible and surface normal


   Am = (Pi / 2 - Ain) / 2
    X = Hbs * Tan(Ain)
    Asn = Pi / 2 - (Am + Ain)

'find distances from the center of mirror (X.Y)
    x1 = 2.54 * Cos(Asn) / 2
    y1 = 2.54 * Sin(Asn) / 2
```

```
    x2 = X + x1
    y2 = Hbs + Hs + y1

    x1 = X - x1
    y1 = Hbs + Hs - y1

End Sub

Sub Setstyles()
'Table
        ActiveChart.SeriesCollection(1).Select
        With Selection.Border
            .ColorIndex = 1
            .Weight = xlThick
            .LineStyle = xlGray75
        End With
        With Selection
            .MarkerBackgroundColorIndex = xlAutomatic
            .MarkerForegroundColorIndex = xlAutomatic
            .MarkerStyle = xlNone
            .Smooth = False
            .MarkerSize = 9
            .Shadow = False
        End With
'Stage
        ActiveChart.SeriesCollection(2).Select
        With Selection.Border
            .ColorIndex = 1
            .Weight = xlThick
            .LineStyle = xlGray75
        End With
        With Selection
            .MarkerBackgroundColorIndex = xlAutomatic
            .MarkerForegroundColorIndex = xlAutomatic
            .MarkerStyle = xlNone
            .Smooth = False
            .MarkerSize = 9
            .Shadow = False
        End With

'Surface normal
        ActiveChart.SeriesCollection(3).Select
        With Selection.Border
            .ColorIndex = 48
            .Weight = xlThin
            .LineStyle = xlDash
```

```
        End With
        With Selection
            .MarkerBackgroundColorIndex = xlAutomatic
            .MarkerForegroundColorIndex = xlAutomatic
            .MarkerStyle = xlNone
            .Smooth = False
            .MarkerSize = 5
            .Shadow = False
        End With

'Inc. IR
        ActiveChart.SeriesCollection(5).Select
        With Selection.Border
            .ColorIndex = 3
            .Weight = xlThin
            .LineStyle = xlContinuous
        End With
        With Selection
            .MarkerBackgroundColorIndex = xlNone
            .MarkerForegroundColorIndex = xlAutomatic
            .MarkerStyle = xlNone
            .Smooth = False
            .MarkerSize = 5
            .Shadow = False
        End With


        ActiveChart.SeriesCollection(7).Select
        With Selection.Border
            .ColorIndex = 3
            .Weight = xlThin
            .LineStyle = xlContinuous
        End With
        With Selection
            .MarkerBackgroundColorIndex = xlNone
            .MarkerForegroundColorIndex = xlAutomatic
            .MarkerStyle = xlNone
            .Smooth = False
            .MarkerSize = 5
            .Shadow = False
        End With

        ActiveChart.SeriesCollection(8).Select
        With Selection.Border
            .ColorIndex = 1
            .Weight = xlThick
```

```
            .LineStyle = xlGray75
        End With
        With Selection
            .MarkerBackgroundColorIndex = xlNone
            .MarkerForegroundColorIndex = xlAutomatic
            .MarkerStyle = xlAutomatic
            .Smooth = False
            .MarkerSize = 9
            .Shadow = False
        End With
End Sub

Sub Reset()

fname = ActiveSheet.Name
Range("A1:AZ150").Clear
    Range("A1:Z100").Interior.Color = Black
    Range("B2:I2").Select
    With Selection
        .WrapText = False
        .Orientation = 0
        .AddIndent = False
        .IndentLevel = 0
        .ShrinkToFit = False
        .MergeCells = True
        .Font.Size = 16
        .Font.Bold = True
        .Font.Italic = False
        .Font.ColorIndex = 2
        .Font.Name = "Courier New"
        .Value = "SF ANGLE CALCULATIONS"
    End With
    With Selection
        .HorizontalAlignment = xlCenter
        .VerticalAlignment = xlCenter
    End With

    msg = "     The program calculates the new mirror position relative to"
    msg = msg & " visible delivery and draws the Vis and SF delivery charts. Charts
are in actual"
    msg = msg & " dimentions (cm).  Colors of the beams in the table denotes the color
of the beam in"
    msg = msg & " the chart."
    Range("B3:I4").Select
    With Selection
        .HorizontalAlignment = xlLeft
```

```
        .VerticalAlignment = xlCenter
        .WrapText = True
        .Orientation = 0
        .AddIndent = False
        .IndentLevel = 0
        .ShrinkToFit = False
        .MergeCells = True
        .Font.Size = 8
        .Font.Bold = False
        .Font.Italic = True
        .Font.Name = "Arial"
        .Font.ColorIndex = 48
        .Value = msg
    End With

    msg = "To recalculate with new angle either change the values in the table or"
    msg = msg & " change the values in the pop-up window when ""calculate from angles"""
    msg = msg & " is pressed. ""Reset"" button resets the default values."

    Range("B5:I6").Select
    With Selection
        .HorizontalAlignment = xlLeft
        .VerticalAlignment = xlCenter
        .WrapText = True
        .Orientation = 0
        .AddIndent = False
        .IndentLevel = 0
        .ShrinkToFit = False
        .MergeCells = True
        .Font.Size = 8
        .Font.Bold = False
        .Font.Italic = True
        .Font.Name = "Arial"
        .Font.ColorIndex = 48
        .Value = msg
    End With
    Range("A1").Select

With Worksheets(fname).Range("A11:F11")
    .Font.Size = 10
    .Font.Bold = False
    .Font.Italic = True
    .Font.Name = "Arial"
End With
```

```
With Worksheets(fname).Range("A10")
    .Value = "Solid/Air Interface"
    .Font.Bold = True
    .Font.Italic = False
    .Font.Size = 12
    .Font.ColorIndex = 1
    .Font.Name = "Arial"
End With

Range("A12").Value = "Visible"
Range("A12:E12").Font.ColorIndex = 5
Range("A13").Value = "Infrared"
Range("A13:E13").Font.ColorIndex = 3
Range("A14").Value = "Sum Frequency"
Range("A14:E14").Font.ColorIndex = 6
Range("A11:E11").Font.ColorIndex = 42
Range("B11").Value = "Wavelength (nm)"
Range("C11").Value = "Wavenumber (cm-1)"
Range("D11").Value = "Ref. Index (n)"
Range("E11").Value = "Angle w/surface normal"

Range("B11:E11").Columns.AutoFit
Range("A12:E14").HorizontalAlignment = xlHAlignCenter
Range("A12:E14").VerticalAlignment = xlVAlignCenter

With Worksheets(fname).Range("H10")
    .Value = "Equation"
    .Font.Bold = True
    .Font.Italic = False
    .Font.Size = 12
    .Font.Name = "Arial"
    .Font.ColorIndex = 2
End With

With Worksheets(fname).Range("A16:C18").Font
    .Bold = False
    .Italic = False
    .Size = 10
    .Name = "Arial"
End With

Range("A16:B17").Font.ColorIndex = 42
Range("A16").Value = "Beam Height"
Range("A17").Value = "Stage Height"
Range("B16").Value = "  " & Hb & " cm"
Range("B17").Value = "   " & Hs & " cm"
```

```
'format drawing region

With Worksheets(fname).Range("AA26")
    .Font.Size = 12
    .Font.Bold = False
    .Font.Italic = False
    .Font.Name = "Courier New"
    .Value = "Drawing informations for delivering visible"
End With

With Worksheets(fname).Range("AA38")
    .Font.Size = 12
    .Font.Bold = False
    .Font.Italic = False
    .Font.Name = "Courier New"
    .Value = "Drawing informations for delivering SFG"
End With


With Worksheets(fname).Range("AA28:AO29").Font
    .Size = 10
    .Bold = True
    .Italic = False
    .Name = "Arial"
End With

With Worksheets(fname).Range("AA30:AO46")
    .Font.Size = 10
    .Font.Bold = False
    .Font.Italic = False
    .Font.Name = "Arial"
    .NumberFormat = "###0.00"

End With

    Range("AA31").Value = "X1"
    Range("AA41").Value = "X1"
    Range("AA32").Value = "X2"
    Range("AA42").Value = "X2"
    Range("AA33").Value = "X3"
    Range("AA43").Value = "X3"
    Range("AA34").Value = "Y1"
```

```
    Range("AA44").Value = "Y1"
    Range("AA35").Value = "Y2"
    Range("AA45").Value = "Y2"
    Range("AA36").Value = "Y3"
    Range("AA46").Value = "Y3"

With Worksheets(fname).Range("B2")
    .Font.Size = 16
    .Font.Bold = True
    .Font.Italic = False
    .Font.Name = "Courier New"
    .Value = "SF ANGLE CALCULATIONS"
End With

With Worksheets(fname).Range("A11:F11")
    .Font.Size = 10
    .Font.Bold = False
    .Font.Italic = True
    .Font.Name = "Arial"
End With

With Worksheets(fname).Range("A10")
    .Value = "Solid/Air Interface"
    .Font.Bold = True
    .Font.Italic = False
    .Font.Size = 12
    .Font.Name = "Arial"
End With

Range("A12").Value = "Visible"
Range("A13").Value = "Infrared"
Range("A14").Value = "Sum Frequency"

Range("B11").Value = "Wavelength (nm)"
Range("C11").Value = "Wavenumber (cm-1)"
Range("D11").Value = "Ref. Index (n)"
Range("E11").Value = "Angle w/surface normal"

Range("B11:E11").Columns.AutoFit
Range("A12:E14").HorizontalAlignment = xlHAlignCenter
Range("A12:E14").VerticalAlignment = xlVAlignCenter

With Worksheets(fname).Range("H10")
    .Value = "Equation"
    .Font.Bold = True
    .Font.Italic = False
```

```
    .Font.Size = 12
    .Font.Name = "Arial"
End With

With Worksheets(fname).Range("A15:C118").Font
    .Bold = False
    .Italic = False
    .Size = 10
    .Name = "Arial"
End With

Worksheets(fname).Range("B12:E14").NumberFormat = "###0.00"

    Range("A16").Value = "Beam Height"
    Range("A17").Value = "Stage Height"
    Range("B16").Value = "  " & 14.3 & " cm"    'height of beam
    Range("B17").Value = "    " & 5.2 & " cm"    'height of stage

    Range("B12").Value = 775  'vis wavelength
    Range("B13").Value = 3300  'Ir wavelength
    Range("B14").Value = 627.6 'SF wavelength

    Range("C12").Value = 12903
    Range("C13").Value = 3030.3
    Range("C14").Value = 15933.3

    Range("D12").Value = 1 'ref index for vis
    Range("D13").Value = 1  ' for ir
    Range("D14").Value = 1  ' for SF

    Range("E12").Value = 34.83
    Range("E13").Value = 52.4
    Range("E14").Value = 37.71
End Sub
```

A.2. Igor routine for data transfer and processing

The routine is modified from build-in procedures.

```
#pragma rtGlobals=1             // Use modern global access method.

#include <File Name Utilities>

Menu "Load Waves"
        "Load WinSpec Binary File...", LoadWinSpecBinaryFileDialog()
        "Load All WinSpec Binary Files In Folder...",  LoadWinSpecFilesDialog()
```

```
End

static Function ReadSignedByte(refNum, offset)
	Variable refNum
	Variable offset

	Variable byteOrder=3		// See documentation for /B flag to FBinRead operation
	Variable val

	FSetPos refNum, offset
	FBinRead/B=(byteOrder)/F=1 refNum, val
	return val
End

static Function ReadUnsignedByte(refNum, offset)
	Variable refNum
	Variable offset

	Variable byteOrder=3		// See documentation for /B flag to FBinRead operation
	Variable val

	FSetPos refNum, offset
	FBinRead/B=(byteOrder)/F=1/U refNum, val
	return val
End

static Function ReadSignedShort(refNum, offset)
	Variable refNum
	Variable offset

	Variable byteOrder=3		// See documentation for /B flag to FBinRead operation
	Variable val

	FSetPos refNum, offset
	FBinRead/B=(byteOrder)/F=2 refNum, val
	return val
End

static Function ReadUnsignedShort(refNum, offset)
	Variable refNum
	Variable offset
```

```
	Variable byteOrder=3		// See documentation for /B flag to FBinRead operation
	Variable val

	FSetPos refNum, offset
	FBinRead/B=(byteOrder)/F=2/U refNum, val
	return val
End

static Function ReadSignedLong(refNum, offset)
	Variable refNum
	Variable offset

	Variable byteOrder=3		// See documentation for /B flag to FBinRead operation
	Variable val

	FSetPos refNum, offset
	FBinRead/B=(byteOrder)/F=3 refNum, val
	return val
End

static Function ReadUnsignedLong(refNum, offset)
	Variable refNum
	Variable offset

	Variable byteOrder=3		// See documentation for /B flag to FBinRead operation
	Variable val

	FSetPos refNum, offset
	FBinRead/B=(byteOrder)/F=3/U refNum, val
	return val
End

static Function ReadDouble(refNum, offset)
	Variable refNum
	Variable offset

	Variable byteOrder=3		// See documentation for /B flag to FBinRead operation
	Variable val

	FSetPos refNum, offset
	FBinRead/B=(byteOrder)/F=5 refNum, val
	return val
```

```
End

static Function/S GetNewWaveName(fileName)
	String fileName

	String baseName, newName, front, rest, TWave, Pol
	Variable v1, SPEPos, TPos, DPos

	newName = fileName
	//print newName
	// Eliminate extension.
	SPEPos = strsearch(newName, ".SPE", 0)
	if (SPEPos > 1)
		newName = newName[0, SPEPos-1]		// Eliminate extension.
	endif

	sscanf newName[0,6], "%i", v1
	If (v1)
		//DPos = strsearch(newName, "-", 8)
		TPos = strsearch(newName, "-S1", 6)
		TPos=TPos - 5
		front = newName [7, TPos-1]
		TWave = newName [TPos, TPos+5]
		If (strsearch(newName, "SSP", 30) > 0)
			Pol = "SSP"
		Elseif (strsearch(newName, "SPS", 30) > 0)
			Pol = "SPS"
		Else
			Pol = "PPP"
		Endif
		NewName = front + TWave + Pol
	Endif
	newName = CleanupName(newName, 0)		// I avoid liberal names because they introduce programming complexities
	return newName
End

// Filters the cosmic lines from the wave
Function ApplyFilter2Wave(nWave)
	Wave nWave
	Variable j, avg,avg1,avg2, p1, p2

	WaveStats /Q nWave
	j = 12
	Do
```

```
		If ( j == 1328)
			break
		Endif

		p1 = j - 12
		p2 = j + 13
		avg1 = faverage(nWave, p1, j-2)
		avg2 = faverage(nwave,j+2,p2)
		avg = (avg1 + avg2)/2
		If (abs(nWave[j] - avg) > (5*V_sdev))
			nWave[j] = avg
		Endif
		j += 1
	While(1)
END

static Function CalibrateWave(w, X_dim, XCalbOrder, xOffset, Xfactor4Scale, XPolCoeff, LaserLine)
	Wave w, XPolCoeff
	Variable X_dim, XCalbOrder, xOffset, Xfactor4Scale, LaserLine

	// Assumes for 2nd or 3rd order polynomial
	If (XCalbOrder == 2)
		Variable i = 0, w1
		Print " Laser Line : ", LaserLine
		Do
			w1= XPolCoeff [0] + XPolCoeff[1]*(i+1) + XPolCoeff[2]*(i+1)*(i+1)
			w1 = (1/w1- 1/LaserLine) *10000000
			w [i] = w1
			i +=  1
		While (i < X_dim)
	Endif
	//Since 3rd order calibration of the data is never used during the spectrometer calibration, the procedure skipped
	//If (XCalbOrder == 3)
	//	FSetPos refNum, 3263

	//	FBinRead/F=3/B=3/U refNum, XPolCoeff1
	//	FBinRead/F=3/B=3/U refNum, XPolCoeff2
	//	FBinRead/F=3/B=3/U refNum, XPolCoeff3
	//	Variable jj = 0
	//	Do
	//		w[jj] = XoffSet + XPolCoeff1*(jj+1) + XPolCoeff2*(jj+1) + XPolCoeff3*(jj+1)
	//		jj += 1
```

```
	//		While (jj < X_dim)
	//Endif
	// This is left as an exercise for the user.
End


Function LoadWinSpecBinaryFile(pathName, fileName)		// Output wave is always named WinSpecTemp0
	String pathName		// Name of an Igor symbolic path.
	String fileName			// Name of file.

	Variable refNum
	Variable xDim, yDim, numFrames, winSpecDataType
	Variable runningOnMac = strsearch(IgorInfo(2), "Macintosh", 0) >= 0

	// First open file and use FBinRead to read various header fields.

	Open/R/P=$pathName refNum as fileName

	xDim = ReadUnsignedShort(refNum, 42)
	winSpecDataType = ReadSignedShort(refNum, 108)		// 0 = float, 1 = long, 2 = short, 3 = unsigned short
	yDim = ReadUnsignedShort(refNum, 656)
	numFrames = ReadSignedLong(refnum, 1446)

	 //Print xDim, yDim, numFrames		// For debugging only.

	Variable xOffset, Xfactor4Scale, XCalbOrder, xUnitAsByte, LaserLine
	xOffset = ReadDouble(refNum, 3000)			// offset for absolute data scaling
	Xfactor4Scale = ReadDouble(refNum, 3008)			// factor for absolute data scaling
	xUnitAsByte = ReadUnsignedByte(refNum, 3016)		// selected scaling unit
	XCalbOrder = ReadSignedByte(refNum, 3101)		// ORDER of calibration POLYNOM

	Wave XPolCoeff
	Make /N=4 XPolCoeff
	XPolCoeff [0] = ReadDouble(refNum, 3263)			// Coefficients of polynomial
	XPolCoeff [1] = ReadDouble(refNum, 3271)
	XPolCoeff [2] = ReadDouble(refNum, 3279)
	XPolCoeff [3] = ReadDouble(refNum, 3287)
	LaserLine = ReadDouble(refNum, 3311)			// LaserLine for Rel Wavenumber
```

```
	// Print "PolCoeff", XPolCoeff[0], XPolCoeff[1], XPolCoeff [2], XPolCoeff
[3]	// debug only

	String xUnitStr = num2char(xUnitAsByte)

	// Printf "xOffset=%g, Xfactor4Scale=%g, XCalbOrder=%g,
xUnitAsByte=%g, xUnitStr=\"%s\"\r", xOffset, Xfactor4Scale, XCalbOrder,
xUnitAsByte, xUnitStr

	Close refNum

	// Now use GBLoadWave to load the bulk of the data

	// NOTE: This Assumes data is unsigned byte. Change to suit your data if
necessary.
	Variable inputDataType, outputDataType

	switch(winSpecDataType)
		case 0:					// float
			inputDataType = 2
			break

		case 1:					// long
			inputDataType = 32
			break

		case 2:					// short
			inputDataType = 16
			break

		case 3:					// unsigned short
			inputDataType = 16 + 64
			break

		default:
			Abort "Invalid data type was read from WinSpec file"
	endswitch

	outputDataType = inputDataType		// Use this if you want the
Igor data to be the same type as the WinSpec data
	// outputDataType = 2			// Use this if you want the
Igor data to always be float


	// Apply calibration
```

```
	Wave XWinSpecTemp0
	Make /O/N=(xDim)  XWinSpecTemp0
	CalibrateWave(XWinSpecTemp0, XDim, XCalbOrder, xOffset,
Xfactor4Scale, XPolCoeff, LaserLine)

	KillWaves XPolCoeff
	// Since GBLoadWave is an external operation, it can not be called directly
from a user function.
	//
GBLoadWave/Q/O/B/T={dataType,dataType}/S=4100/W=1/N=winSpec/P=$pathNa
me fileName
	String cmd
	Sprint cmd,
"GBLoadWave/Q/O/B/T={%d,%d}/S=4100/W=1/N=winSpecTemp/P=$\"%s\"
\"%s\"", inputDataType, outputDataType, pathName, fileName
	// Print cmd                                                    // For debugging
only
	Execute cmd

	If (yDim >1)
		if (numFrames > 1)                                  //  Multi-dimensional
data?
			Redimension/N=(xDim, yDim, numFrames) WinSpecTemp0
		// Creates 3D wave
		else
			Redimension/N=(xDim, yDim) WinSpecTemp0
			// Creates 2D wave
		endif
	endif
	ApplyFilter2Wave(WinSpecTemp0)
End

Function LoadWinSpecBinaryFileDialog()
	String filePath = ""
	Variable refNum

	Variable runningOnMac = strsearch(IgorInfo(2), "Macintosh", 0) >= 0

	if (runningOnMac)
		Open/D/R/T="????" refNum as ""
	else
		Open/D/R/T=".spe" refNum as ""
	endif

	filePath = S_fileName                          // S_fileName is set by Open/D
and it's really a full path
```

```
	if (strlen(filePath) == 0)			// User cancelled?
		return -1
	endif

	LoadWinSpecBinaryFile("", filePath)		// Wave name is always
"winSpecTemp0"

	if (WaveExists(winSpecTemp0))
		String fileName = FileNameOnly(filePath)
		String newName
		newName = GetNewWaveName(fileName)
		if (WaveExists($newName))
			newName = UniqueName(newName, 1, 0)
		endif
		Rename winSpecTemp0, $newName
		//Printf "Loaded %s and X%s\r", newName, newName
		NewName = "X_" + NewName
		Duplicate/O XWinSpecTemp0, $NewName
		KillWaves/Z winSpecTemp0, XWinSpecTemp0
	endif

End

Function BoxAverage()
	Wave BoxedAvSFG
	Variable i

	Duplicate /O SumSFG, BoxedAvSFG

	i = 5
	Do
		If (i == 1330)		// exits for box average of 11
			break
		Endif
		BoxedAvSFG [i] = faverage(SumSFG, (i - 5), (i + 5))
		i += 1
	While(1)
End

Function SumWaves(nWaves, ListofWaves)

	Variable nWaves
	String ListofWaves
	Variable i
	Wave SumSFG
```

```
	String cmd, NameWave, SumSF = " "
	i = 0
	Make /N = 1340 SumSFG

	Do
		If (i == nWaves)
			break
		Endif
		NameWave = StringFromList (i, ListofWaves, ",")
		If (i < (nWaves-1))
			SumSF = SumSF + NameWave +  "+ "
		Else
			SumSF = SumSF + NameWave
		Endif
		i += 1
	While (1)
	SumSF = "SumSFG = " + SumSF
	sprintf cmd, SumSF
	//Print cmd                                                    // For debugging
only
	Execute cmd
End

//Function AmpDatawrtMin(nWaves, listofWaves)      //Amplifies data according to
//loaded wave numbers
//	Variable nWaves

//	String ListofWaves
//	String namewave, txt

//	Wave TempWave
//	Variable i = 0, j = 0     // i  = number of waves ; j = number of points in a wave
= 1340
//	Variable avg25, sum25, yavg, p1, p2
//	Variable stringend

//	Do
//		If (i == nWaves)
//			break
//		Endif

		//Wave TempWave
//		namewave = StringFromList (i, ListofWaves, ", ")
//		If (i >=1)
//			stringend = strlen(namewave)
//			namewave = namewave [1,stringend]
```

```
//		Endif
//		Duplicate /O $namewave, TempWave
//		WaveStats /Q TempWave
//		yavg = V_avg
//		ApplyFilter2Wave(TempWave)
//
//		j = 12
//		Do
//			If ( j == 1328)
//				break
//			Endif
//
//			p1 = j - 12
//			p2 = j + 13
//			Sum25 = Sum (TempWave, p1, p2)
//			If (Sum25 > (yavg * 25*1.1))
//				If (TempWave[j] <= 1)
//					TempWave [j] = TempWave [j] + yavg
//				Else
//					TempWave [j] = TempWave [j] * (nWaves) -
(nWaves-1)*yavg
//				Endif
//			Endif
//			j += 1
//		While (1)
//			txt  = namewave + "= TempWave"
//			//sprintf cmd, txt
//			//Print txt                                                    //
For debugging only
//			Execute txt
//		i += 1
//	While (1)
//	KillWaves/Z TempWave
//End


//	LoadWinSpecFiles(pathName, overwriteMode)
//
//	pathName is the name an Igor symbolic path that references the folder
containing the wave files.
//	 Create the path using Misc->New Path.
//

Function LoadWinSpecFiles(pathName, overwrite)
	String pathName		// Name of an Igor symbolic path.
	Variable overwrite		// 1 to overwrite, 0 to not overwrite
```

```
	Variable i, Tpos
	String fileName, txt
	String listOfWavesLoaded = ""
	Variable numWavesLoaded = 0
	String Exp_Name, Trest
	Variable Tstart, Tend, Twave

	i = 0
	do
		fileName = IndexedFile($pathName, i, ".spe")		// Reads filename from directory
		if (strlen(fileName) == 0)
			break 					// All done
		endif
		//040119-1C9OH-T3550-SSP-S1=125mm-S2=150um-180s.SPE //typical file name
		// generate Title for graph
		TPos = strsearch(fileName, "-T3", 10)   // position for Slit 1
		Exp_Name = fileName[0,Tpos+1]
		Twave = str2num(fileName[Tpos+2,Tpos+5])
		If (i ==0)
			Tstart = Twave
			Tend = Twave
		Endif

		If (Twave < Tstart)
			Tstart = Twave
		Elseif (Twave > Tend)
			Tend = Twave
		Endif
		Trest = fileName[Tpos+6, strlen(fileName)-5]

		// Load wave using temporary names.
		LoadWinSpecBinaryFile(pathName, fileName)		// Wave name is always "winSpecTemp0"
		// Rename the waves based on the file name.
		String newName, baseName
		//baseName = GetNewWaveName(fileName)	// names are long and changed to Twavelength
		basename = "T" + Num2Str(Twave)

		if (overwrite)
			newName = baseName
		else
			if (WaveExists($baseName))
```

```
                        newName = UniqueName(baseName, 1, 0)
                    endif
                endif
                Duplicate/O winSpecTemp0, $newName
                //Printf "Loaded %s and X%s\r", newName, newName     //Debug only

                if (numWavesLoaded > 0)
                    listOfWavesLoaded += ", "
                endif
                listOfWavesLoaded += newName
                NewName = "X_" + newName
                Duplicate/O XWinSpecTemp0, $newName
                KillWaves/Z winSpecTemp0, XWinSpecTemp0
                numWavesLoaded += 1

                i += 1
            while (1)                                   // Continue till break above

            Printf "%d waves loaded:\r %s\r", numWavesLoaded, listOfWavesLoaded
            AmpDatawrtMin(numWavesLoaded, listOfWavesLoaded)
            SumWaves (numWavesLoaded, listOfWavesLoaded)    // Sums all the Y data
            BoxAverage()
             // BoxAverages the Summed SFG data
            // generating the graph and modifying
            txt = stringfromlist(1, listOfWavesLoaded, ",")
            txt = "X_" + txt[1, strlen(txt)]
            txt = "SumSFG, BoxedAvSFG vs "  + txt
            execute "Display /W = (100,200, 850, 650) " + txt
            SetAxis bottom, 3100, 2700
            ModifyGraph noLabel(left) = 1, lblLatPos(left) =0, axOffset(left) = -4.5,
axisEnab(left)={0,0.9}, lblMargin(left)=5
            ModifyGraph
rgb(SumSFG)=(65280,21760,0),rgb(BoxedAvSFG)=(0,0,13056)
            Label left, "SFG Intensity (a.u.)"
            Label bottom, "Wavenumber (cm-1)"
            txt = Exp_Name + num2str(Tstart) + "-" + Num2Str(Tend) + Trest
            FileName = txt
            txt = "\\Z18" + txt
            TextBox /N=text1/F=0/A=MT/X=0/Y=0 txt
            //Saving experiment
            FileName = FileName + ".pxp"
            Variable refNum, outputPath
            Print fileName
            Open /D/P=home /M="File Name"  refNum as FileName
            SaveExperiment as S_fileName
```

```
	//Layout is generated for printing purposes but not saved
	NewLayout /C=1/P=Landscape
	txt = "AppendToLayout graph0"
	Execute txt
	ModifyLayout frame=0, width(graph0)=648,height(graph0)=468
	DoAlert 1, "\r	Would you like to print the graph"
	If (V_flag == 1)
	  txt =  " PrintLayout /C=0 layout0"
	  Execute txt
	Endif
End

Function LoadWinSpecFilesDialog()
	String pathName = "home"
	Prompt pathName, "Choose path", popup PathList("*", ";", "")
	Variable overwriteMenuSelection = 1
	Prompt overwriteMenuSelection, "Overwrite pre-existing waves?", popup
"Yes;No (use unique wave names)"
	DoPrompt "Load WinSpec Files", pathName, overwriteMenuSelection
	if (V_Flag)
		return -1 // User canceled
	endif
	LoadWinSpecFiles(pathName, overwriteMenuSelection==1)
End
```

References

(1) Rosen, M. J. *Surfactants and Interfacial phenomena*; John Wiley & Sons, 1978.
(2) Lu, J. R.; Lee, E. M.; Thomas, R. K.; Penfold, J.; Flitsch, S. L. *Langmuir* **1993**, *9*, 1353.
(3) Ocko, B. M.; Wu, X. Z.; Sirota, E. B.; Sinha, S. K.; Gang, O.; Deutsch, M. *Phys. Rev. E* **1997**, *55*, 3164.
(4) Pfohl, T.; Beaglehole, D.; Riegler, H. *Chem. Phys. Lett.* **1996**, *260*, 82.
(5) Buck, M.; Himmelhaus, M. *J. Vac. Sci. Technol. A.* **2001**, *19*, 2717.
(6) Zhang, X. Y.; Esenturk, O.; Walker, R. A. *J. Am. Chem. Soc.* **2001**, *123*, 10768.
(7) Zhang, X.; Walker, R. A. *Langmuir* **2001**, *17*, 4486.
(8) Macphail, R. A.; Strauss, H. L.; Snyder, R. G.; Elliger, C. A. *J. Phys. Chem.* **1984**, *88*, 334.
(9) Aljibury, A. L.; Snyder, R. G.; Strauss, H. L.; Raghavachari, K. *J. Chem. Phys.* **1986**, *84*, 6872.
(10) Sirota, E. B.; King, H. E.; Shao, H. H.; Singer, D. M. *J. Phys. Chem.* **1995**, *99*, 798.
(11) Klein, M. L. *J. Chem. Soc. Faraday Trans.* **1992**, *88*, 1701.
(12) Craievich, A.; Doucet, J.; Denicolo, I. *Phys. Rev. B* **1985**, *32*, 4164.
(13) Snyder, R. G.; Strauss, H. L.; Elliger, C. A. *J. Phys. Chem.* **1962**, *86*, 5145.
(14) Snyder, R. G. *J. Chem. Soc. Faraday Trans.* **1992**, *88*, 1823.
(15) Zerbi, G.; Abbate, S. *Chem. Phys. Lett.* **1981**, *80*, 455.
(16) Wunder, S. L.; Merajver, S. D. *J. Chem. Phys.* **1981**, *74*, 5341.
(17) Richter, L. T.; Petralli-Mallow, T. P.; Stephenson, J. C. *Opt. Lett.* **1998**, *23:(20)*, 1594.
(18) Yang, C. S. C.; Richter, L. J.; Stephenson, J. C.; Briggman, K. A. *Langmuir* **2002**, *18*, 7549.
(19) Sefler, G. A.; Du, Q.; Miranda, P. B.; Shen, Y. R. *Chem. Phys. Lett.* **1995**, *235*, 347.
(20) Earnshaw, J. C.; Hughes, C. J. *Phys. Rev. A* **1992**, *46*, R4494.
(21) Fuhrmann, D.; Graham, A. P.; Criswell, L.; Mo, H.; Matthies, B.; Herwig, K. W.; Taub, H. *Surface Sci.* **2001**, *482*, 77.
(22) Braden, D. A.; Parker, S. F.; Tomkinson, J.; Hudson, B. S. *J. Chem. Phys.* **1999**, *111*, 429.
(23) Earnshaw, J. C. *J. Dispersion Sci. Technol.* **1999**, *20*, 743.
(24) Shen, Y. R. *Nature* **1989**, *337*, 519.
(25) Bain, C. D. *J. Chem. Soc. Faraday Trans.* **1995**, *91*, 1281.
(26) Richmond, G. L. *An. Chem. News* **1997**, *69*, 536A.
(27) Harris, A. L.; Levinos, N. J. *Appl. Opt.* **1987**, *26*, 3996.
(28) Guyotsionnest, P.; Hunt, J. H.; Shen, Y. R. *Phys. Rev. Lett.* **1987**, *59*, 1597.
(29) Braun, R.; Casson, B. D.; Bain, C. D.; van der Ham, E. W. M.; Vrehen, Q. H. F.; Eliel, E. R.; Briggs, A. M.; Davies, P. B. *J. Chem. Phys.* **1999**, *110*, 4634.

(30) Bloombergen, N.; Pershan, P. S. *Phys. Rev.* **1962**, *128*, 606.
(31) Zhu, X. D.; Suhr, H.; Shen, Y. R. *J. Opt. Soc. Am. B* **1986**, *3*, 252.
(32) Hunt, J. H.; Guyotsionnest, P.; Shen, Y. R. *Chem. Phys. Lett.* **1987**, *133*, 189.
(33) Harris, A. L.; Chidsey, C. E. D.; Levinos, N. J.; Loiacono, D. N. *Chem. Phys. Lett.* **1987**, *141*, 350.
(34) Chen, Z.; Ward, R.; Tian, Y.; Baldelli, S.; Opdahl, A.; Shen, Y. R.; Somorjai, G. A. *J Am. Chem. Soc.* **2000**, *112*, 10615.
(35) Brown, M. G.; Walker, D. S.; Raymond, E. A.; Richmond, G. L. *J. Phys. Chem. B* **2003**, *107*, 237.
(36) Oh-e, M.; Hong, S. C.; Shen, Y. R. *J Phys. Chem. B* **2000**, *104: (31)*, 7455.
(37) Zhu, X. D.; Suhr, H.; Shen, Y. R. *Phys. Rev. B* **1987**, *35:(6)*, 3047.
(38) Shen, Y. R. *Sur. Sci.* **1994**, *299/300*, 551.
(39) Du, Q.; Freysz, E.; Shen, Y. R. *Science* **1994**, *264*, 826.
(40) Du, Q.; Freysz, E.; Shen, Y. R. *Phys. Rev. Lett.* **1994**, *72*, 238.
(41) Stanners, C. D.; Du, Q.; Chin, R. P.; Cremer, P.; Somorjai, G. A.; Shen, Y. R. *Chem. Phys. Lett.* **1995**, *232*, 407.
(42) Stanners, C. D.; Du, Q.; Chin, R. P.; Cremer, P.; Somorjai, G. A.; Shen, Y. R. *Chem. Phys. Lett.* **1995**, *232*, 407.
(43) Raduge, C.; Pflumio, V.; Shen, Y. R. *Chem. Phys. Lett.* **1997**, *274:(1-3)*, 140.
(44) Miranda, P. B.; Pflumio, V.; Saijo, H.; Shen, Y. R. *Chem. Phys. Lett.* **1997**, *264:(3-4)*, 387.
(45) Su, X.; Shen, Y. R.; Somorjai, G. A. *Chem. Phys. Lett.* **1997**, *280:(3-4)*, 302.
(46) Zhang, D.; Ward, R. S.; Shen, Y. R.; Somorjai, G. A. *J Phys. Chem. B* **1997**, *101:(44)*, 9060.
(47) Shen, Y. R. *Solid State Commun.* **1998**, *108*.
(48) Zhang, D.; Gracias, D. H.; Ward, R.; Gauckler, M.; Tian, Y.; Shen, Y. R.; Somorjai, G. A. *J Phys. Chem. B* **1998**, *102*, 6225.
(49) Zhuang, X.; Miranda, P. B.; Kim, D. S.; Shen, Y. R. *Phys. Rev. B* **1999**, *59:(19)*, 12632.
(50) Wei, X.; Hong, S. C.; Zhuang, X.; Goto, T.; Shen, Y. R. *Phys. Rev. E* **2000**, *62:(4)*, 5160.
(51) Baldelli, S.; Eppler, A. S.; Anderson, E.; Shen, Y. R.; Somojai, G. A. *J. Chem. Phys.* **2000**, *113*, 5432.
(52) Oh-e, M.; Lvovsky, A. I.; Wei, X.; Shen, Y. R. *J Chem. Phys.* **2000**, *113:(19)*, 8827.
(53) Belkin, M. A.; Kulakov, T. A.; Ernst, K. H.; Yan, L.; Shen, Y. R. *Phys. Rev. Lett.* **2000**, *85:(21)*, 4474.
(54) Edgar, R.; Huang, J. Y.; Popovitz-Biro, R.; Kjayer, K.; Bouwman, W. G.; Howes, P. B.; Als-Nielsen, J.; Shen, Y. R.; Lahav, M.; Leiserowitz, L. *J Chem. Phys. B* **2000**, *104*, 6843.
(55) McGuire, J. A.; Beck, W.; Wei, X.; Shen, Y. R. *Opt. Lett.* **2000**, *24:(24)*, 1877.
(56) Miranda, P. B.; Pflumio, V.; Saijo, H.; Shen, Y. R. *J. Am. Chem. Soc.* **1998**, *120*, 12092.
(57) Richmond, G. L. *Annu. Rev. Phys. Chem.* **2001**, *52*, 357.
(58) Walker, R.; Smiley, B. L.; Richmond, G. L. *Spectroscopy* **1999**, *14*, 18.

(59) Walker, R.; Gruetzmacher, J. A.; Richmond, G. L. *J Am. Chem. Soc.* **1998**, *120*, 6991.
(60) Richmond, G. L. *Chem. Rev.* **2002**, *102*, 2693.
(61) Gragson, D. E.; Richmond, G. L. *J Chem. Phys.* **1997**, *107:(22)*, 9687.
(62) Gragson, D. E.; Richmond, G. L. *J Phys. Chem. B* **1998**, *102:(20)*, 3847.
(63) Gragson, D. E.; Richmond, G. L. **1998**, *102*, 569.
(64) Allen, H. C.; Raymond, R. A.; Richmond, G. L. *J Phys. Chem. A* **2001**, *105*, 1649.
(65) Allen, H. C.; Raymond, R. A.; Richmond, G. L. *J Phys. Chem. A* **2000**.
(66) Allen, H. C.; Gragson, D. E.; Richmond, G. L. *J Phys. Chem. B* **1999**, *103:(4)*, 660.
(67) Scatena, L. F.; Richmond, G. L. *J. Chem. Phys. B* **2001**, *105*, 11240.
(68) Watry, M. R.; Richmond, G. L. *J Am. Chem. Soc.* **2000**, *122:(5)*, 875.
(69) Brown, M. G.; Raymond, R. A.; Allen, H. C.; Scatena, L. F.; Richmond, G. L. *J Phys. Chem. A* **2000**, *104*, 10220.
(70) Gragson, D. E.; Richmond, G. L. **1998**, *120*, 366.
(71) Smiley, B. L.; Richmond, G. L. *Biopolymers* **2000**, *57:(2)*, 117.
(72) Watry, M. R.; Tarbuck, T. L.; Richmond, G. L. *J. Phys. Chem. B.* **2003**, *107*, 512.
(73) Wilson, P. T.; Richter, J. E.; Wallace, W. E.; Briggman, K. A.; Stephenson, J. C. *Chem. Phys. Lett.* **2002**, *363*, 161.
(74) Briggman, K. A.; Richter, L. J.; Stephenson, J. C. *Opt. Lett.* **2001**, *26*, 238.
(75) Briggman, K. A.; Stephenson, J. C.; Wallace, W. E.; Richter, J. E. *J Phys. Chem. B* **2001**, *105*, 2785.
(76) Stephenson, J. C. *Personal communication*, 2004.
(77) Bell, G. R.; Bain, C. D. *J. Chem. Soc. Faraday Trans.* **1996**, *92*, 515.
(78) Potterton, E. A.; Bain, C. D. *J Elec. Anal. Chem.* **1996**, *409*, 109.
(79) Bain, C. D. *J. Chem. Soc. Faraday Trans.* **2001**, *91*, 1281.
(80) Braun, R.; Casson, B. D.; Bain, C. D. *Chem. Phys. Lett.* **1995**, *245*, 326.
(81) McKenna, C. E.; Knock, M. M.; Bain, C. D. *Langmuir* **2000**, *16*, 5853.
(82) Bain, C. D. *Biosen. & Bioelec.* **1995**, *10*, 917.
(83) Knock, M. M.; Bell, G. R.; Hill, E. K.; Turner, H. J.; Bain, C. D. *J. Phys. Chem. B* **2003**, *107*, 10801.
(84) Ward, R. N.; Duffy, D. M.; Davies, P. B.; Bain, C. D. *J. Phys. Chem.* **1994**, *98*, 8536.
(85) Kim, J.; Cremer, P. S. *Chem.Phys.Chem.* **2001**, *8-9*, 543.
(86) Zimdars, D.; Dadap, J. I.; Eisenthal, K. B.; Heinz, T. F. *Chem. Phys. Lett.* **1999**, *301*, 112.
(87) Pluchery, O.; Tadjeddine, M.; Flament, J. P.; Tadjeddine, A. *Phys. Chem. Chem. Phys.* **2001**, *3*, 3343.
(88) Morita, A.; Hynes, J. T. *J. T. Chem. Phys.* **2000**, *258*, 371.
(89) Schnitzer, C.; Baldelli, S.; Shultz, M. J. *Chem. Phys. Lett.* **1999**, *313*, 416.
(90) Simonelli, D.; Shultz, M. J. *J. Chem. Phys.* **2000**, *112*, 6804.
(91) Schnitzer, C.; Baldelli, S.; Shultz, M. J. *J. Phys. Chem.* **2000**, *104*, 585.
(92) Pizzolatto, R. L.; TYang, Y. J.; Wolf, L. K.; Messmer, M. C. *Anal. Chim. Acta.* **1999**, *397*, 81.

(93) Rupprechter, G. *Phys. Chem. Chem. Phys.* **2001**, *3*, 4621.
(94) Williams, C. T.; Beattie, D. A. *Surface Sci.* **2002**, *500*, 545.
(95) Beattie, D. A.; Haydock, S.; Bain, C. D. *Vib. Spectrosc.* **2000**, *24*, 109.
(96) Berg, O.; Klenerman, D. *J. Am. Chem. Soc.* **2003**, *125*, 5493.
(97) Du, Q.; Xiao, X. D.; Charych, D.; Wolf, F.; Frantz, P.; Shen, Y. R.; Salmeron, M. *Phys. Rev. B* **1995**, *51*.
(98) Kawai, T.; Neivandt, D. J.; Davies, P. B. *J. Am. Chem. Soc.* **2000**, *122*, 12301.
(99) Kuhnke, K.; Hoffmann, D. M. P.; Wu, X. C.; Bittner, A. M.; Kern, K. **2003**, *83*, 3830.
(100) Cho, M. *Phys. Rev. A.* **2000**, *61*, 3406.
(101) Hirose, C.; Akamatsu, N.; Domen, K. *Appl. Spectrosc.* **1992**, *46*, 1051.
(102) Dick, B.; Gierulski, A.; Marowsky, G. *Appl. Phys. B.* **1985**, *38*, 107.
(103) Shen, Y. R. *Appl. Phys. B - Las. Opt.* **1999**, *68:(3)*, 295.
(104) Wei, X.; Hong, S. C.; Lvovsky, A. I.; Held, H.; Shen, Y. R. *J Phys. Chem. B* **2000**, *104: (14)*, 3349.
(105) Boyd, R. W. *Nonlinear Optics*; Academic Press, c1992: Boston, 1992.
(106) Hirose, C.; Akamatsu, N.; Domen, K. *J. Chem. Phys.* **1992**, *96*, 997.
(107) Wilson, P. T.; Briggman, K. A.; Wallace, W. E.; Stephenson, J. C. *Appl. Phys. Lett.* **2002**, *80*, 3084.
(108) Rhee, J. K.; Sosnowwski, T. S.; Norris, T. B. *Optics Lett.* **1994**, *19*, 1550.
(109) Snyder, R. G.; Kim, Y. *J. Phys. Chem.*. **1991**, *95*, 602.
(110) Snyder, R. G.; Aljibury, A. L.; Strauss, H. L.; Casal, H. L.; Gough, K. M.; Murphy, W. F. *J. Chem. Phys.* **1984**, *81*, 5352.
(111) Hill, I. R.; Levin, W. I. *J. Chem. Phys.* **1979**, *70*, 842.
(112) Marinkovic, T.; Oss, S. *Phys. Chem. Comm.* **2003**, *6*, 42.
(113) Wunder, S. L.; Bell, M. I.; Zerpi, G. *J. Chem. Phys.* **1986**, *85*, 3827.
(114) Zerbi, G.; Zoppo, M. D. *J. Chem. Soc. Faraday Trans.* **1992**, *88*, 1835.
(115) Macphail, R. A.; Snyder, R. G.; Strauss, H. L. *J. Chem. Phys.* **1982**, *77*, 1118.
(116) Lide, D. R. *Chemical Rubber Company Handbook of Chemistry and Physics*, 77 ed.; CRC Press: New York, 2003; Vol. Student edition.
(117) Marcus, Y. *The properties of solvents*, 1999; Vol. 4.
(118) Steel, W. H.; A., W. R. *NATURE* **2003**, *424*, 296.
(119) Zhang, X.; Steel, W. H.; Walker, R. A. *J. Phys. Chem. B* **2003**, *107*, 3829.
(120) Ocko, B. M.; Sirota, E. B.; Deutsch, M.; DiMasi, E.; Coburn, S.; Strzalka, J.; Zheng, S.; Tronin, A.; Gog, T.; Venkataraman, C. *Phys. Rev. E* **2001**, *63*, 03602.
(121) Habenschuss, A.; Narten, A. H. *J. Chem. Phys.* **1990**, *92*, 5692.
(122) Wu, X. Z.; Ocko, B. M.; Sirota, E. B.; Sinha, S. K.; Deutsch, M.; Cao, B. H.; Kim, M. W. *Science* **1993**, *261*, 1018.
(123) Wu, X. Z.; Sirota, E. B.; Sinha, S. K.; Ocko, B. M.; Deutsch, M. *Phys. Rev. Lett.* **1993**, *70*, 958.
(124) Hughes, C. J.; Earnshaw, J. C. *Phys. Rev. E* **1993**, *47*, 3485.
(125) Gang, O.; Wu, X. Z.; Ocko, B. M.; Sirota, E. B.; Deutsch, M. *Phys. Rev. E* **1998**, *58*, 6086.
(126) Hommel, E. L.; Allen, H. C. *Analyst* **2003**, *128*, 750.
(127) Snyder, R. G.; Strauss, H. L. *J. Phys. Chem.* **1982**, *86*, 5145.

(128) Zhang, D.; Shen, Y. R.; Somorjai, G. A. *Chem. Phys. Lett.* **1997**, *218:(4-6)*, 394.
(129) Dragoslaw, M.; Tikhonov, A. M.; Li, M.; Huang, Z.; Shlossman, M. L. *Phys. Rev. Lett.* **2000**, *85*, 582.
(130) Zhang, D.; Gutow, J. H.; Eisenthal, K. B. *J. Chem. Soc. Faraday Trans.* **1996**, *92*, 539
(131) Zhang, D.; Gutow, J. H.; Eisenthal, K. B.; Heinz, T. F. *J. Chem. Phys.* **1993**, *98*, 5099.
(132) Vieceli, J.; Benjamin, I. *J. Phys. Chem. B* **2002**, *106*, 7898.
(133) Mugele, F.; Baldelli, S.; Somorjai, G. A.; Salmeron, M. *J. Phys. Chem. B.* **2000**, *104*, 3140.
(134) Casson, B. D.; Braun, R.; Bain, C. D. *Faraday Discuss.* **1996**, *104*, 209.
(135) Du, Q.; Superfine, R.; Freysz, E.; Shen, Y. R. **1993**, *70*, 2313.
(136) Benjamin, I. **1994**, *73*, 2083.
(137) Dogonadze, R. R.; Kalman, E.; Kornyshev, A. A.; Ulstrup, J. *The Chemical Physics of Solvation. Part A. Theory of Solvation*; Elsevier Science Publishing Company Inc.: Amsterdam, The Netherlands, 1985; Vol. 38A.
(138) Pimentel, G. C. *J. Am. Chem. Soc.* **1957**, *79*, 3323.
(139) Pawelka, Z.; Palasek, B.; Puszko, A. *J. Phys. Org. Chem.* **1997**, *10*, 835.
(140) Getahun, Z.; Huang, C.-Y.; Wang, T.; Leon, B. D.; DeGrado, W. F.; Gai, F. *J. Am. Chem. Soc.* **2003**, *125*, 405.
(141) Milischuk, A.; Matyushov, D. V. *J. Phys. Chem. A* **2002**, *106*, 2146.
(142) Khajehpour, M.; Kauffman, J. F. *J. Phys. Chem. A* **2000**, *104*, 7151.
(143) Abboud, J. L. M.; Notario, R. *Pure Appl. Chem.* **1999**, *71*, 645.
(144) Kuc, T.; Pawelka, Z.; Sobczyk, L. *Phys. Chem. Chem. Phys.* **2001**, *3*, 5201.
(145) Huang, D. M.; Chandler, D. *J. Phys. Chem. B* **2002**, *106*, 2047.
(146) Suppan, P.; Ghoneim, N. *Solvatochromism*; Royal Society of Chemistry, 1997.
(147) Benjamin, I. *J. Phys. Chem. A* **1998**, *102*, 9500.
(148) Debolt, S. E.; Kollman, P. A. *J. Am. Chem. Soc.* **1990**, *112*, 7515.
(149) Reichardt, C. *Chem. Rev.* **1994**, *94*, 2319.
(150) Kamlet, M. J.; Abboud, J. L.; Taft, R. W. *J. Am. Chem. Soc.* **1977**, *99*, 6027.
(151) Onsager, L. *J. Am. Chem. Soc.* **1936**, *58*, 1486.
(152) Kirkwood, J. *J. Chem. Phys.* **1934**, *2*, 351.
(153) Roux, B.; Simonson, T. *Biophys. Chem.* **1999**, *78*, 1.
(154) Diakovitch, V. A.; Arnaudov, M. G.; Shishkova, L. M.; Ilieva, M. B. *J. Mol. Liq.* **1984**, *28*, 115.
(155) Brady, J. E.; Carr, P. W. *J. Phys. Chem.* **1985**, *89*, 5759.
(156) Wong, M. W.; Frisch, M. J.; Wiberg, K. B. *J. Am. Chem. Soc.* **1991**, *113*, 4776.
(157) Mennucci, B. *J. Am. Chem. Soc.* **2002**, *124*, 1506.
(158) Aquino, A. J. A.; Tunega, D.; Haberhauer, G.; Gerzabek, M. H.; Lischka, H. *J. Phys. Chem. A* **2002**, *106*, 1862.
(159) Zierkiewicz, W.; Michalska, D.; Havlas, Z.; Hobza, P. *ChemPhysChem* **2002**, *3*, 511.

(160) Rocha, W. R.; De Almeida, K. J.; Coutinho, K.; Canuto, S. *Chem. Phys. Lett.* **2001**, *345*, 171.
(161) Kryachko, E. S.; Nguyen, M. T. *J. Phys. Chem. A* **2002**, *106*, 4267.
(162) Malaspina, T.; Coutinho, K.; Canuto, S. *J. Chem. Phys.* **2002**, *117*, 1692.
(163) Lipkowski, P.; Koll, A.; Karpfen, A.; Wolschann, P. *Chem. Phys. Lett.* **2002**, *360*, 256.
(164) Medina, F.; Poyato, J. M. L.; Pardo, A.; Rodriguez, J. G. *J. Photochem. Photobiol. A-Chem.* **1992**, *67*, 301.
(165) Schmidt, M. W.; Baldridge, K. K.; Boatz, J. A.; Elbert, S. T.; Gordon, M. S.; Jensen, J. H.; Koseki, S.; Matsunaga, N.; Nguyen, K. A.; Su, S. J.; Windus, T. L. GAMESS VERSION = 6; From Iowa State Univ., JUN 1999.
(166) Southall, N. T.; Dill, K. A. *J. Phys. Chem. B* **2000**, *104*, 1326.
(167) Novaki, L. P.; ElSeoud, O. A. *Ber. Bunsen-Ges. Phys. Chem. Chem. Phys.* **1997**, *101*, 105.
(168) Korter, T. M.; Borst, D. R.; Butler, C. J.; Pratt, D. W. *J. Am. Chem. Soc.* **2001**, *123*, 96.
(169) Suppan, P. *J. Photochem. Photobiol. A-Chem.* **1990**, *50*, 293.
(170) NIST Chemistry Database, http://webbook.nist.gov/chemistry.
(171) Hermansson, K. *J. Phys. Chem. A* **2002**, *106*, 4695.
(172) Laha, A. K.; Das, P. K.; Bagchi, S. *J. Phys. Chem. A* **2002**, *106*, 3230.
(173) Kolling, O. W. *J. Phys. Chem.* **1996**, *100*, 16087.
(174) Kolling, O. W. *J. Phys. Chem.* **1992**, *96*, 6217.